A SOIL CO_2 GAS SURVEY OVER THE LIGHTNING DOCK KNOWN GEOTHERMAL RESOURCE AREA, ANIMAS VALLEY, NEW MEXICO

By

Kristie S. McLin

Thesis
Submitted in Partial Fulfillment of the Requirements
for the Degree of Master of Science in Geochemistry

New Mexico Institute of Mining and Technology
Socorro, New Mexico

May, 2004

ABSTRACT

Soil CO_2 flux measurements were taken over the Lightning Dock Known Geothermal Resource Area located in the Animas Valley, New Mexico to determine if structures could be identified using these measurements. The Animas Valley, located southwest of Lordsburg, NM, trends N-S, typical of Basin and Range extension. The Animas Valley fault is a normal fault bounding the eastern edge of the valley. A shallow geothermal reservoir at greater than 100^{o} C lies approximately 26 m below the surface in the valley fill sediments. Originally, it was thought that geothermal fluids were degassing beneath the surface and that these gases were diffusing to the surface through valley fill sediments above these faults. Soil CO_2 flux measurements ranging from 0 to 11 g m^{-2} day^{-1} were measured over the area, and a cumulative probability plot indicated the possibility of multiple populations of flux data. However, stable isotope and compositional analysis of soil gases sampled over the LDKGRA indicate that vegetation and soil properties, not geothermal gas flux, are the dominant controls on soil CO_2 flux values in this area.

The $\delta^{13}C$ values for soil CO_2 at 50 cm depth range between -9.2 and -22.1 $^{o}/_{oo}$ relative to PDB. The $\delta^{13}C$ values indicate various degrees of mixing between vegetative and atmospheric end members of CO_2 within the soil. Lighter $\delta^{13}C$ values correspond to high flux values, indicating the strong influence of root respiration from C_3 vegetation in

the area. The $\delta^{18}O$ values for soil CO_2 at 50 cm depth range from 24.4 to 44.0 $^{o}/_{oo}$ relative to SMOW. Oxygen isotope values indicate that either soil water $\delta^{18}O$ values are not homogeneous throughout the study area or that various soil properties are influencing the rate at which soil CO_2 isotopically equilibrates with soil water. Compositional analyses of the soil gas samples also indicate that plant respiration and atmosphere contribute to the CO_2 found in soil gases in this area. Small inputs of organic molecules such as CH_4 and C_2H_6 correlating with CO_2 values in soil indicate that there are small areas within the soils where anaerobic processes dominate. Although anomalously high soil CO_2 fluxes (>4 g m^{-2} day^{-1}) coincide with the Animas Valley fault, the coincidence is not related to a geothermal flux. A NE-SW trend in flux anomalies is also observed. More productive vegetation or changes in soil properties over the fault may explain the correlation between high soil CO_2 flux measurements and the location of the Animas Valley fault. Future work should include full descriptions of soil properties, vegetation type and quantity, as well as soil gas sampling at 10 cm increments throughout the soil profile to fully understand the processes influencing soil gases and soil CO_2 flux.

ACKNOWLEDGEMENTS

I would like to express my gratitude to those who have supported me throughout this project. This project was supported financially by Roy Cunniff and Roger Bowers of Lightning Dock Geothermal, Inc. They were also more than generous with their time and support. The New Mexico Geological Society provided a Grant-In-Aid for this project. I would like to thank my advisory committee for their prompt reviews and for making time for my defense during the busiest time of the semester. I would like to thank Dr. Philip Kyle, who convinced me to come back to Tech, encouraged my work, and was incredibly flexible with all the surprises that came along. Dr. David Norman allowed me to work on this project when the previous thesis project did not pan out and also provided encouragement. Dr. Andrew Campbell was extremely patient with my continuous questioning. He made time for me when I needed it the most. I would like to thank Dylan Canales, who handed the project over to me with a considerable amount of measurements made. Roger Bowers was always there for me to bounce ideas off of, for field assistance, for references, for company in Lordsburg, and for ice cold drinks on hot September afternoons in the desert Southwest. Dave Lorge spent a considerable amount of time staking out measurement locations for me in September, 2003. I would also like to thank the residents of the area over the LDKGRA who allowed me access to their land and gave interesting observations and assistance in determining measurement locations. I would like to thank Jody Diehl for assisting me in soil gas sampling, as well as for her support and love. I would like to thank Greg, Elisa, and Alaina Diehl for their love and support as well. I am grateful to Steve and Debbie McLin for their love, support, and pickup truck. I would like to thank my grandfather, who I take after.

Finally, I would like to thank my husband, Ryan McLin, who made this all possible. He commuted to Albuquerque to work when I said I wanted to come back to school. He took care of me when all I had time to do was type. He came to Lordsburg to assist me in the field for weeks at a time. He has loved and supported me throughout this project and I could not have done this without him.

TABLE OF CONTENTS

LIST OF FIGURES

LIST OF TABLES

This thesis is accepted on behalf of the
Faculty of the Institute by the following committee:

David L. Noon / Philip Reyes

Advisor

Andrew Campbell

4/29/04

Date

I release this document to the New Mexico Institute of Mining and Technology.

4/29/04

Student's Signature

Date

1. INTRODUCTION

Soil gas measurements are used as a geochemical exploration tool in the petroleum industry and have been used to explore for geothermal resources (e.g. Bertrami et al, 1990; Vakin and Layanlin, 1990; Hinkle, 1991; Finlayson, 1992; Klusman et al, 2000; Bergfeld et al, 2001; Norman et al, 2002). Soil CO_2 has also often been studied to understand volcanism (e.g. Baubron et al, 1990; Allard et al, 1991; O'Keeffe, 1994; Farrar et al, 1995; Gerlach et al, 2001) and to understand the formation of calcium carbonate in arid soils (e.g. Cerling et al, 1989, 1991; Vindum, 1998). It is important to understand the relationship between the flux, concentration, and isotope composition of CO_2 in soils to determine its sources. Bertrami et al (1990) determined that CO_2 anomalies in soil over geothermal areas on Vulcano Island are associated with fractures. Finlayson (1992) suggested that soil gas studies can validate or invalidate conclusions reached on flow patterns in a geothermal field using other methods. Vakin and Lyanlin (1990) determined that CO_2 can be used as a detector of geothermal conduits up to 1000 m below the surface. Non-volcanic degassing can contribute significant CO_2 to the global carbon cycle (Kerrick, 2001). The Taupo volcanic zone of New Zealand and other back arcs of western Pacific subduction zones emit an estimated 10^{12} mol/yr CO_2. Geothermal systems in the Salton Trough, California emit approximately 10^9 mol/yr CO_2 (Kerrick, 2001). The Salton Trough, however, is a unique example because carbonate-bearing sediments are metamorphosed to produce CO_2 in these geothermal systems. Continental rifts and major fault zones may provide conduits to the atmosphere for deeply derived CO_2 (Kerrick, 2001). The Basin and Range province, characterized with

high heat flow and thin crust, may be contributing deeply derived CO_2 to the atmosphere as well.

The Lightning Dock Know Geothermal Resource Area (LDKGRA) is located in the Animas Valley SW of Lordsburg, NM. The valley was formed during Basin and Range extension (Elston et al, 1983). Chemical geothermometers have indicated that subsurface geothermal fluids are at temperatures between 160 and 180^{o} C (Elston et al, 1983; Norman and Bernhardt, 1982), although temperatures measured in wells are only about 115 ^{o} C (Elston et al, 1983). The reservoir water contains about 1% of the dissolved N_2 that air saturated groundwater would normally contain (Norman and Bernhardt, 1982). Geophysical and geochemical exploration methods were not suitable to locate subsurface faults over the LDKGRA where there are no surface expressions of the geothermal field other than a surface heat anomaly (Kintzinger, 1956).

The working hypothesis for this study is that low-level CO_2 emissions over the Lightning Dock Known Geothermal Resource Area (LDKGRA) are related to faults conducting geothermal fluid in the subsurface (McLin et al, 2004). These faults are possible conduits bringing geothermal CO_2 to the surface and therefore can be detected using soil CO_2 flux measurements. The valley fill sediments are hundreds of meters thick in this area, so soil CO_2 flux measurement was an ideal exploration method to find faults buried by these sediments. Dylan Canales conducted the first portion of the soil CO_2 flux survey over the LDKGRA in July, 2002 to examine fluxes and their relationship to known structures. The results were promising because anomalously high soil CO_2 fluxes (>4 g m $^{-2}$ day^{-1}) correlated with a known fault in the 0.8 km^2 area (Norman et al, 2002). The study area was then expanded to include a 7 km^2 area over Kintzinger's (1956)

surface thermal anomaly so hidden structures could be located. The soil CO_2 flux measurements taken over the LDKGRA indicated patterns associated with a known fault, as well as possible patterns related to inferred faults from previous studies (McLin et al, 2004). The working hypothesis was tested by sampling soil gas in the study area and analyzing the stable carbon and oxygen isotopes in the CO_2 and the composition of the soil gas. A geothermal influence on the soil CO_2 would be detected through these measurements. Sources of the soil CO_2 related to varying fluxes over the LDKGRA were determined, and patterns in the data were re-examined and compared to known and inferred structural features.

1.1 Soils and CO_2

Soil gases are generally the same as those present in the atmosphere (O'Keeffe, 1994). These include N_2, O_2, Ar, and CO_2 as the major components of both atmosphere and soil gas. The concentration of CO_2 in soil naturally increases with depth due to the decreasing influence of atmosphere, increasing influence of plant root respiration, and decreasing diffusion of gases out of soil with depth (Amundson et al, 1998). In atmosphere, the global average concentration of CO_2 is continually increasing, giving rise to the greenhouse effect (Keeling and Whorf, 2002). Atmospheric CO_2 concentrations vary spatially and are reported at 373 ppmv over Manoa Loa and 370 ppmv over Antarctica (Keeling and Whorf, 2002).

The soil CO_2 flux is a measure of the quantity of CO_2 diffusing through a soil to the surface and into the atmosphere. Fluxes are usually reported in grams per square meter per day ($g\ m^{-2}\ day^{-1}$). Concentrations of CO_2 in soils can be significantly higher than in atmosphere, even in desert environments with sparse vegetation. The vegetation

usually found on the surface of these arid soils is mixed grasses, shrubs, and succulents often referred to as C_3, C_4, and CAM vegetation (Cerling, 1989). C_3, C_4, and CAM refer to the different methods of metabolism for this vegetation. The top few centimeters of any soil mainly contain gases contributed by the atmosphere or gases that have mixed with the atmosphere. Usually, greater values of CO_2 flux correspond to an increase in the influence of plant respiration on the CO_2 concentration in a soil (Amundson et al, 1998). Soil gas CO_2 produced by plant respiration is usually considered to be secondary in the generation of gas anomalies in volcanic and geothermal areas (O'Keeffe, 1994). Thus, if there is an input of geothermal CO_2, soil CO_2 flux in geothermal areas will be affected by background flux from plant respiration, atmospheric CO_2, and geothermal CO_2. Unless the geothermal CO_2 flux exceeds that of background vegetation related flux levels, anomalous flux values related to geothermal input cannot be easily identified.

In order to supply O_2 to a plant's roots, a soil must be aerated. Aeration is the gaseous exchange that must take place between soil gases and atmospheric gases in order to prevent an excess of CO_2 and a deficiency of O_2 within a soil (Hillel, 1998). Aeration can occur more easily in dry soils because the rate of exchange from atmosphere decreases with increasing water in pore spaces in a soil. Mechanical compaction of soil can severely impede aeration, as can poor drainage or water logging. Aeration of a soil strongly depends on the air capacity of the soil. The air capacity of a soil depends on soil texture as well as the moisture content of a soil (Hillel, 1998). With an increase in fine components such as clay and silt in the soil, there is a decrease in the air capacity of a soil. A strongly compacted soil may contain less than 5% air by volume, a clay-rich soil

may contain less than 10% air by volume, and sandy soils may contain 25% or more air by volume (Hillel, 1998)

1.2 Stable Isotopes

Since there are many sources of CO_2 in soils, it is important to understand the contributions of these sources when interpreting anomalies in the flux data. The various sources of carbon influence the $\delta^{13}C$ of CO_2. $\delta^{13}C$ is a value that represents the ratio of ^{13}C to ^{12}C in a sample compared to a standard as follows (Hoefs, 1997):

$$\delta^{13}C_{(CO2)} = (((^{13}C/^{12}C)_{sample}/(^{13}C/^{12}C)_{standard})-1) \times 10^3 \ (^{o}/_{oo}) \quad \text{(Equation 1)}$$

The carbon standard PDB (Pee Dee Belemnite) has been exhausted; however $\delta^{13}C$ values are reported relative to this standard (Hoefs, 1997). Various natural processes fractionate carbon, giving a variety of $\delta^{13}C$ values for various sources of carbon. Different types of vegetation use different photosynthetic pathways and fractionate carbon isotopes differently. C_3 plants respire CO_2 that has a $\delta^{13}C$ ratio between -30 and -20 $^{o}/_{oo}$ relative to PDB (Hoefs, 1997), and C_4 plant CO_2 has a $\delta^{13}C$ ratio on average - 13 $^{o}/_{oo}$ relative to PDB (Cerling et al, 1991). CAM vegetation uses both C_3 and C_4 photosynthetic pathways and can therefore respire values of $\delta^{13}C$ anywhere between -13 $^{o}/_{oo}$ and -30 $^{o}/_{oo}$. Atmospheric CO_2 has a $\delta^{13}C$ ratio averaging -8 $^{o}/_{oo}$ (Amundson, 1998), and mantle CO_2 has a $\delta^{13}C$ ratio between -8 and -4 $^{o}/_{oo}$ relative to PDB (Hoefs, 1997). By analyzing the soil gases in an area for stable isotopes in CO_2, it should be possible to determine the influence of vegetation on soil CO_2 flux measurements, as well as interpret sources for the soil CO_2.

Although oxygen isotope data are seldom reported for CO_2 stable isotope studies, the $\delta^{18}O$ value of CO_2 may also help to constrain the possible sources of CO_2 in soil.

$\delta^{18}O$ is a value that represents the ratio of ^{18}O to ^{16}O in a sample compared to a standard as follows (Hoefs, 1997):

$$\delta^{18}O_{(CO2)} = (((^{18}O/^{16}O)_{sample}/(^{18}O/^{16}O)_{standard})-1) \times 10^3 \quad (^{o}/_{oo}) \quad \text{(Equation 2)}$$

The $\delta^{18}O$ is usually reported relative to the standard SMOW (standard mean ocean water). Very few studies have examined the processes that control the $\delta^{18}O$ in soil CO_2 (Stern et al, 1999). Four processes are thought to control the oxygen isotope ratio in soil CO_2. These include the respiration of CO_2 by plants, varying mass affecting the diffusivity of the various masses of CO_2 through a soil to the surface, the mixing of atmosphere with soil gas by diffusion and advection, and isotope exchange with soil water (Stern et al, 1999). Oxygen in CO_2 respired by plants is thought to be in isotopic equilibrium with the oxygen in soil water. Oxygen in atmospheric CO_2 in a soil also equilibrates with oxygen in soil water. Oxygen in atmospheric CO_2 usually has a value of 42 $^{o}/_{oo}$ relative to SMOW, but can increase or decrease in soils due to these various processes. Some studies also suggest that plants may discriminate against heavier oxygen as well in their intake of CO_2, O_2, and H_2O (Berry et al, 1994). This and other biological activities can account for the heavy $\delta^{18}O$ found in atmospheric gases.

1.3 Photosynthesis, Photorespiration, and the Cycling of CO_2

Photosynthesis is the process by which a plant creates the energy it needs to grow by reducing atmospheric CO_2 to organic forms of carbon by the following overall reaction (Schlesinger, 1997):

$$CO_2 + H_2O \rightarrow CH_2O + O_2 \quad \text{(Equation 3)}$$

A five carbon molecule, ribulose 1,5-bisphosphate (RuBP), fixes carbon from the CO_2 (Karp, 1996). Plants use different photosynthetic pathways to fix carbon: C_3, C_4, and

CAM methods of metabolism. Overall, plants that use the C_3 pathway for photosynthesis make up about 90% of vegetation on Earth today (Hoefs, 1997). C_4 plants differ from C_3 plants because they have developed a method for concentrating CO_2 relative to O_2, therefore fixing a greater amount of carbon (Karp, 1996). Both C_3 and C_4 plants have small openings in their leaves called stomata that open during the daytime to allow CO_2 in. These openings do allow for the evaporation of water from these plants by a process called transpiration. CAM plants have also developed a method to concentrate CO_2, but unlike C_3 and C_4 plants, they do not open their stomata in the daylight hours (Karp, 1996).

A less well known process called photorespiration also occurs in plants. This process involves the uptake of O_2 and the release of CO_2 and wastes the plant's energy (Karp, 1996). This process may account for a loss of up to 50% of a plant's carbon taken in through photosynthesis. The process of photorespiration is unavoidable, although many have tried to breed plants that do not engage in photorespiration with virtually no success (Karp, 1996). Photorespiration occurs mainly in the roots of plants, therefore enriching the soil atmosphere with CO_2 while depleting it in O_2.

As discussed in section 1.2, the stable isotope ratio of carbon respired by vegetation can vary between -30 $^{o}/_{oo}$ and -13 $^{o}/_{oo}$. C_3 plants can show large variation in $\delta^{13}C$ values depending on their water-use efficiency (Ehleringer, 1991). When there is a shortage of available water, plants tend to close their stomata to decrease the effects of transpiration (Schlesinger, 1997). At lower stomatal conductance, the water-use efficiency of a plant increases. Also, at lower stomatal conductance, discrimination

between $^{12}CO_2$ and $^{13}CO_2$ is not as great (Schlesinger, 1997). The greater the water-use efficiency of a plant, the more ^{13}C will be fixed during photosynthesis.

2. PREVIOUS STUDIES

2.1 Volcanology

Soil CO_2 flux studies have been conducted on several active volcanoes to understand the contribution of diffuse emissions of CO_2 to the global carbon cycle, as well as to monitor volcanic activity (Baubron et al, 1990; Allard et al, 1991; O'Keeffe, 1994; Farrar et al, 1995; Gerlach et al, 2001). Faults and fractures channel the volcanic gases to the surface, where they are diffused into the soil and to the surface (Delmelle and Stix, 2000). The quantity of gases released through the flanks of a volcano may equal or surpass the quantity released through the crater. The first volcano to be extensively studied for diffuse emissions of CO_2 was Mt. Etna, one of the world's most actively degassing volcanoes (Allard et al, 1991). Mt. Etna, in Sicily, is a strato-volcano that produces alkaline basaltic lava and emits large quantities of CO_2 through its crater, as well as along fractures and faults along its flanks. The carbon isotope ratios of the diffuse flank gases indicates that the source of the CO_2 is magmatic, derived from a deep mantle source ($\delta^{13}C = -3.7\pm0.3^{o}/_{oo}$) (Allard et al, 1991). Soil gas concentrations of CO_2 varied from 0.25 to 27.9% by volume on the flanks of Mt. Etna. These measurements were made using a stainless steel probe at a depth of 80 cm in the volcanic soil (Allard et al, 1991). Soil CO_2 concentrations were measured and used to find hidden structures near the Pernicana fault, which is considered to be one of the most active and important faults on Mt. Etna (Giammanco et al, 1999). A teflon probe was inserted to a depth of 50 cm for these measurements. Gas monitoring has also indicated that Mt. Etna's plumbing

system extends at least 40 km SW from the boundary of the volcano, where 200 tonnes of gas are discharged each day (Caracausi et al, 2003). By examining diffuse emissions of CO_2 and other gases on the flanks of Mt. Etna, faults and fractures can be mapped and magmatic processes can be explored.

Mammoth Mountain, CA is also studied extensively for its diffuse degassing of CO_2 through faults and fractures along its flanks. Mammoth Mountain is a dacitic volcano on the edge of the Long Valley Caldera that has been recently active (Farrar et al, 1995). Tree kills were noticed after a 1989 earthquake swarm and soil gas studies were initiated in these areas (Farrar et al, 1995). Soil gas samples were collected at 30 to 60 cm depths and analyzed for CO_2 volume percents, as well as for $\delta^{13}C$, nitrogen, oxygen depletion, and He concentrations and isotope ratios. Farrar et al (1995) also estimated the percent of soil CO_2 in and away from the tree kill areas produced through biologic processes. Within the tree kill areas, the percent of biogenic CO_2 was negligible, ranging from 0.1 to 1.4 %. Percentages were significantly higher in areas with living trees, ranging from 4.7 to 100%. The $\delta^{13}C$ values for the CO_2 in the live tree areas ranged from -19.9 to -3.0 $^{o}/_{oo}$ relative to PDB, and in the kill zones the $\delta^{13}C$ values for the CO_2 ranged from -4.7 to -3.0 $^{o}/_{oo}$ relative to PDB. Gerlach et al (2001) conducted soil CO_2 flux surveys in tree kill areas using the closed circulation accumulation chamber method. In this method a chamber is placed open ended onto the ground, and as the CO_2 accumulates in the chamber, the gas is circulated through an external analyzer and back to the chamber. The soil CO_2 flux in one tree kill area, near the Horseshoe Lake tree kill, ranged from 1 to greater than 10,000 g m^{-2} day^{-1} (Gerlach et al, 2001). Gerlach et al (2001) also determined that the non-normality of their flux data for the Horseshoe Lake

tree kill did not seriously distort kriging models used for contouring their data. Rogie et al (2001) examined the variability of soil CO_2 flux measurements taken on Mammoth Mountain continuously from 1997 to 2000. Variations in flux were related to atmospheric pressure and wind speed, not to geological processes. Degassing of CO_2 was relatively consistent throughout the study, and only meteorological variations caused changes in flux measured.

2.2 Geothermal

The Roosevelt Hot Springs KGRA, located in Utah, is a hot-water-dominated system that is structurally controlled by several faults within the field (Hinkle, 1991). It is also an area where soil CO_2 studies were conducted to understand the natural variation of this and other gases in soils (Hinkle, 1991). Soil gases were collected regularly at four sites in the KGRA over several months and analyzed for volume percent CO_2, and measurements of soil temperature, air temperature, barometric pressure, rainfall, and snowfall were collected to understand these influences on the CO_2 percents. The soil concentrations of CO_2 varied dramatically over the seasons. As the soil temperatures increased, the concentrations of CO_2 decreased. Hinkle (1991) hypothesized that the seasonal variation is related to varying rates of root respiration and microbiological activity during the different times of year. She also determined that either soil gas surveys should be done under the same meteorological conditions in a very short period of time, or the data should be normalized to the soil temperature at the time that the measurements are taken.

Soil He, CO_2, H_2, and CH_4 were investigated in geothermal and non-geothermal zones in Italy by Bertrami et al (1990). Vulcano Island was the geothermal region

investigated in this study. Soil CO_2 anomalies correlated to He anomalies in the geothermal regions. The He anomalies corresponded to lineaments in the geothermal regions on Vulcano Island. Baubron et al (1990) also investigated the diffuse emissions of CO_2 on Vulcano Island, but the purpose of their study was to monitor volcanic activity and diffuse degassing related to the Fossa active cone. This island is an active volcano, so it would be difficult to distinguish between CO_2 anomalies related to geothermal processes and those related to degassing of the intrusion. However, anomalous CO_2 concentrations correspond to faults and fractures in either case.

Vakin and Lyanlin (1990) conducted a soil gas survey over the Mutnovsky Geothermal Field in Kamchatka and determined that radon and CO_2 were the best indicators of conduits in this area. Gas samples were extracted using a steel probe at a depth of 1 m and then analyzed for concentrations of various gases. Vakin and Lyanlin (1990) determined that the maximum distance between sample locations should be no more than 100 m, and the sample grid could be altered if the geologic features investigated are elongate and the strike is known. The distance between profiles perpendicular to the strike of the features could be increased, but the distance between points on these profiles should be decreased. Vakin and Lyanlin (1990) also developed an approach that should be used in soil gas surveys. First, the survey area and scale choice should be based on geochemical and geophysical data. Background values of the indicator gas should be determined, and an arrangement of routine observation points should be made. Mapping of observations, as well as computer treatment of the data should follow, and lastly, the results should be tested through reconnaissance drilling (Vakin and Lyanlin, 1990). By following this method, Vakin and Lyanlin (1990) assert

that it should be possible to discover areas of concealed discharge, even at depths up to 1000 m in geothermal systems.

A soil gas survey was conducted over the Rotorua Geothermal Field in New Zealand by Finlayson (1992). Gas was sampled from 1-meter depth using a probe and analyzed for CO_2, H_2S, and CH_4. Finlayson (1992) discovered through stable isotope analysis of the carbon in the CO_2 that much of the soil CO_2 in geothermal areas could still be contributed largely through biogenic processes. The $\delta^{13}C$ values within the area ranged from -4.2 to -25.0 $^{o}/_{oo}$, and an off-field site sample yielded a $\delta^{13}C$ of -25.9 $^{o}/_{oo}$.

3. STUDY AREA

The Lighting Dock Known Geothermal Resource Area (LDKGRA) is located SW of Lordsburg, New Mexico in the Animas Valley (Fig. 1). The Animas Valley trends N-S and is typical of Basin and Range extension (Elston et al, 1983). Water with a temperature of 115 ^{o} C was discovered in 1948 at a depth of 26.5 meters. Since the discovery of boiling water in the valley, more than forty wells have been drilled in the area to further explore the geothermal resource. Groundwater was used to irrigate crops such as cotton and pecans when the geothermal system was discovered, and now the hot water is used in greenhouses to grow roses and raise fish fingerlings. Kintzinger (1956) investigated and mapped a surface high heat anomaly. Preliminary wells drilled in the early 1950's show that there is about 50 feet of sand and clay deposited on the surface of the valley (Kintzinger, 1956). This soil is underlain by what is described as "warm-water-bearing gravel," which is above an 8-ft thick layer of clay. Below the clay is a rock described as "hot rhyolite." Kintzinger (1956) measured the temperature of the ground one and two meters below the surface using resistance thermometers, and the

highest temperature recorded at 1 m below the surface was 23° C. The temperatures were 12° C higher than measurements taken outside of the anomalous region. Many greenhouses are now located on the thermal anomaly mapped by Kintzinger (1956).

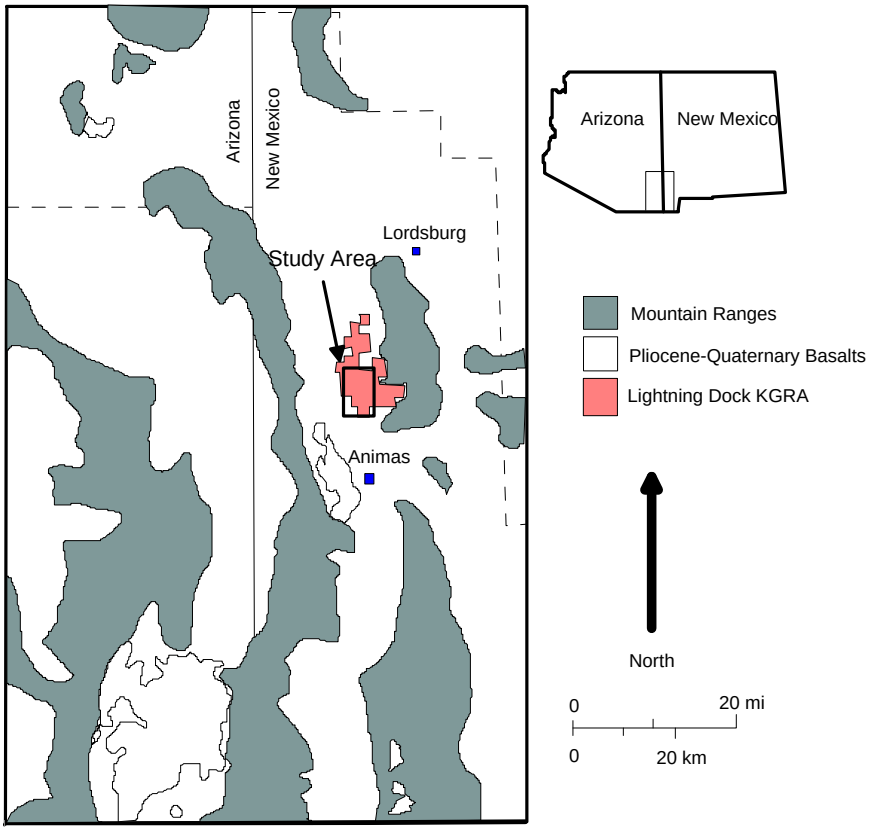

Figure 1. Map of Lordsburg, NM area, including the location of the Lighting Dock KGRA and the study area location. Map modified from Elston et al, 1983.

Lordsburg, NM, located northeast of the Animas Valley, receives an average of 3.1 cm precipitation annually. The average daytime highs in this area range from 15° C in January to 37° C in July. The hydrologic gradient in the valley is from South to North, with flow also from the sides to the center of the valley (Elston et al, 1983). Playa lakes and evaporite deposits develop north of the valley where the groundwater table occasionally reaches the surface, ponds up, then evaporates. The Animas Valley is filled

with alluvial fan deposits from surrounding hill slopes, as well as by windblown loess (Fleischhauer and Stone, 1982). The area is arid, with most of the year's precipitation falling during the summer rains, and there is very little natural vegetation.

The Animas Valley fault is a normal N-S trending bounding fault of this valley that is Miocene age and was still active in the Holocene (Fleischhauer and Stone, 1982). The recent offset observed on this fault is greater to the north, and the surface expression of this fault is not visible to the south of the hot wells. There are no definite surface expressions of other faults in the valley, but many are hypothesized using interpretations from geophysical and geochemical data, including a fault trending NE-SW (Elston et al, 1983). Many normal faults are observed trending in directions other than N-S, though, in the Pyramid Mountains (Elston et al, 1983). The Pyramid Mountain volcanic complex to the East of the valley consists of deposits ranging from rhyolitic lava flows and ignimbrites to basaltic andesite lava flows. The Muir Cauldron structure with bounding ring faults is part of the Pyramid Mountain volcanic complex, and ring faults may influence the flow of groundwater in the Animas Valley (Elston et al, 1983). Tuff erupted from the Muir Cauldron was dated at 35.23 ± 0.13 Ma using $^{40}Ar/^{39}Ar$ methods on a biotite crystal from the tuff of Woodhaul Canyon (McIntosh and Byran, 2000). Quaternary basaltic volcanism is found approximately 30-km southwest of the hot wells (Elston et al, 1983). The basaltic lava flows in the Animas Valley are dated at 0.544 ± 0.050 Ma using K-Ar methods (Lynch, 1978). There is evidence for widespread fault-controlled hot-spring activity within the past 20 million years in the area, and there is a significant amount of hydrothermal alteration in the Pyramid Mountains. This alteration, however, is thought to be related to the Pyramid Mountain volcanic complex and not to

the recent geothermal activity in the area. Travertine and calcite deposits are evidence for the existence of hot springs in the area, but they are not found within the study area. Local mineralization trending NE includes veins containing fluorite, calcite, manganese, silver, copper, pyrite, and stibnite (Elston et al, 1983). Elston et al (1983) hypothesize that the geothermal water found in the LDKGRA reservoir is a mixture of 75% meteoric groundwater and 25% geothermal fluids heated by basaltic magma. Geochemical evidence shows that the heated water seeps into a shallow cold aquifer through a system of faults SE of the LDKGRA (Elston et al, 1983).

The ground waters of the Animas Valley are found in unconfined aquifers and in valley fill sediments (Elston et al, 1983). Using oxygen and hydrogen stable isotope measurements, the geothermal water and groundwaters in the Animas Valley were determined by Elston et al (1983) to be meteoric in origin, but the waters have been modified by evaporation, boiling, and mixing. Although the majority of the precipitation falls during summer rains, winter precipitation is most likely the source of recharge to these aquifers. This is because summer rainfall events are short duration, and evaporation does not allow for infiltration to the water table (Elston et al, 1983). Three wells with high surface temperatures, as well as 42 cooler wells in the valley, were sampled under the supervision of C.A. Swanberg as part of an initial survey of the geothermal potential in the Animas Valley (Elston et al, 1983). The water samples from these three hot wells, named samples P2, P3, and P4, in the LDKGRA were measured at temperatures of 85.0, 81.0, and 71.0^{o} C, respectively, at the surface. These samples also show low total dissolved solids (1116, 1024, 1608 ppm, respectively) and relatively high fluoride (12.6, 12.0, 7.25 ppm, respectively). The geothermal waters are thought to be a

mix of high temperature geothermal fluids and cold shallow groundwater. Wells SW of the hot wells and Kintzinger's (1956) thermal anomaly show the geochemical signature of deep geothermal reservoir water even though these wells are up gradient from the thermal anomaly (Elston et al, 1983). This evidence leads Elston et al (1983) to hypothesize that the main geothermal reservoir is located SW of the surface thermal anomaly.

The LDKGRA is a convective geothermal resource (Witcher, 1988). The convective geothermal systems in southwestern New Mexico often exhibit water chemistry that reflects the reservoir lithology. These systems also occur mainly where Paleocene to lower Miocene rocks overlie Paleozoic and Precambrian rocks. These are areas of Laramide and Mesozoic uplifts. Convective geothermal resources are also favored where there are deep sediment-filled basins and where there are lacustrine and playa lake deposits because these areas have higher temperature gradients. The combination of uplift, a Tertiary cauldron complex (Muir Cauldron), and late Tertiary horst block structures is found at the LDKGRA, as well as lacustrine and playa lake deposits and a deep sediment-filled basin.

Geophysical data indicate that a structure trends within the Animas Valley from an area SW of the main surface heat anomaly and continues through the LDKGRA to the NE. Several Bouguer gravity anomaly maps of the area show this trend clearly (Wynn, 1981; Lance et al, 1982; O'Brien and Stone, 1984), as do the resistivity highs observed by Jiracek and Smith (1976).

The area of the LDKGRA examined in this study consists of Quaternary alluvial fan deposits and Quaternary eolian and sheetflood deposits (Elston et al, 1983) (Fig. 2).

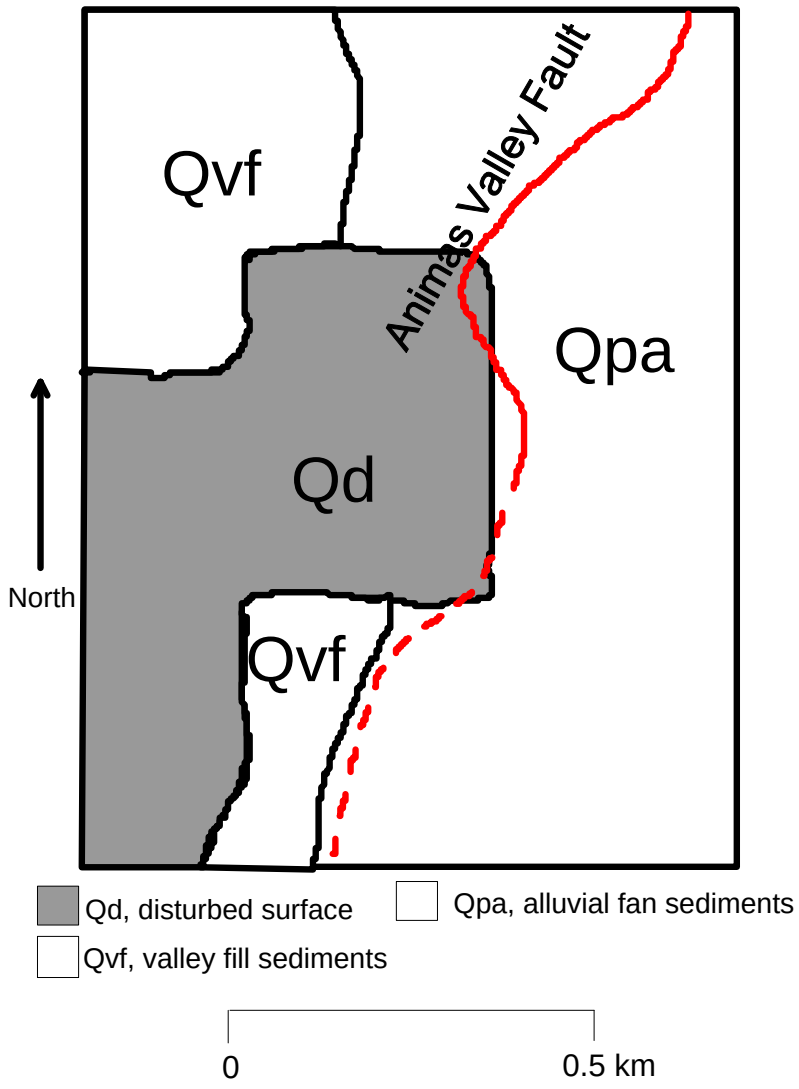

Figure 2. A map of Quaternary surficial deposits after the Geologic Map of Southern Part of Pyramid Mountains, Hidalgo County, New Mexico (Elston et al, 1983). Map has been modified to include areas disturbed by human activity, as well as adjustments to boundaries observed in the field.

The fan deposits consist of poorly sorted gravels and sands, with a parent material of rhyolites, tuffs, and amorphous quartz materials eroded from the Pyramid Mountains east of the area. The Quaternary eolian and sheetflood deposits are fine sand and silt that fill the Animas Valley. Much of the surface in the study area has been disturbed by human activity, including farming, building, and roads. Some areas that were previously farmed have not re-vegetated since farming ceased. These areas also have no gravel, while small

amounts of gravel can be found throughout the valley deposits. Calcium carbonate has concentrated in the soil horizons formed on fans surrounding and within the study area, but the soils above Kintzinger's (1956) thermal anomaly have negligible quantities of calcium carbonate in the upper horizons (Bowers, personal communication 2003).

Parts of the study area remain relatively undisturbed by human activity. These areas have vegetation that consists almost solely of creosote (*Larrea tridentada*) (Fig. 3).

Figure 3. A picture of the NE end of the study area looking east to the Pyramid Mountains. The vegetation here is creosote (a C_3 plant).

The creosote mainly grow in the gravely areas and in some areas where sand dunes have formed. The creosote is taller and denser in the Qpa alluvial sediments. Within the disturbed areas, there is a considerable amount of non-native vegetation. Non-native grasses grow surrounding the rose greenhouses in the area. Some residents in the area have brought in the grass for lawns, and it has spread to the well watered areas surrounding the greenhouse structures. The soil in the greenhouse area has also been

extremely compacted. The vegetation observed in the field area (creosote and non-native grasses) uses the C_3 photosynthetic pathway, with some CAM (yucca) plants in the Southern part of the area.

4. METHODS

4.1 Soil CO_2 Flux

For this study, soil CO_2 flux measurements were taken in a 7 km^2 area near the hottest wells mostly at 50-meter spacing in the E-W direction except where not possible due to cultural features. The measurement locations were chosen based on the location of the Animas Valley fault, mapped surface heat anomalies (Kintzinger, 1956), and various inferred structures and lineaments observed on the surface using aerial photography. The 50-meter spacing was chosen because measurements taken at 100-meter spacing showed multiple one point anomalous values of soil CO_2 flux. A total of 467 measurements were taken. Dylan Canales performed the first 126 measurements in July, 2002. I took the remaining measurements in January and September, 2003 and in March, 2004. I also measured atmospheric pressure, air speed, atmospheric temperature and soil temperature at each measurement location. Soil temperature measurements were made using a probe at a depth of 15 cm. General descriptions of the surface deposits and vegetation type and coverage were also made. A global positioning systems unit was used to find UTM coordinates for each site using NAD 27 as datum. Soil CO_2 flux measurements were taken at least once every field day at a standard measurement location to determine seasonal variation and reproducibility of measurements. This standard measurement location was chosen because it is easily accessible and has sparse vegetation.

A LI-COR® brand 6262 CO_2 analyzer and a closed accumulation chamber were used for measuring the soil CO_2 flux (Fig. 4). Air was circulated through a closed loop between the analyzer and the chamber so suction or pressure was not created within the chamber that may have altered the flux measurement (Welles et al, 2001). The accumulation chamber used was a 9.39-liter volume aluminum box with a fan inside to circulate the air. Circulation inside the chamber is important to correctly sample the changing concentration of CO_2 within the chamber (Welles et al, 2001). Measurements were not taken within a day of a recent precipitation event, which would increase soil moisture, affecting the flux measurements. The open end of the box was placed on the surface approximately one centimeter into the soil and away from vegetation. Because water vapor has a diluting effect on the concentration of CO_2, it was removed from the chamber using a magnesium perchlorate trap before the gas was analyzed. Carbon dioxide was scrubbed from the accumulation chamber until the concentration in the chamber was slightly below atmospheric concentration, or about 356 micromoles per mole. The CO_2 was accumulated in the box, fed into a flow meter, and then analyzed by the LI-COR®. The CO_2 concentration was averaged and logged by an HP Palmtop® once every second for over 100 seconds (some exceptions in July 2002 measurements). The gas was then pumped back into the accumulation chamber, preventing a vacuum from forming inside the box. The LI-COR® was calibrated once a day by scrubbing out the CO_2 from the lines and zeroing the analyzer. It was also calibrated once a day using a standard 3500 parts per million (molar) CO_2 gas.

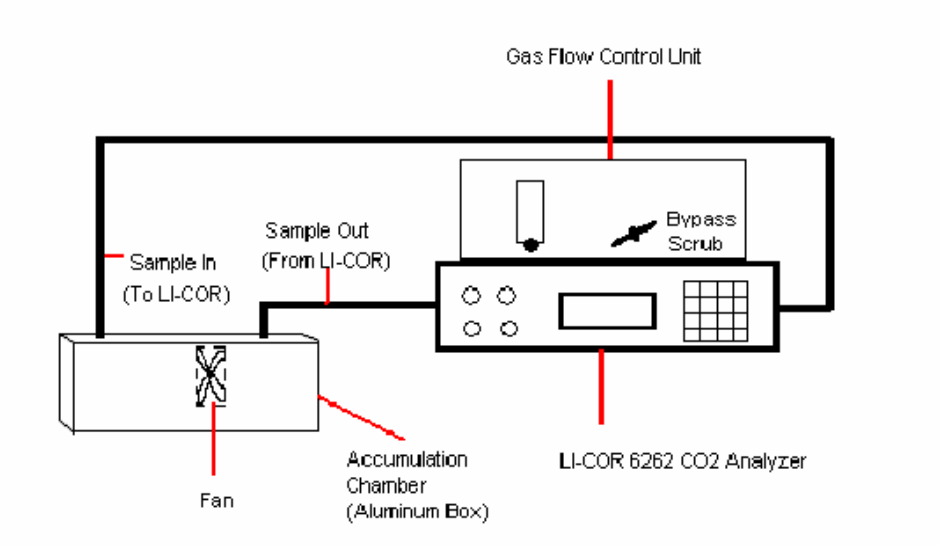

Figure 4. Schematic diagram of the LI-COR® 6262 CO_2 analyzer and accumulation chamber.

From the concentration and time data logged, a plot with time on the X-axis (seconds) and concentration (micromoles per mole) on the Y-axis gives a slope of change in concentration over change in time (dX/dt). The slope is taken at the point where the concentration of CO_2 is near atmosphere, usually within the first 50 to 100 seconds of measurement. This slope ($\mu mol\ mol^{-1}\ s^{-1}$) was then used in the equation for flux:

$$Flux = (PV/RT*dX/dt)/A \qquad \text{(Equation 4)}$$

where P is atmospheric pressure (atm), V is the volume in the accumulation chamber (L), R is the gas constant (L atm K^{-1} mol^{-1}), T is atmospheric temperature (K), and A is surface area underneath the accumulation chamber (m^2). Flux is usually reported in units of grams per square meter per day (g m^{-2} day^{-1}). The measurement locations and flux values are plotted on various maps using Golden Software's Surfer 7 program. The soil CO_2 flux image and contour maps are compared to known structural features to observe correlations in the data.

4.2 Soil Gas Stable Isotope Analysis

Ten soil gas samples were collected from a depth of 0.5 meters using a hollow metal soil probe. The gas was pumped into evacuated sample bags through a septum using a hypodermic needle. 1.6 liters of soil gas were collected for stable isotope analysis at ten sample locations. At each sample location, flux measurements, air and soil temperature, air speed, atmospheric pressure, and UTM coordinates were taken. Notes were also made concerning the soil type, vegetation type, and vegetation density at each location. The gas samples were returned to the Stable Isotope lab in the Earth and Environmental Sciences Department at the New Mexico Institute of Mining and Technology for preparation and analysis. The soil gases were prepared and analyzed for stable isotopes within 48 hours of sampling.

In the Stable Isotope lab, an aliquot of soil gas was released from the sample bags into a glass vacuum extraction line. CO_2 and H_2O were cryogenically separated and trapped. Once adequate time had passed to freeze all the water and CO_2 into the traps, the non-condensable gases were pumped away. The procedure was repeated until the bag was empty. The CO_2 was allowed to melt, transferred to a cold finger, and the gas pressure was measured. Finally, samples were moved into evacuated sample bottles for transfer to the mass spectrometer. The sample bottle was then sealed until the gas was analyzed. This is the same method reported by Wardell et al (2003) for separation of CO_2 from other gases in the NMIMT Stable Isotopes lab.

The CO_2 samples were analyzed for $\delta^{13}C$ relative to PDB and $\delta^{18}O$ relative to SMOW using a Thermo Finnigan Delta Plus XP mass spectrometer. The samples were run with a duel inlet system against an Oztech® gas standard. The data resulting from

stable isotope analyses of the gases were then compared to a variety of factors such as sample size, flux, vegetation type, and vegetation density to examine possible relationships.

4.3 Soil Gas Compositional Analysis

Ten 0.3-liter soil gas samples were collected for compositional analysis at the same sites and using the same method as the stable isotope gas samples. These samples were analyzed in the Quadropole Mass Spectrometer lab at the New Mexico Institute of Mining and Technology. In the lab, background values were measured for the mass spectrometer. 1-cc air samples from the lab were injected through a septum into a glass vacuum extraction line. Two dry ice traps froze water out of the gas samples before they were analyzed by the mass spectrometer. 1-cc size samples from the soil gases were extracted from the sample bags and then injected into the extraction line using a syringe. These samples were analyzed and recorded for ten two-second cycles, then evacuated from the line. Two background measurements, seven air measurements, and ten soil gas measurements were made. The mass spectrometer analyzed for and recorded values for He, CH_4, N_2, C_2H_6, O_2, Ar, CO_2, and SO_2. Background levels were subtracted from the analyzed sample values, and all values were ratioed to N_2. These gas ratios were then ratioed to the air samples taken before and after the analysis. Ratios for each gas were plotted versus flux to examine possible relationships, as well as plotted versus CO_2. Gases were also plotted against each other to look for correlations between gases.

5. RESULTS

5.1 Soil CO_2 Flux

All soil CO_2 flux measurements taken in the study area lie within the range of 0 to 11 g m^{-2} day^{-1}. Flux measurements do not show a normal distribution (Fig. 5). An arithmetic cumulative probability plot (Fig. 6) of the flux data indicates that there could be multiple populations within these data. This is indicated by the linearity of the plot, as well as the distinct breaks in slope of the plotted values and probabilities. The 22 control point flux measurements averaged 2 g m^{-2} day^{-1} with a standard deviation of 0.2 g m^{-2} day^{-1}. The control point measurements did show a normal distribution with one anomalously higher measurement (Fig. 7). No seasonal effects were observed within the control data, most likely because vegetation is sparse near this control point and temperature corrections are made by the LI-COR®. A contour map was constructed for the soil CO_2 flux data using Golden Software's Surfer 7 program (Fig. 8). Many one-point soil CO_2 flux highs are observed within the study area.

5.2 Soil Gas Stable Isotope Analysis

The $\delta^{13}C$ of the soil CO_2 ranged from -22.1 $^{o}/_{oo}$ to -9.2 $^{o}/_{oo}$ relative to PDB (Table 2). The $\delta^{18}O$ values ranged from 24.4 $^{o}/_{oo}$ to 44.0 $^{o}/_{oo}$ relative to SMOW (Table 1). Carbon and oxygen isotope values positively correlated (Fig. 9), giving the following equation:

$$\delta^{18}O = 1.6\,\delta^{13}C - 60.0 \qquad \text{(Equation 5)}$$

When the $\delta^{13}C$ values are plotted with the flux measurements taken at the time of soil gas sampling, two distinct linear trends are observed (Fig. 10). The two trends shown give the following equations:

$$\text{Flux} = -0.2872\ \delta^{13}C - 2.3784 \qquad \text{(Equation 6)}$$

$$\text{Flux} = -1.0981\ \delta^{13}C - 8.3618 \qquad \text{(Equation 7)}$$

Similar trends are observed when $\delta^{18}O$ values are plotted with flux measurements (Fig. 11).

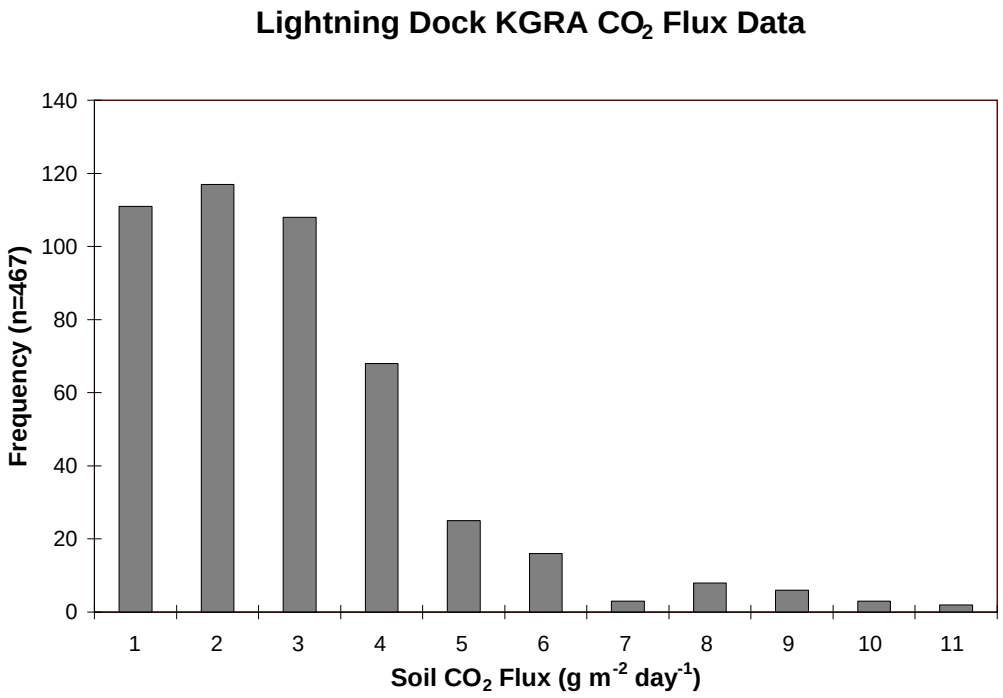

Figure 5. Distribution of all soil CO_2 flux measurements taken over the LDKGRA.

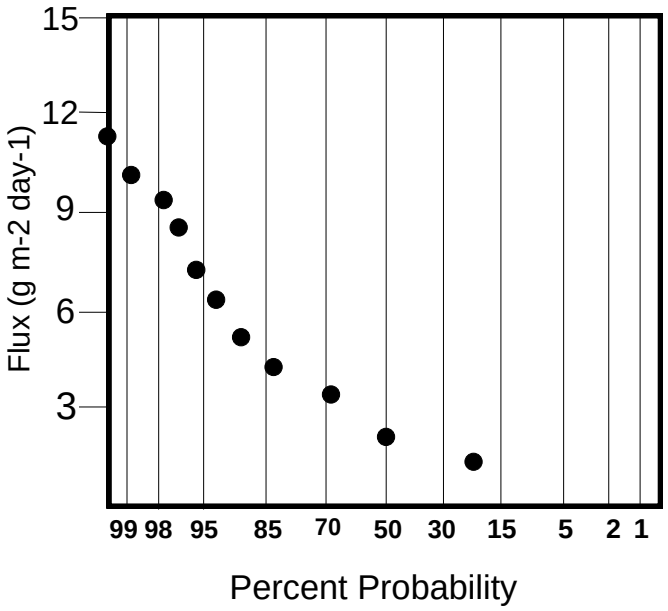

Figure 6. Plot showing the probability that a flux value will be less than a given value.

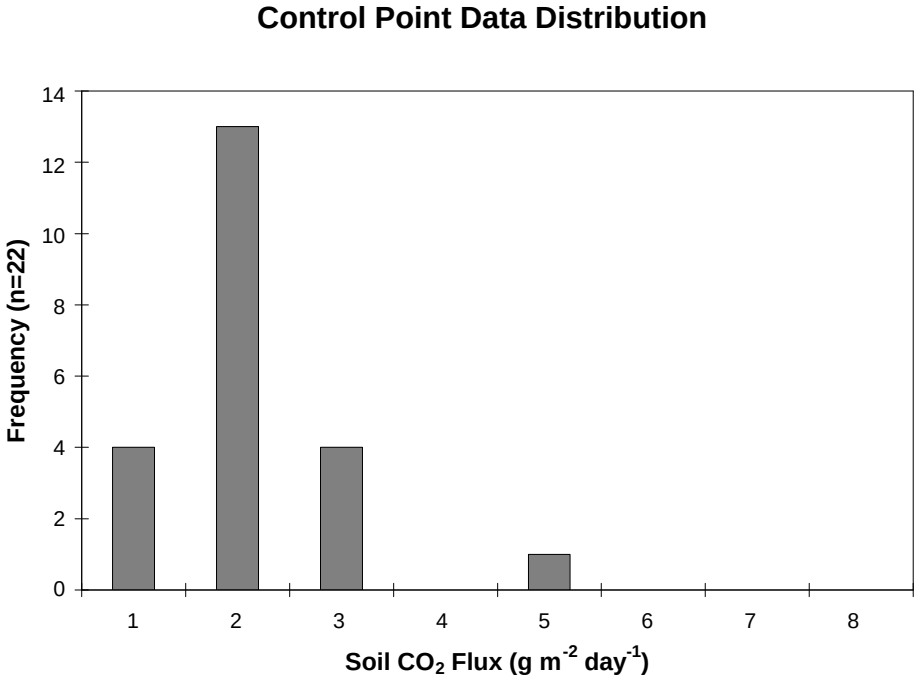

Figure 7. Graph illustrating the distribution of CO_2 flux values at the control point.

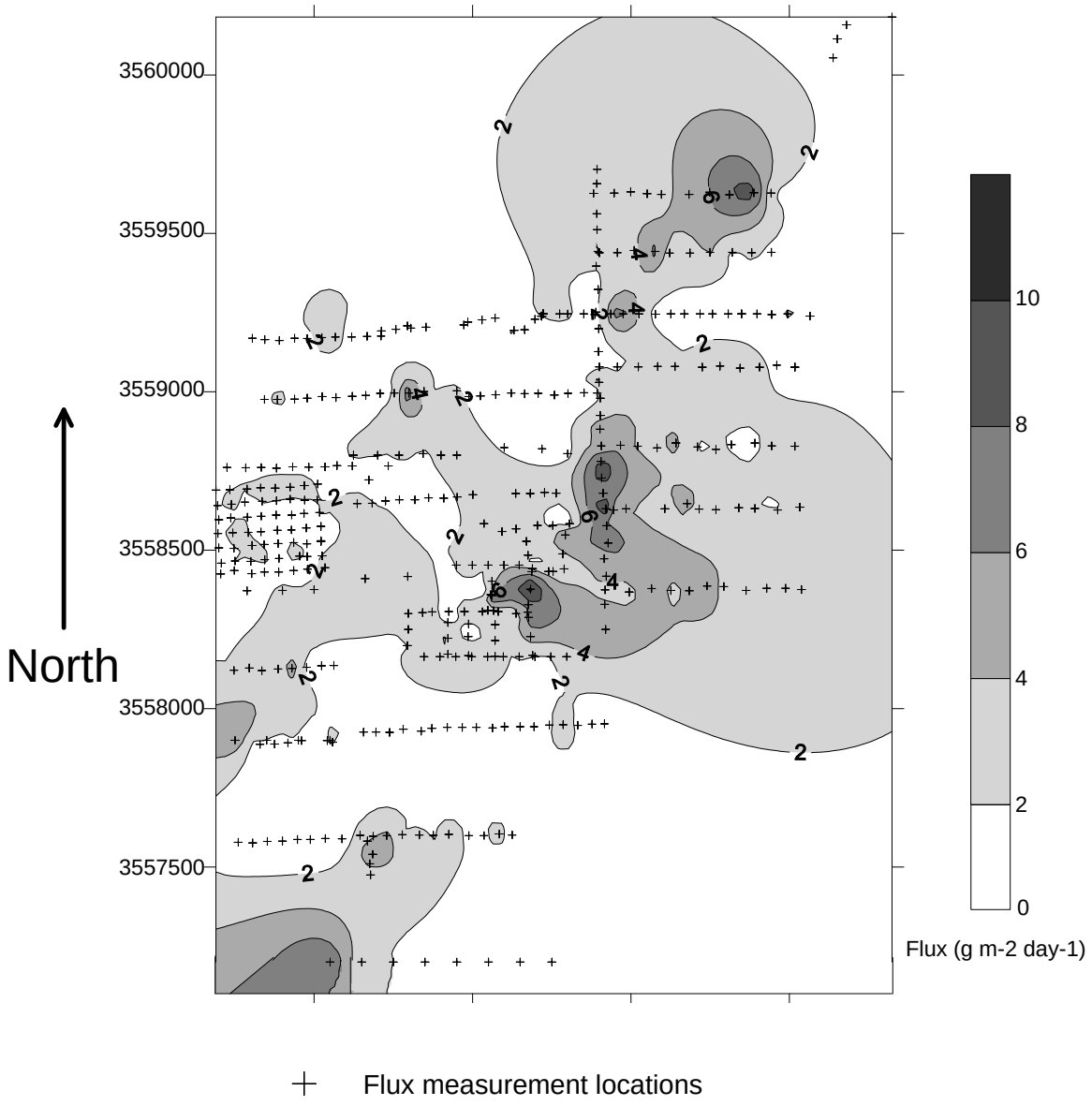

Figure 8. Map showing the soil CO_2 flux measurements and contours showing values of flux in the study area. Coordinates correspond to 12 N UTM locations using NAD 27 as datum.

Table 1. Table shows $\delta^{13}C$ and $\delta^{18}O$ values related to flux and nearby vegetation. Analytical error given in parenthesis is one σ.

Sample	$\delta^{13}C$ (PDB)	$\delta^{18}O$ (SMOW)	Flux ($g\ m^{-2}\ day^{-1}$)	Vegetation
SG1	-14.6(0.1)	40.7(0.1)	2	sparse ground cover
SG2	-16.2(0.1)	34.8(0.1)	2	sparse grass
SG3	-22.1(0.7)	24.4(1.5)	4	dense grass
SG4	-16.8(0.8)	33.6(1.8)	2	moderate grass
SG5	-19.5(0.5)	28.1(1.0)	0	none
SG6	-16.5(0.1), -16.3(0.1)	34.6(0.1), 34.8(0.1)	10	large bush
SG7	-14.0(1.0)	35.3(2.4)	2	sparse ground cover
SG8	-10.5(0.1), -10.5(0.1)	43.7(0.2), 43.7(0.1)	3	moderate shrubs
SG9	-13.9(0.2)	38.8(0.3)	7	dense creosote
SG10	-9.2(0.1)	44.0(0.3)	2	sparse creosote

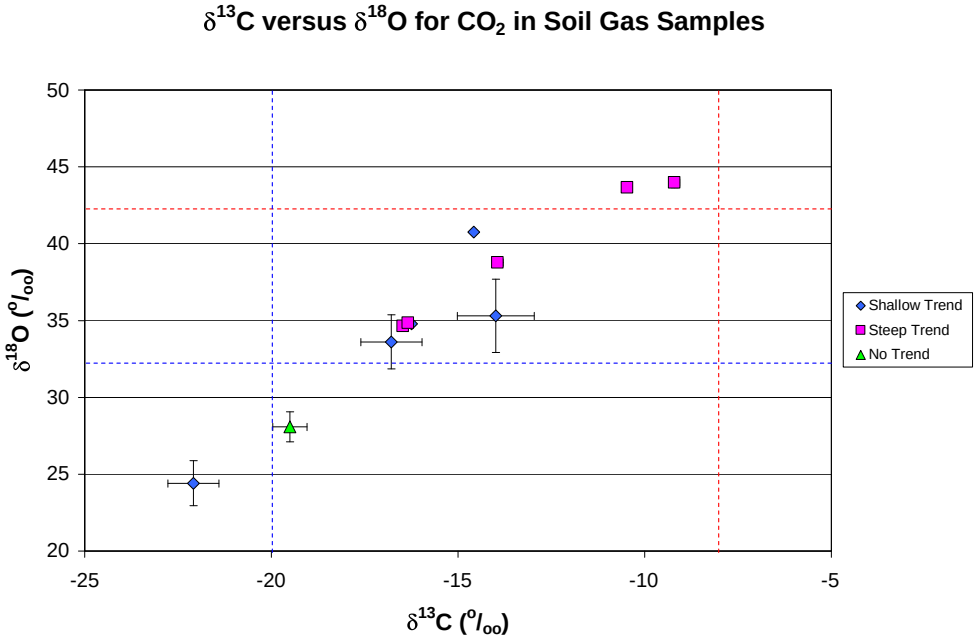

Figure 9. Graph of $\delta^{13}C$ versus $\delta^{18}O$ for CO_2 in soil gas samples taken over the LDKGRA and analyzed in March, 2004. The trends plotted with different symbols refer to the trends observed in Figure 10. The red vertical and horizontal lines represent atmospheric CO_2 isotopic composition (Amundson, 1998). The blue horizontal line represents the heavier end of the $\delta^{13}C$ values associated with C_3 photorespiration (Hoefs, 1997). The blue vertical line represents the $\delta^{18}O$ of soil CO_2 in equilibrium with soil water with a $\delta^{18}O$ of -10 $^{o}/_{oo}$ (Amundson, 1998).

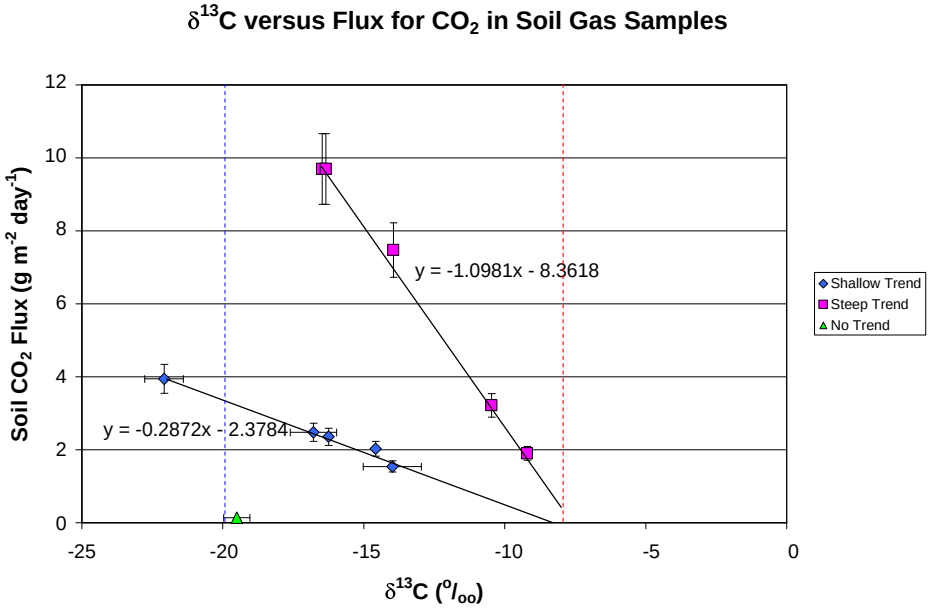

Figure 10. Graph of $\delta^{13}C$ in soil CO_2 versus soil CO_2 flux measured during sampling. Two data trends were fitted assuming that the atmospheric end member for $\delta^{13}C_{CO2}$ of -8 °/oo corresponded to a soil CO_2 flux value of 0 g m^{-2} day^{-1} and assuming that there were two vegetative $\delta^{13}C$ end members. One sample was excluded from these trends (labeled "No Trend"). The red line indicates the $\delta^{13}C$ of atmospheric CO_2 (Amundson, 1998), and the blue line represents the heavier end of the $\delta^{13}C$ values associated with C_3 photorespiration (Hoefs, 1997). Flux errors are based on the 10% standard deviation observed over the standard measurement location.

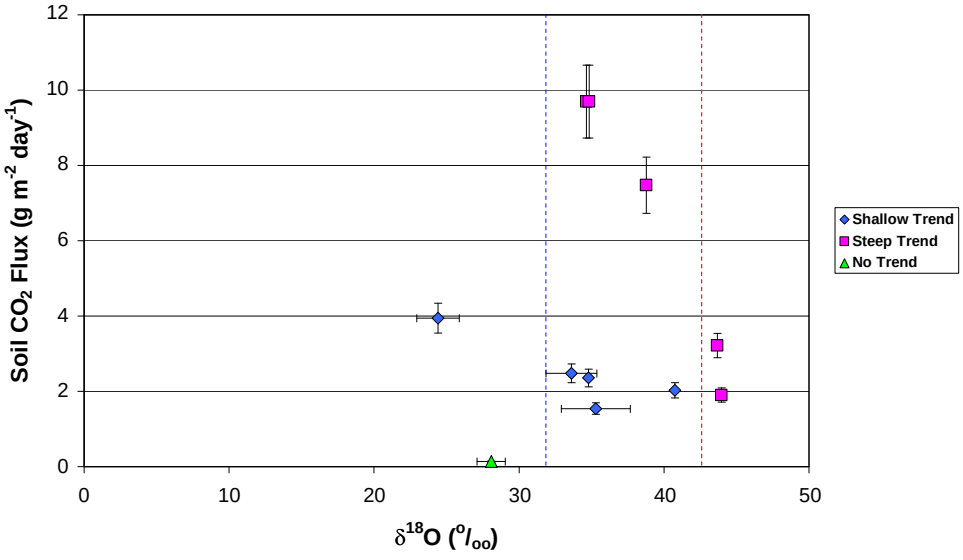

Figure 11. Graph of $\delta^{18}O$ in soil CO_2 versus soil CO_2 flux measured during sampling. The red line indicates the $\delta^{18}O$ of atmospheric CO_2, and the blue line represents the $\delta^{18}O$ associated with soil CO_2 in equilibrium with soil water with a $\delta^{18}O$ of -10 °/oo (Amundson, 1998).

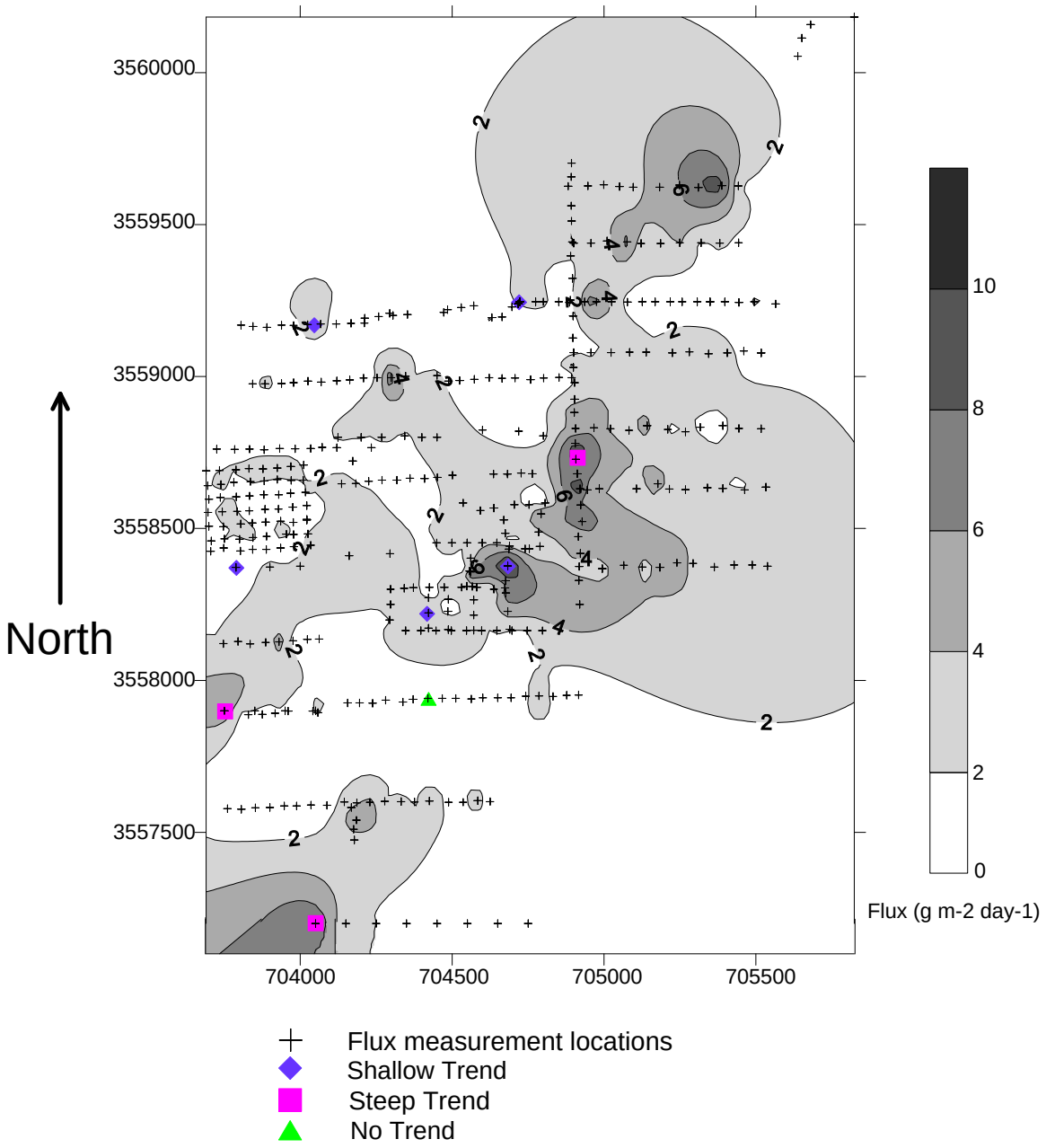

Figure 12. Contour map of soil CO_2 flux measurements and soil gas sample locations. The trends correspond to those observed in Figure 10. Soil gas sample 10 (Sg10) was taken away from the study area and is not shown.

5.3 Soil Gas Compositional Analysis

Concentrations of He, CH_4, C_2H_6, Ar, CO_2, and SO_2 in the soil gas samples were normalized to concentrations of N_2 in the soil gas. The concentrations were then

normalized to concentrations obtained from air samples taken between soil gas analyses. These ratios for soil gas samples are given (Table 2). CO_2 ratios from 50 cm depth roughly correlate with soil CO_2 flux values measured at the time of sampling ($R^2 = 0.45$) (Fig. 13). Other gases did not correlate with soil CO_2 flux. C_2H_6 ratios correlate well with CO_2 ratios when one outlier is excluded ($R^2 = 0.84$) (Fig. 14). CH_4 does not correlate as well, but does show some relationship to CO_2 ratios ($R^2 = 0.59$) (Fig. 15). Ar/N_2 concentrations did not vary substantially among soil gas analyses (Table 3). The N_2, Ar, and He ratios from the soil gas samples taken from the LDKGRA are compared to gas samples analyzed from geothermal and volcanic areas (Fig. 16). The gas ratios from the LDKGRA soil gases cluster around atmospheric ratios, with some deviation towards air saturated groundwater ratios.

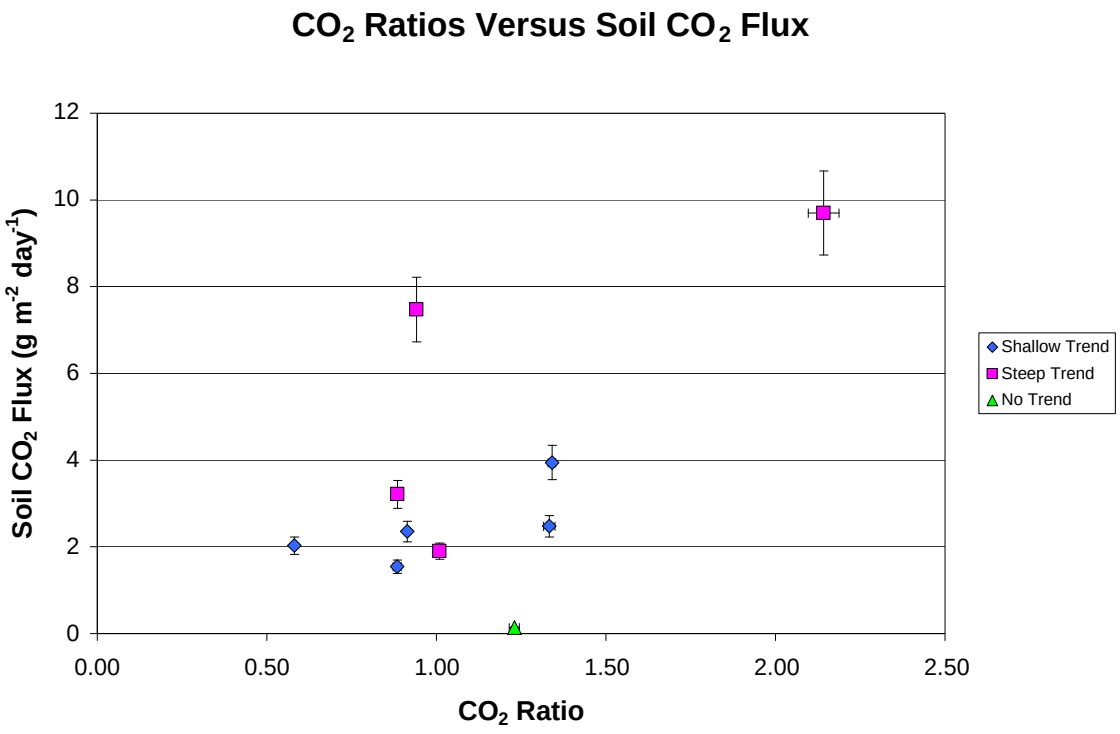

Figure 13. Graph shows correlation between CO_2 ratios and soil CO_2 flux.

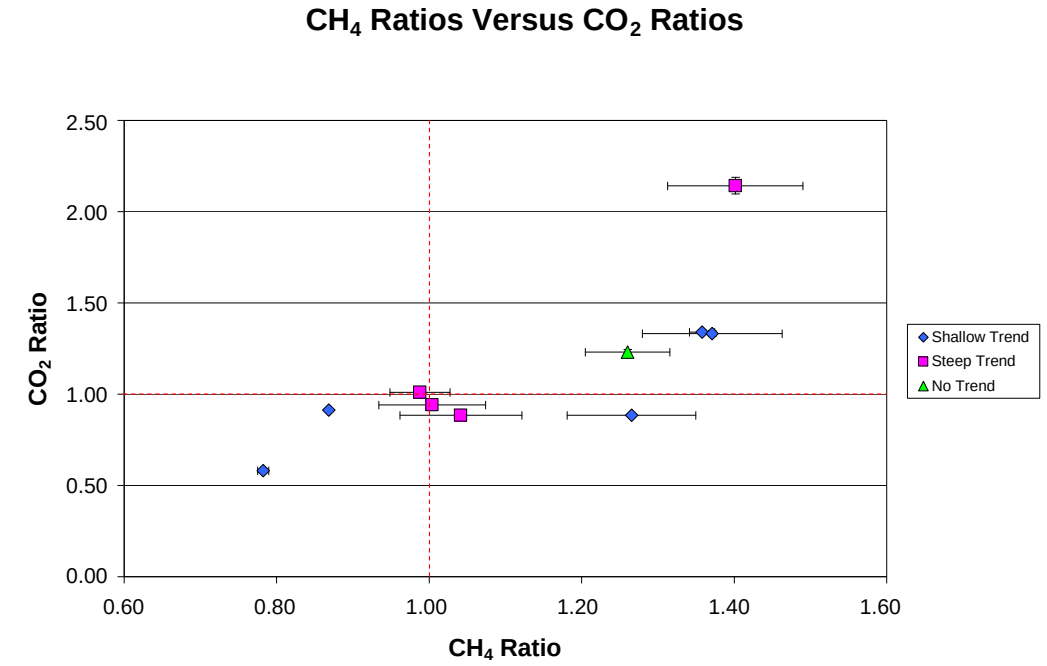

Figure 14. Graph shows correlation between ratios for CH_4 and CO_2 in soil gas samples. The red lines show ratios equal to air.

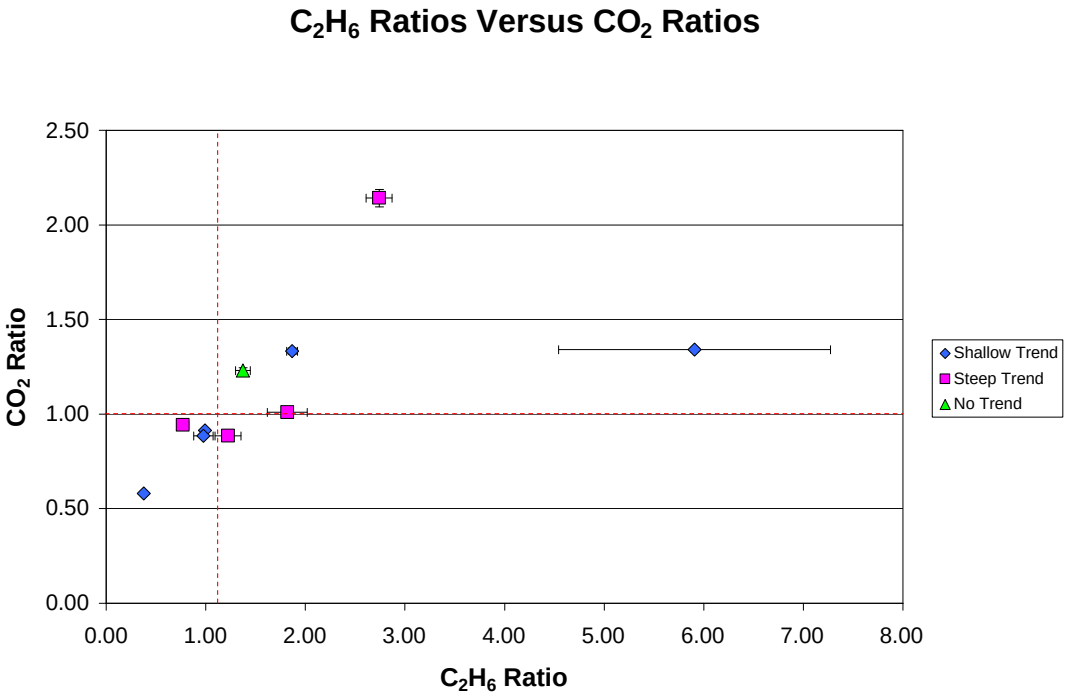

Figure 15. Graph shows correlation between ratios for C_2H_6 and CO_2 in soil gas samples. The red lines show ratios equal to air.

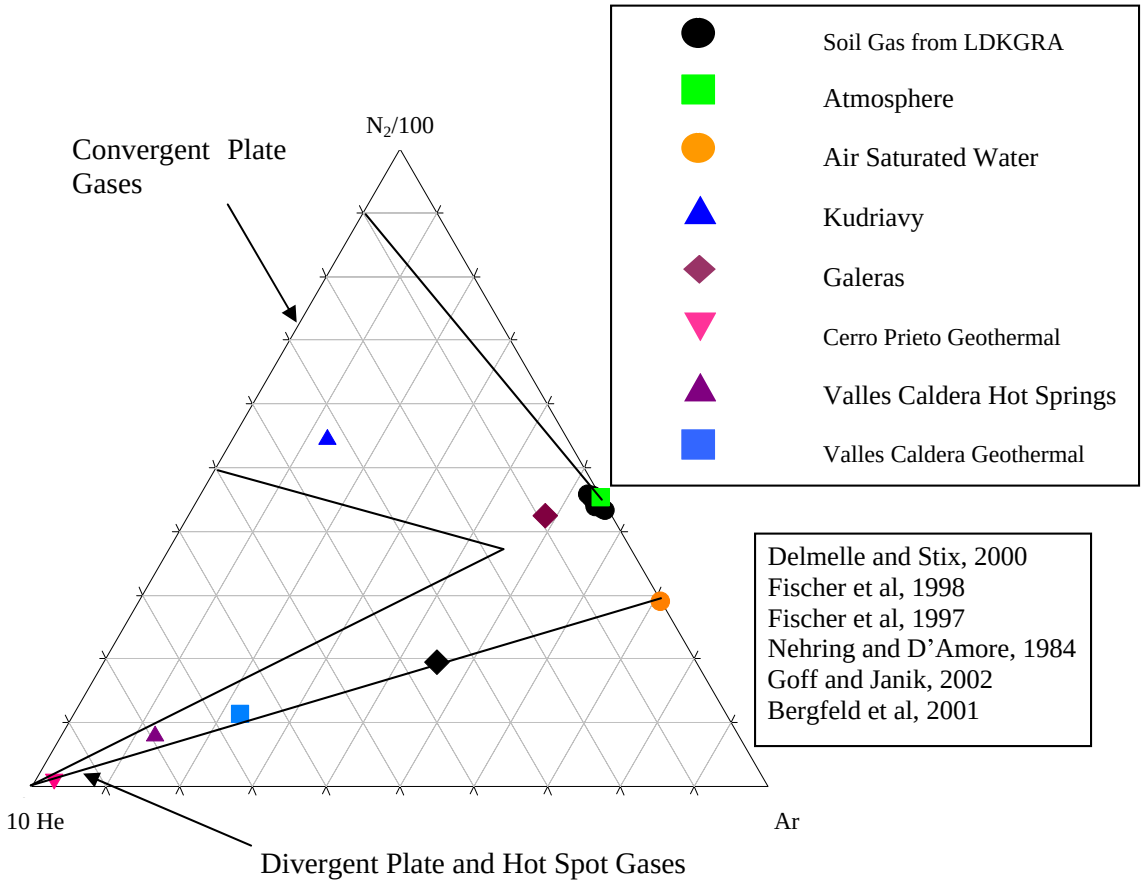

Figure 16. A diagram comparing the soil gas samples analyzed from the LDKGRA to geothermal and volcanic gases measured in other studies. Soil gas samples cluster around atmospheric values, some trending towards air saturated water.

Table 2. Table shows normalized values for compositional analyses for soil gas samples. All gases are normalized to N_2 and then to air samples taken from the lab. Numbers shown for soil gases are (soil gas/N_2)/(air sample/N_2). Values for atmosphere are given in ppmv unless specified (Manahan, 2000; CO_2 from Keeling and Whorf, 2002). Analytical errors are given in percents in parenthesis.

Soil Gas Sample	He	CH_4	C_2H_6	O_2	Ar	CO_2	SO_2	Flux (g m^{-2} day^{-1})
Sg1	1.11(12)	0.78(1)	0.38(2)	1.00(1)	0.99(2)	0.58(1)	0.70(6)	2
Sg2	0.86(11)	0.87(1)	0.99(1)	0.99(2)	1.00(2)	0.91(1)	0.94(7)	2
Sg3	0.92(13)	1.36(1)	5.91(23)	1.01(1)	1.00(1)	1.34(1)	1.51(9)	4
Sg4	1.36(7)	1.37(7)	1.87(3)	1.11(1)	1.04(1)	1.33(1)	1.95(7)	2
Sg5	1.24(6)	1.26(4)	1.37(5)	1.06(1)	1.03(1)	1.23(1)	1.40(5)	0
Sg6	1.15(4)	1.40(6)	2.74(5)	1.05(1)	1.07(2)	2.14(2)	1.56(4)	10
Sg7	1.12(8)	1.27(7)	0.98(10)	1.01(1)	1.08(1)	0.88(1)	1.25(4)	2
Sg8	1.03(7)	1.04(8)	1.22(11)	0.95(1)	0.96(1)	0.89(1)	1.00(3)	3
Sg9	1.01(4)	1.00(7)	0.77(8)	1.00(1)	1.00(1)	0.94(1)	0.84(3)	7
Sg10	0.92(3)	0.99(4)	1.82(11)	0.98(1)	0.98(1)	1.01(1)	0.74(3)	2
Atm.	5.24	1.75	0.0002	21.0%	0.93%	372	0.0002	NA

6. DISCUSSION

6.1 Soil CO_2 Flux

High soil CO_2 flux values in the northeastern portion of the study area crudely correlate with the location of the Animas Valley fault (Fig. 17). Values over 4 g m^{-2} day^{-1} are considered to be anomalously high flux values (McLin et al, 2004) since the vast majority of flux measurements (87%) fall below this cutoff. Compared to areas with magmatic or geothermal input of CO_2 into the soil, these values are low but comparable to vegetation related fluxes measured in Dixie Valley, Nevada (Table 3). Flux values

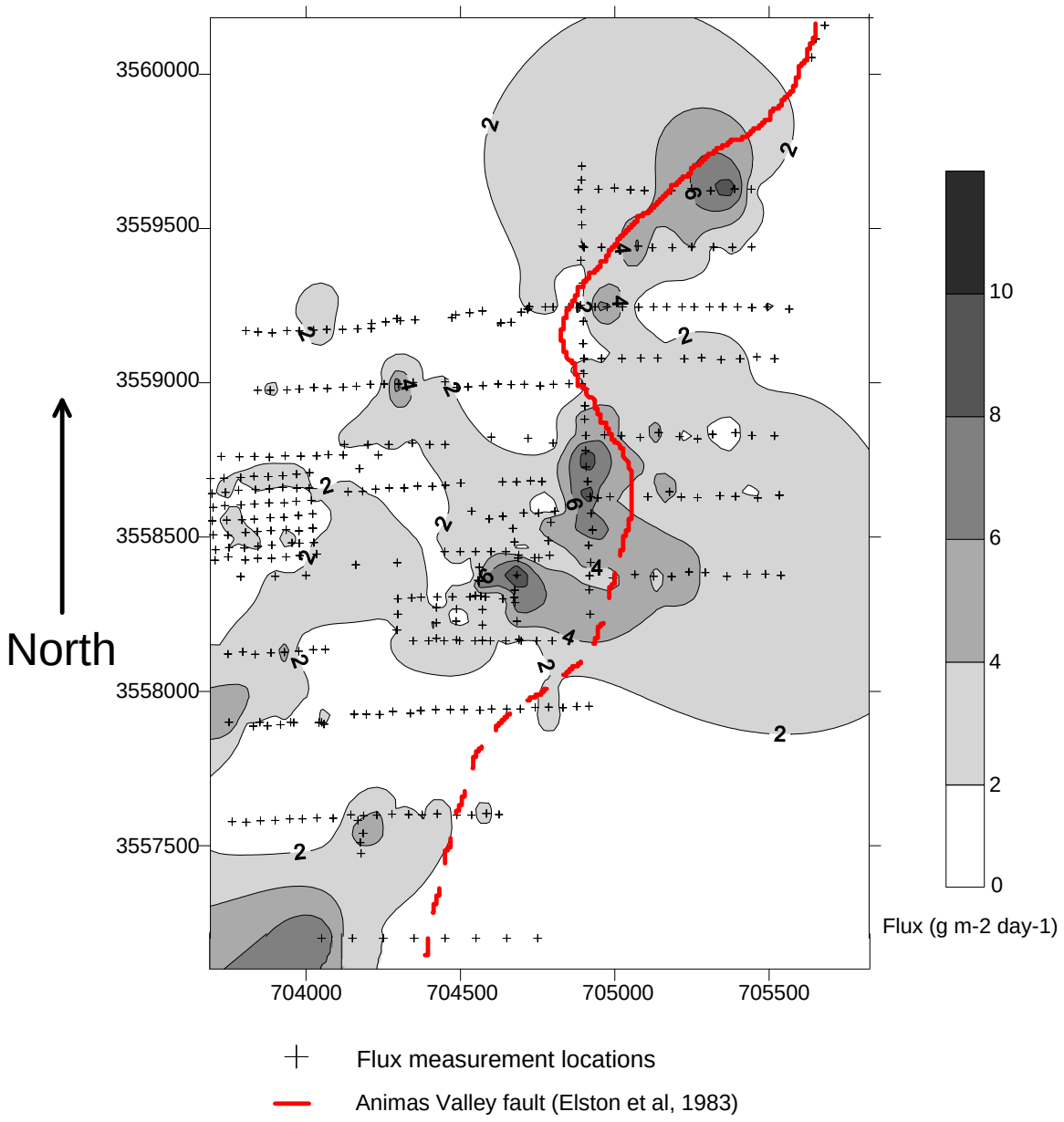

Figure 17. Flux contours and measurement locations relative to the Animas Valley fault (red).

measured over the Animas Valley fault range from 0 to 10 g m^{-2} day^{-1}. However, this correlation is inconsistent and patchy along the northern portion of the fault. High flux values do not correlate well with the inferred southern portion of the fault mapped by Elston and others (1983). High flux values are also measured away from the location of

the northern and southern portions of this fault. A NE-SW trend is also observed when examining the highest flux values in the study area (McLin et al, 2004). This trend may correlate with the inferred NE-SW fault thought to carry geothermal fluids from southwest of the LDKGRA (Elston et al, 1983). There is geophysical and geochemical evidence to support the existence of a fault or fracture zone in the area that trends in this direction. The NE-SW trend of high flux values, however, is also inconsistent and patchy.

Table 3. Table shows the soil CO_2 flux values measured over the LDKGRA compared to those measured in other areas.

Area of Study	CO_2% (volume)	Depth measured	CO_2 Flux (g m^{-2} day^{-1})
Mt. Etna, Italy[a]	0.25 to 27.9	80 cm	35 to 120 (10^9 g day^{-1})
Mammoth Mt., CA[b,c]	<1 to >90	30-60 cm	1 to >10,000
Roosevelt H.S., UT[d,e]	0.03 to 69.7	75 cm	0 to 8.04
Dixie Valley, NV[f]			0 to 570
Cove Fort, UT[g]	0.28 to 0.57	60 cm	0.7 to 3.5
Mutnovsky, Kamchatka[h]	0.1 to 0.26	100 cm	
Vulcano, Italy[i]	0.03 to 80	50 cm	
LDKGRA, NM (This study)	0.05 to 0.12	50 cm	0 to 12

a. Allard et al, 1991
b. Farrar et al, 1995
c. Gerlach et al, 2001
d. Hinkle, 1990
e. Klusman et al, 2000
f. Bergfeld et al, 2001
g. Klusman et al, 2000
h. Vakin and Lyanlin, 1990
i. Bertrami et al, 1990

6.2 Soil Gas Stable Isotopes

At first, vegetation type and quantity, soil texture, and Quaternary deposit type did not seem to correlate with the high flux values measured in the study area (McLin et al, 2004). When soil CO_2 flux contours are plotted over air photos of the study area, some anomalous flux values do not seem to correlate with an increase in vegetation (Fig. 18). However, the stable isotope data for the soil CO_2 indicate that these characteristics are the dominant controls on CO_2 flux in the area. When $\delta^{13}C$ and $\delta^{18}O$ for the ten soil gas samples are plotted, the values strongly correlate (Fig. 9). This correlation indicates that there is a mixing of CO_2 between two, possibly more, source end members giving the linear trend for isotope values. The two samples that have the heaviest carbon ($\delta^{13}C$ = -9.2 and -10.5 $^{o}/_{oo}$) isotope ratios correspond to similar values of carbon (-8 $^{o}/_{oo}$) in atmospheric CO_2 (Amundson, 1998). The sample with the lightest carbon (-22.1 $^{o}/_{oo}$) possibly corresponds to a vegetative end member for carbon in the soil CO_2. Respired CO_2 from C_3 vegetation has a $\delta^{13}C$ significantly lighter that that of atmosphere and can range between -30 and -20 $^{o}/_{oo}$ (Hoefs, 1997). Varying degrees of mixing CO_2 from two distinct sources, respired CO_2 from plants and atmospheric CO_2, explains the strong linear trends observed from the carbon stable isotopes.

When the soil CO_2 flux values measured at the time of sample collection are compared to the $\delta^{13}C$ of a sample, two trends are apparent (Fig. 10). The two trends converge near a flux value of 0 g m^{-2} day^{-1} and a $\delta^{13}C$ value of -8 $^{o}/_{oo}$ (Amundson, 1998). The two trends diverge towards two possible $\delta^{13}C$ end members at higher flux values. When vegetation type is compared to the samples that lie on each trend, a relationship between vegetation type and the isotopic composition emerges. The sample and

measurement locations with creosote nearby have $\delta^{13}C$ and soil CO_2 flux values that follow along the steeper sloping trend (Eqn. 7). The locations with non-native grasses in the disturbed areas follow the shallower trend (Eqn. 6). Although both the creosote and

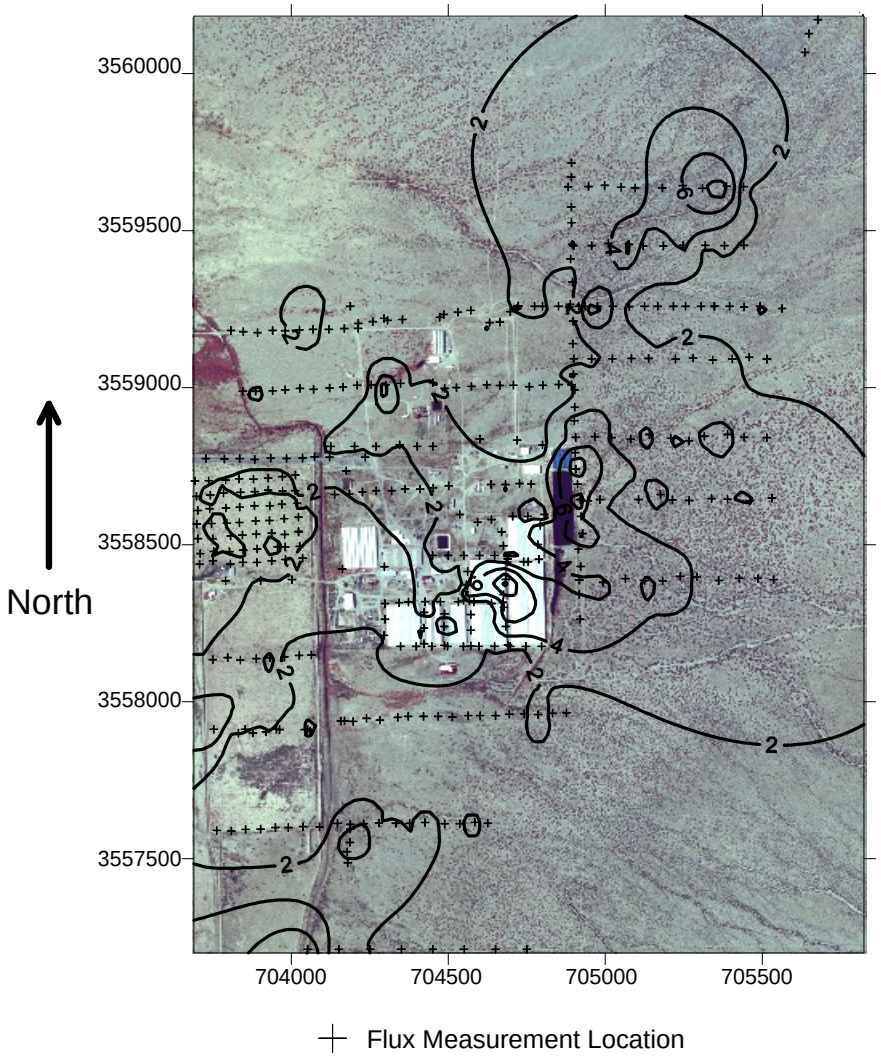

Figure 18. Soil CO_2 flux contours over aerial photograph of the LDKGRA. Greenhouses, roads, farmland, and undisturbed areas are shown. Contour interval is 2 g m^{-2} day^{-1}.

the grass use the C_3 photosynthetic pathway, they would have to have different $\delta^{13}C$ values for the pure vegetative end members to explain the trends observed. Plants with better water-use efficiency fix more ^{13}C during photosynthesis and therefore expel more

$^{13}CO_2$ through their roots during photorespiration. Creosote would have better water-use efficiency than the non-native grass to explain the trends observed in the isotope data, meaning the $\delta^{13}C$ value respired by creosote would be heavier than that respired by the grass. Two $\delta^{13}C$ end members corresponding to different isotopic compositions of CO_2 related to photorespirations should be considered to explain the two trends.

If the degree of mixing between atmospheric CO_2 and plant respired CO_2 is related to soil CO_2 flux, and there are two end member values for $\delta^{13}C$ related to plant respired CO_2, then the two trends on the plot of flux and $\delta^{13}C$ should diverge (Fig. 19). C_3 plants can have varying $\delta^{13}C$ values for the CO_2 they respire based on their water-use efficiency (Schlesinger, 1997). Because creosote is native to this region, it has probably developed better water-use efficiency than the non-native grasses that grow near the greenhouses. The stable isotope data confirm that creosote has a heavier $\delta^{13}C$ associated with the CO_2 it respires than that respired by the grass. However, the difference in slopes between the two vegetation types cannot be explained by a difference in $\delta^{13}C$ respired by the two alone. To fully explain the divergence in slopes for the two trends, less atmospheric CO_2 must be penetrating the soil with the grass than the soil with the creosote.

A soil must be properly aerated for vegetation to grow (Hillel, 1998). This process allows the cycling of O_2 into the soil and CO_2 out of the soil. In compacted soils, the volume of air is significantly lower than the volume of air in a soil that has not been compacted (Hillel, 1998). The creosote in the area is found in soils that have formed on coarser, poorly sorted alluvial fan deposits with sandy soils and on sand dunes formed

further into the valley. The non-native grass grows on the disturbed portions of the study area where human activity has compacted the soil. The soils in these areas also have

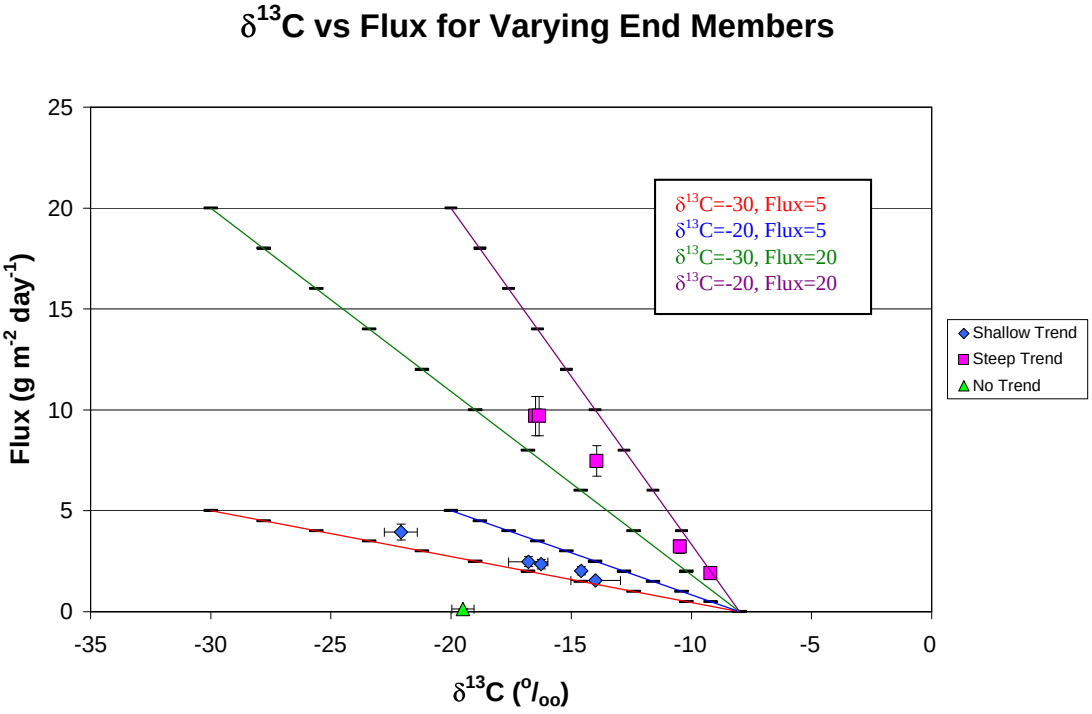

Figure 19. Graph illustrating the trends between $\delta^{13}C$ and Flux for varying $\delta^{13}C$ end members and varying flux values reached for pure plant respired CO_2 in a soil. A $\delta^{13}C$ of -8 $^{o}/_{oo}$ and a flux of O g m $^{-2}$ day^{-1} correspond to a purely atmospheric CO_2 end member in the soil gas. As more plant respired CO_2 mixes with the atmosphere, the trend heads toward a pure plant respired end member. These trends are plotted for $\delta^{13}C$=-30 and -20 $^{o}/_{oo}$ and Flux=5 and 20 g m^{-2} day^{-1} as the end members for 100% plant respired CO_2 in the soil gas. Tic marks on trend lines indicate 10% increments of mixing between atmospheric and vegetation end members of CO_2.

more silt and clay. These differences in soil characteristics can account for the shallower slope of the trend that represents the gas samples collected in the grassy areas and the steeper slope of the trend that represents the gas samples collected near the creosote. Compaction and finer texture of the soil causes these $\delta^{13}C$ versus flux trends to be shallower by decreasing the end member flux value achieved when soil CO_2 is 100% vegetative.

The linear trend of oxygen stable isotope values can also be explained. The heavier values of oxygen isotope ratios (44.0 and 43.7 $^{o}/_{oo}$) are very close to the oxygen isotope values in atmospheric CO_2 of 42 $^{o}/_{oo}$ (Amundson et al, 1998). The lighter values for $\delta^{18}O$ may be related to a variety of processes controlling the exchange of oxygen between soil CO_2 with soil water. Oxygen from atmospheric CO_2 exchanges with soil water, giving a significantly lower $\delta^{18}O$ in soil CO_2 than in atmospheric CO_2 (Stern et al, 1999). The various factors affecting this exchange determine the $\delta^{18}O$ of soil CO_2 at a given depth. The most important factor is the ^{18}O composition of the soil water. Atmospheric CO_2 in equilibrium with soil water with a $\delta^{18}O$ of -10 $^{o}/_{oo}$ will achieve a value of about 32 $^{o}/_{oo}$ (Stern et al, 1999). However, if the CO_2 is not in complete equilibrium with soil water, the $\delta^{18}O$ value of soil CO_2 will fall somewhere between 42 and 32 $^{o}/_{oo}$ for this soil water $\delta^{18}O$ value. Different concentrations of ^{18}O in soil water will change the limits on $\delta^{18}O$ values in soil CO_2. Heavier water values will give heavier values for $\delta^{18}O$ of CO_2 in equilibrium with the water. To achieve $\delta^{18}O$ values in CO_2 of 24.4 and 28.1 $^{o}/_{oo}$ (the lightest values measured in this study) using only this factor, the soil water at 50 cm depth would have to be in equilibrium with waters that have $\delta^{18}O$ of -17.6 and -13.9 $^{o}/_{oo}$ respectively.

All other variation of $\delta^{18}O$ values in the study area could be explained by variations in soil water composition, but these variations can also be explained even if the soil water at 50 cm depth is homogeneous for all sample locations. Assuming the soil water for the sample locations has a similar $\delta^{18}O$ to the -10 $^{o}/_{oo}$ value of groundwater measured in the area, the range of $\delta^{18}O$ values for soil CO_2 can be explained by changing rates of isotope exchange and changing amounts of air-filled pore space. Faster rates of

exchange correspond to lighter $\delta^{18}O$ values at 50 cm depth, and slower rates of exchange result in heavier $\delta^{18}O$ values (Stern et al, 1999). A CO_2 $\delta^{18}O$ value of 33.6 $^{o}/_{oo}$ would indicate that the soil CO_2 has an isotope exchange rate with soil water on the order of 10^{-3} s^{-1}, and a $\delta^{18}O$ value of 38.8 $^{o}/_{oo}$ would indicate a rate on the order of 10^{-6} s^{-1}(Stern et al, 1999). A variety of factors can affect this rate. When temperatures are lower, the isotope exchange rate of oxygen between CO_2 and water is reduced (Stern et al, 1999). When the air-filled pore space in a soil is reduced, the oxygen isotope exchange rate between CO_2 and water increases, giving lighter $\delta^{18}O$ values for soil CO_2 (Stern et al, 1999). The reduced pore space allows the CO_2 to equilibrate with water more quickly because less atmospheric CO_2 enters the soil.

Lighter $\delta^{13}C$ values that lie on the shallow $\delta^{13}C$ versus flux trend are related to compacted soil in the area with the greenhouses. Likewise, lighter $\delta^{18}O$ values can be related to compacted soils, assuming the soil water has a homogeneous $\delta^{18}O$ composition within the field area at 50 cm depth. Thus, variations in soil air-filled pore space can explain the correlation between $\delta^{13}C$ and $\delta^{18}O$ and the similar trends observed when isotope composition is compared to soil CO_2 flux values.

6.3 Soil Gas Composition

Ratios for organic molecules such as CH_4 and C_2H_6 correlate with CO_2 ratios in soil gas samples. If the aeration requirement for a soil is not fulfilled, anaerobic conditions could temporarily develop (Hillel, 1998). This could lead to the formation of gases such as CH_4 and C_2H_6. These organic compounds could also be produced through decomposition of organic matter. However, it seems unlikely that such a severe oxygen deficiency would occur in these soils, considering that O_2 values analyzed for soil gas

samples did not show a significant decrease with increasing CH_4 or C_2H_6. Although a soil may appear to be well aerated, zones of poor aeration may occur within this soil (Hillel, 1998). On a smaller scale, organisms in the pore space of soil can consume oxygen, leaving the pore space anaerobic (Conklin, 2002). Even when a soil is properly aerated, methane can be produced in these pore spaces. When plant roots consume a greater amount of oxygen in a soil, they also produce more CO_2 (Hillel, 1998). This increased consumption of O_2 can lead to an increase in anaerobic pore space, allowing for greater CH_4 and C_2H_6 production within the soil.

6.4 Anomalous Soil CO_2 Flux Measurements

Anomalous soil CO_2 fluxes in the study area are greater than 4 g m^{-2} day^{-1} (McLin et al, 2004). Soil gas samples were taken corresponding to many levels of soil CO_2 flux from 0 to 10 g m^{-2} day^{-1}. At all levels of flux values, the influence of vegetation and atmosphere on the soil CO_2 flux could be observed. No geothermal influence could be detected through stable isotope or compositional analysis of the soil gas samples collected at 50 cm depth over the LDKGRA. Most anomalously high soil CO_2 flux measurements do not correspond to a known structural feature. The high flux values may, however, correspond to a NE-SW trending structure observed by other methods (Elston et al, 1983). Because vegetation and soil texture control the flux rates, as shown by stable carbon isotope data, these properties should be related to structural controls in order to use soil CO_2 flux as the sole method of locating structural features in this study area. Faults or fracture zones may create zones of preferential flow for water, providing an ideal location for desert vegetation to grow. The vegetation along a fault may increase or become more productive. However, aerial photographs and field inspection do not

show increased vegetation along the Animas Valley fault. Another explanation is that a fault may considerably increase the aeration capabilities in the soil forming on this structure. Further study is required to understand the relationship of structures to anomalous soil CO_2 flux measurements.

7. CONCLUSIONS

High values of soil CO_2 flux over the LDKGRA crudely correlate with a known fault in the area. It is unknown if the NE-SW trend observed in the flux data corresponds to faults or fractures in the subsurface. The working hypothesis of CO_2 leakage from faults acting as geothermal conduits was not supported by the stable isotope data, which showed that the CO_2 in the soil was contributed by photorespiration and atmospheric gases, not a geothermal source. Flux values did not increase with heavier $\delta^{13}C$ values, which was expected for a geothermal influence on soil CO_2. Compositional analyses also do not support the working hypothesis; instead, the analyses strengthen the evidence of mixing of the vegetative and atmospheric end members of CO_2 in the soil.

Stable isotope and compositional analyses show no evidence for a geothermal input of CO_2 into the soils over the LDKGRA, and thus do not support the working hypothesis. Vegetation and soil texture exert a strong influence on the stable isotope composition of the soil CO_2, as well as on the soil CO_2 flux rates in the study area. Creosote should respire CO_2 with a heavier $\delta^{13}C$ than the non-native grasses in the area due to increased water-use efficiency, explaining two different $\delta^{13}C$ end members for C_3 plants. The compacted soils in the disturbed areas also restrict aeration, while the sandy soils in the gravely alluvial fan deposits allow atmosphere to circulate into the soil to a

greater extent. Fault detection using soil CO_2 fluxes was not based on an input of geothermal CO_2, but could be related to soil properties and preferential flow of water.

Using soil CO_2 flux measurements alone, faults cannot definitively be detected in this study area. Even when correlations are found between high fluxes and known structures, the relationship of these structures to the geothermal reservoir below cannot be determined by using this technique over the LDKGRA. In areas where geothermal fluids have higher dissolved gas concentrations, it may be possible to use this technique to detect structures that act as conduits for geothermal fluids. Geothermal CO_2 was not detected over the LDKGRA in this study.

The stable isotope trends seen in the soil gas samples collected over the LDKGRA should be examined further in future studies. Soil gas samples should be taken at 10 cm depth increments within a soil to examine the changes in stable isotope values with depth. Soil water samples should be taken at 10 cm depth intervals to correspond to the soil CO_2 samples. Soils should be thoroughly described and soil properties such as bulk density should be measured to examine the influence of these properties on soil CO_2 flux and soil CO_2 stable isotope composition. These measurements should refine our understanding of the processes that influence the flux and composition of soil CO_2, as well as understand the various end members that contribute to soil CO_2. The influence of structures on vegetation and soil CO_2 flux in this area should be examined as well.

8. REFERENCES

Allard, P., Carbonnelle, J., Dajlevic, D., Le Bronec, J., Morel, P., Robe, M.C., Maurenas, J.M., Faivre-Pierret, R., Martin, D., Sabroux, J.C., Zettwoog, P. (1991), "Eruptive and diffusive emissions of CO_2 from Mount Etna," *Nature*, 351, 387-391.

Amundson, R., Stern, L., Baisden, T., and Wang, Y. (1998) "The isotopic composition of soil and soil respired CO_2," *Geoderma*, 82, 83-114.

Baubron, J.C., Allard, P., Toutain, J.P. (1990), "Diffuse volcanic emissions from Vulcano Island, Italy," *Nature*, 344, 51-53.

Bergfeld, D., Goff, F., Janik, C.J. (2001) "Elevated carbon dioxide flux at the Dixie Valley geothermal field, Nevada; relations between surface phenomena and the geothermal reservoir," *Chemical Geology*, 177, 43-66.

Berry, J.A., Collatz, G. J., Guy, R. D., Fogel, M. D. (1994), "The Compensation Point: Can a Physiological Concept Be Applied to Global Cycles of Carbon and Oxygen?" Regulation of Atmospheric CO_2 and O_2 by Photosynthetic Carbon Metabolism. New York, Oxford University Press, 234-248.

Bertrami, R., Ceccarelli, A., Pandeli, E., Pieri, S. (1990), "Soil gases in geothermal exploration: comparison of results from geothermal and non-geothermal zones," Geochemistry of gaseous elements and compounds. Athens, Greece, Theophrastus Publ., 243-268.

Caracausi, A., Favara, R., Giammanco, S., Italiano, F., Paonita, A., Pecoraino, G., Rizzo, A. (2003), "Mount Etna; geochemical signals of magma ascent and unusually extensive plumbing system," *Geophysical Research Letters*, 30, 1057.

Cerling, T. E., Quade, J., Wang, Y., Bowman, J. R. (1989), "Carbon isotopes in soils and paleosols as ecology and palaeoecology indicators," *Nature*, 341, 138-139.

Cerling, T. E., Solomon, D. K., Quade, J., Bowman, J. R. (1991), "On the isotopic composition of carbon in soil carbon dioxide," *Geochimica et Cosmochimica Acta*, 55, 3404-3405.

Conklin Jr., A.R. (2002), "Soil Microorganisms," *Soil Sediment & Water*, http://www.aehsmag.com/issues/2002/january/microorganisms.

Delmelle, P., Stix, J. (2000), "Volcanic Gases." Encyclopedia of Volcanoes. Sigurdsson, H., ed. San Diego, Academic Press, 803-815.

Ehleringer, J. R. (1991), "$^{13}C/^{12}C$ Fractionation and its Utility in Terrestrial Plant Studies," Carbon Isotope Techniques. Coleman, D. C., Fry, B., ed. San Diego, Academic Press, 187-200,

Elston, W.E., Deal, E.G., Logsdon, M.J. (1983), "Geology and geothermal waters of Lightning Dock region, Animas Valley, and Pyramid Mountains, Hidalgo County, New Mexico." New Mexico Bureau of Geology Circular 177, 1-44.

Farrar, C. D., Sorey, M.L., Evans, W.C., Howle, J.F., Kerr, B.D., Kennedy, B.M, King, C.Y., Southon, J.R. (1995), "Forest-killing diffuse CO_2 emission at Mammoth Mountain as a sign of magmatic unrest," *Nature*, 376, 675-678.

Finlayson, J.B. (1992), "A soil gas survey over Rotorua Geothermal Field, Rotoura, New Zealand," Geothermics, 21, 181-195.

Fischer, T. P., Sturchio, N. C., Stix, J., Arehart, G. B., Counce, D., Williams, S. N. (1997), "The chemical and isotopic composition of fumerolic gases and spring discharges from Galeras Volcano, Columbia," *Journal of Volcanology and Geothermal Research*, 77, 229-253.

Fischer, T. P., Giggenbach, W. F., Sano, Y., Williams, S. N. (1998), "Fluxes and sources of volatiles discharged from Kudriavy, a subduction zone volcano, Kurile Islands," Earth and Planetary Science Letters, 160, 81-96.

Fleischhauer, Jr., H.L. and Stone, W.J. (1982), "Quaternary geology of Lake Animas, Hidalgo County, New Mexico," New Mexico Bureau of Geology Circular 174, 1-25

Gerlach, T.M., Doukas, M.P., McGee, K.A., Kessler, R. (2001), "Soil efflux and total emission rates of magmatic CO_2 at the Horseshoe Lake tree kill, Mammoth Mountain, California 1995-1999," *Chemical Geology*, 177, 101-116.

Giammanco, S., Gurreieri, S., Valenza, M. (1999), "Geochemical investigations applied to active fault detection in a volcanic area: the North-East Rift on Mt. Etna (Sicily, Italy)," *Geophysical Research Letters*, 26, 2005-2008.

Goff, F., Janik, C. J. (2002) "Gas geochemistry of the Valles caldera region, New Mexico and comparisons with gases at Yellowstone, Long Valley and other geothermal systems," Journal of Volcanology and Geothermal Research, 116, 299-323.

Hillel, D. (1998), Environmental Soil Physics. San Diego, Academic Press, 1-771.

Hinkle, M.E. (1991), "Seasonal and geothermal production variations in concentrations of He and CO_2 in soil gases, Roosevelt Hot Springs Known Geothermal Resource Area, Utah, U.S.A.," *Applied Geochemistry*, 6, 35-47.

Hoefs, J. (1997), Stable Isotope Geochemistry. Germany, Springer-Verlag Berlin Heidelberg, 1-201.

Jiracek, G. R., Smith, C. (1976), "Deep resistivity investigations at two known geothermal resource areas (KGRAS) in New Mexico; Radium Springs and Lightning Dock," New Mexico Geological Society Special Publication, 6, 71-76.

Karp, G. (1996), Cell and Molecular Biology. New York, John Wiley & Sons, Inc., 1-773.

Keeling C. D., Whorf, T. P. (2002), Atmospheric CO_2 records from sites in the SIO air sampling network. In Trends: A Compendium of Data on Global Change. Carbon Dioxide Information Analysis Center, Oak Ridge National Laboratory, U.S. Department of Energy, Oak Ridge, Tenn., U.S.A., http://cdiac.ornl.gov/trends/co2/sio-mlo.htm.

Kerrick, D. M. (2001), "Present and Past Nonanthropogenic CO_2 Degassing from the Solid Earth," *Reviews of Geophysics*, 39, 565-585.

Kintzinger, P.R. (1956), "Geothermal survey of hot ground water near Lordsburg, New Mexico," *Science*, 124, 629-630.

Klusman, R.W., Moore, J.N., LeRoy, M.P. (2000), "Potential for surface gas measurements in exploration and evaluation of geothermal resources," *Geothermics*, 29, 637-670.

Lance, J. O. Jr., Keller, G. R., Aiken, C. L. V. (1982), "A regional geophysical study of the western overthrust belt in southwestern New Mexico, West Texas, and Northern Chihuahua," Rocky Mountain Association of Geologists Field Conference Guidebook, 123-130.

Lynch, D. J. (1978) "The San Bernardino Volcanic Field of Southern Arizona," New Mexico Geological Society Guidebook, 29, 261-268.

Manahan, S. E. (2000), Environmental Chemistry. Boca Raton, Lewis Publishers, 1-898.

McIntosh, W. C., Bryan, C. (2000), Chronology and Geochemistry of the Boot Heel Volcanic Field, New Mexico," New Mexico Geological Society Guidebook, 51, 157-174.

McLin, K., Norman, D., Kyle, P. (2004), "Mapping Faults in the Lightning Dock Known Geothermal Area, Animas Valley, New Mexico Using Soil CO_2 Flux Measurements," *Proceedings of the 29th Stanford Geothermal Workshop*, in press.

Nehring, N. L., D'Amore, F. (1984), Gas chemistry and thermometry of the Cerro Prieto, Mexico," Geothermics, 13, 75-89.

Norman, D. I., Bernhardt, C. A. (1982), "Assessment of geothermal reservoirs by analysis of gases in thermal waters," N.M. Energy Research and Development Inst., Santa Fe, NM, United States.

Norman, D. I., Blamey, N., Kurilovitch, L. (2002), "New Applications of Geothermal Gas Analysis to Exploration," *Geothermal Resources Council Transactions*, 26, 335-341.

O'Brien, K. M., Stone, W. J. (1984), "Role of Geological and Geophysical Data in Modeling a Southwestern Alluvial Basin," *Ground Water*, 22, 717-727.

O'Keeffe, M. K. (1994), "Soil CO_2 Gas Concentrations and Emissions at Kilauea Volcano, Hawaii," Thesis, Department of Earth and Environmental Sciences, New Mexico Institute of Mining and Technology, Socorro, 1-87.

Rogie, J. D., Kerrick, D. M., Sorey, M. L., Chiodini, G., Galloway, D. L. (2001), "Dynamics of carbon dioxide emission at Mammoth Mountain, California," *Earth and Planetary Science Letters*, 188, 535-541.

Schlesinger, W.H. (1997), Biogeochemistry: an analysis of global change, San Diego, Academic Press, 1-588.

Stern, L., Baisden, W.T., Amundson, R. (1999), "Processes controlling the oxygen isotope ratio of soil CO2: Analytic and numerical modeling," *Geochimica et Cosmochimica Acta*, 63, 799-814.

Vakin, E.A., Lyanlin, G.N. (1990), "Soil Gas Anomalies and the detection of water-conducting fracture zones within geothermal systems," Geochemistry of gaseous elements and compounds. Athens, Greece, Theophrastus Publ., 243-268.

Vindum, C. M. (1998), "Controls on isotopic composition of pedogenic carbonate in the Sevilleta National Wildlife Refuge, New Mexico," Independent Study, Department of Earth and Environmental Sciences, New Mexico Institute of Mining and Technology, Socorro, 1-72.

Wardell, L. J., Kyle, P. R., Campbell, A. R. (2003), "Carbon dioxide emissions from fumarolic ice towers, Mount Erebus volcano, Antarctica," *Volcanic Degassing*, Geological Society, London, Special Publications, 213, 231-246.

Welles, J.M., Demetriades-Shah, T.H., McDermitt, D.K. (2001), "Considerations for measuring ground CO_2 effluxes with chambers," *Chemical Geology*, 177, 3-13.

Witcher, J. C. (1998), "Geothermal Resources of Mew Mexico and Southeastern Arizona," New Mexico Geological Society Guidebook, 39, 191-196.

Wynn, J. C. (1981), "Complete Bouguer Anomaly Map of the Silver City $1^o x 2^o$ Quadrangle, New Mexico-Arizona." U.S. Geological Survey Miscellaneous Investigation Series Map I-1310-A.

APPENDIX A

These graphs show the concentrations measured and averaged each second for 467 soil CO_2 flux measurements taken over the LDKGRA. Time in seconds is on the x axis, and concentration of CO_2 in μmol/mol is on the y axis. The measurement name is given at the top of the graph. The black line is the data, and the red line was used to obtain a slope dX/dt that was used to calculate the soil CO_2 flux in g m^{-2} day^{-1}.

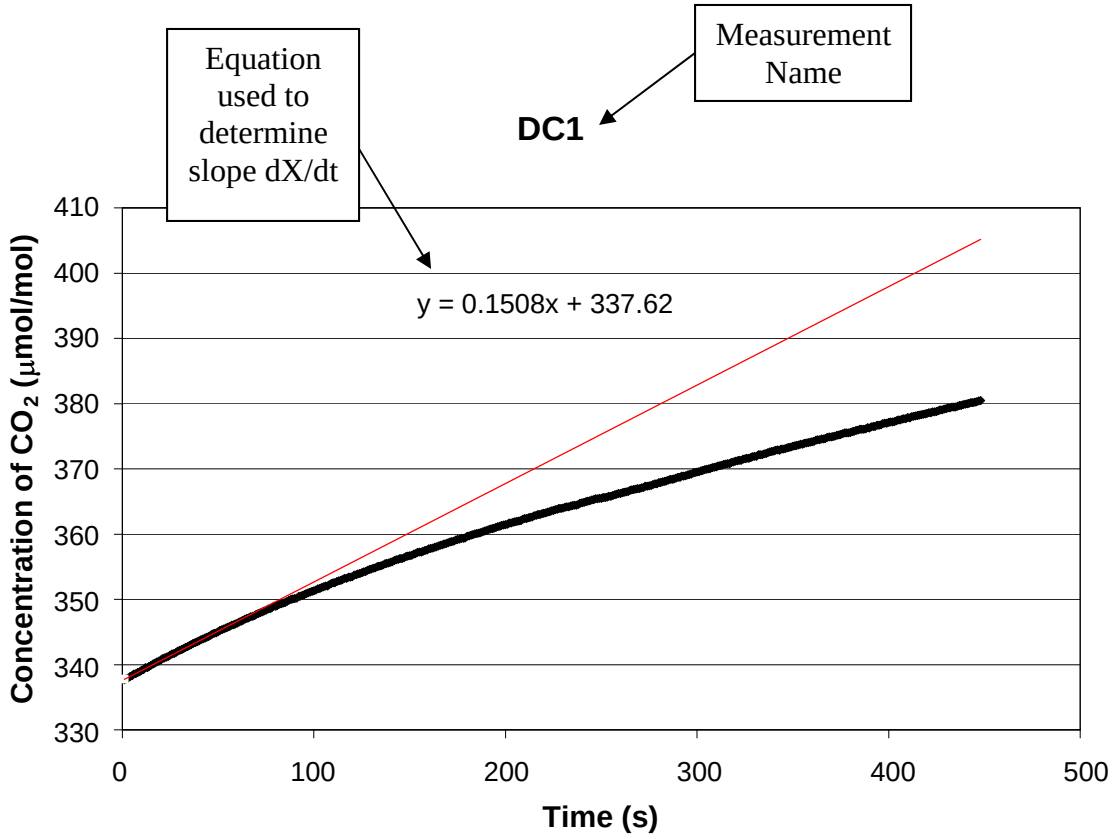

DC1

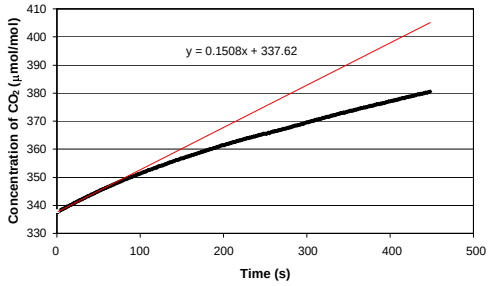

DC4

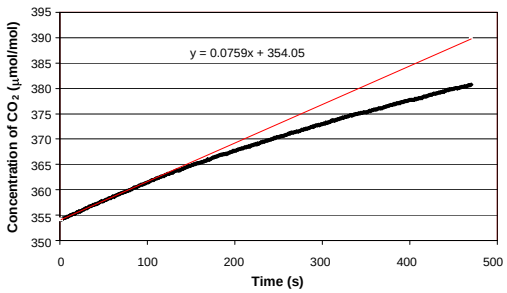

DC7

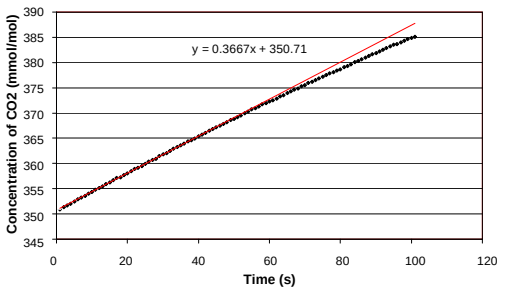

DC2

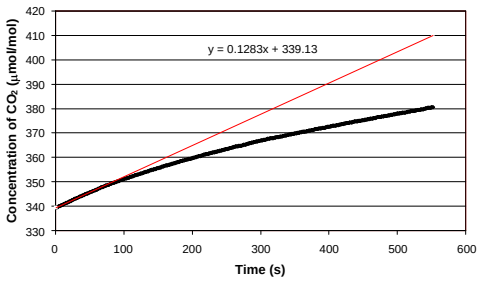

DC5

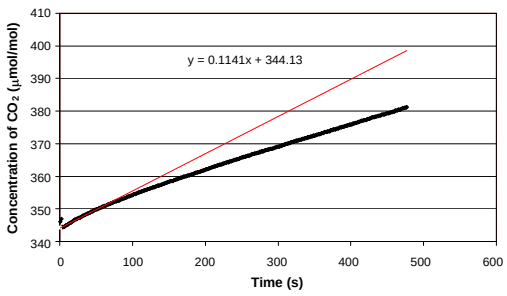

DC8

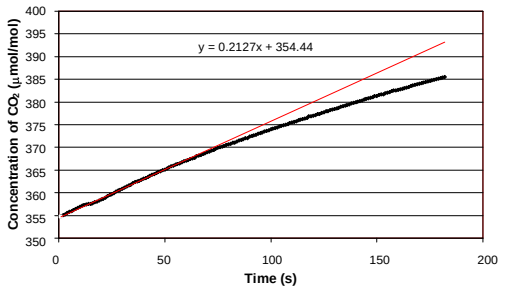

DC3

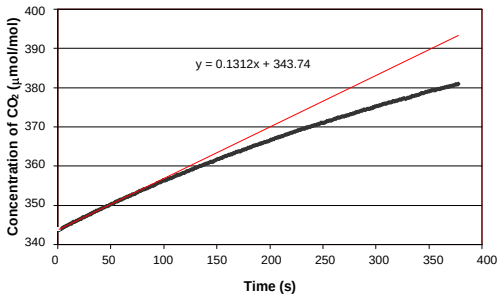

DC6

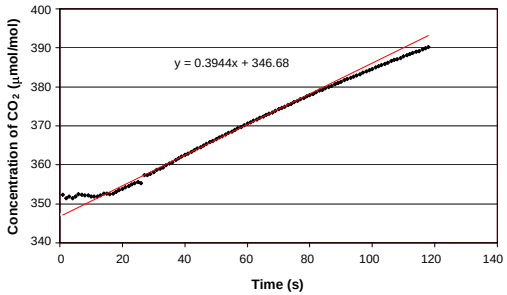

DC9

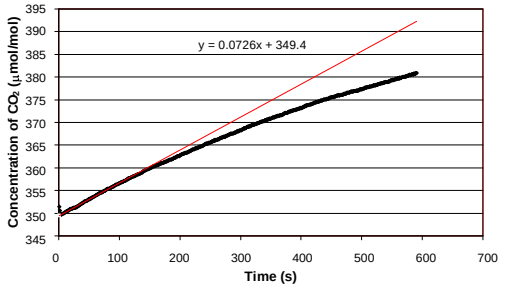

DC10

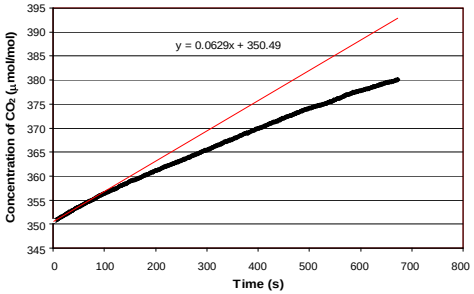

DC13

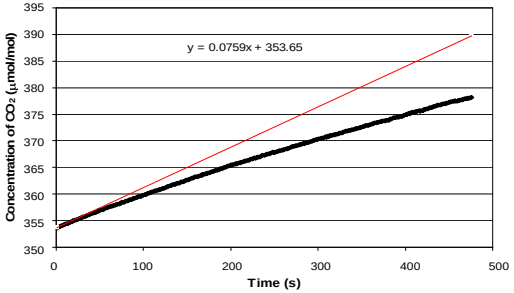

DC15B

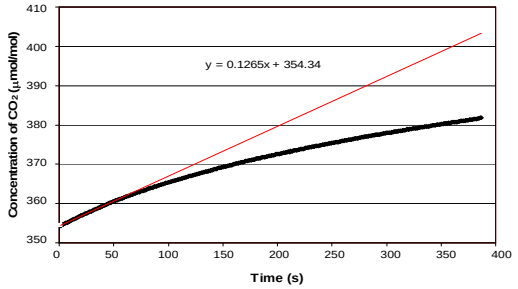

DC11

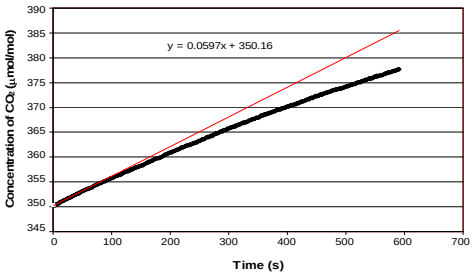

DC14

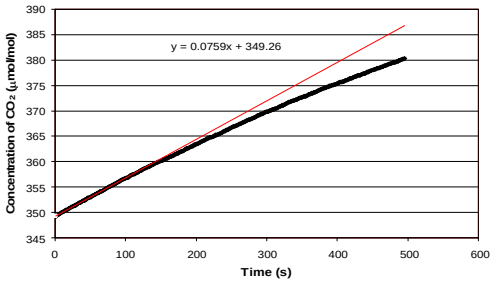

DC16

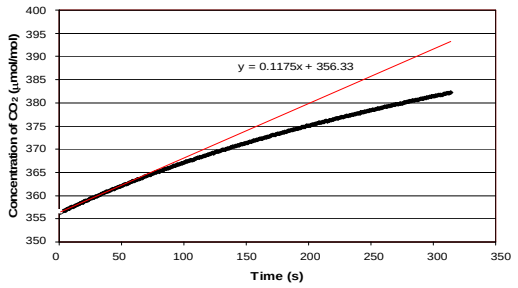

DC12

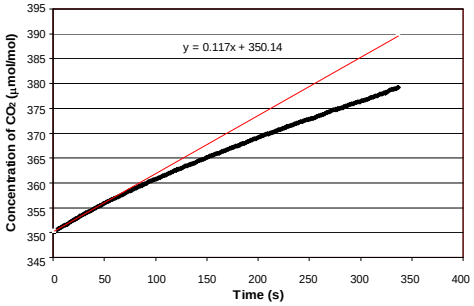

DC15

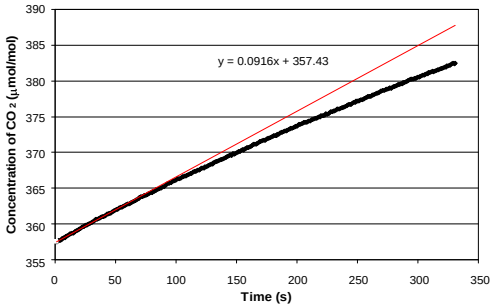

DC17

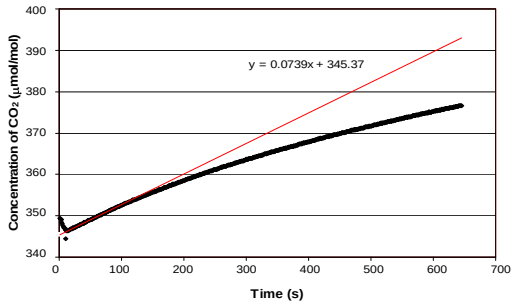

DC18

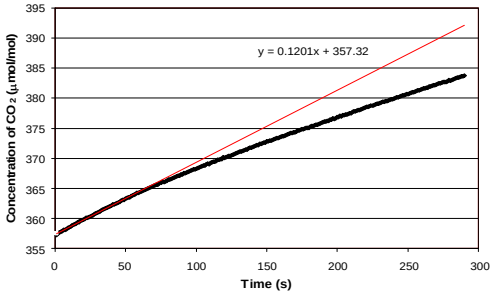

DCN17

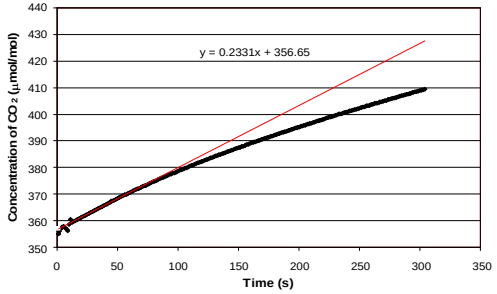

DCN20

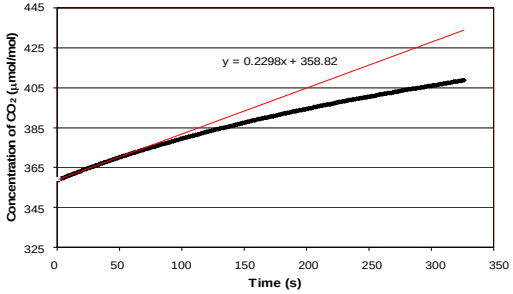

DC19

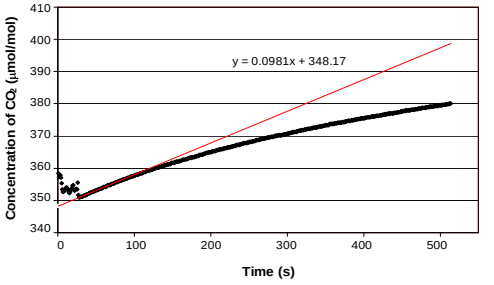

DCN18

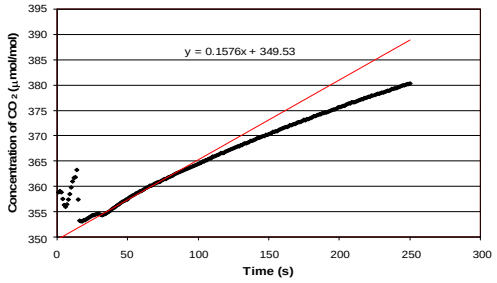

DCN21

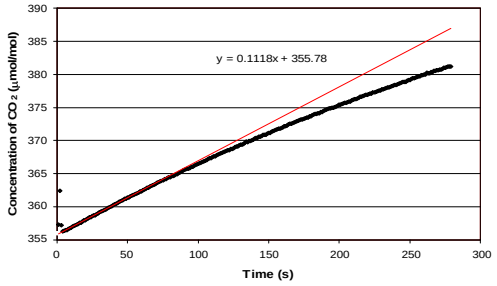

DCN16

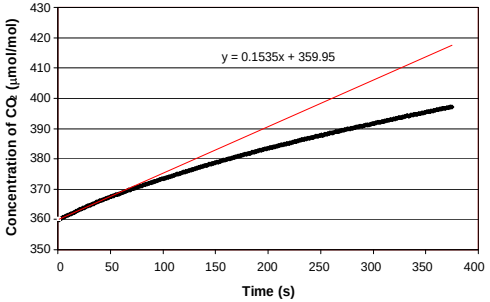

DCN19

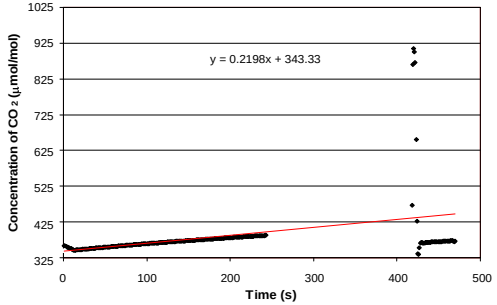

DCN22

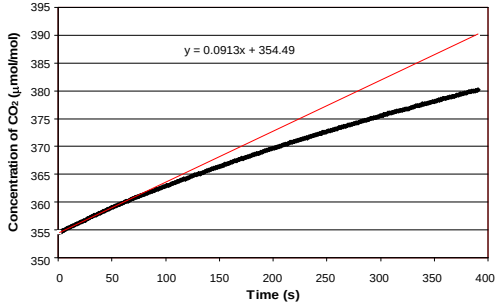

DCN23

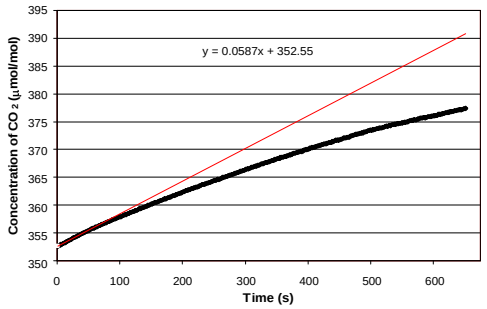

DCN25

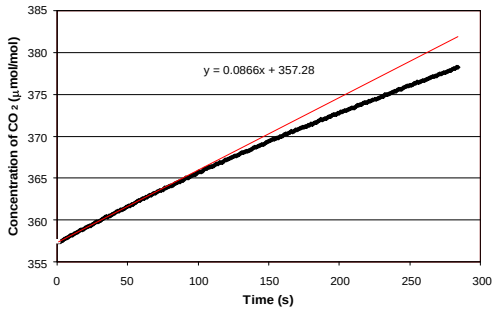

DCN28

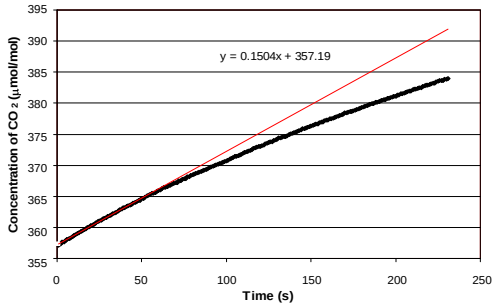

DCN24

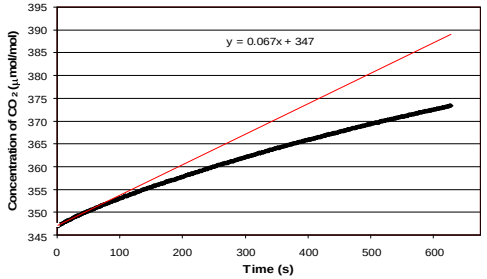

DCN26

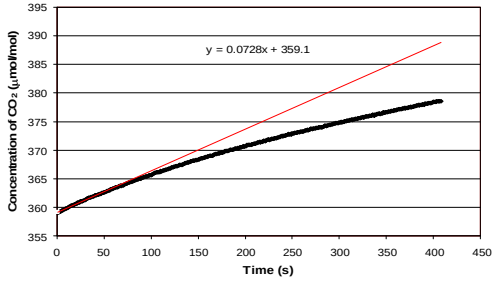

DCN29

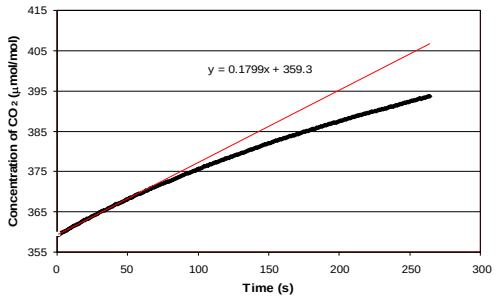

DCN24B

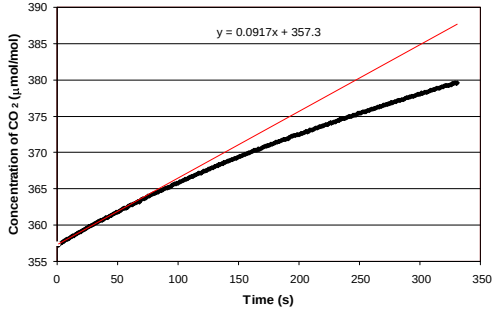

DCN27

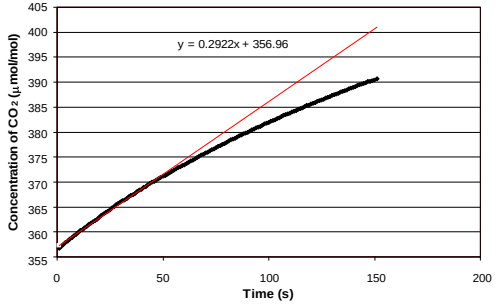

DCN30

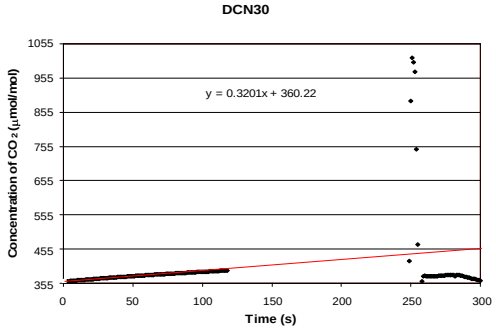

DCN31

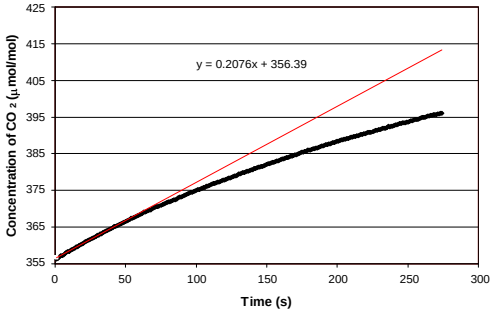

DCN34

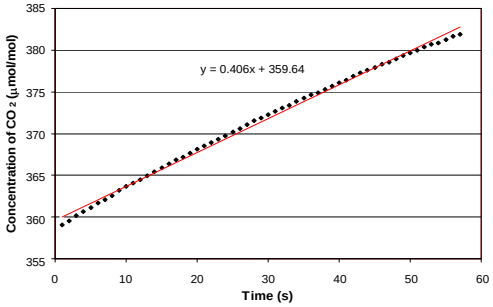

DCN37

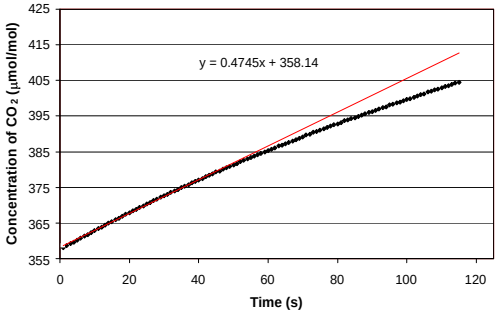

DCN32

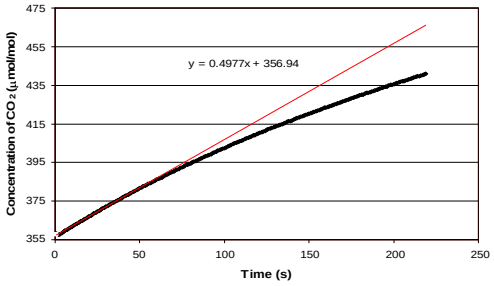

DCN35

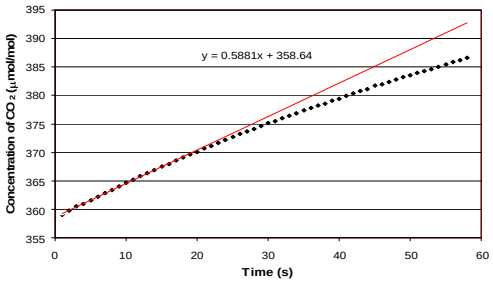

DCN37B

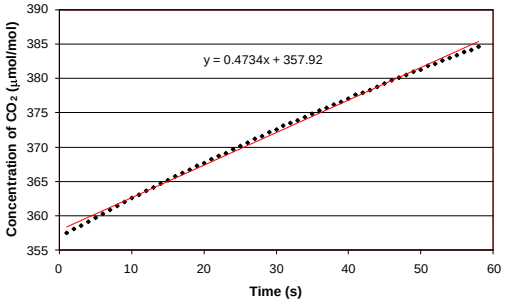

DCN33

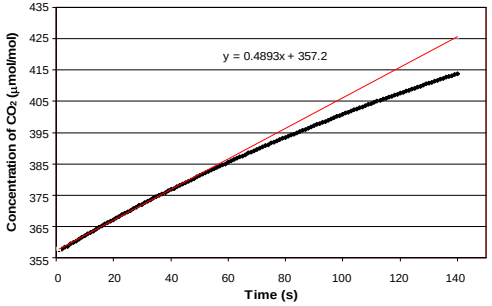

DCN36

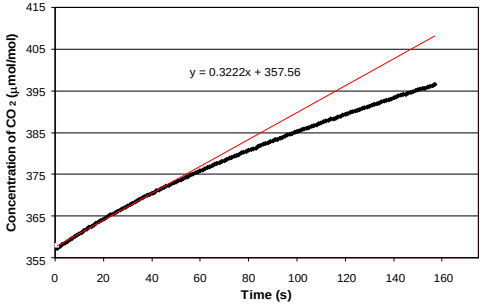

DCN38

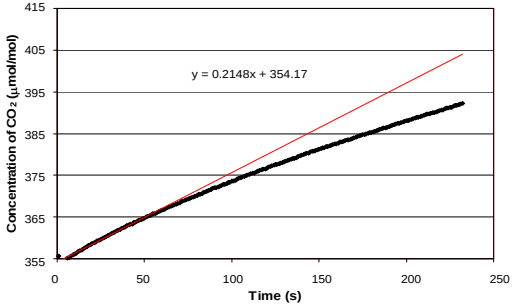

DCN39

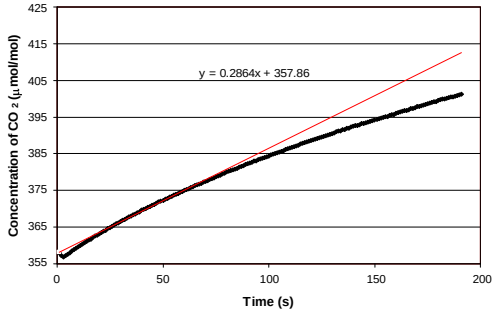

DCN42

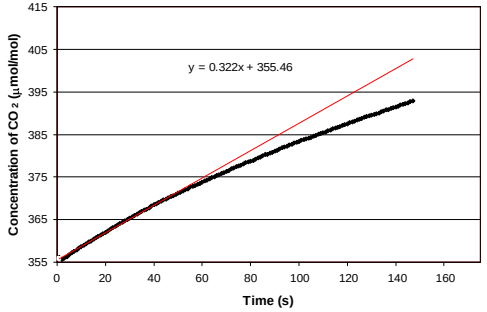

DCG3

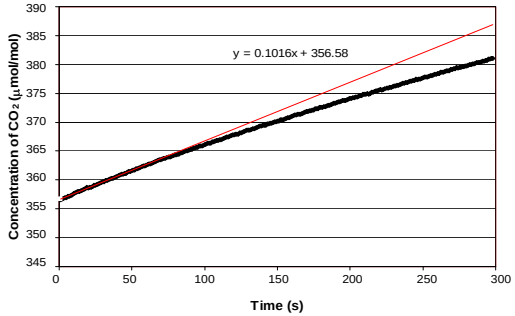

DCN40

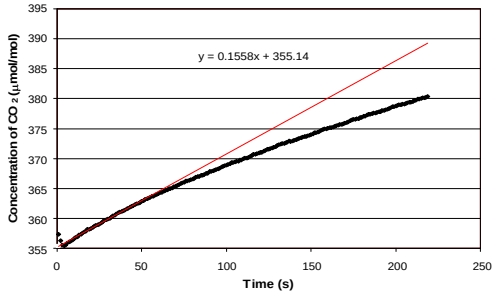

DCG1

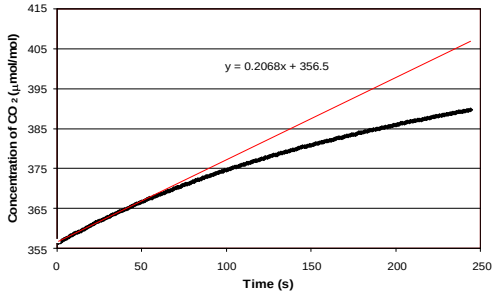

DCG4

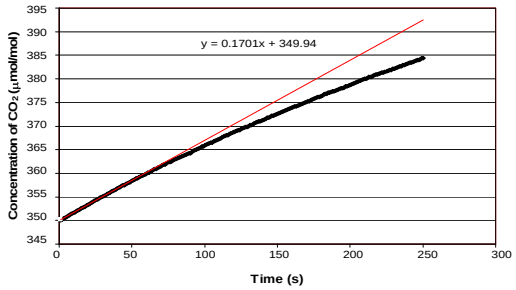

DCN41

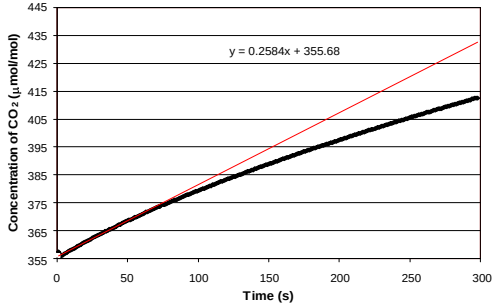

DCG2

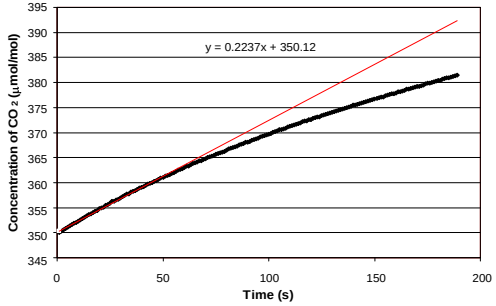

DCG5

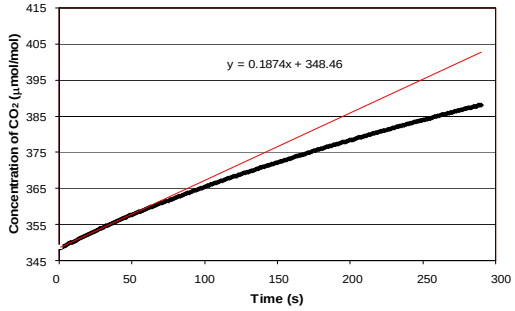

DCG6

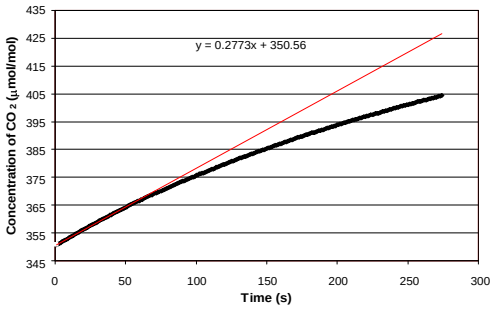

DCG9

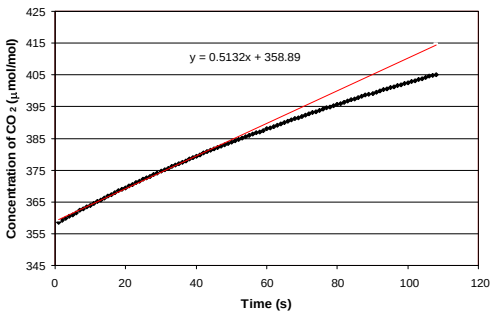

DCG12

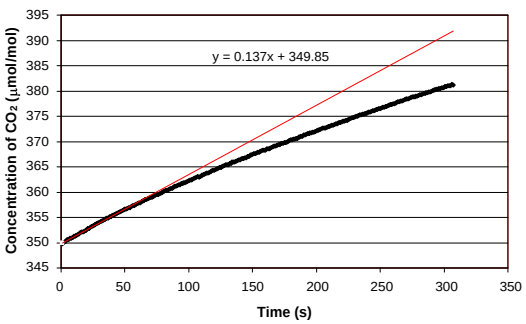

DCG7

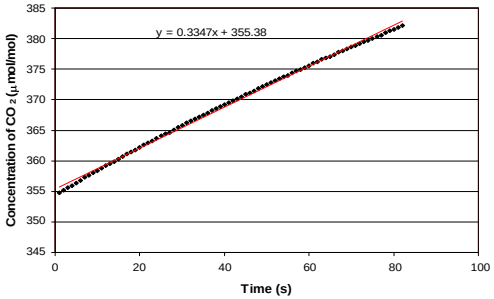

DCG10

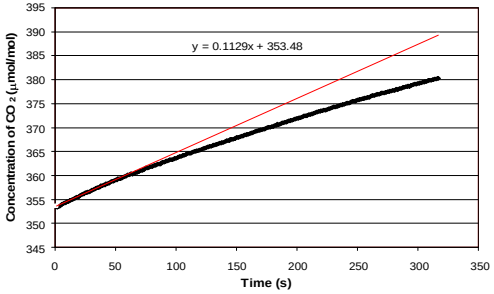

DCG13

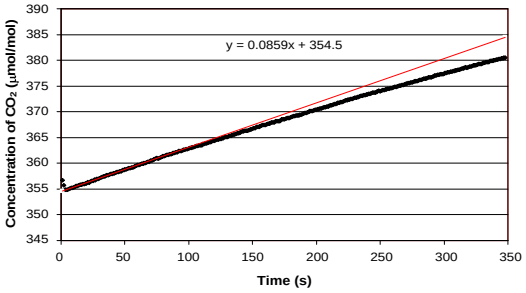

DCG8

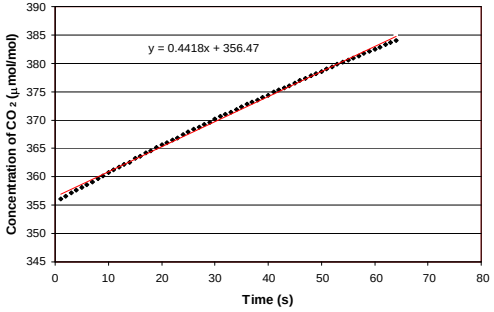

DCG11

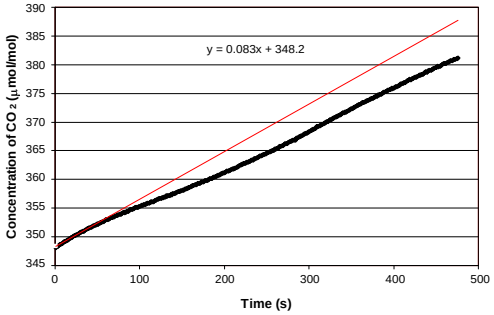

DCG14

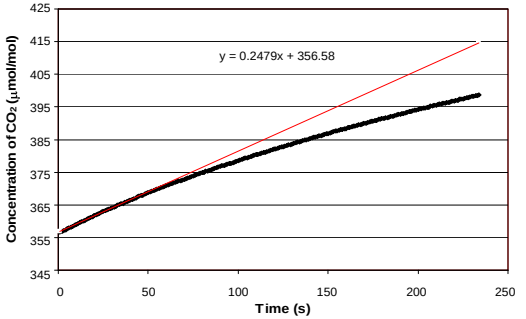

DCG15

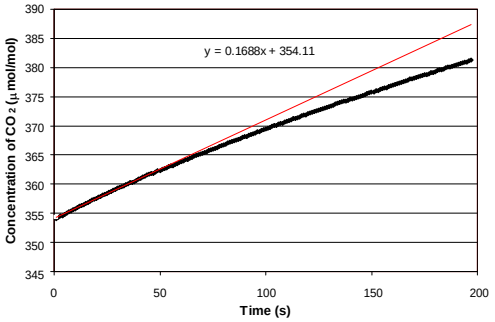

DCG18

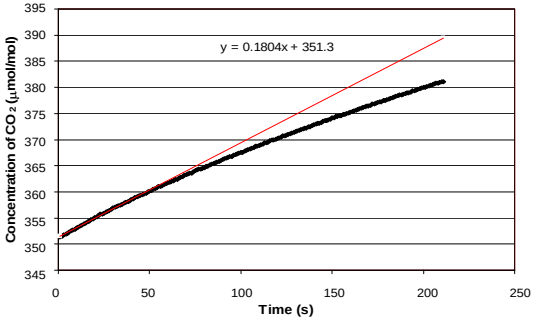

DCG20B

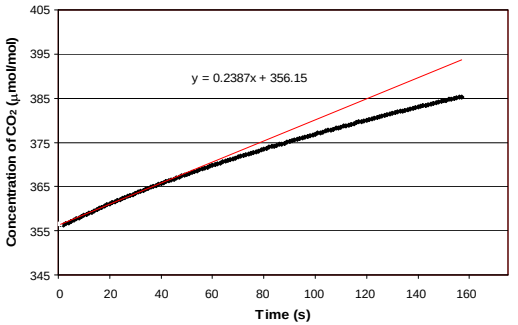

DCG16

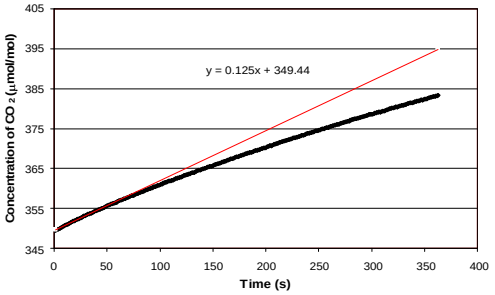

DCG19

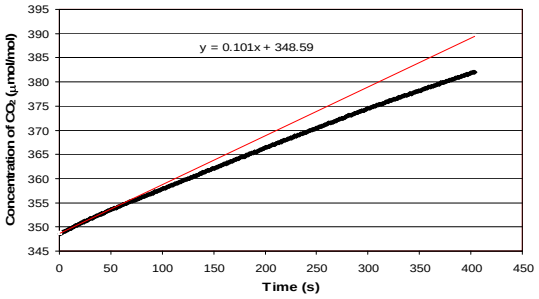

DCG21

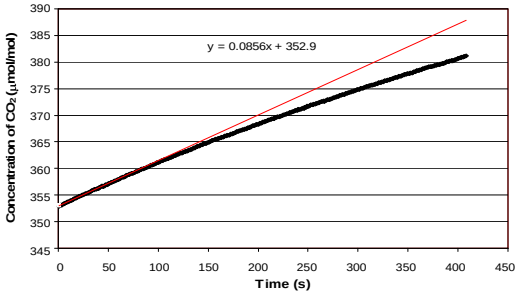

DCG17

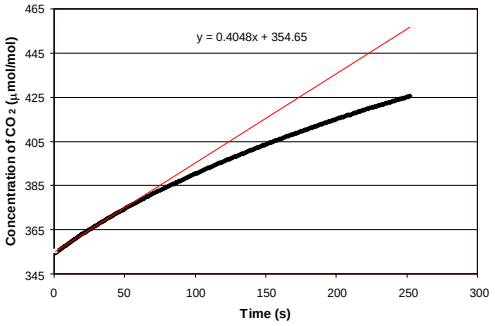

DCG20

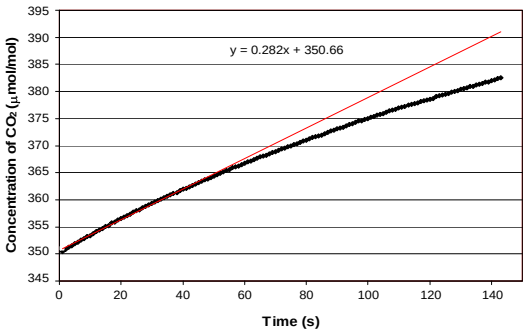

DCG22

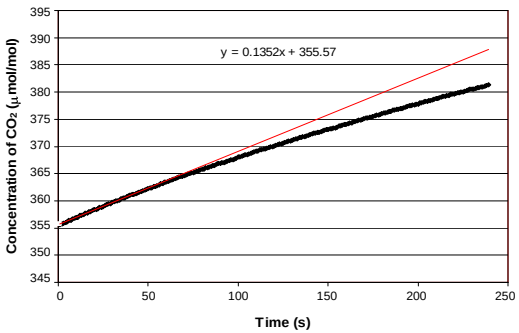

DCG23

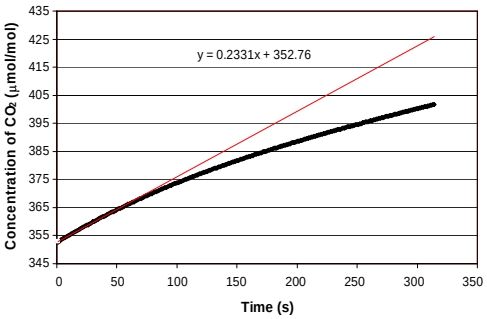

DCG26

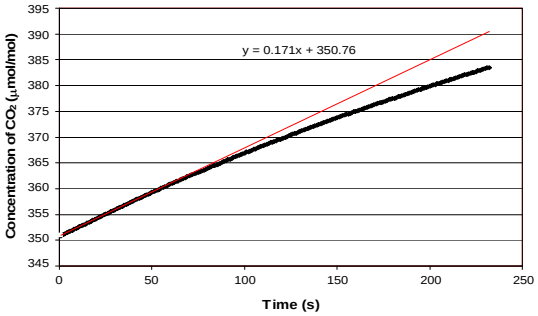

DCG29

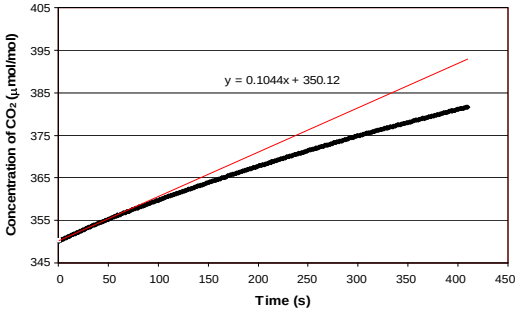

DCG24

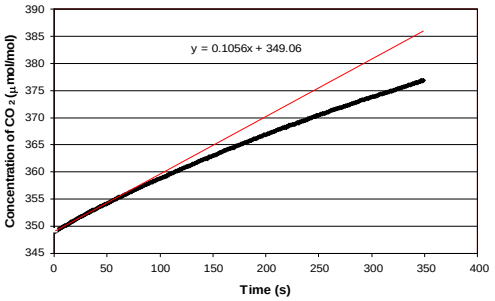

DCG27

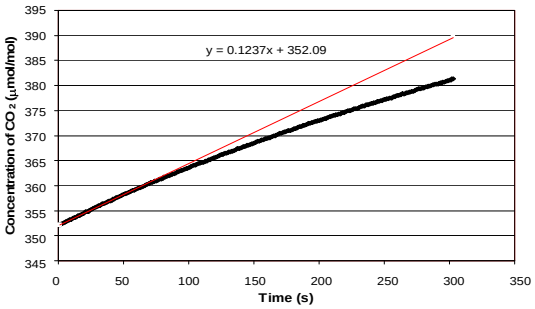

DCG30

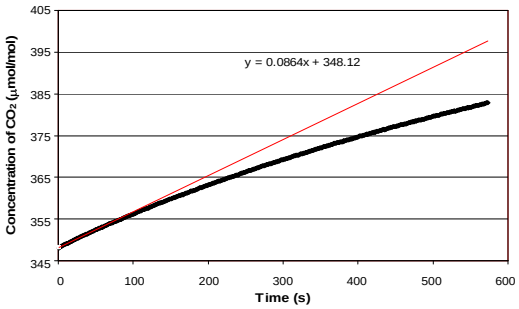

DCG25

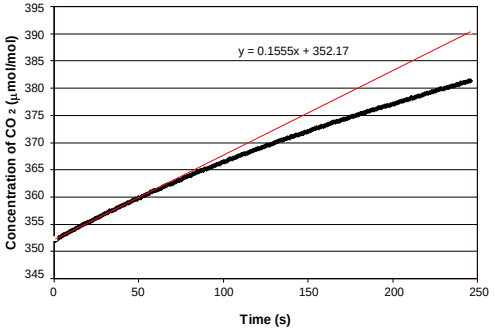

DCG28

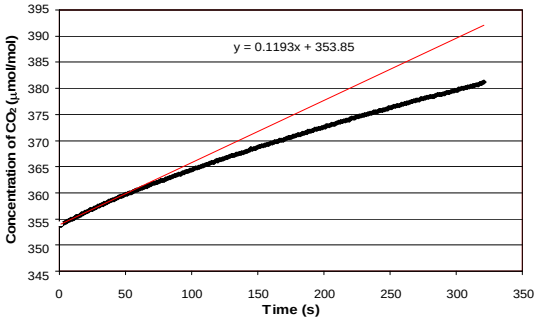

DCG30B

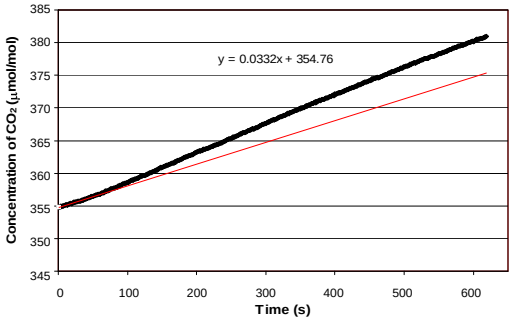

DCG31

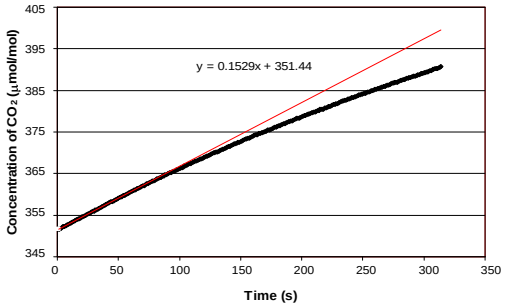

DCG34

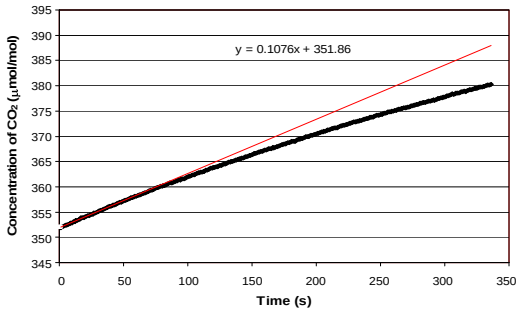

DCG37

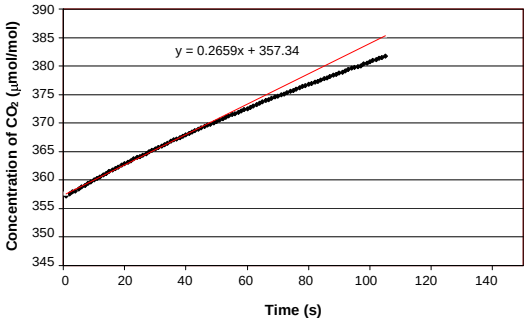

DCG32

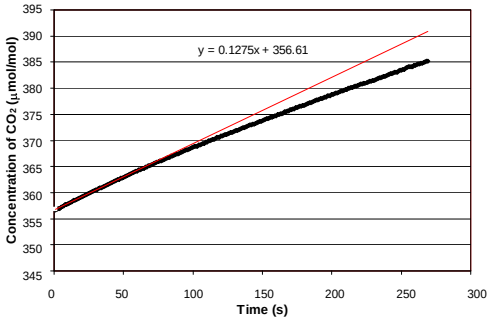

DCG35

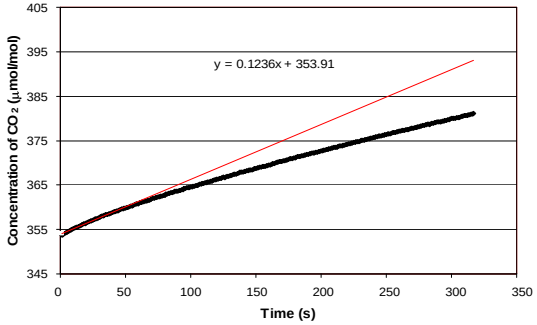

DCG37B

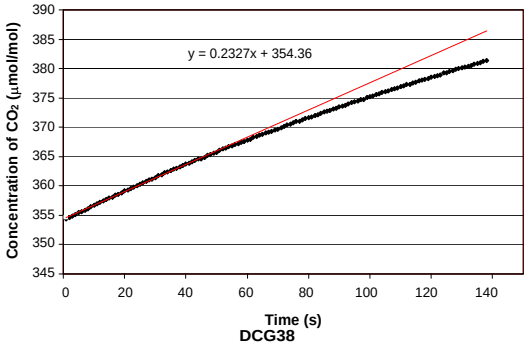

DCG33

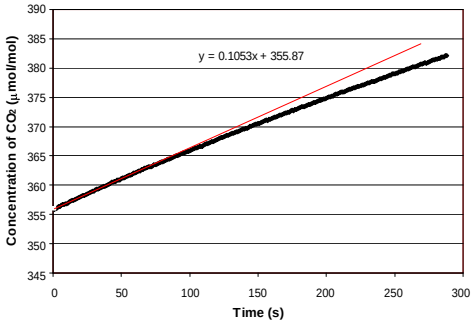

DCG36

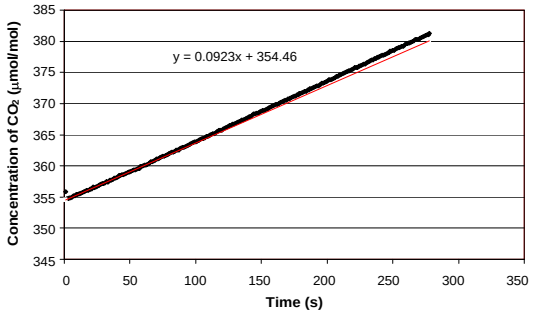

DCG38

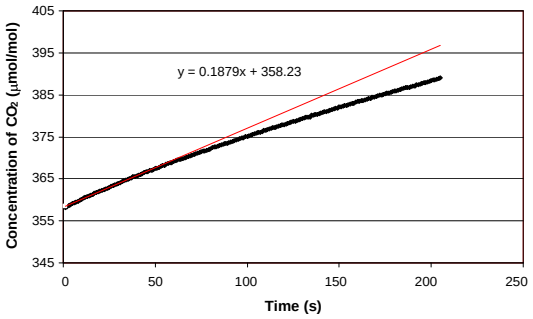

DCG39

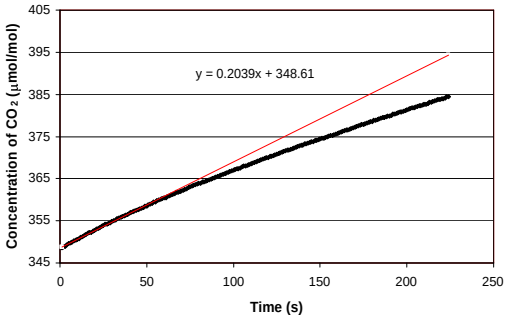

DCG42

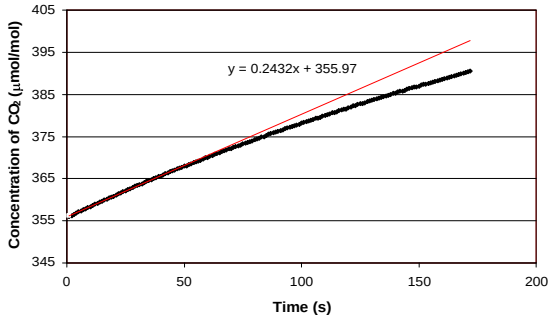

DCG45

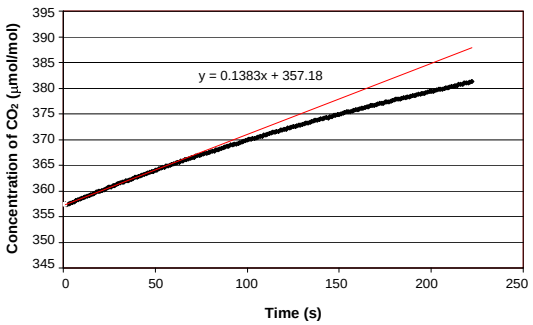

DCG40

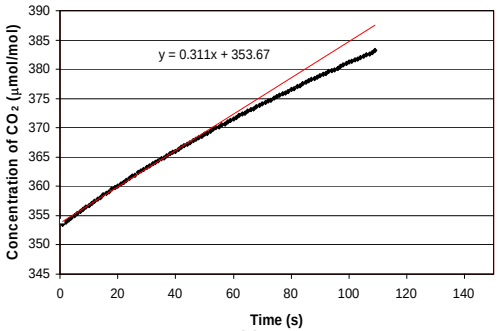

DCG43

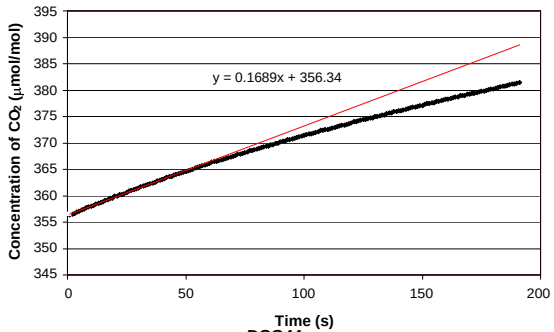

DCG46

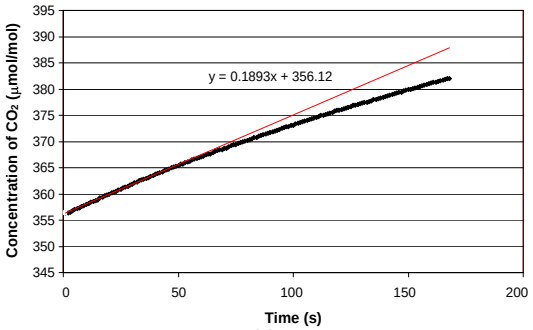

DCG41

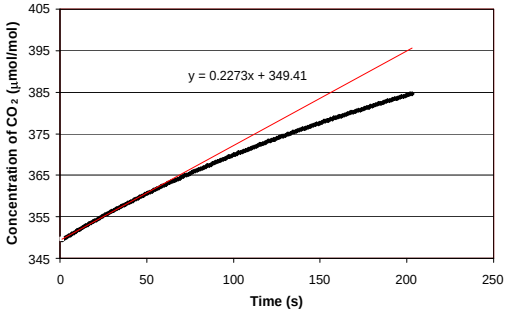

DCG44

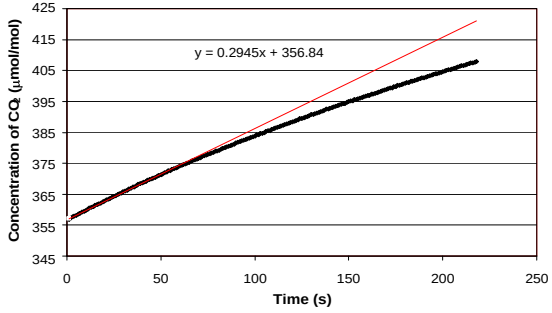

DCG47

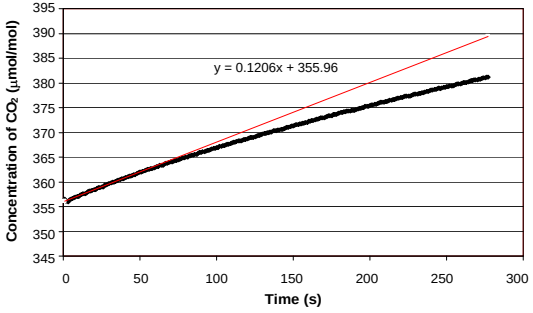

DCG48

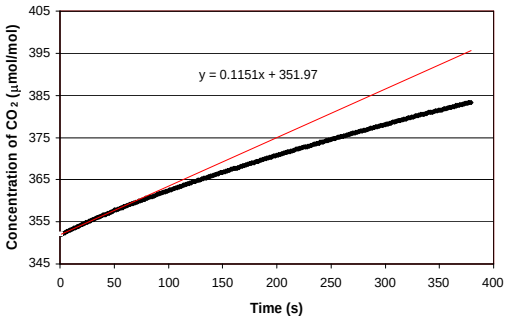

DCG50B

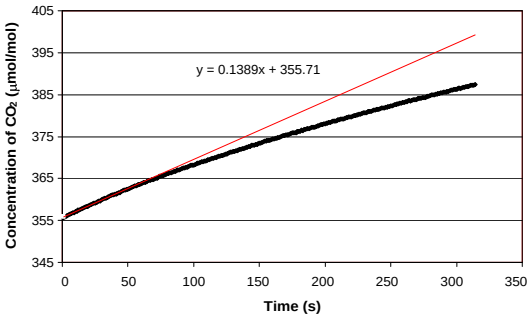

DCG53

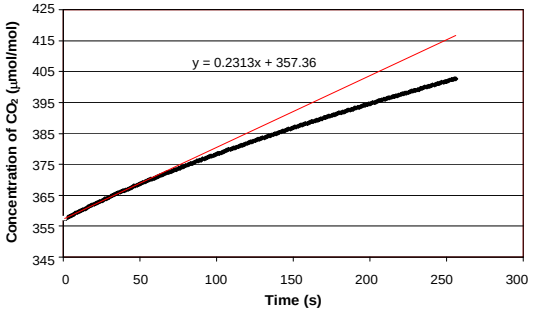

DCG49

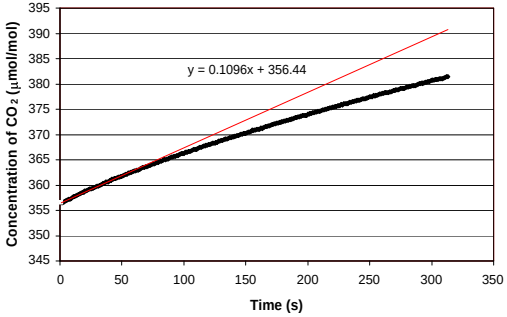

DCG51

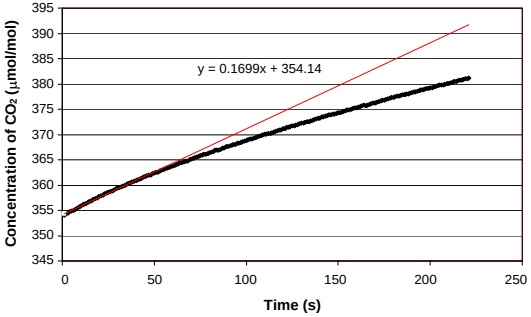

DCG54

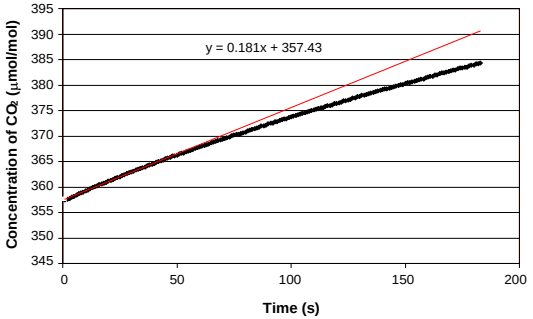

DCG50

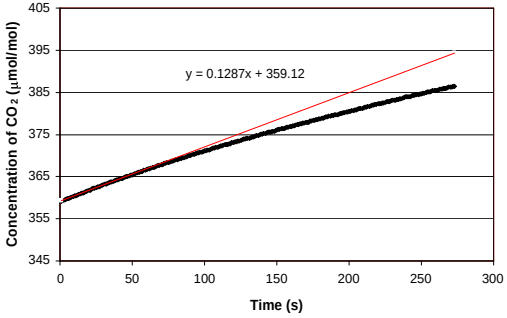

DCG52

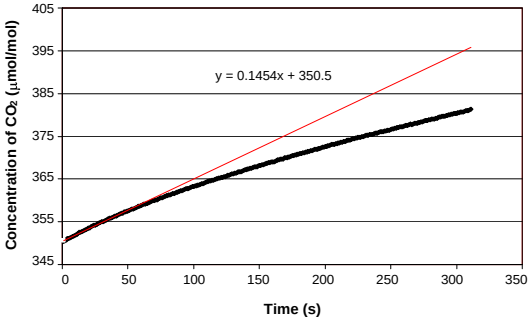

DCG55

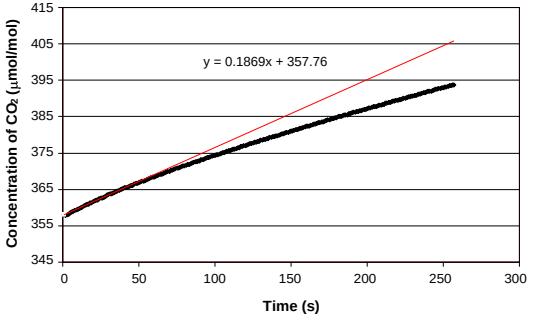

DCG56

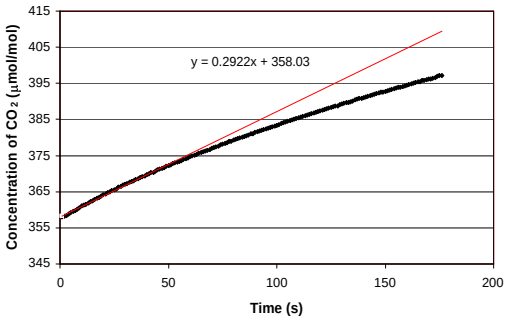

DCG59

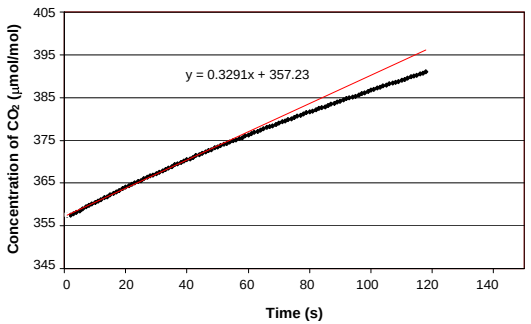

DCC1

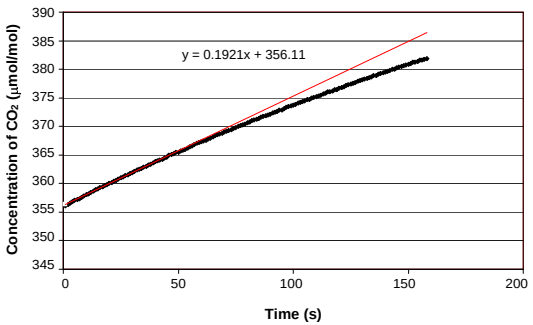

DCG57

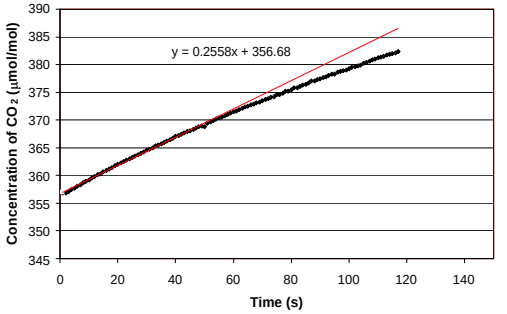

DCG60

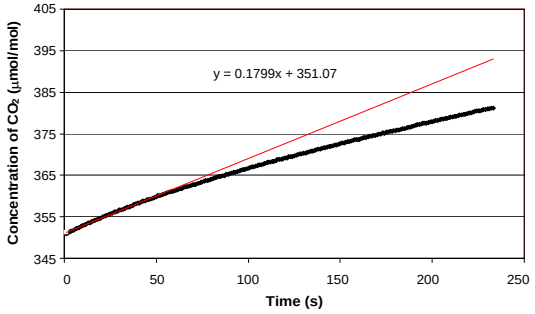

DCC2

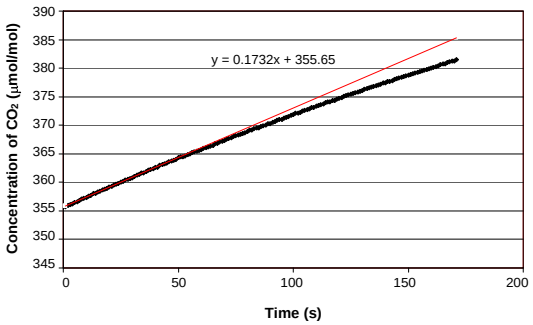

DCG58

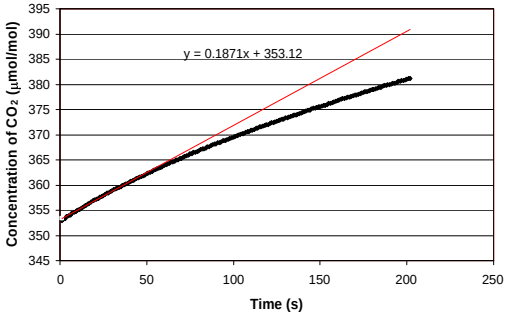

DCG60B

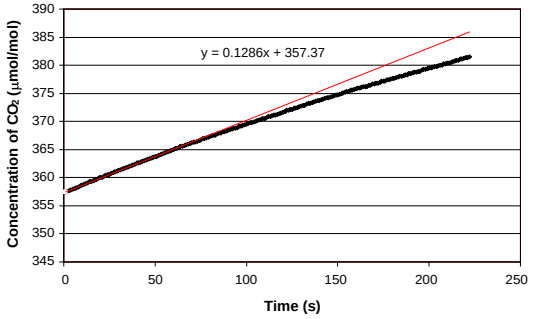

DCC3

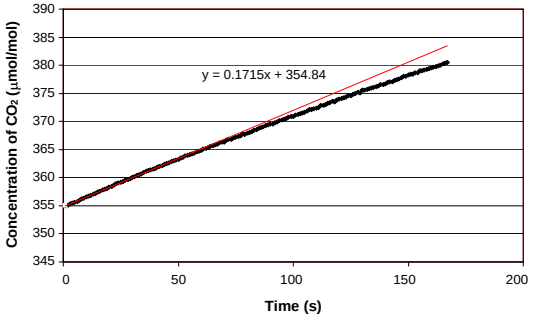

DCC4

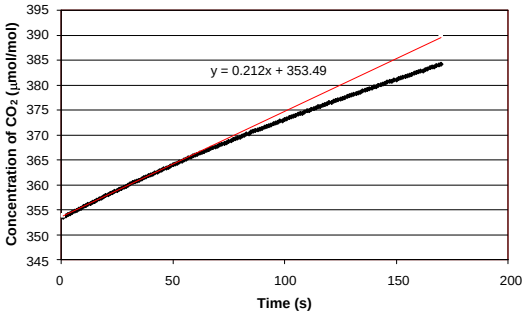

DCC7

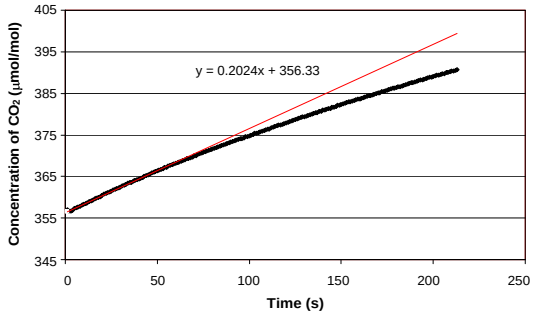

DCC10

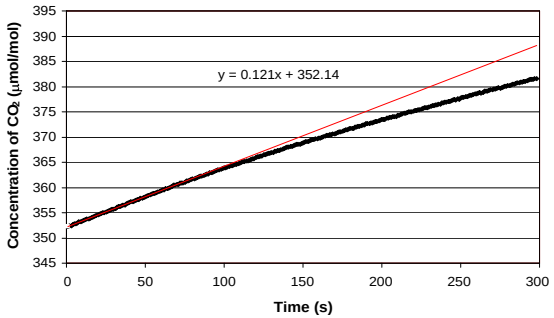

DCC5

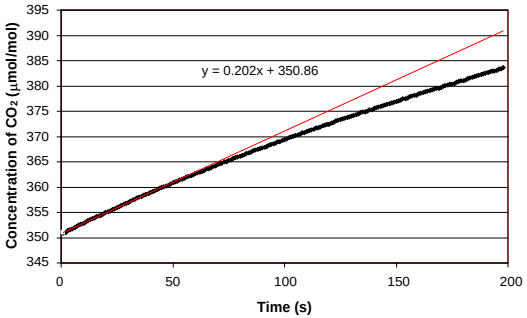

DCC8

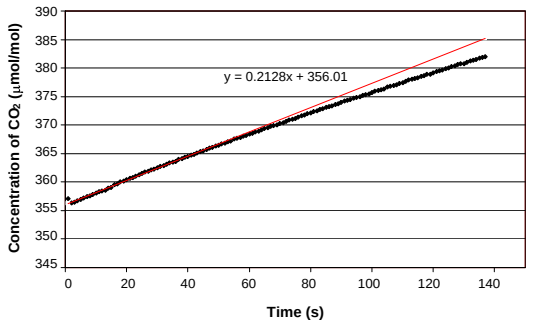

DCC11

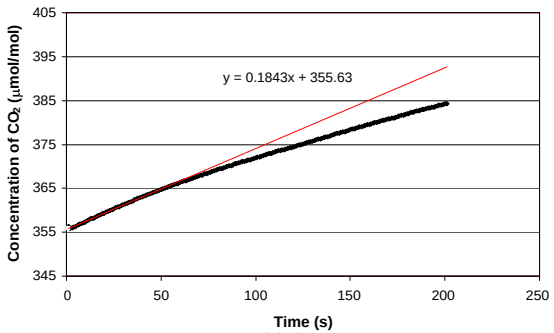

DCC6

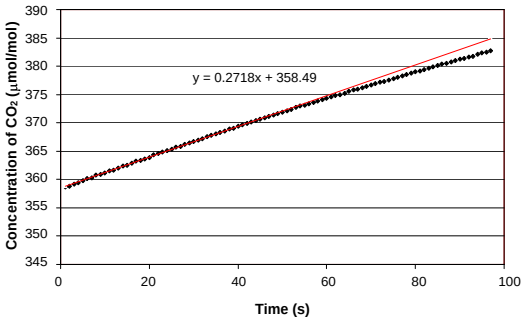

DCC9

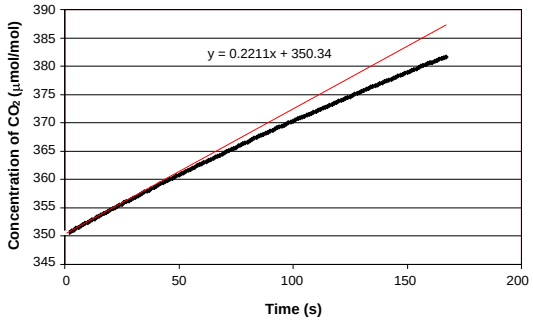

DCC12

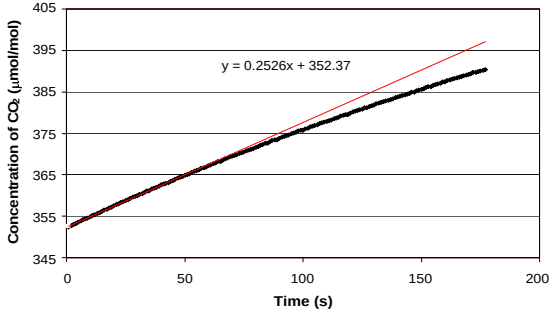

DCB

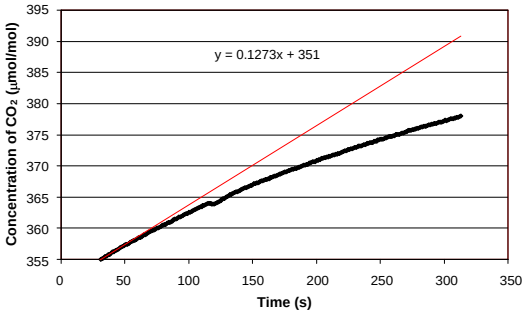

DCB4

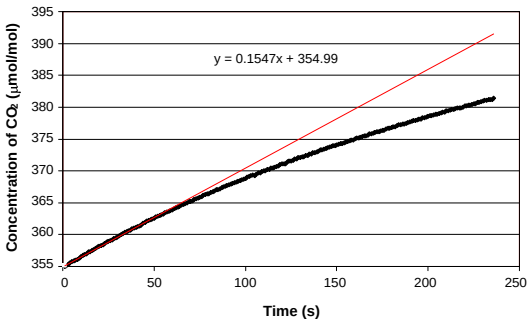

KM01040301

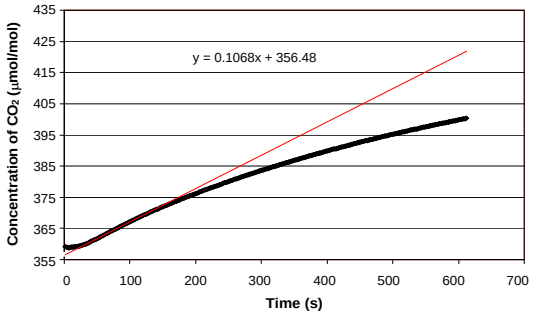

DCB2

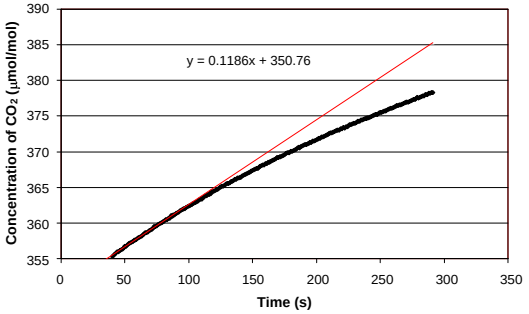

DCB5

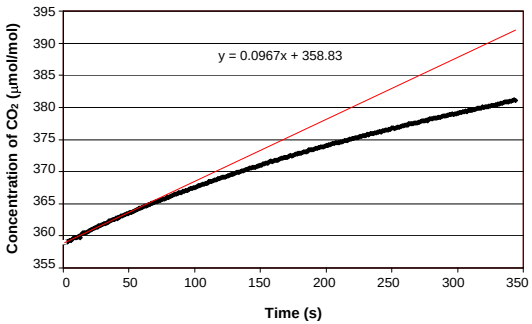

KM01040302

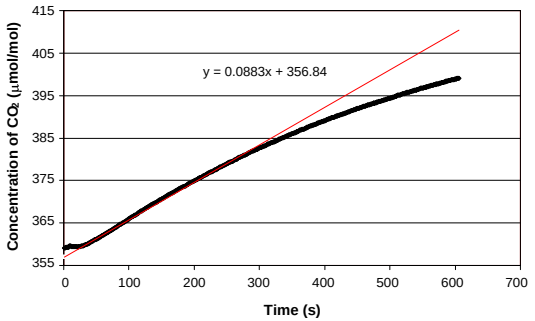

DCB3

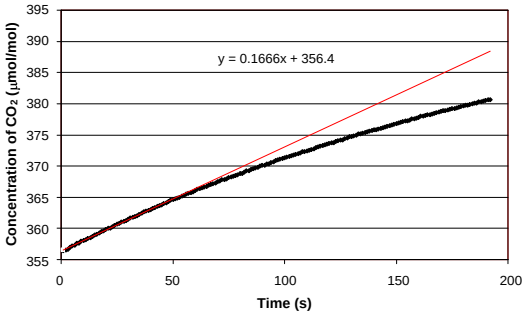

DCB6

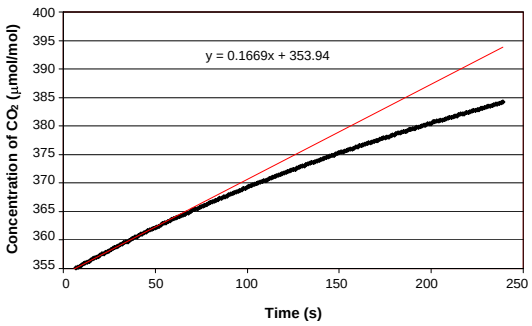

KM01040303

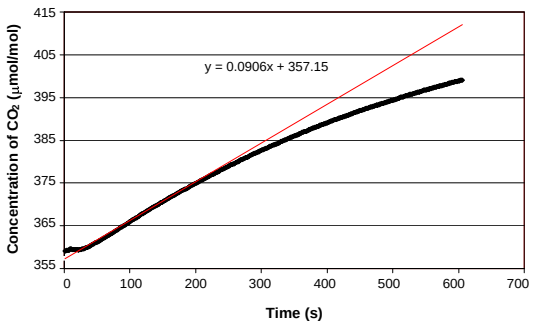

KM01040304

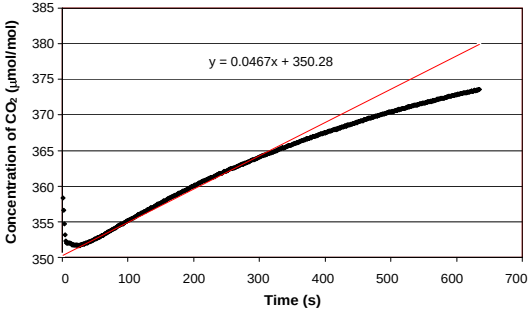

KM01040307

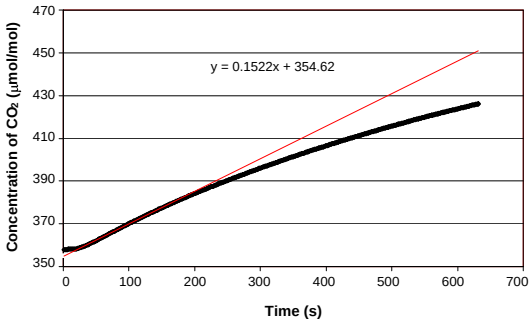

KM01040310

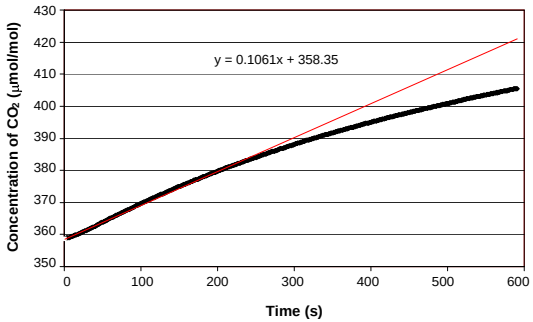

KM01040305

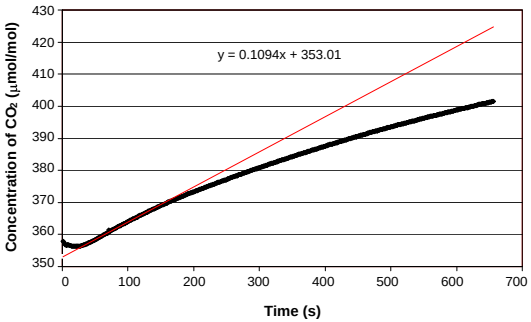

KM01040308

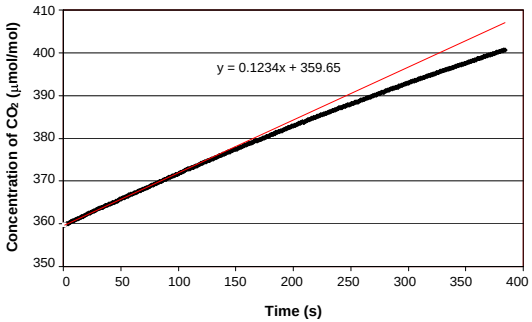

KM01040311

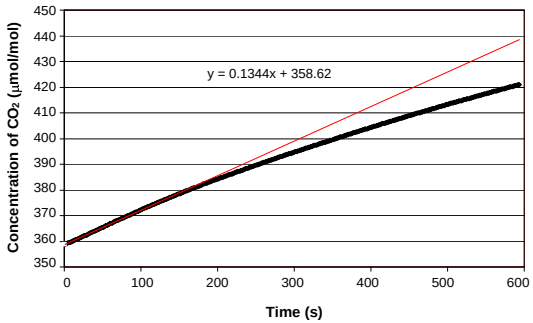

KM01040306

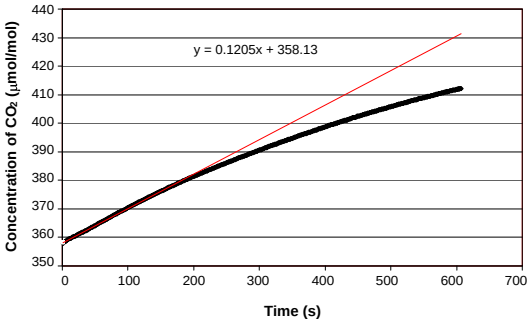

KM01040309

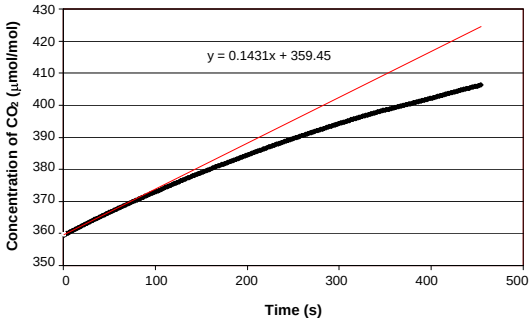

KM01040312

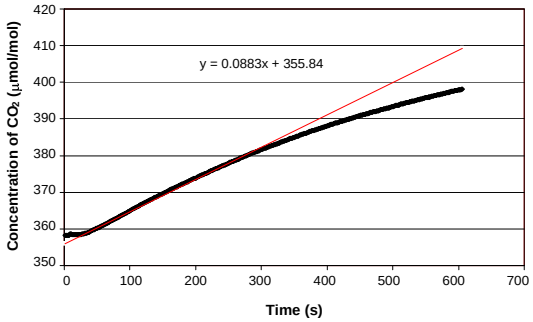

KM01040313

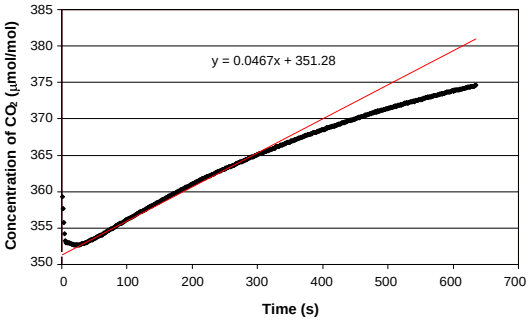

KM01040316

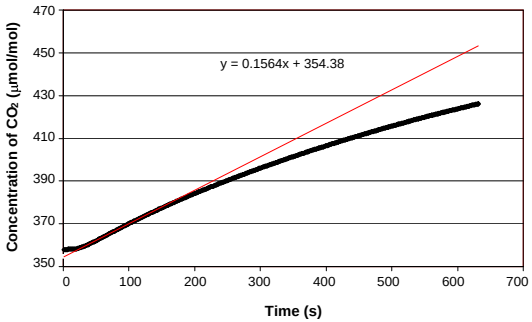

KM01040319

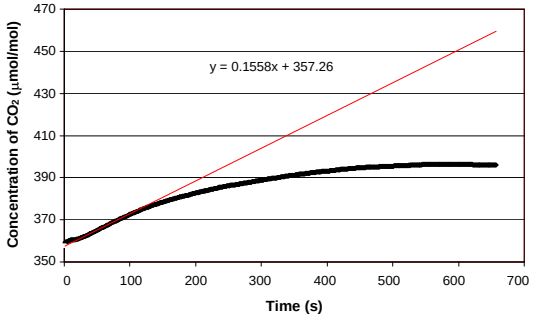

KM01040314

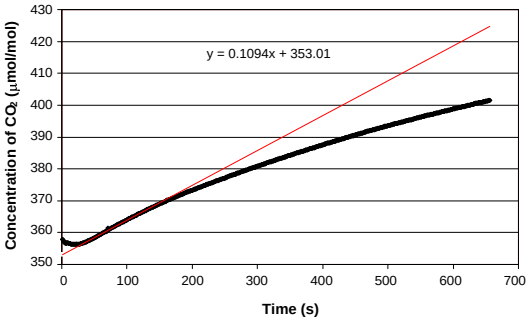

KM01040317

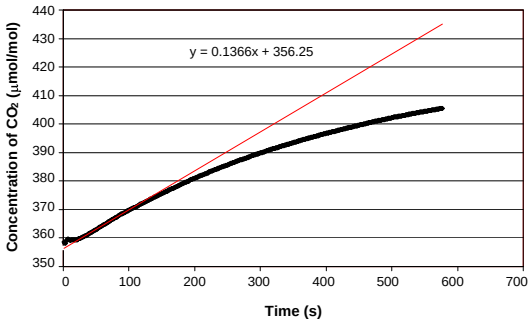

KM01040320

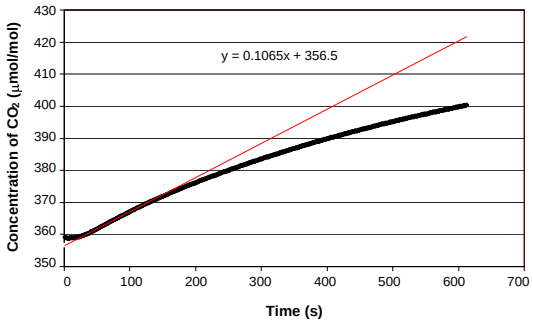

KM01040315

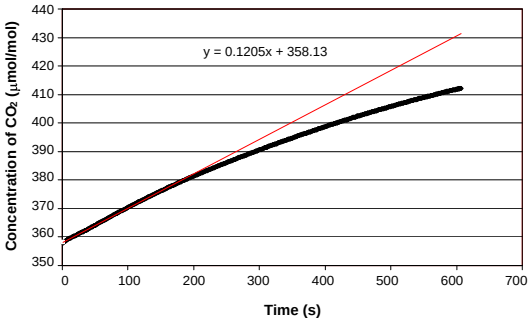

KM01040318

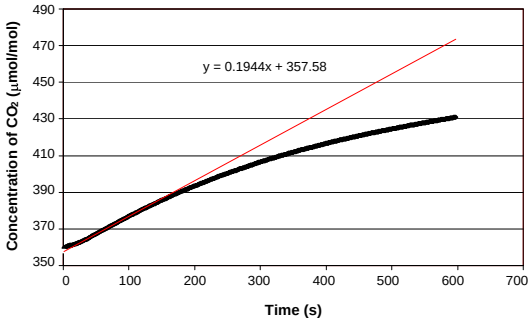

KM01050301

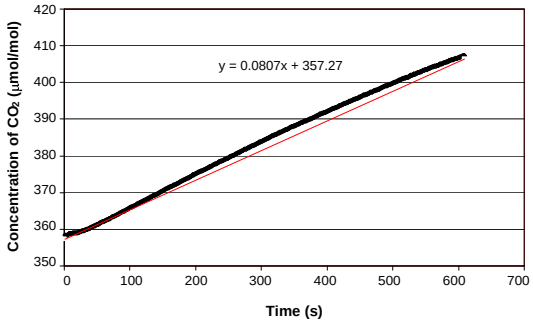

KM01050302

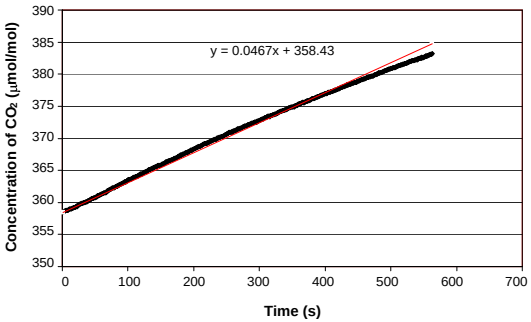

KM01050305

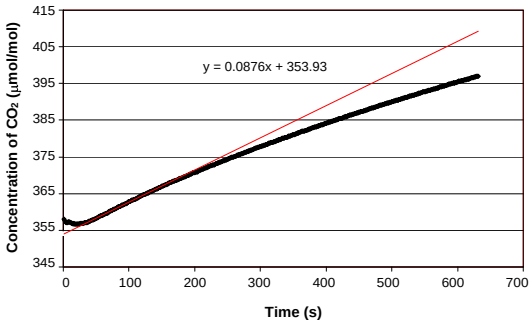

KM01050308

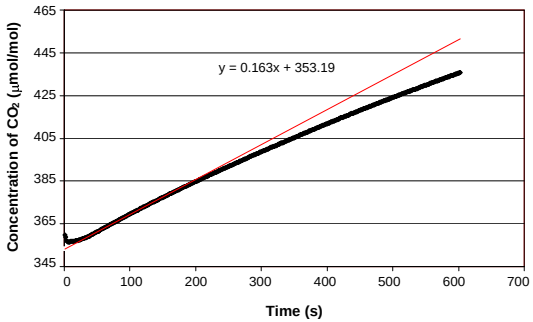

KM01050303

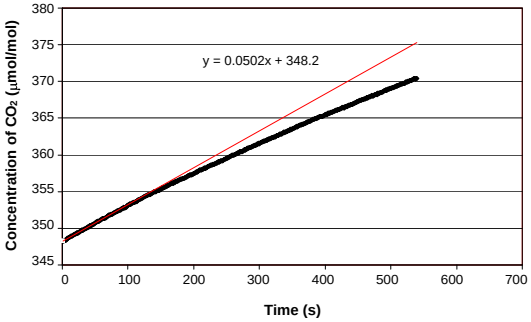

KM01050306

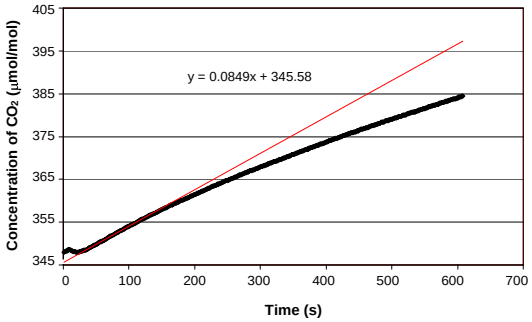

KM01050309

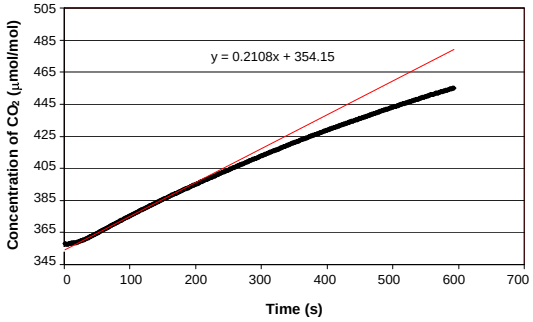

KM01050304

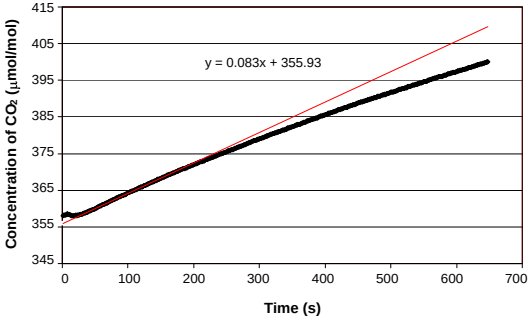

KM01050307

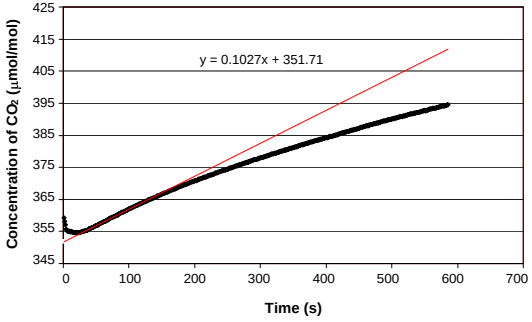

KM01050310

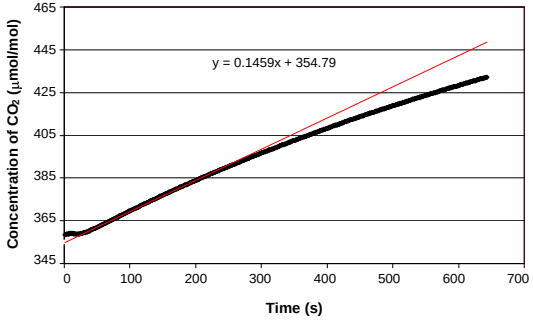

KM01050311

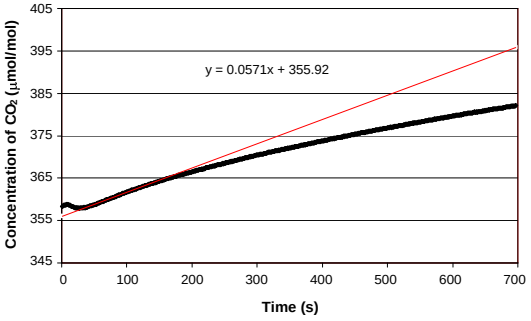

KM01070302

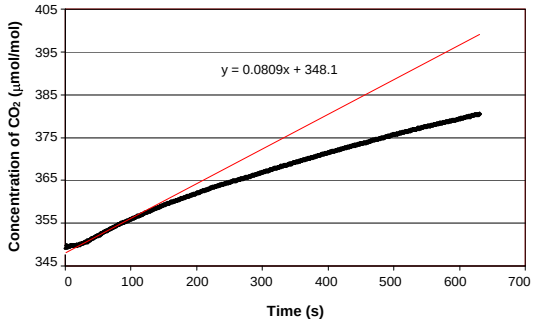

KM01070305

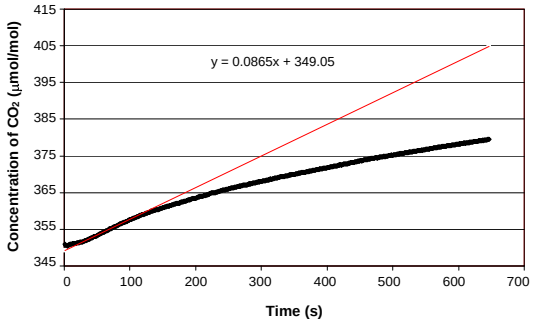

KM01050312

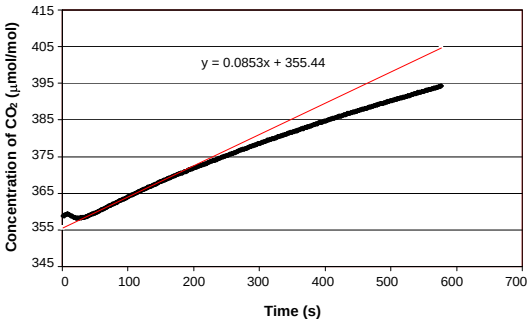

KM01070303

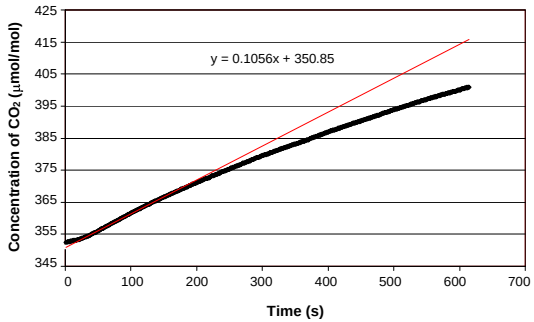

KM01070306

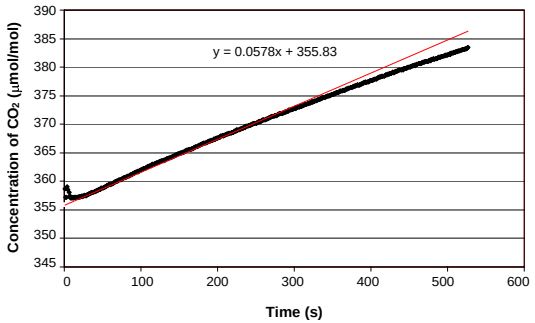

KM01070301

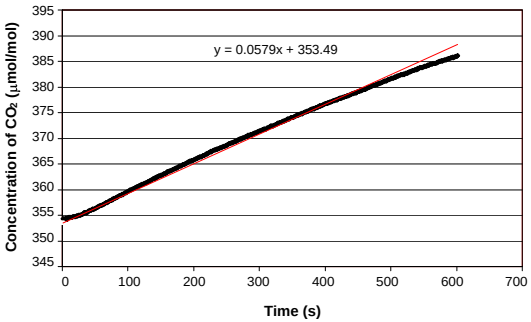

KM01070304

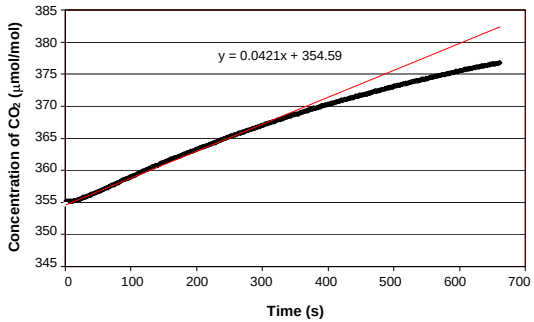

KM01070307

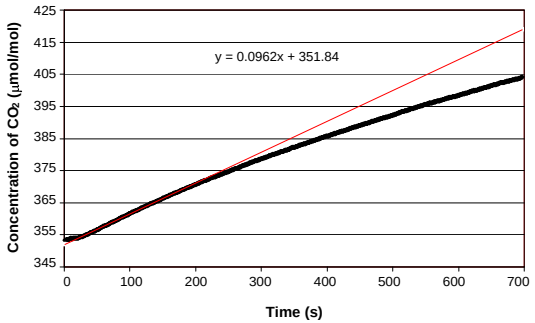

KM01070308

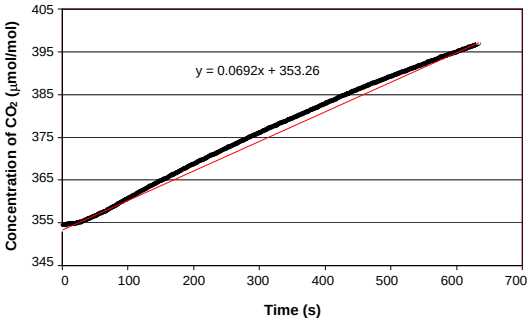

KM01070311

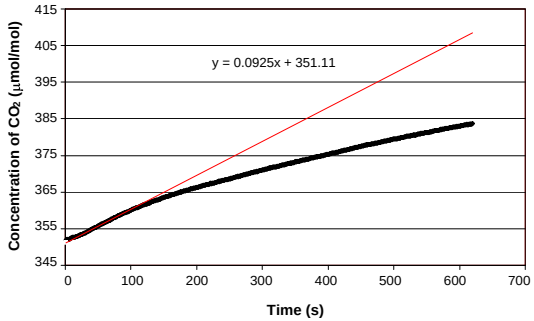

KM01100301

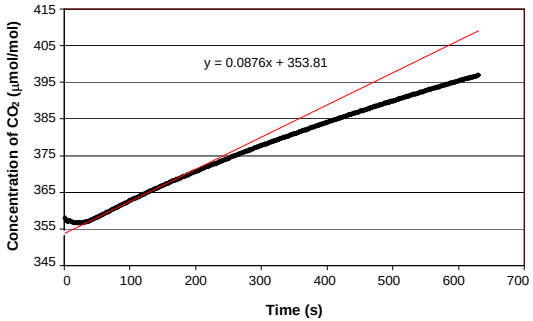

KM01070309

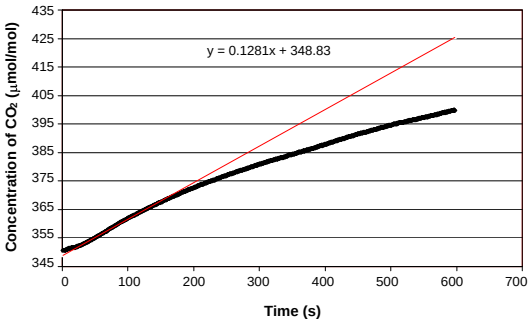

KM01070312

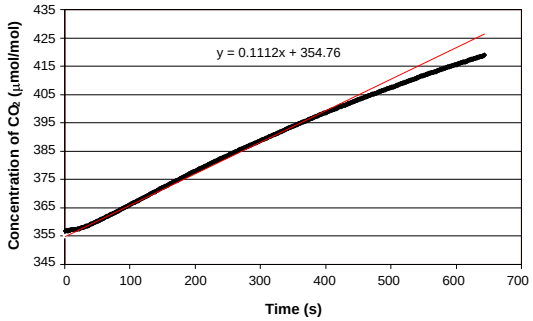

KM01100302

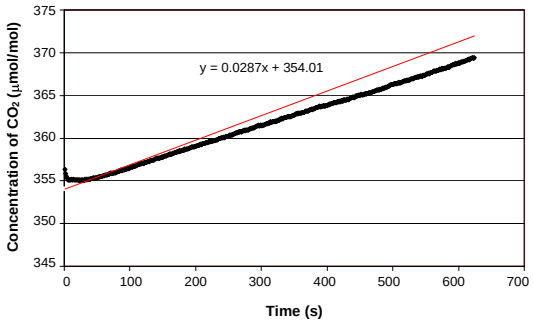

KM01070310

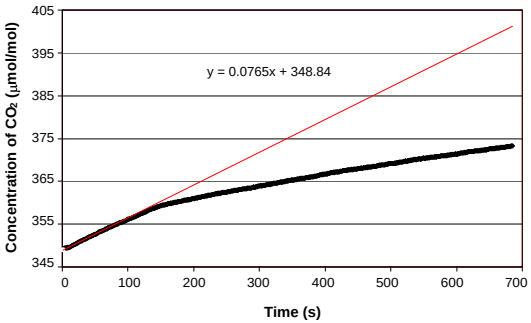

KM01070313

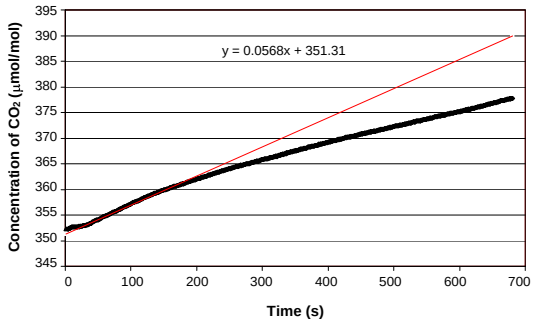

KM01100303

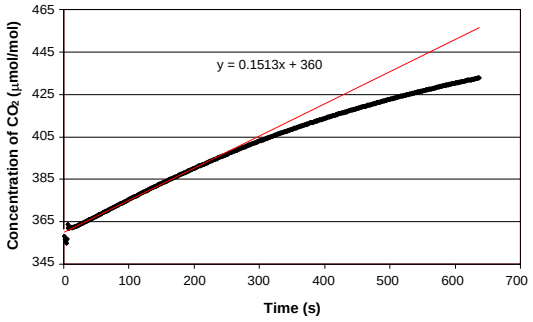

KM01100304

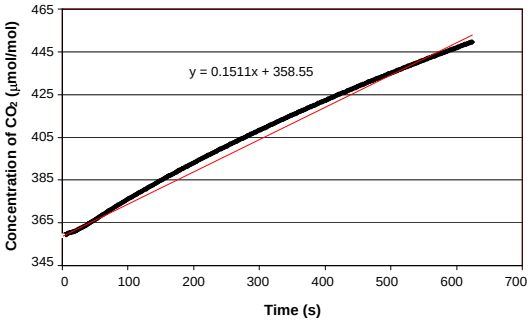

KM01100307

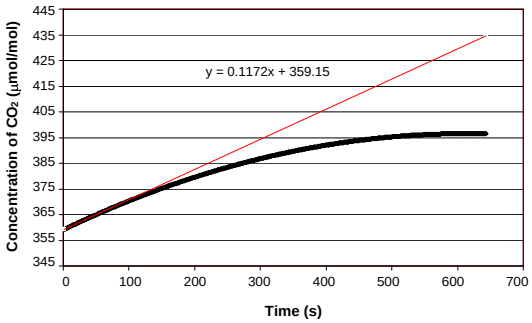

KM01100310

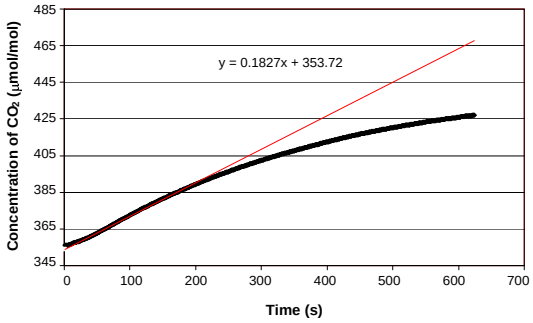

KM01100305

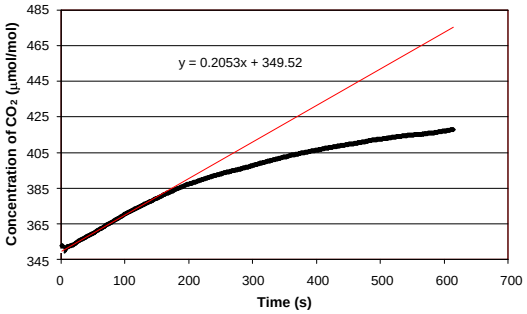

KM01100308

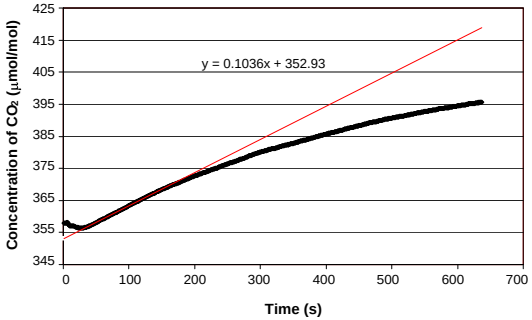

KM01100311

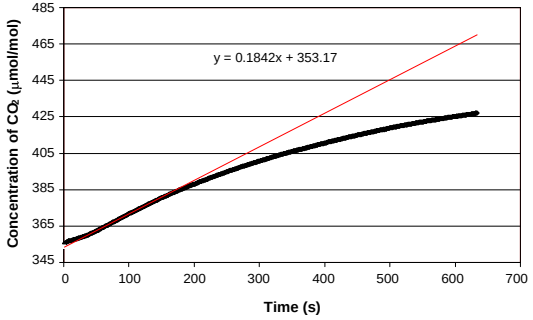

KM01100306

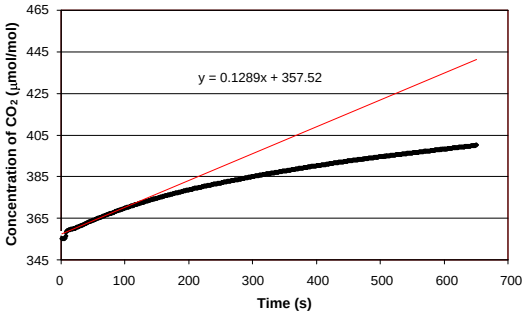

KM01100309

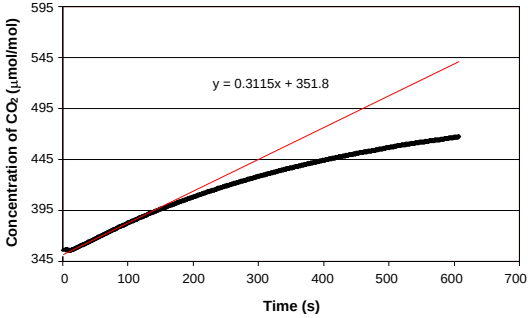

KM01100312

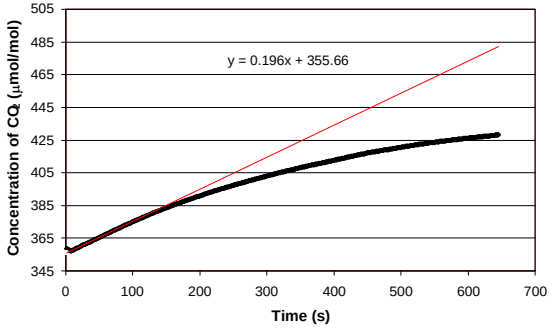

KM01100313

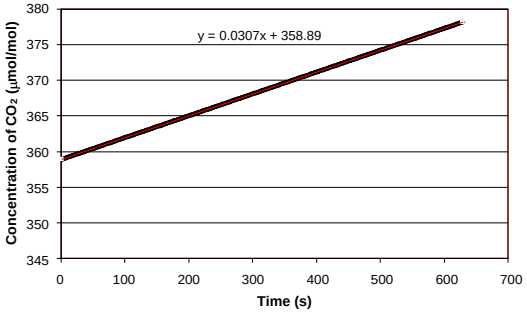

KM01100316

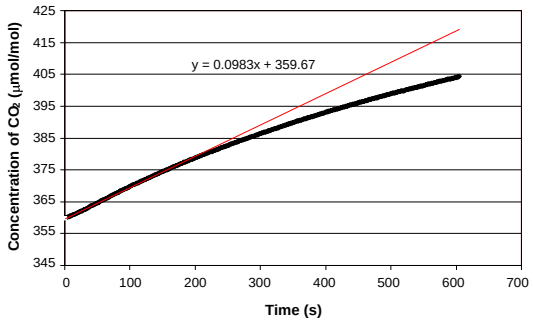

KM01100319

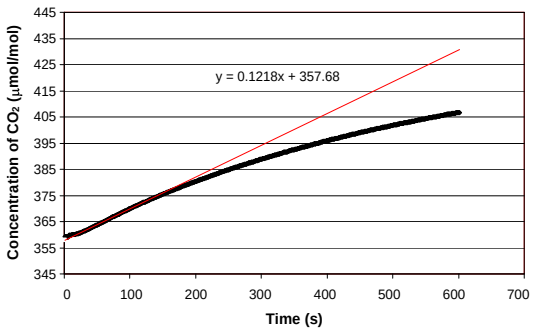

KM01100314

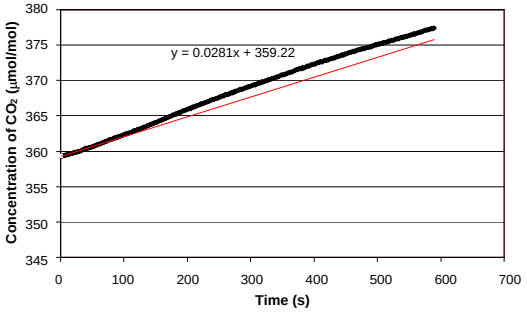

KM01100317

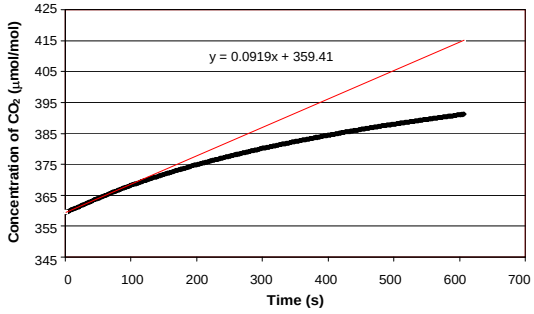

KM01100320

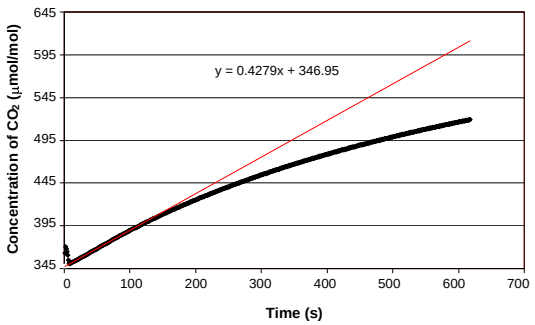

KM01100315

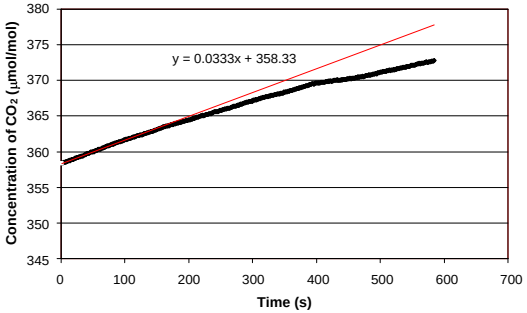

KM01100318

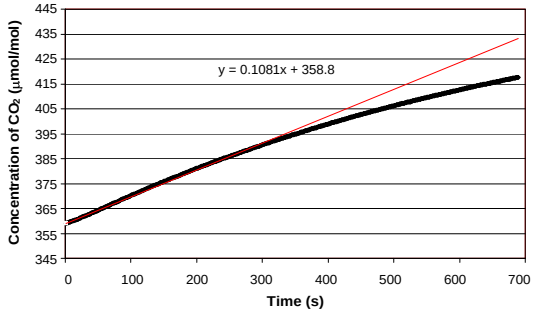

KM01110301

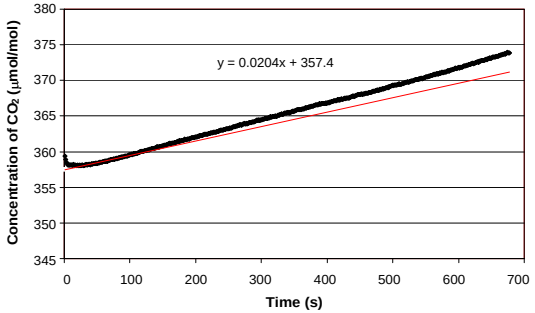

KM01110302

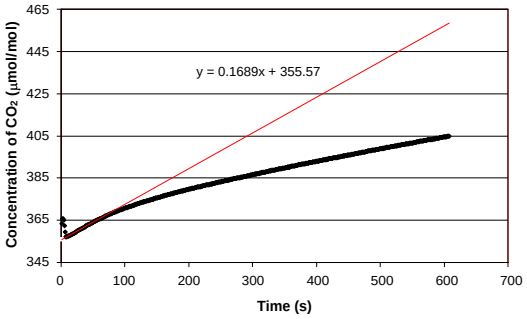

KM01110305

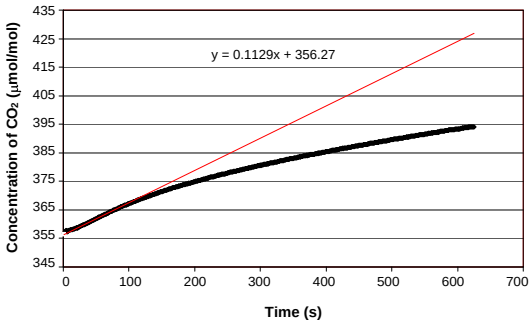

KM01110308

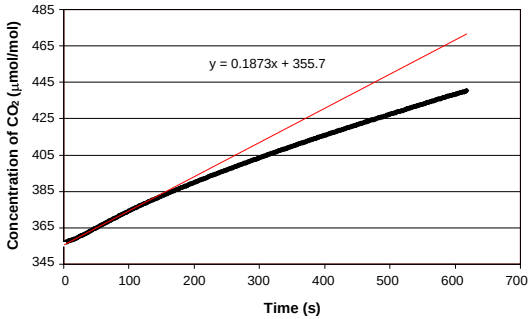

KM01110303

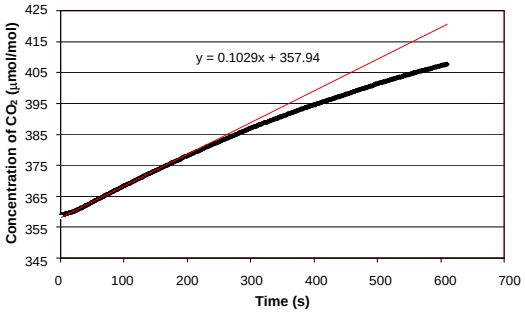

KM01110306

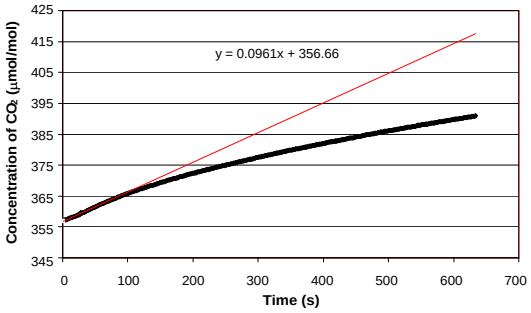

KM01110309

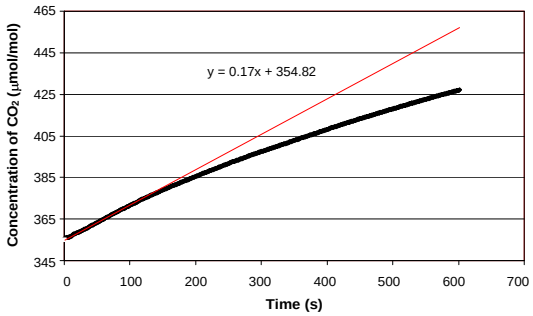

KM01110304

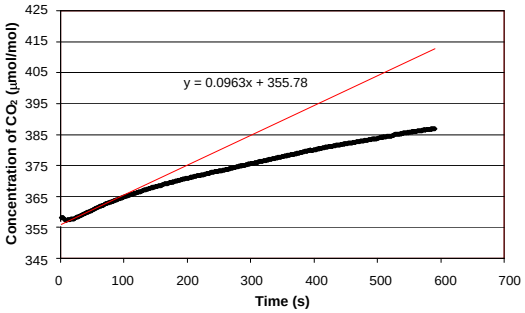

KM01110307

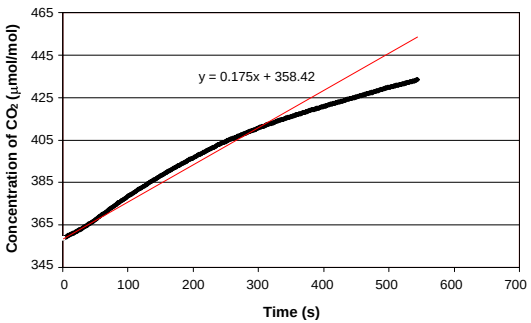

KM01110310

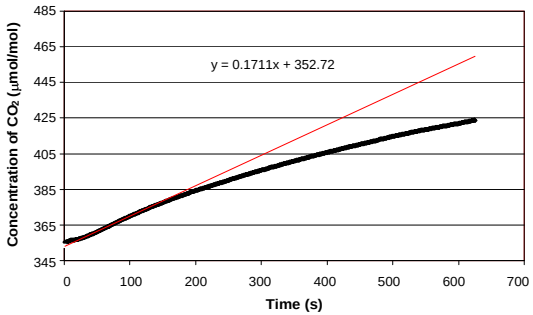

KM01110311

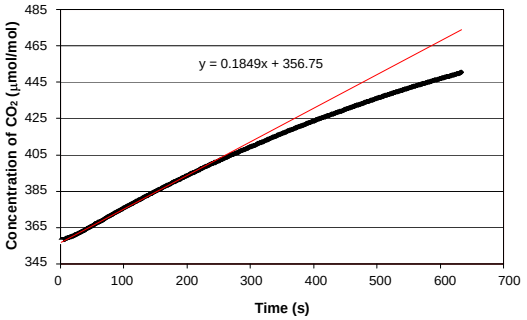

KM01110314

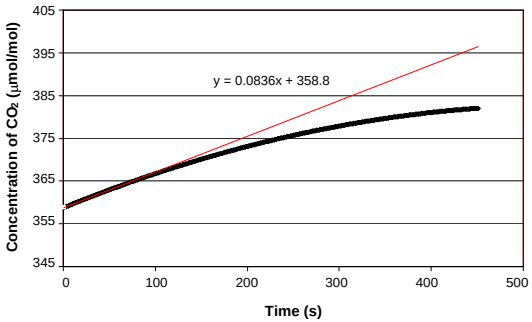

KM01110317

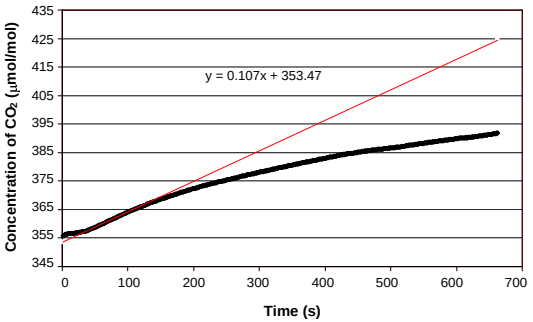

KM01110312

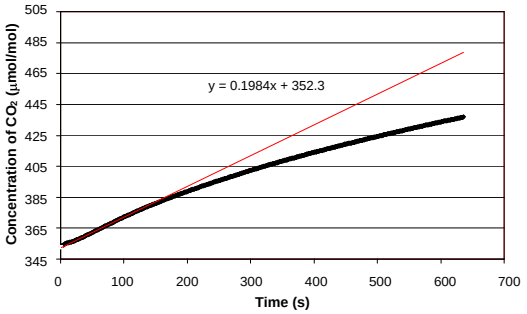

KM01110315

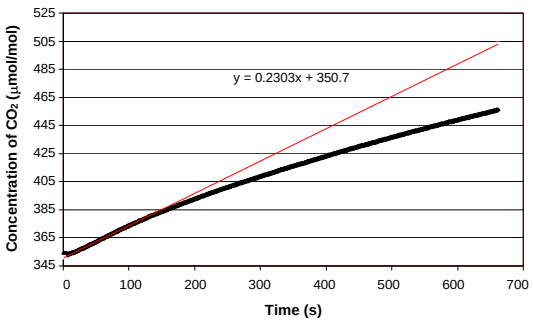

KM01110318

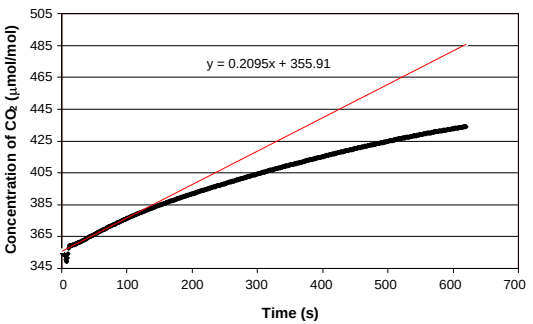

KM01110313

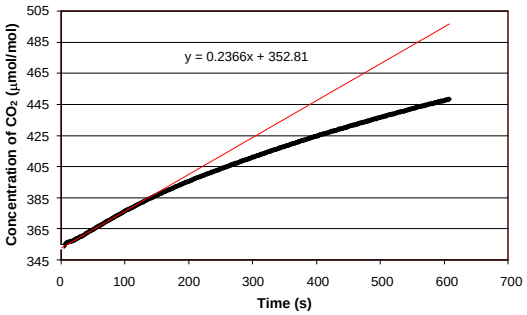

KM01110316

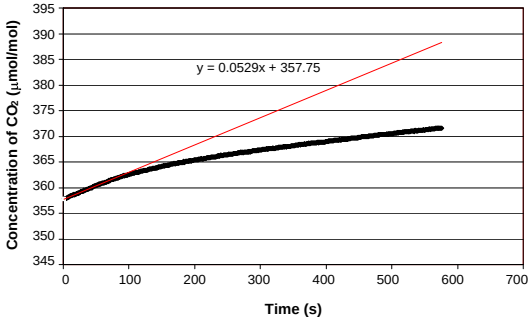

KM01110319

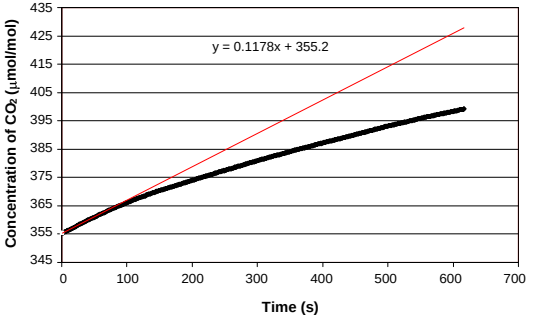

KM01110320

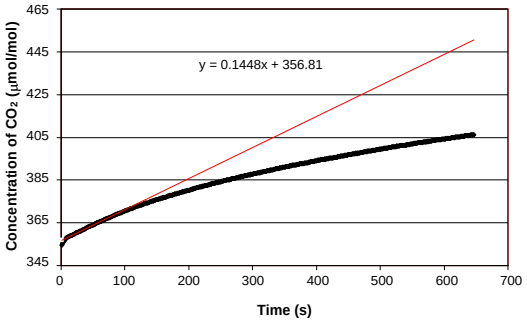

KM01110323

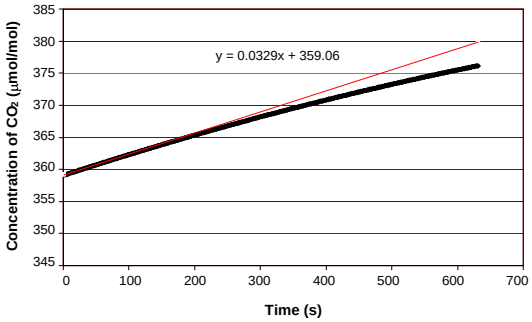

KM01120302

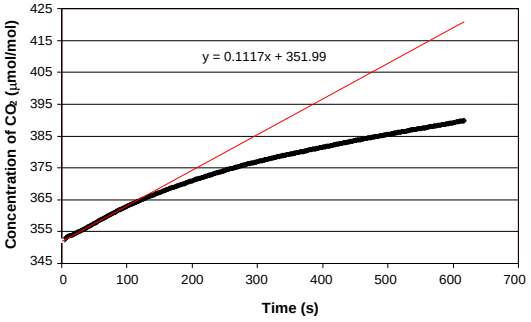

KM01110321

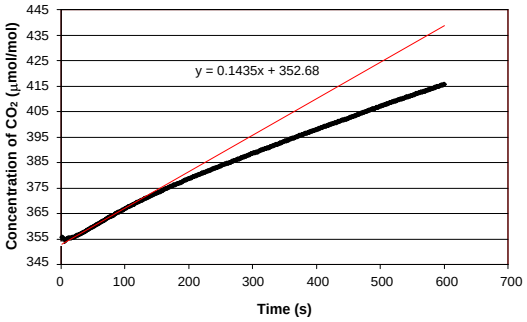

KM01110324

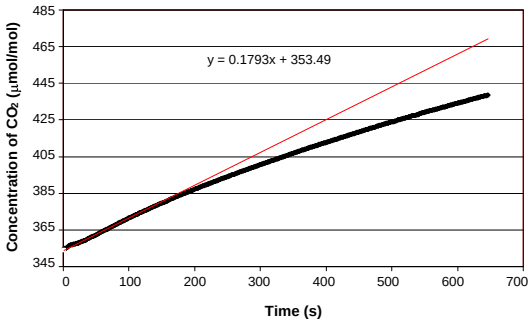

KM01120303

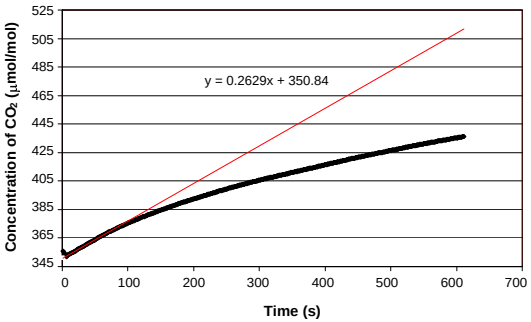

KM01110322

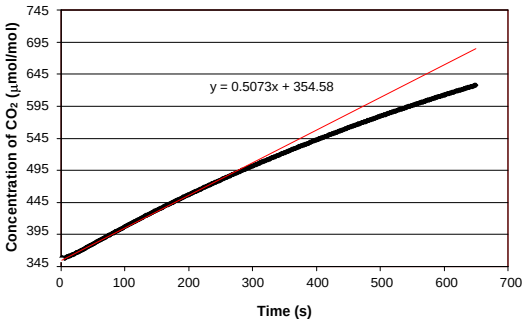

KM01120301

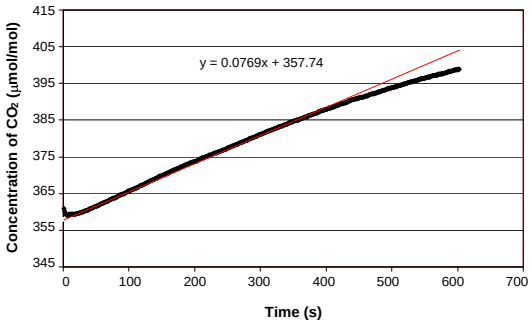

KM01120304

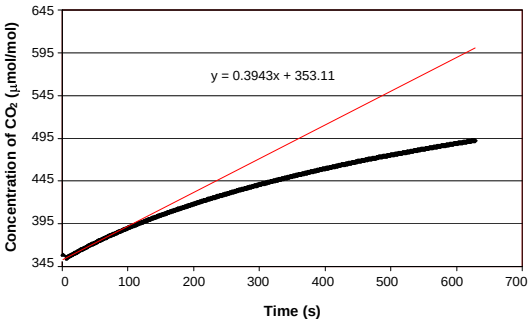

KM01120305

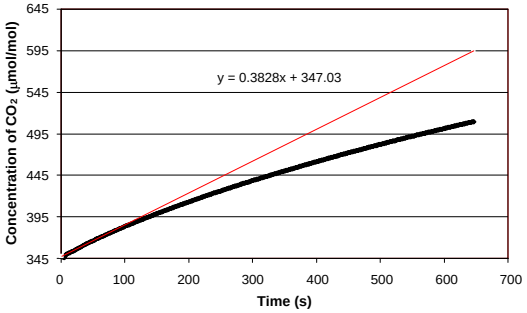

KM01120308

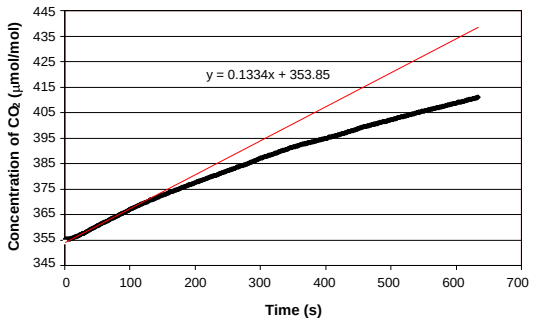

KM01120311

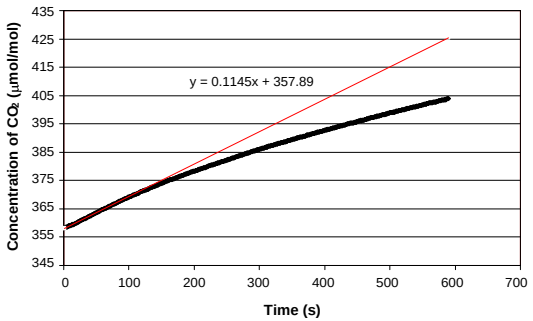

KM01120306

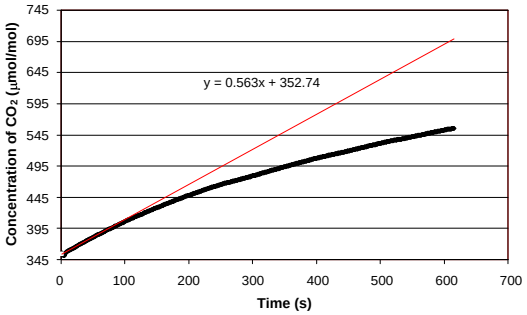

KM01120309

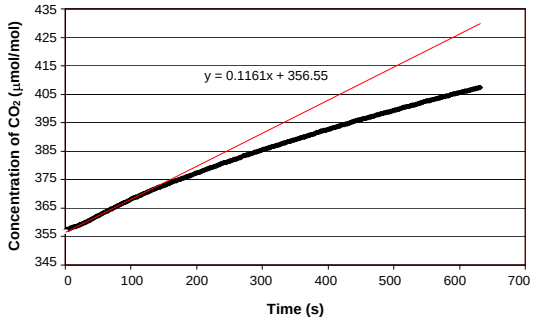

KM01120312

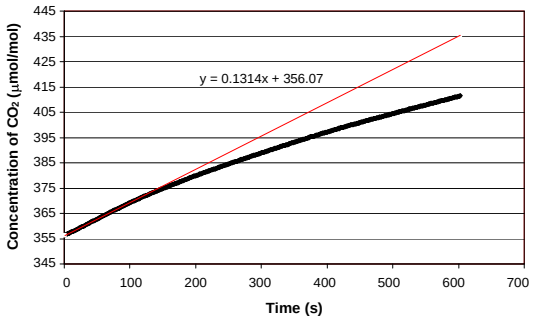

KM01120307

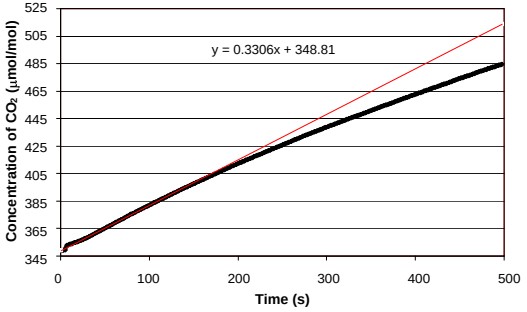

KM01120310

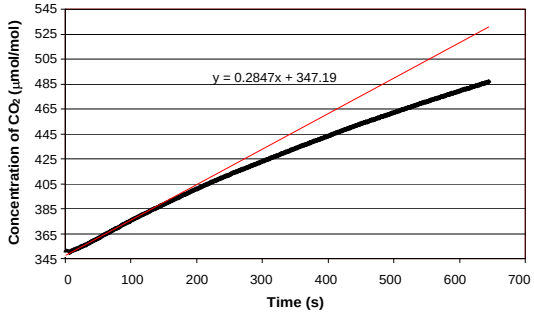

KM01120313

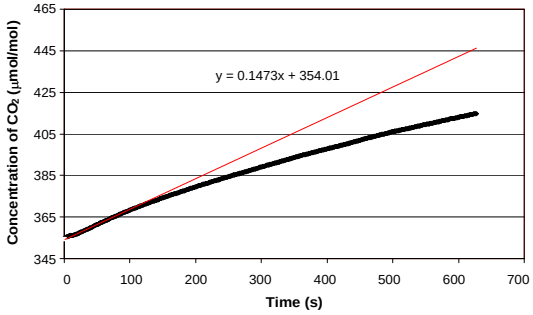

KM01120314

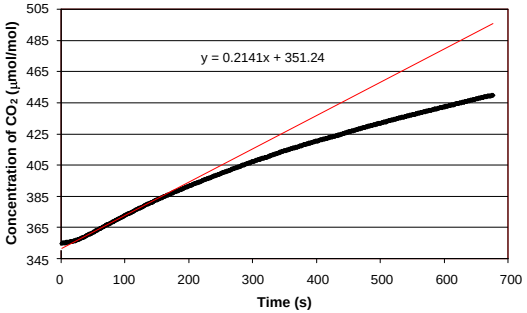

KM01120317

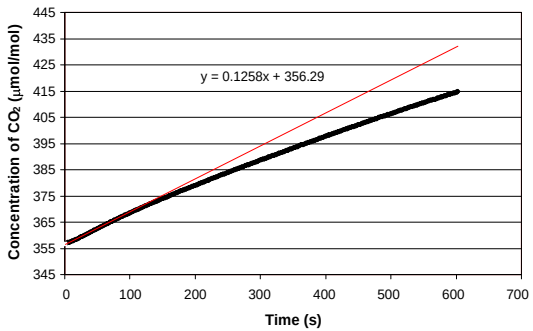

KM01130301

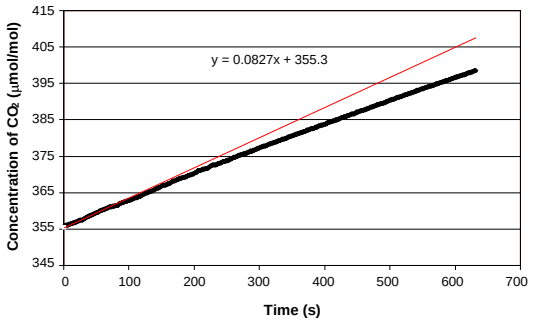

KM01120315

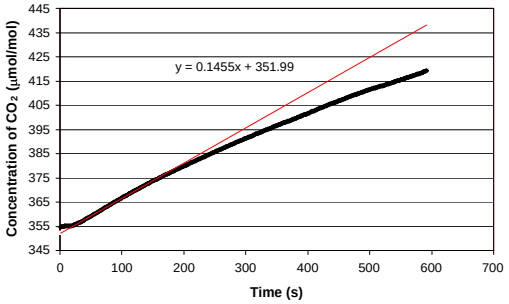

KM01120318

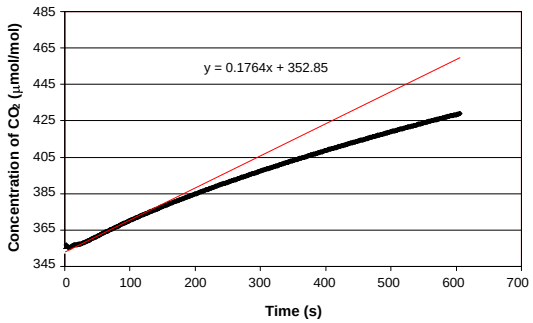

KM01130302

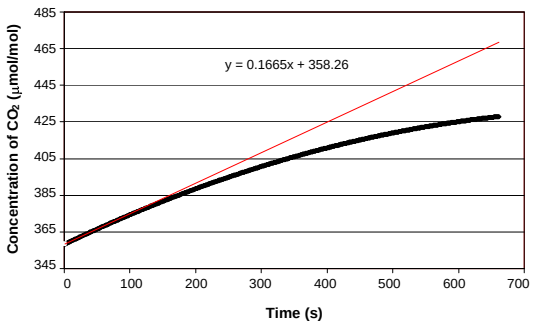

KM01120316

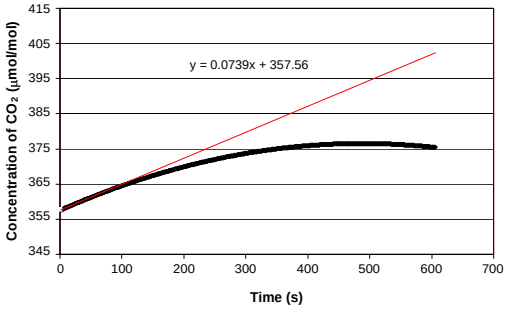

KM01120319

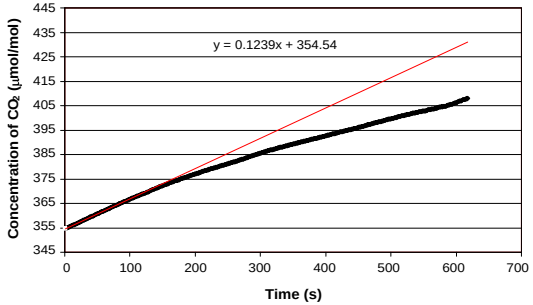

KM01130303

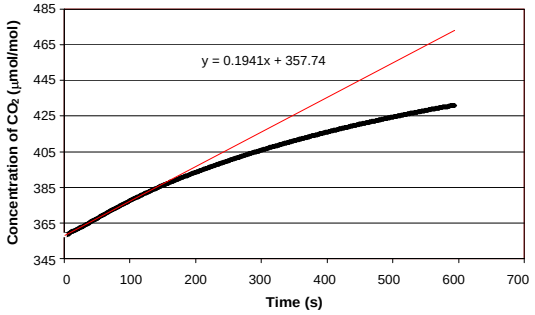

KM01130304

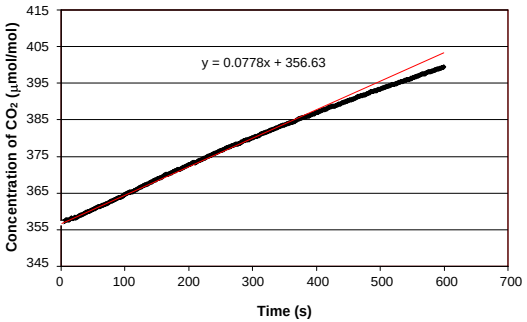

KM01130307

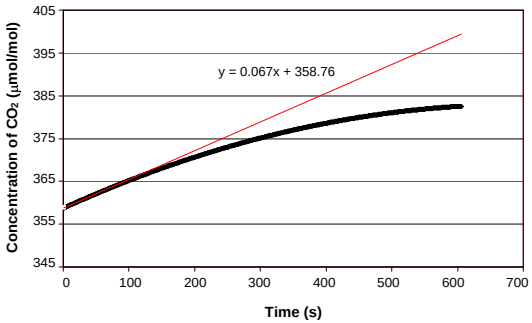

KM01130310

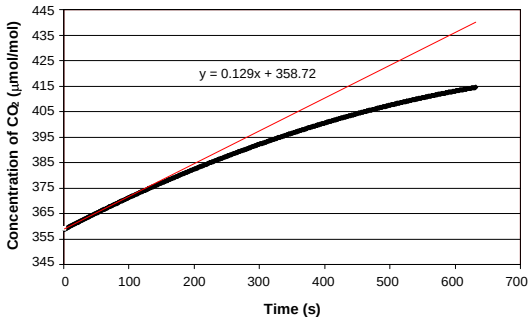

KM01130305

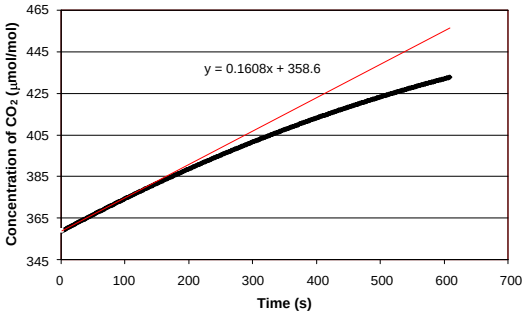

KM01130308

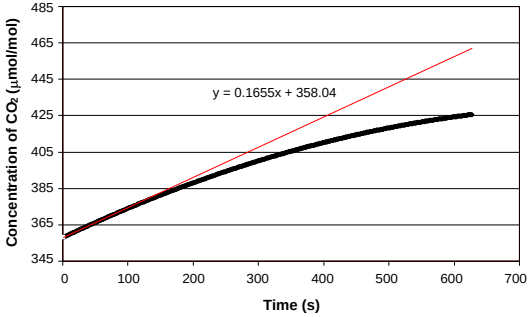

KM01130311

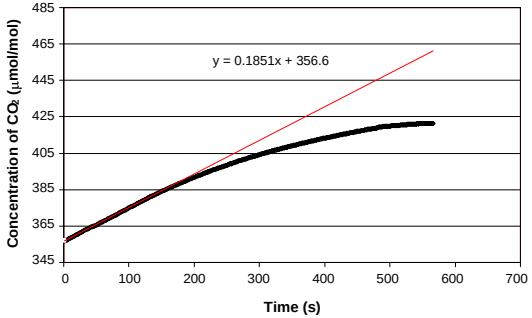

KM01130306

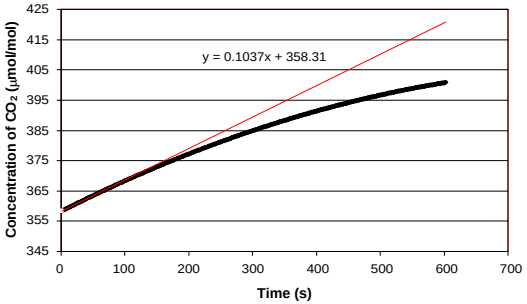

KM01130309

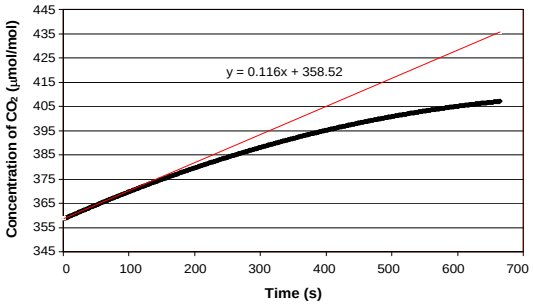

KM01130312

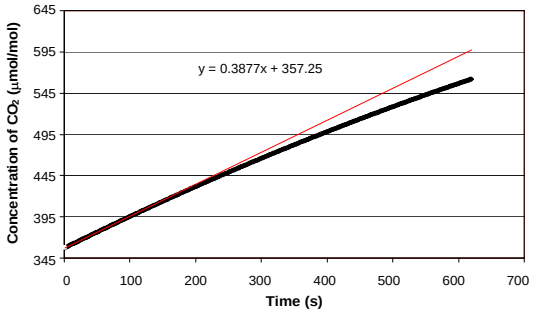

KM01130313

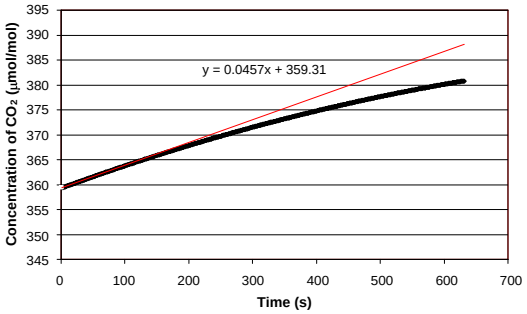

KM01130316

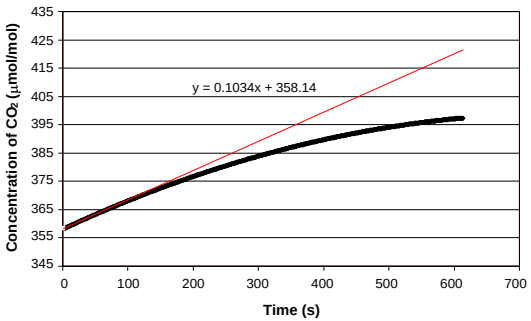

KM01140301

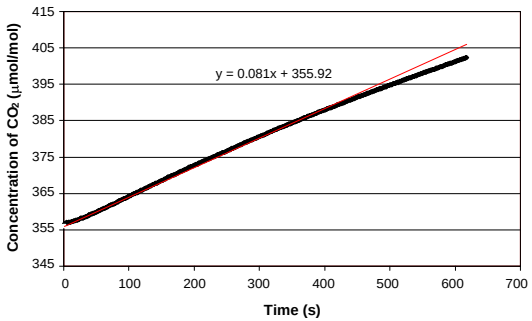

KM01130314

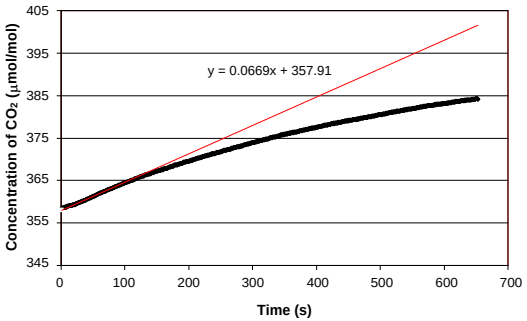

KM01130317

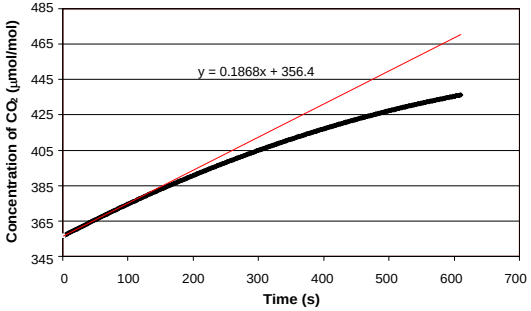

KM01140302

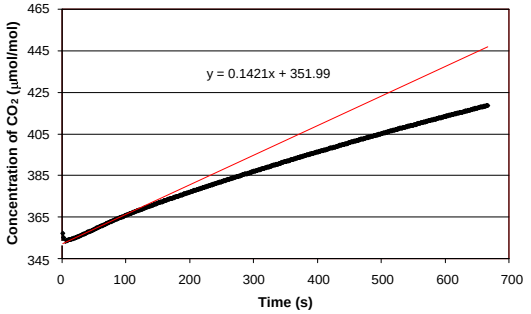

KM01130315

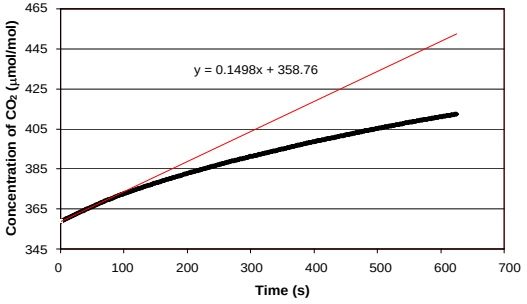

KM01130318

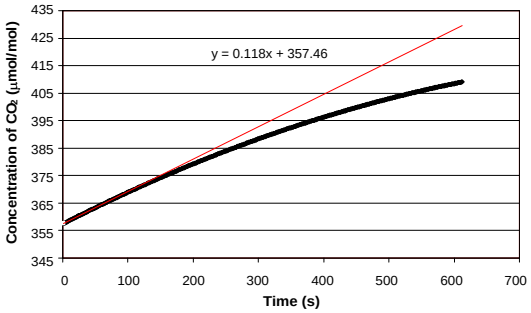

KM01140303

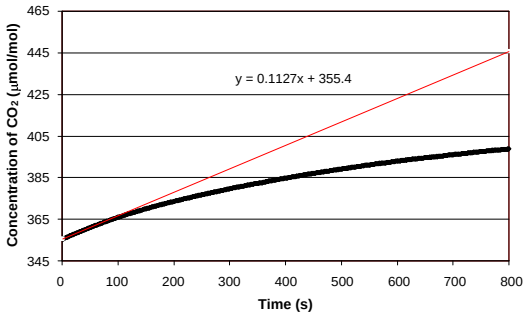

KM01140304

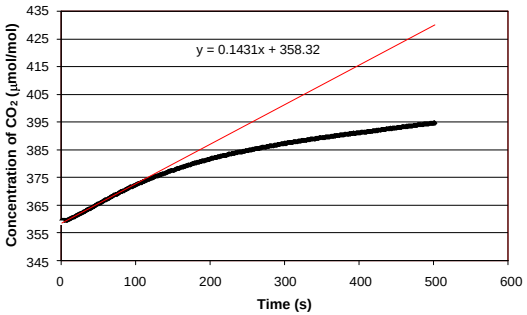

KM01140307

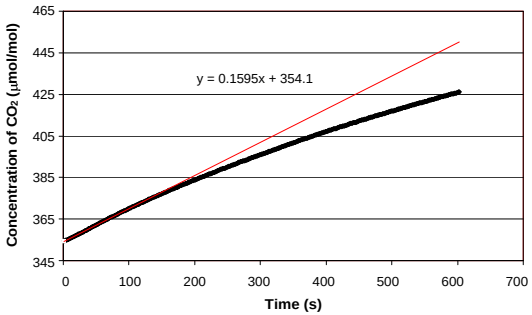

KM01140310

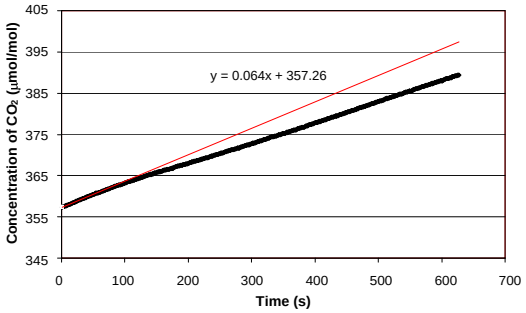

KM01140305

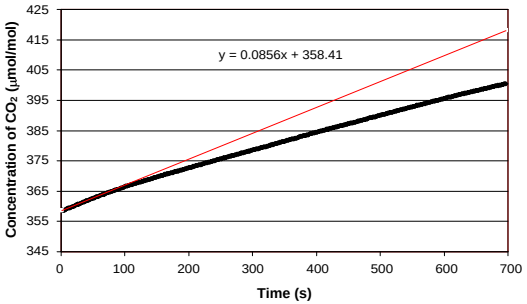

KM01140308

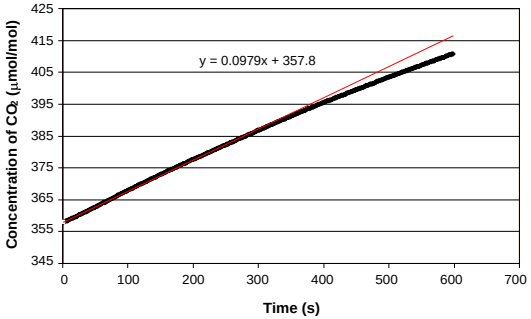

KM01140311

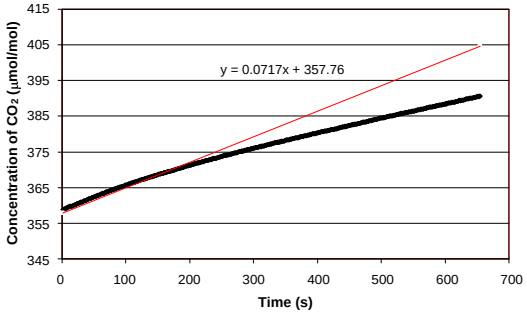

KM01140306

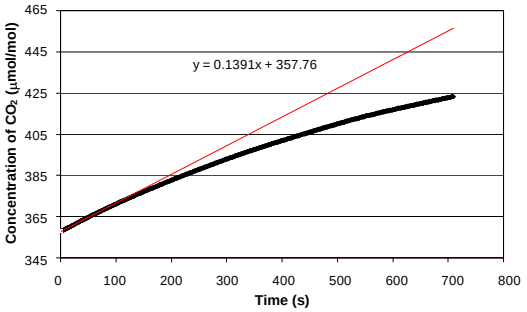

KM01140309

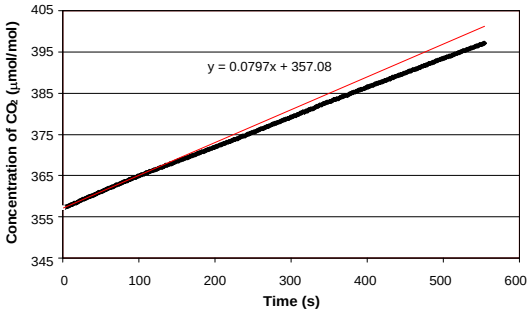

KM09170301

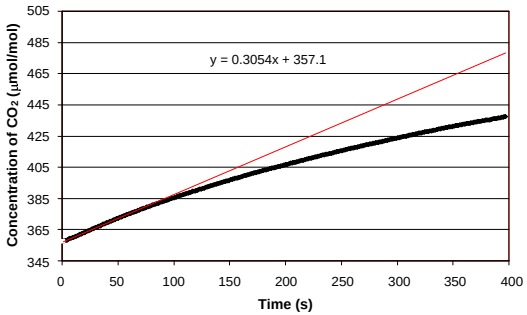

KM09170302

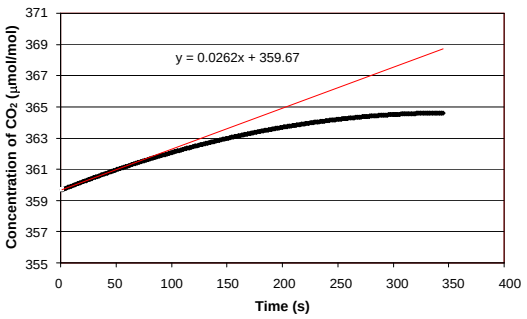

KM09170305

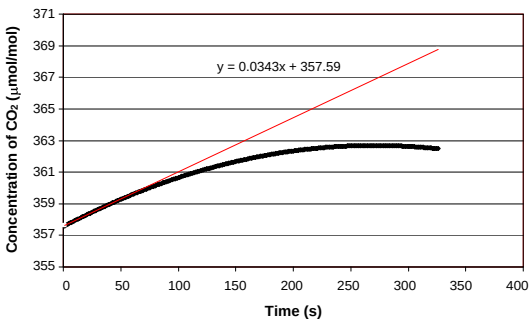

KM09170308

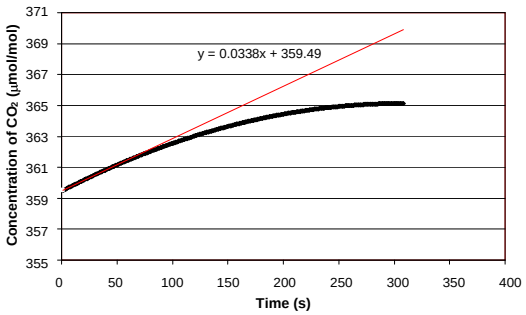

KM09170303

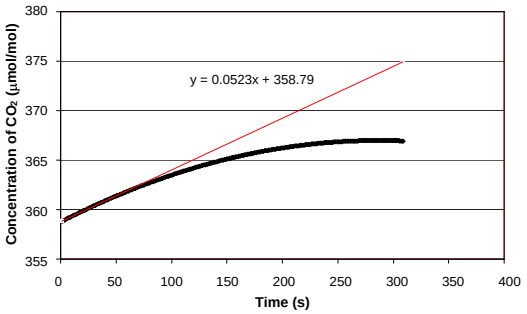

KM09170306

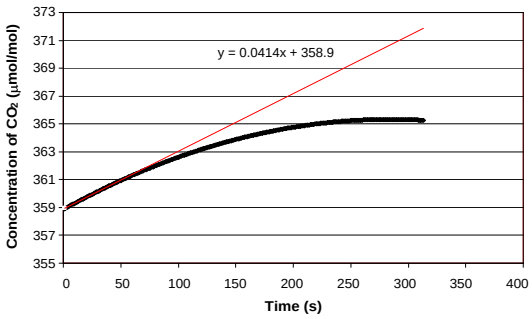

KM09170309

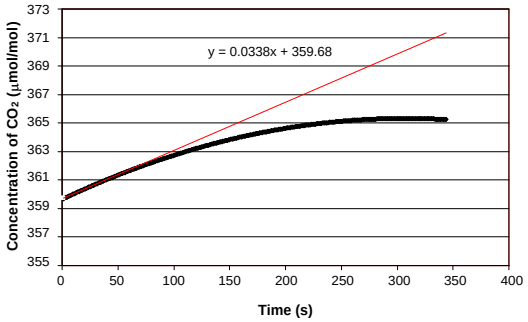

KM09170304

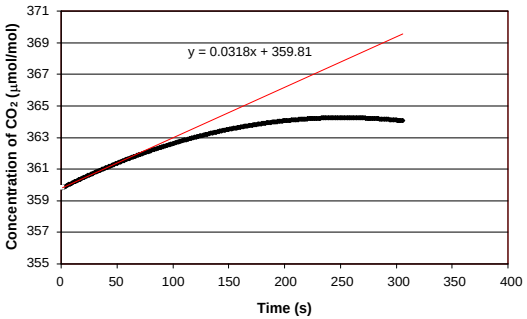

KM09170307

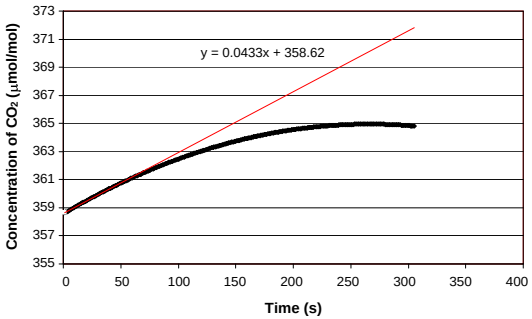

KM09170310

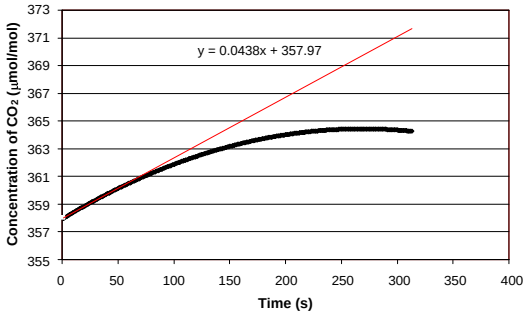

KM09170311

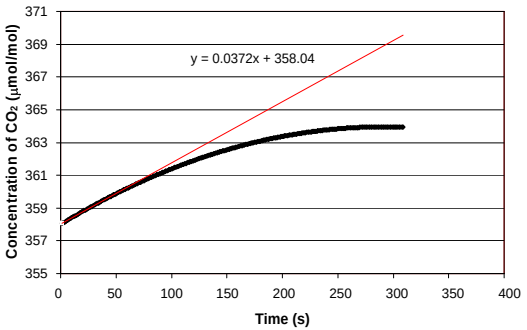

KM09170314

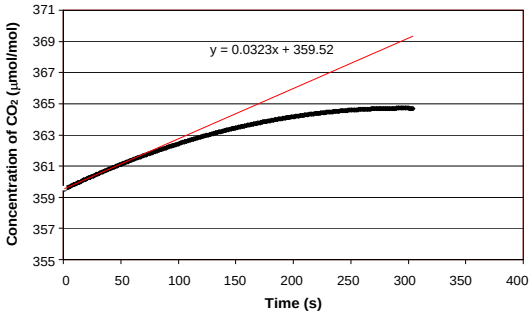

KM09170317

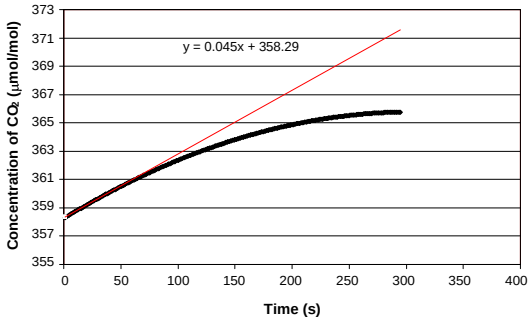

KM09170312

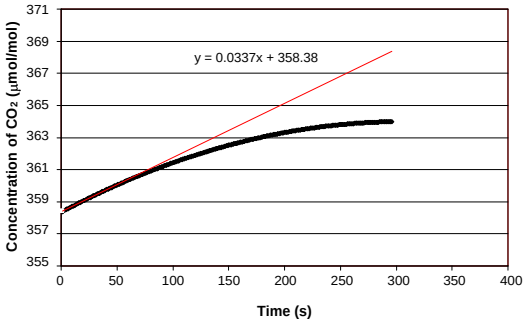

KM09170315

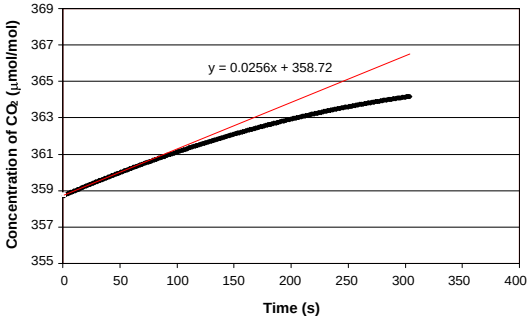

KM09170318

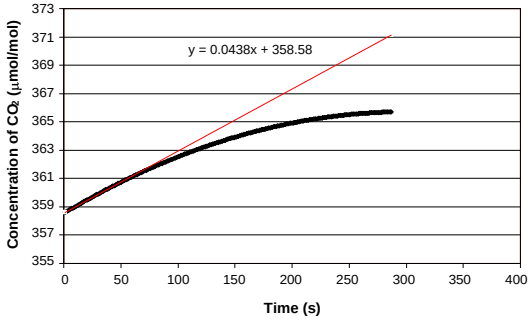

KM09170313

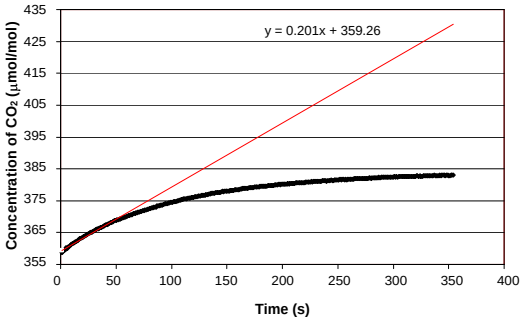

KM09170316

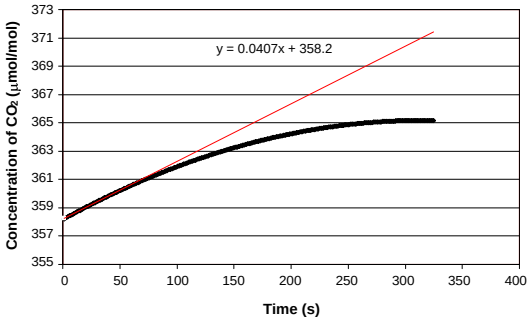

KM09170319

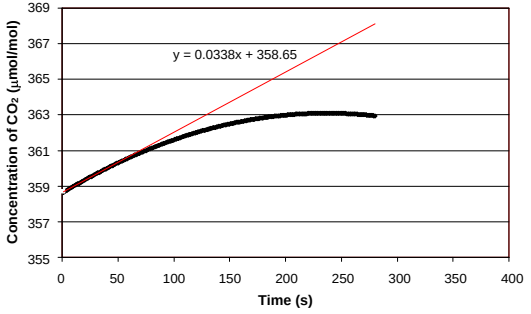

KM09170320

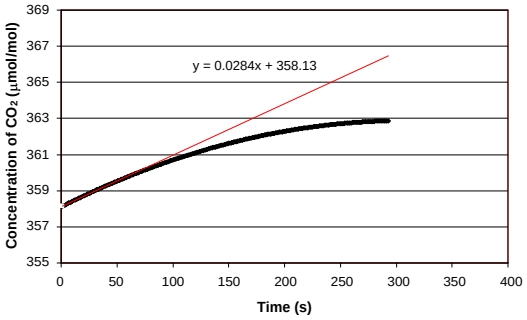

KM09180303

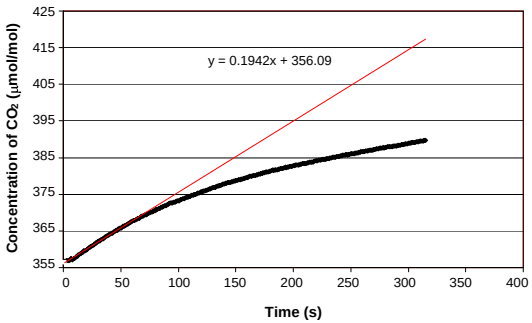

KM09180306

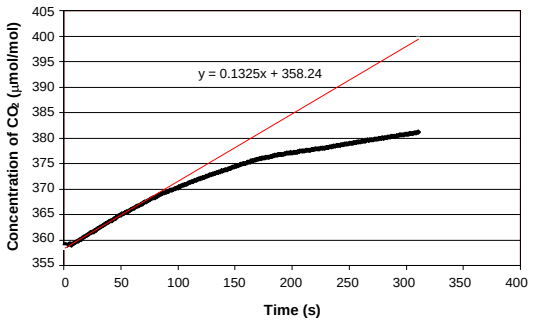

KM09180301

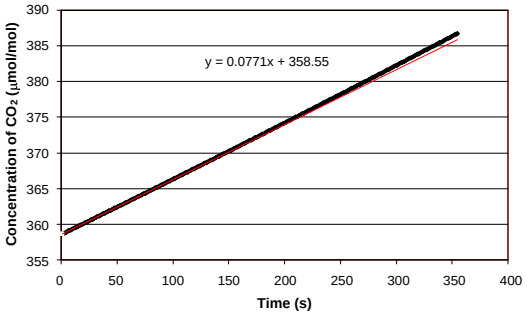

KM09180304

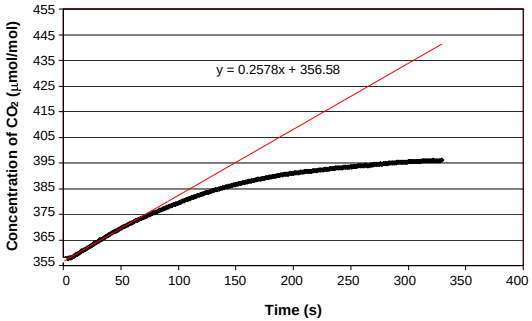

KM09180307

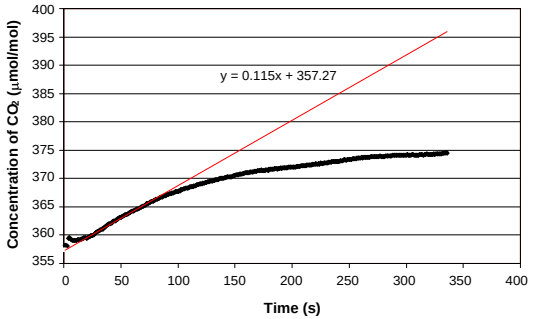

KM09180302

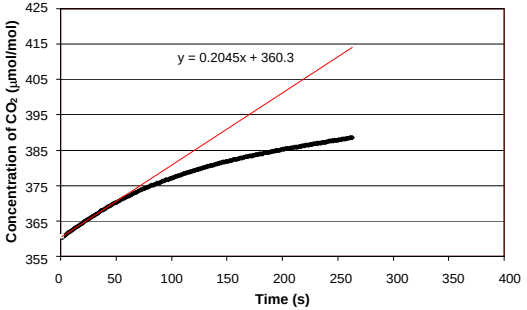

KM09180305

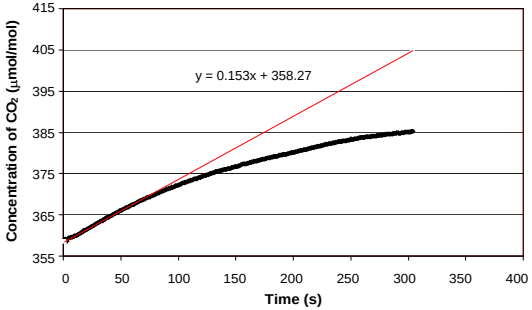

KM09180308

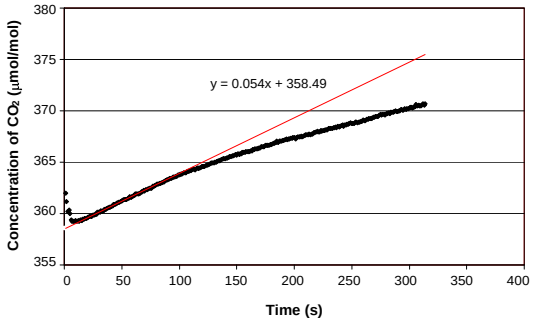

KM09180309

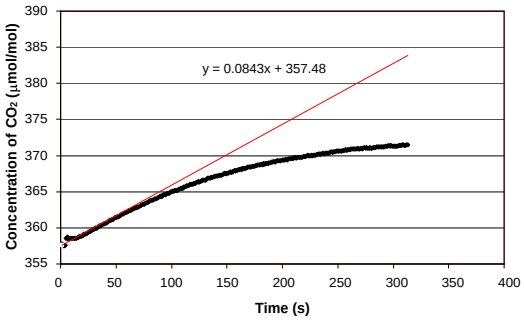

KM09180312

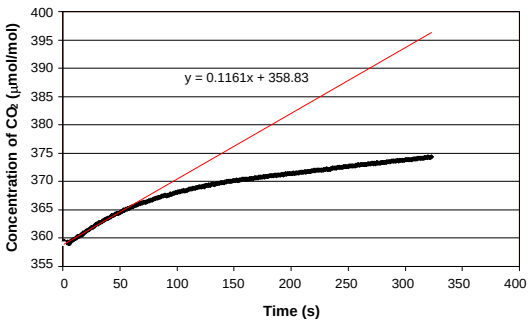

KM09180315

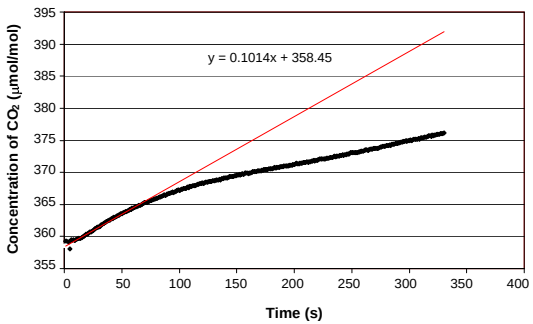

KM09180310

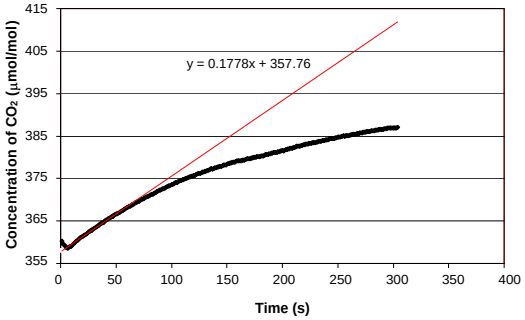

KM09180313

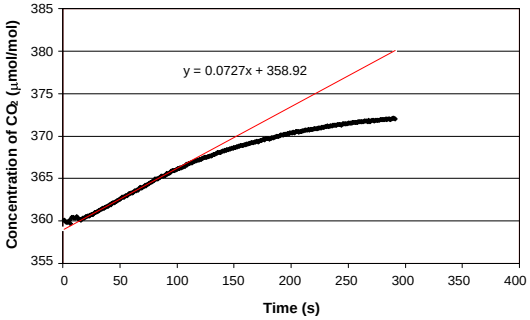

KM09180316

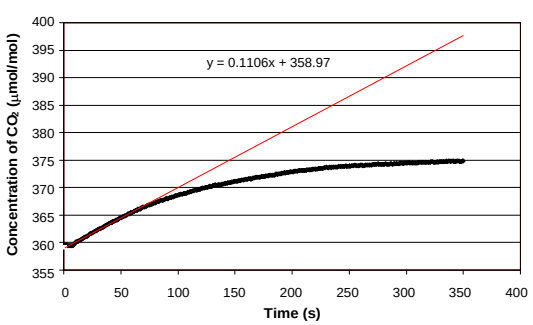

KM09180311

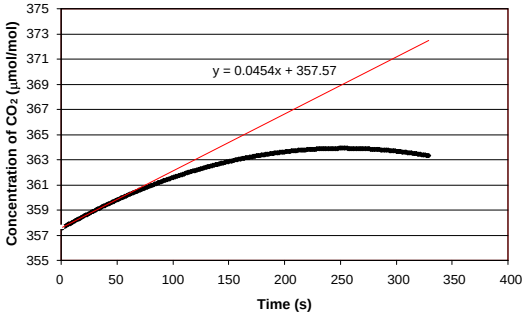

KM09180314

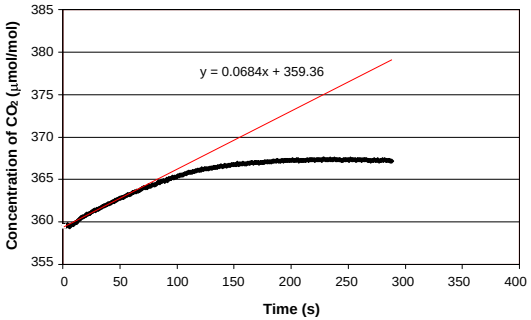

KM09180317

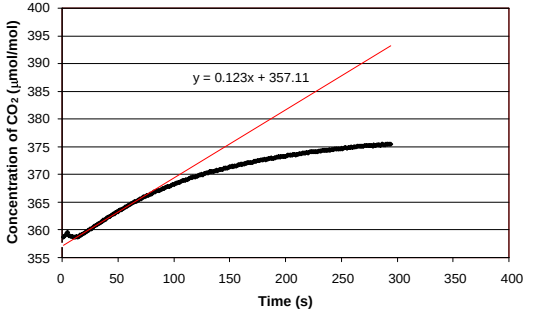

KM09180318

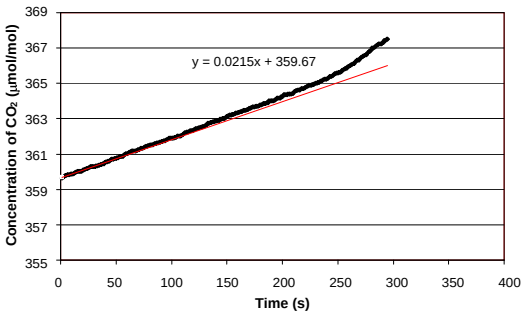

KM09180321

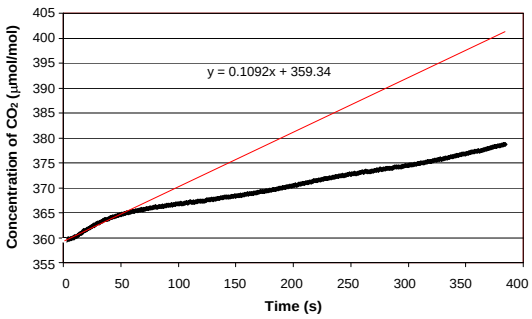

KM09180324

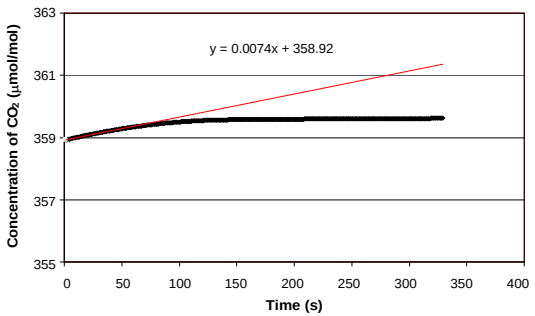

KM09180319

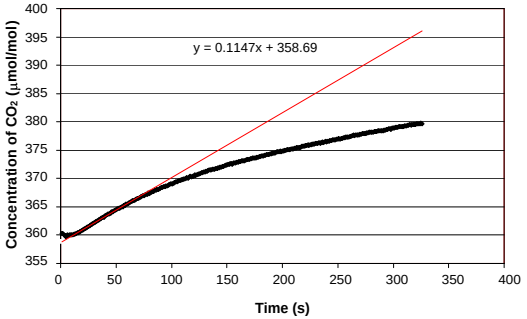

KM09180322

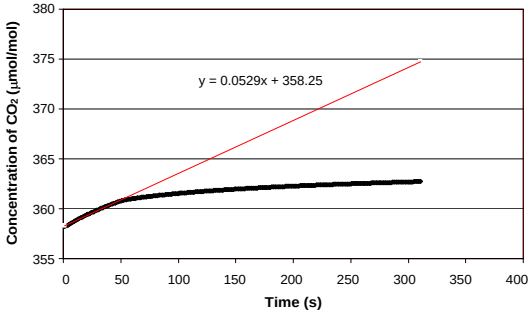

KM09180325

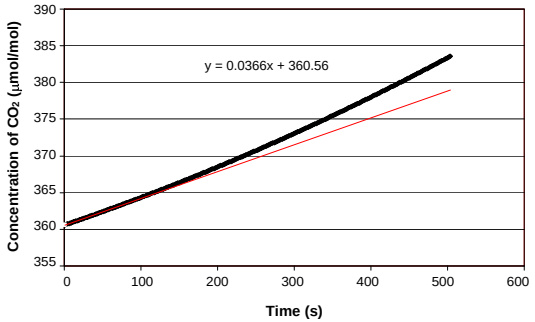

KM09180320

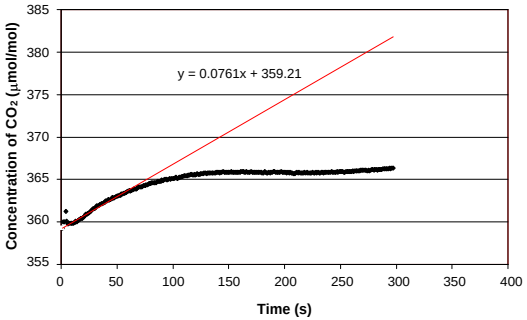

KM09180323

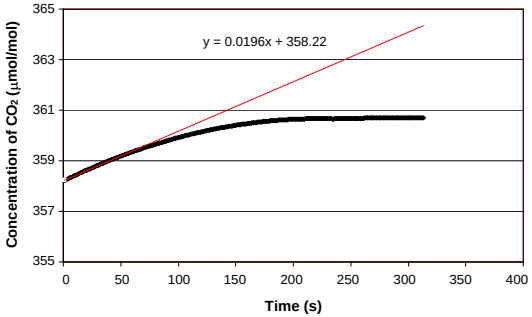

KM09180326

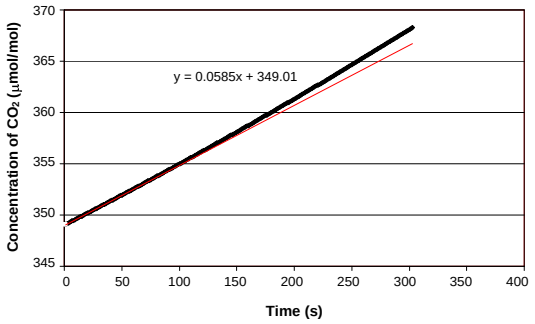

KM09180327

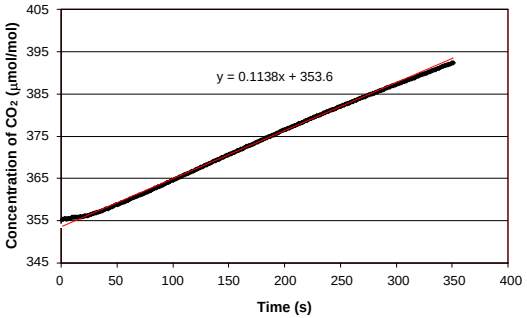

KM09180330

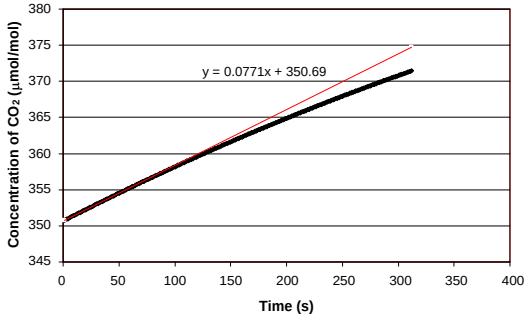

KM09180333

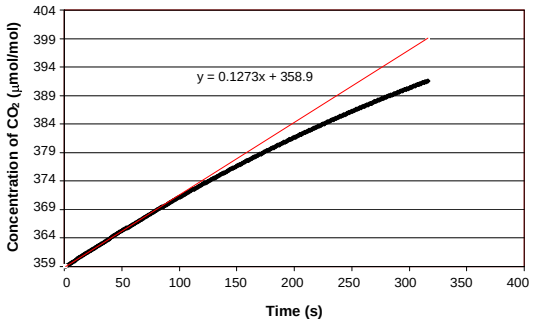

KM09180328

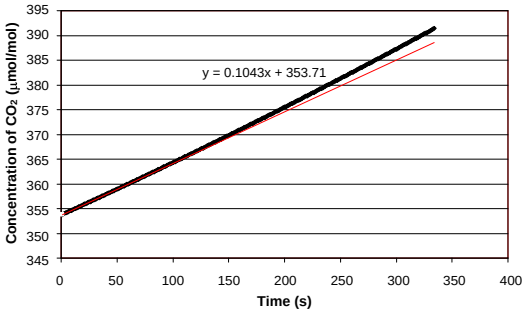

KM09180331

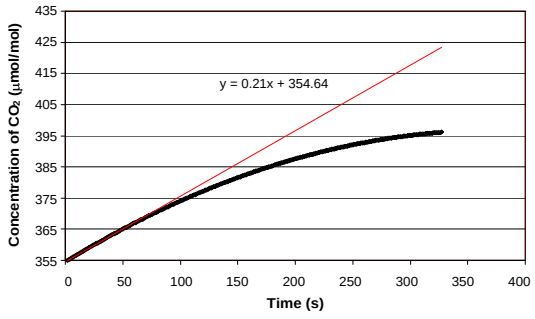

KM09180334

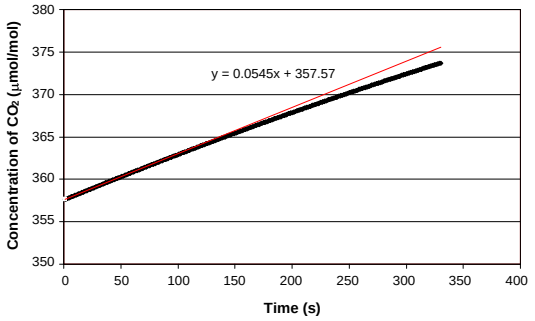

KM09180329

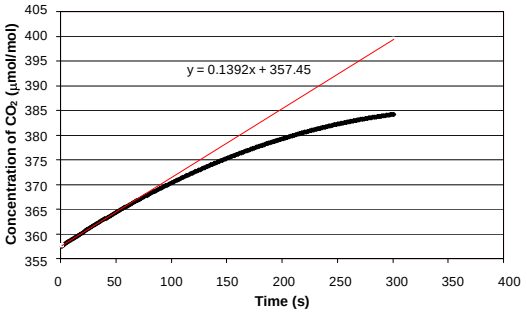

KM09180332

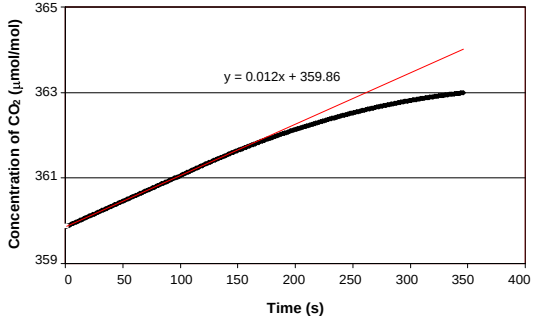

KM09180335

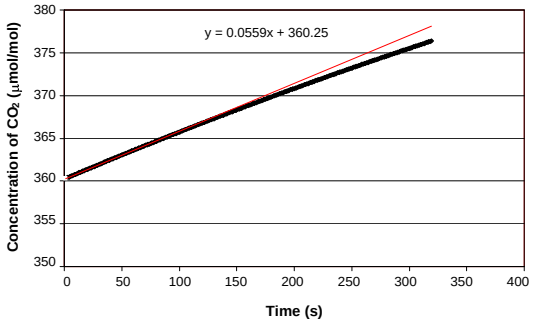

KM09180336

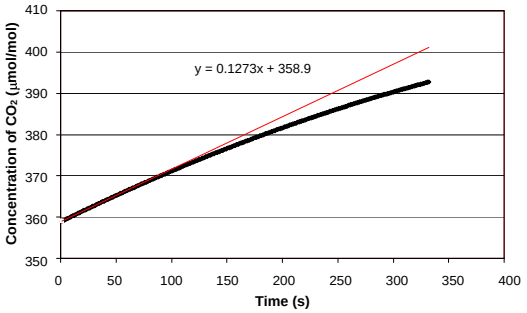

KM09180339

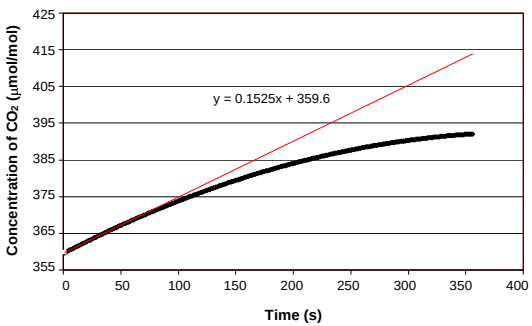

KM09190302

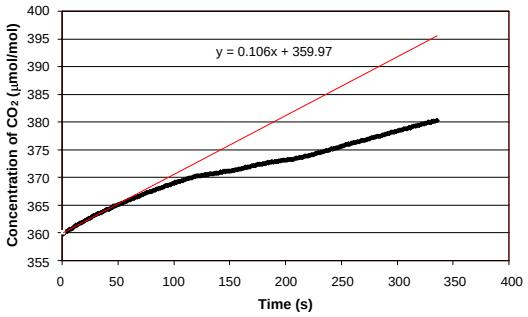

KM09180337

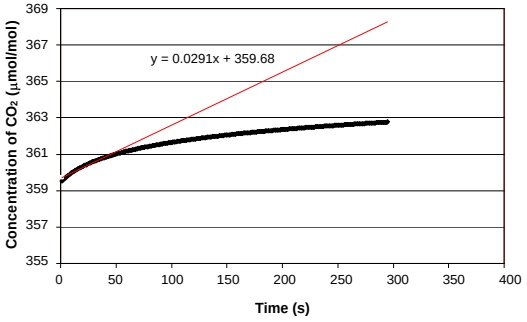

KM09180340

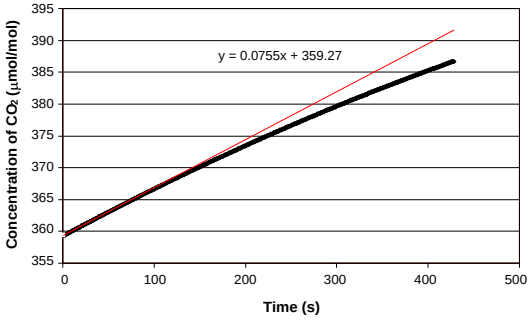

KM09190303

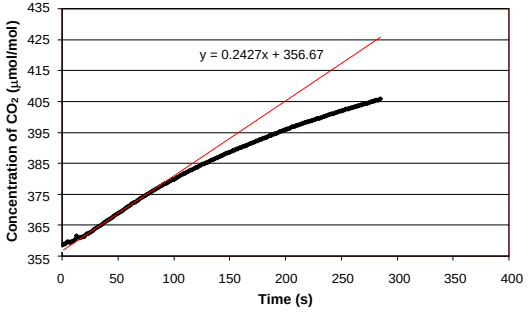

KM09180338

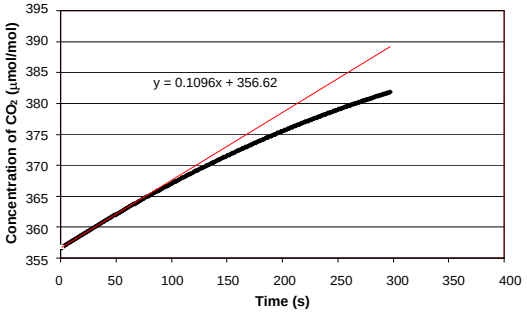

KM09190301

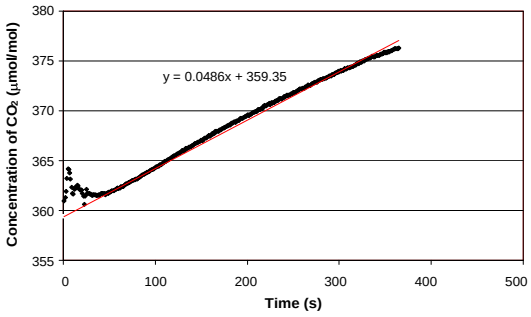

KM09190304

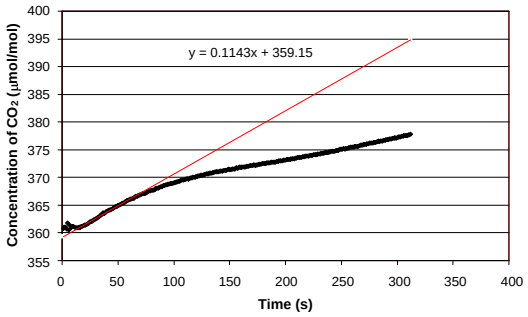

KM09190305

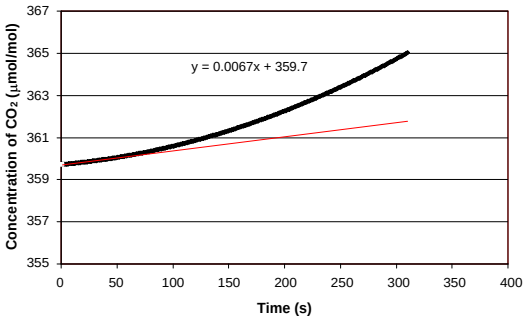

KM09190308

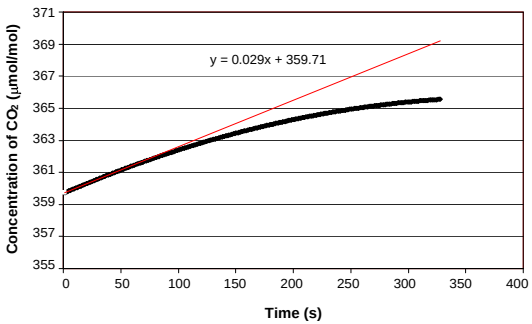

KM09190311

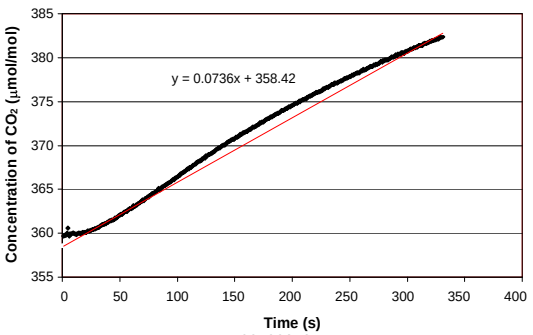

KM09190306

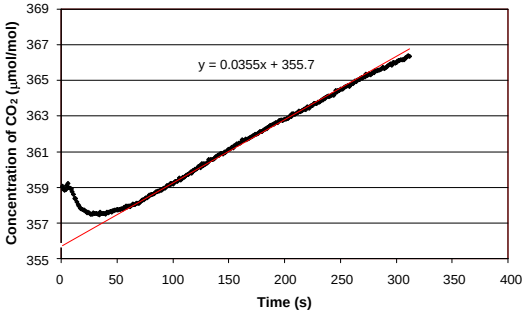

KM09190309

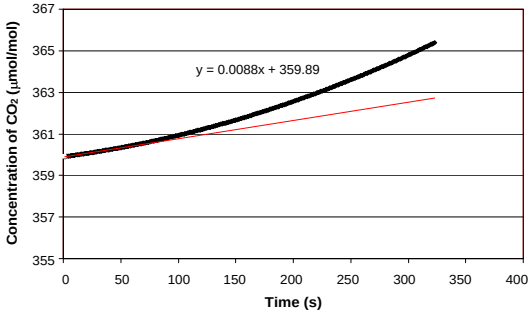

KM09190312

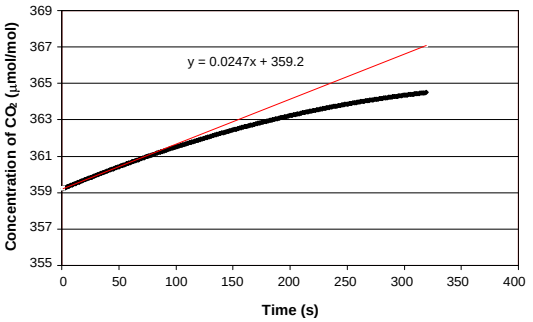

KM09190307

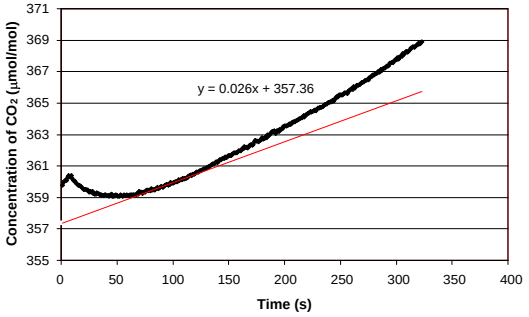

KM09190310

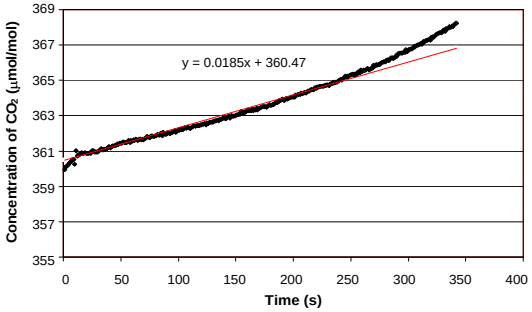

KM09190313

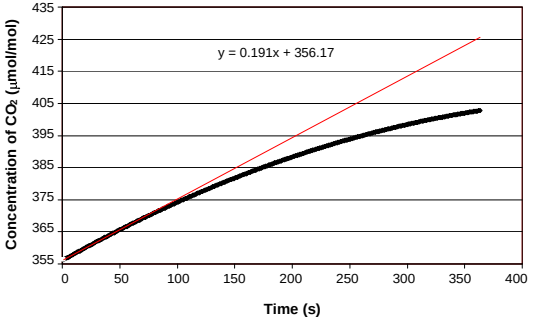

KM09190314

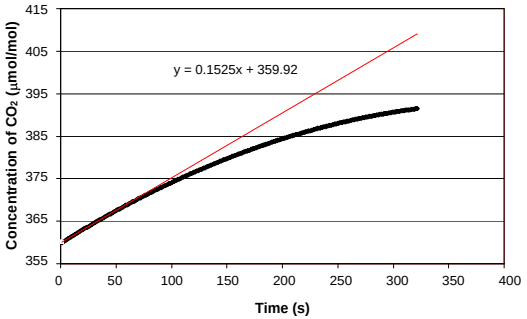

KM09190317

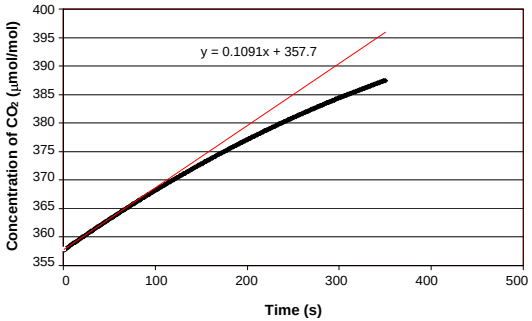

KM09190320

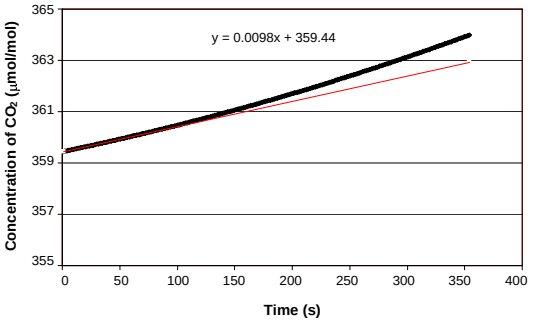

KM09190315

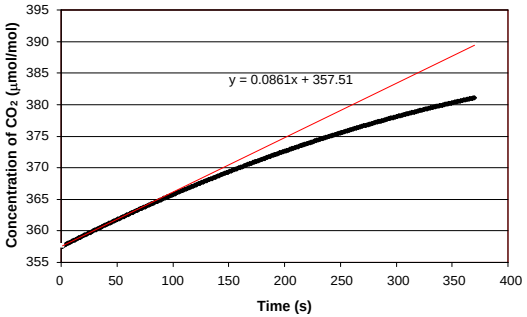

KM09190318

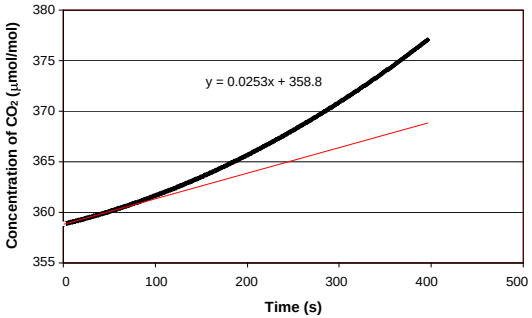

KM09190321

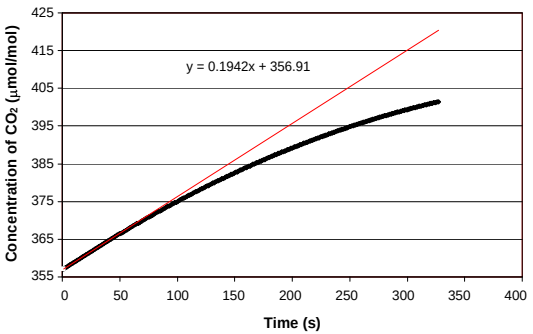

KM09190316

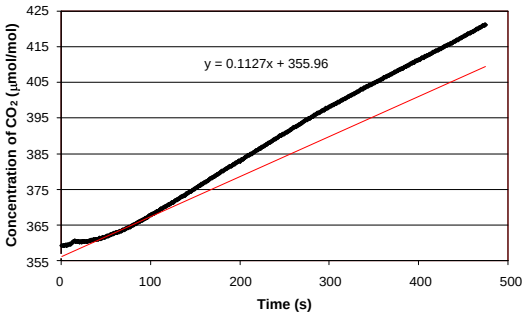

KM09190319

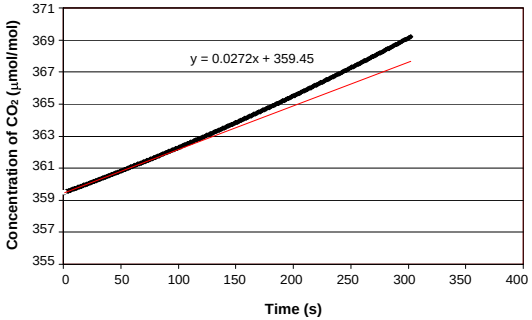

KM09190322

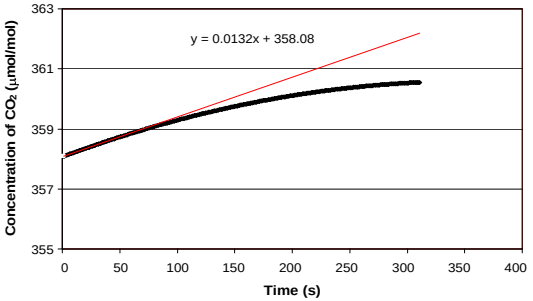

KM09190323

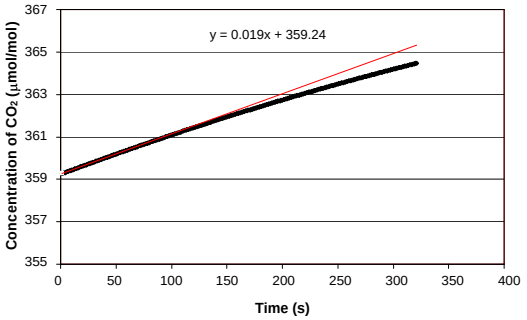

KM09190326

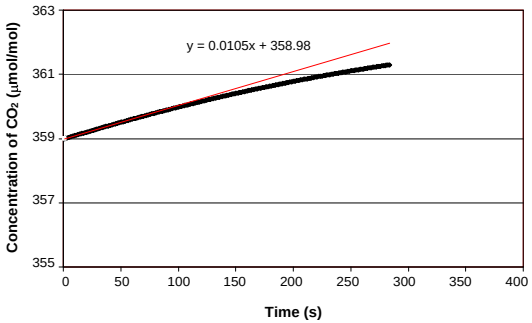

KM09190329

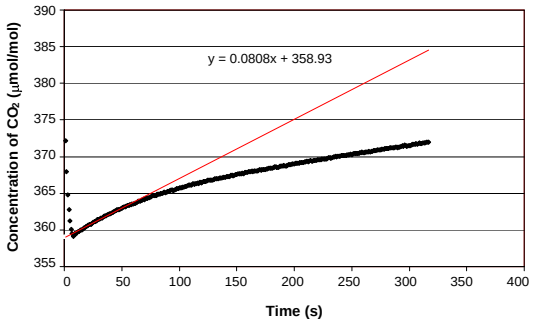

KM09190324

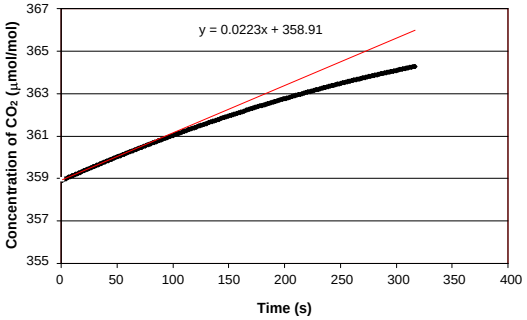

KM09190327

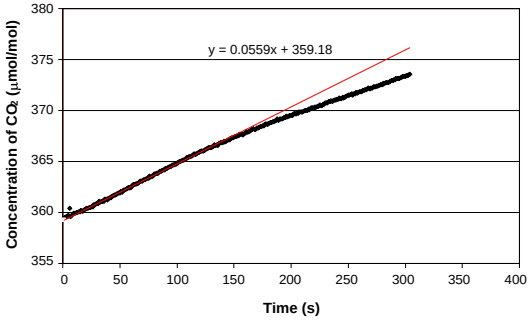

KM09190330

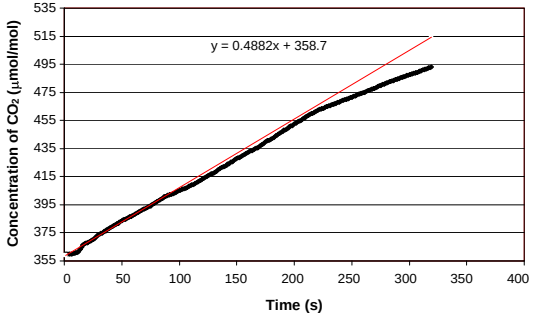

KM09190325

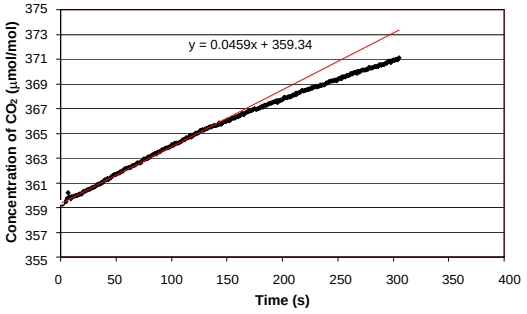

KM09190328

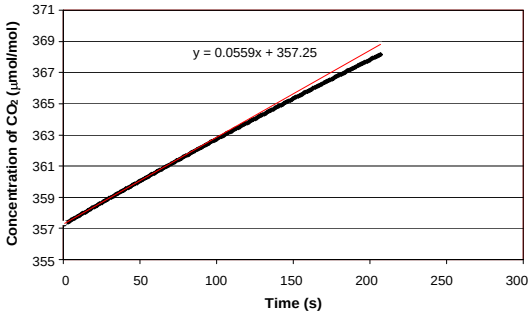

KM09190331

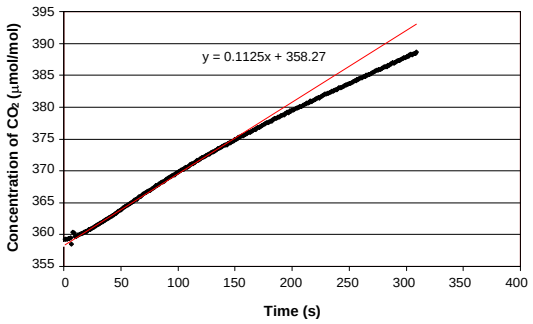

KM09200301

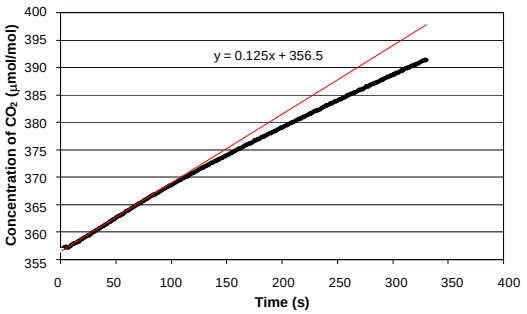

KM09200304

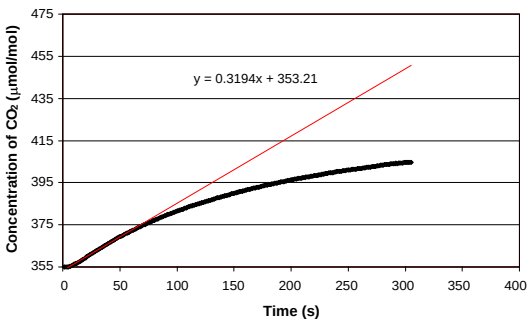

KM09200307

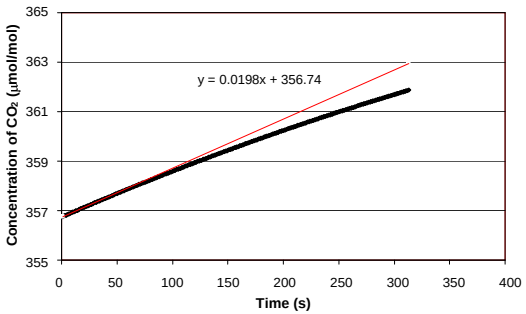

KM09200302

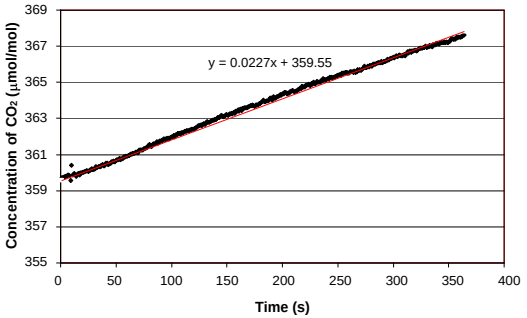

KM09200305

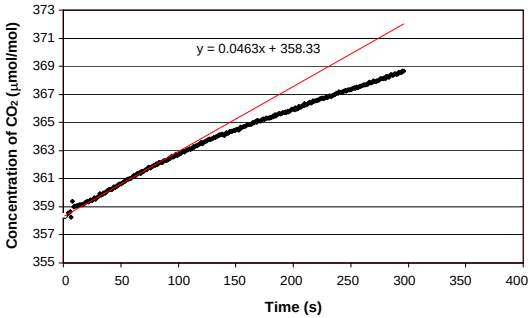

KM09200308

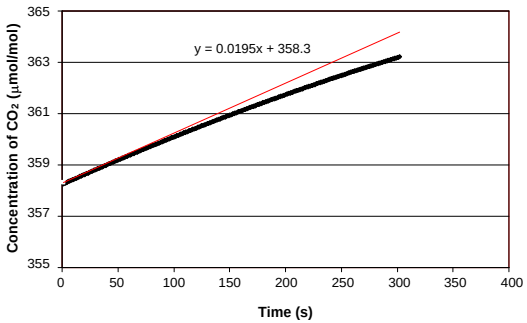

KM09200303

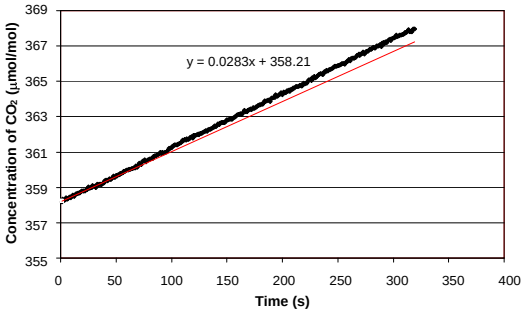

KM09200306

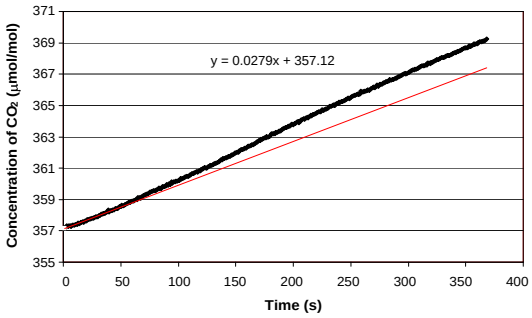

KM09200309

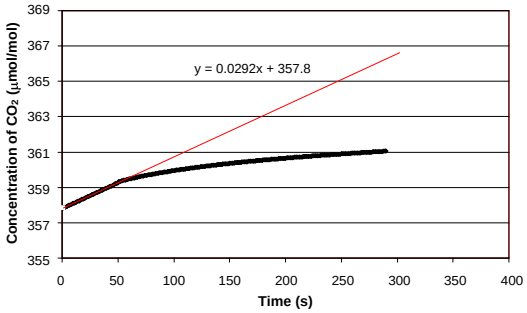

KM09200310

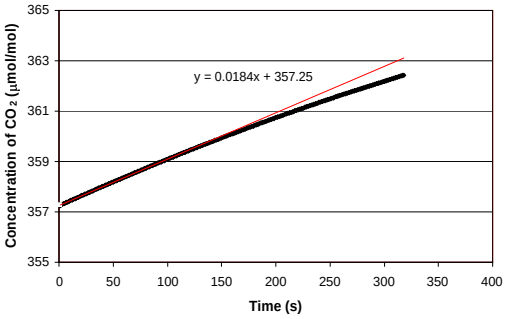

KM09200313

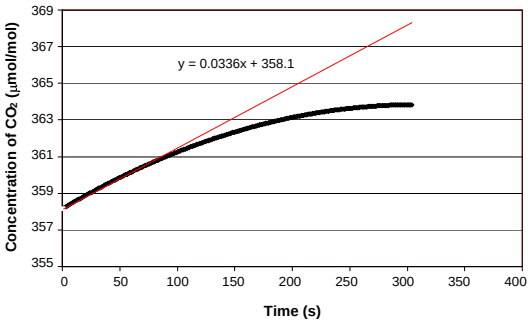

KM09200316

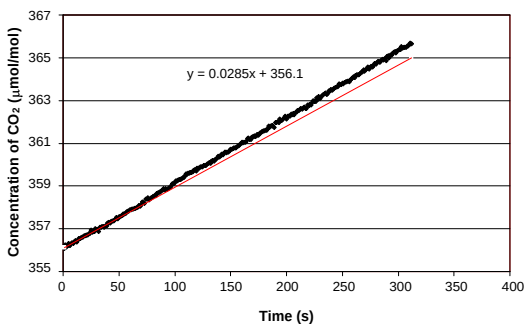

KM09200311

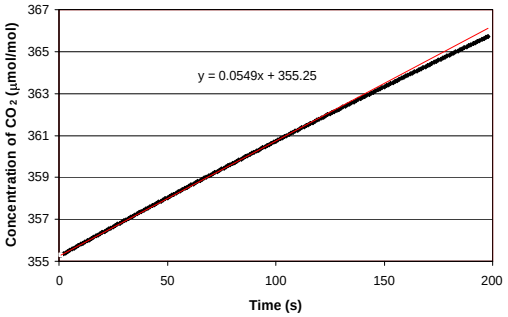

KM09200314

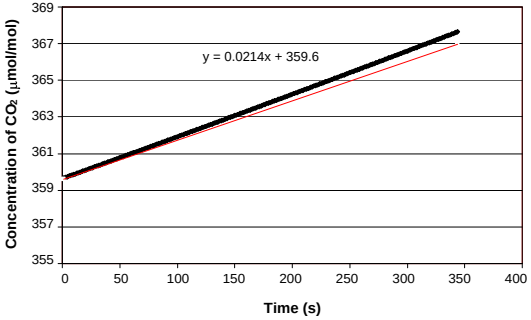

KM09200317

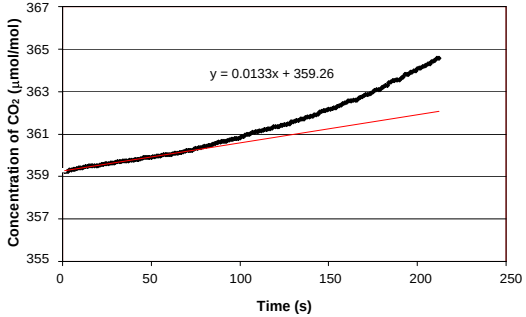

KM09200312

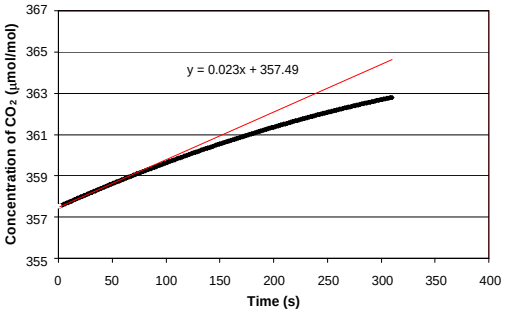

KM09200315

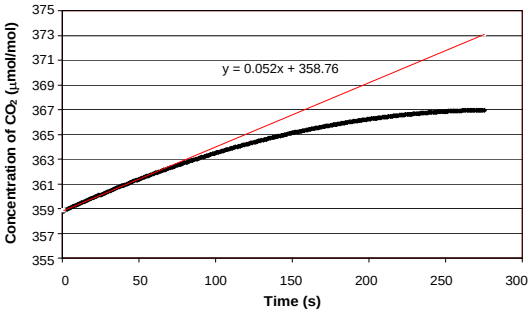

KM09200318

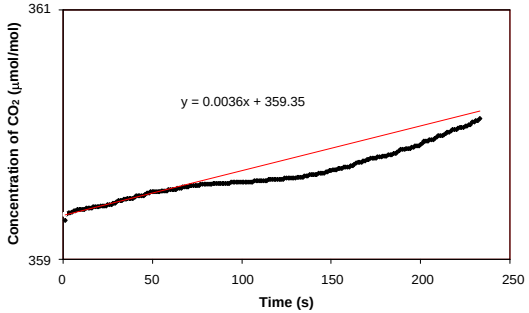

KM09200319

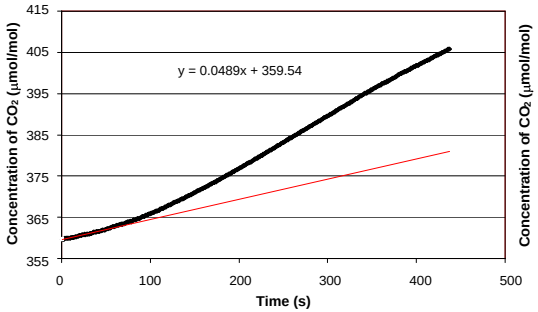

KM09210303

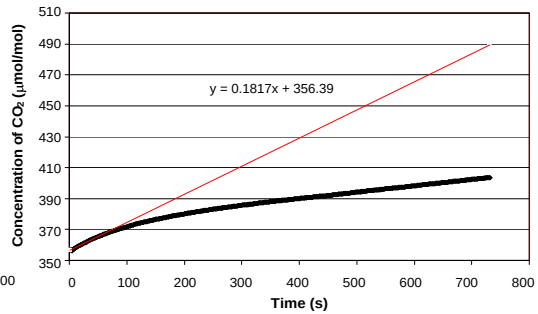

KM09210306

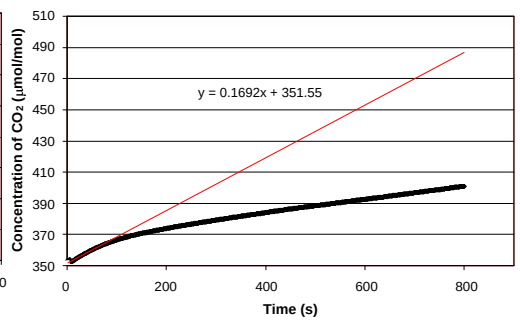

KM09210301

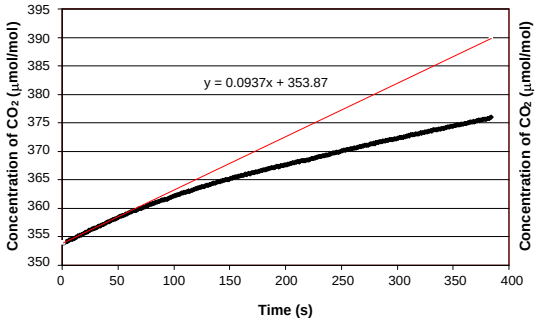

KM09210304

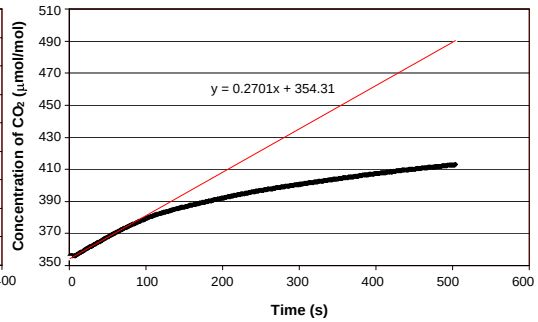

KM09210307

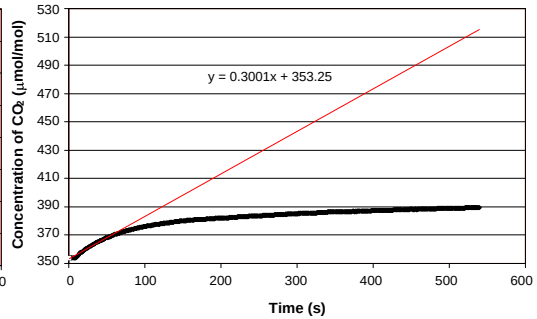

KM09210302

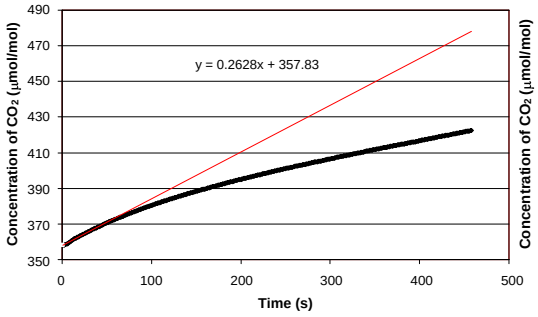

KM09210305

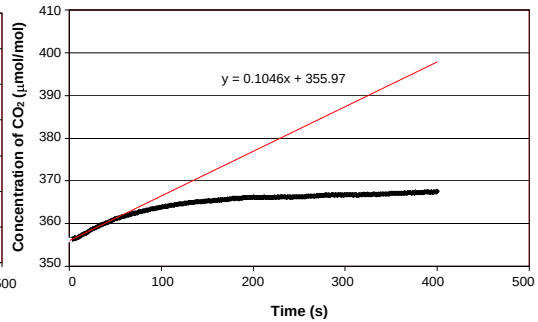

KM09210308

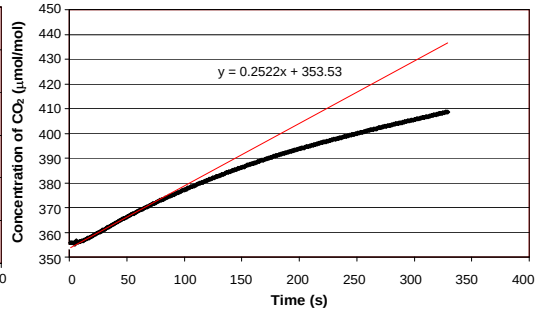

KM09210309

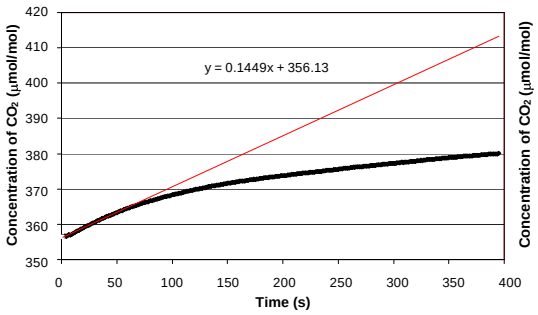

KM09210312

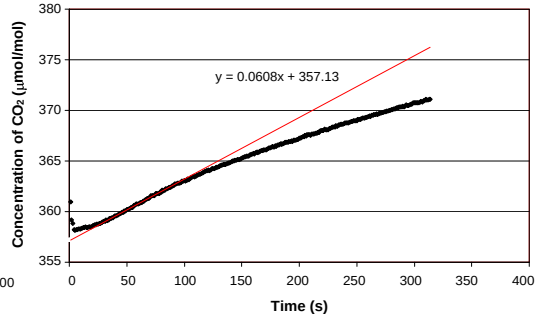

KM09220302

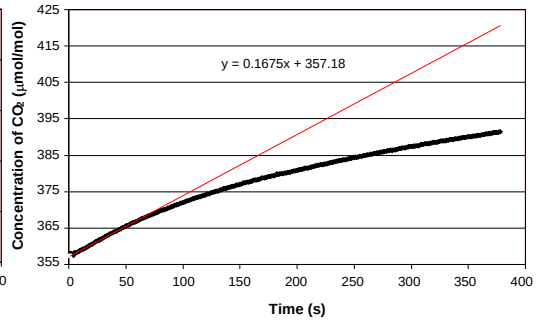

KM09210310

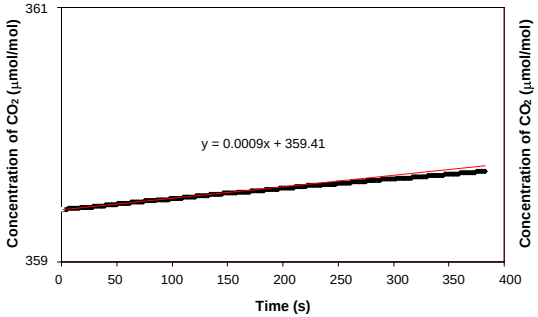

KM09210313

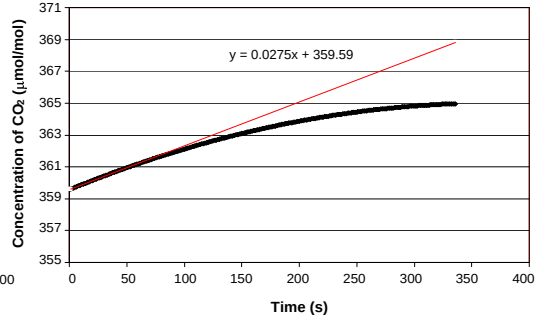

KM09220303

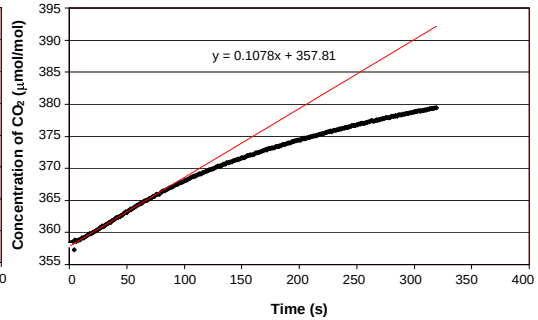

KM09210311

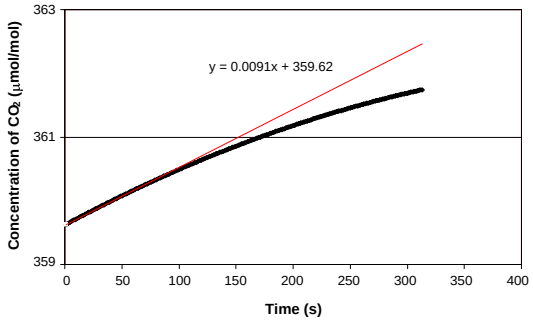

KM09220301

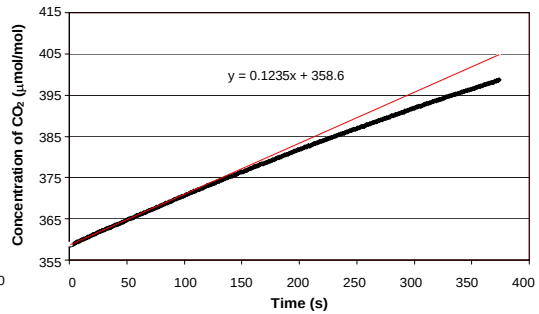

KM09220304

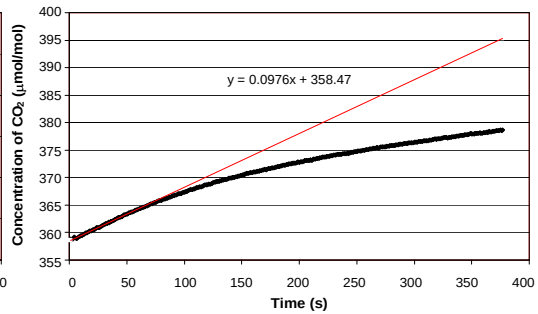

KM09220305

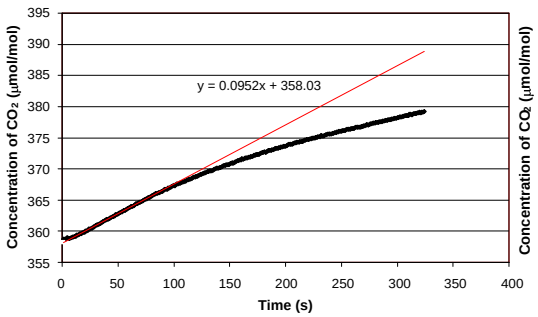

KM09220308

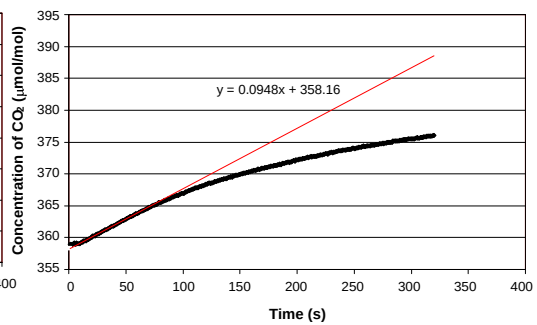

KM09220311

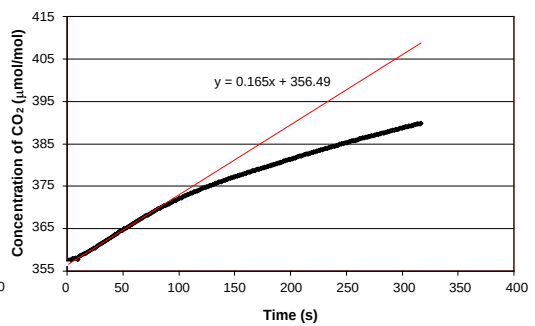

KM09220306

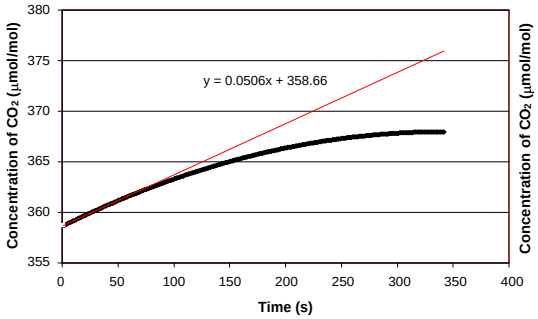

KM09220309

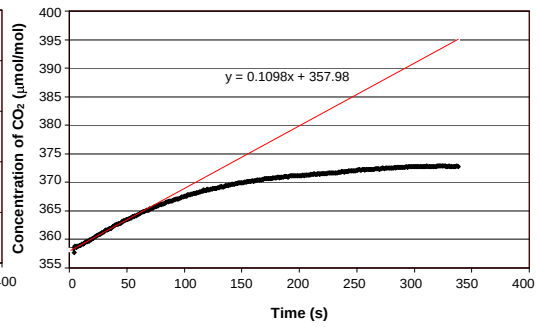

KM09220312

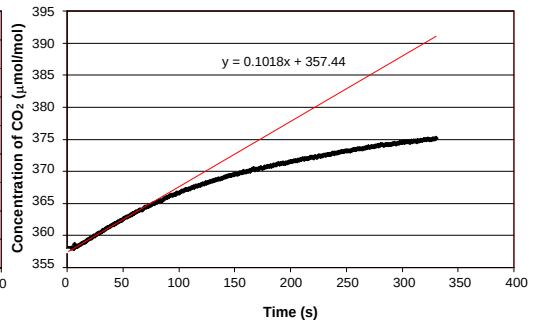

KM09220307

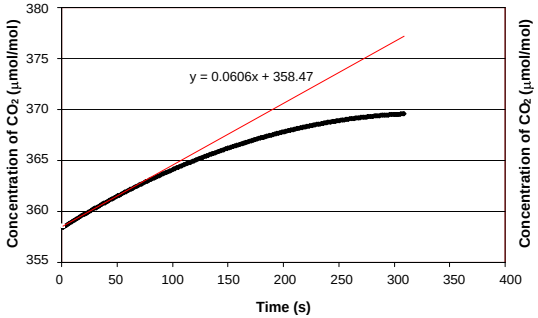

KM09220310

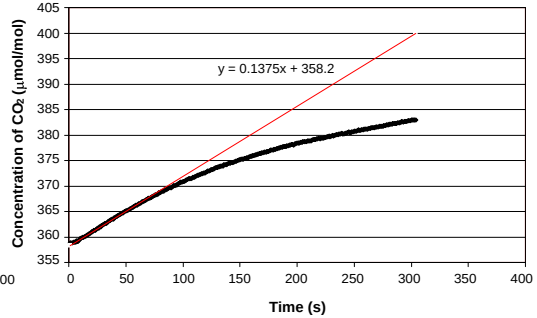

KM09220313

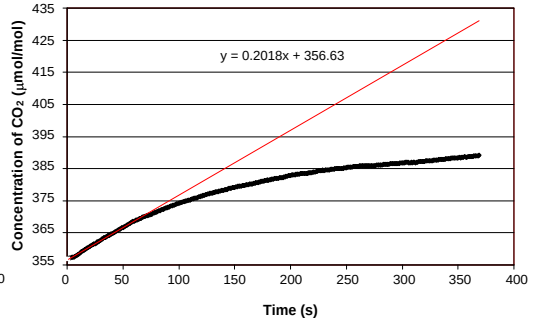

KM09220314

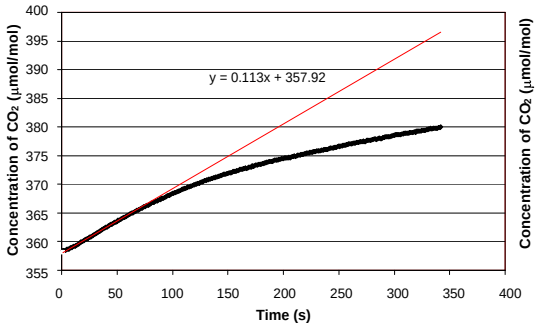

KM09220317

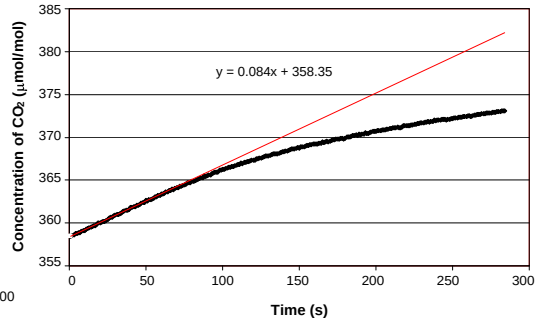

KM09220320

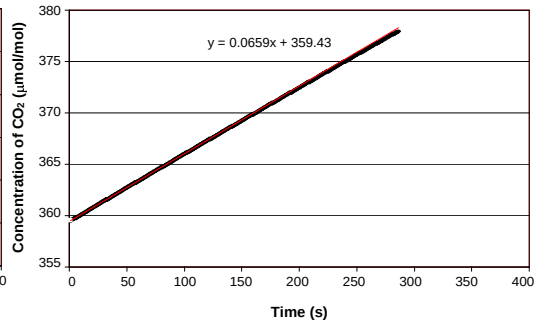

KM09220315

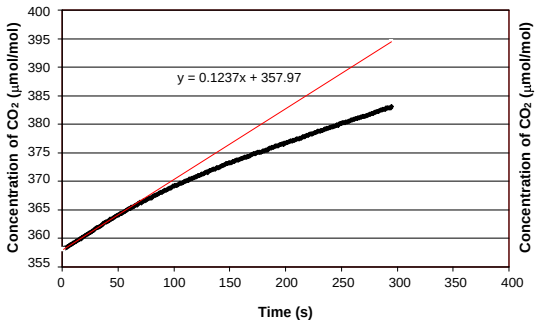

KM09220318

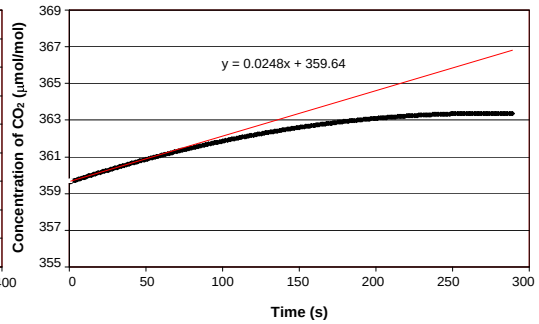

KM09220321

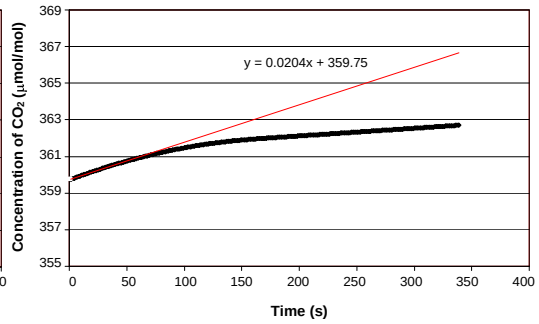

KM09220316

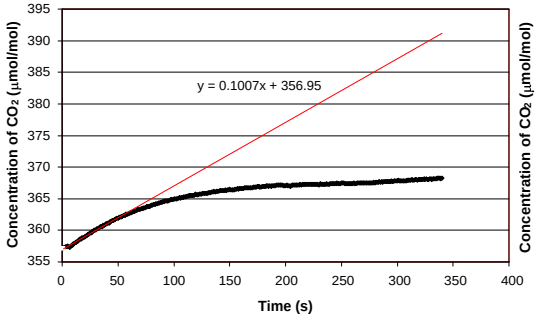

KM09220319

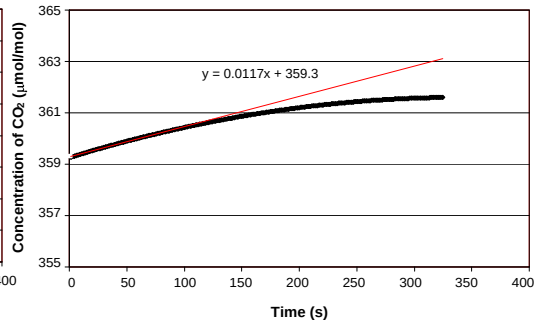

KM09220322

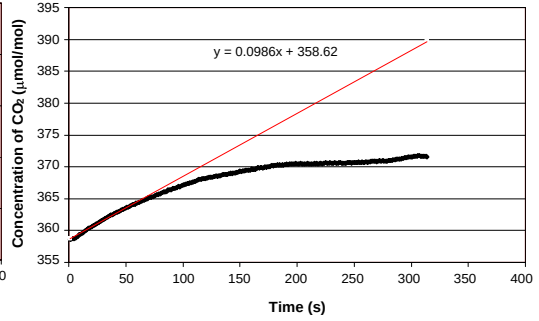

KM09220323

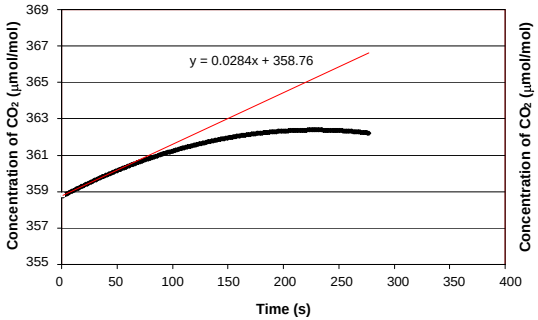

KM09220326

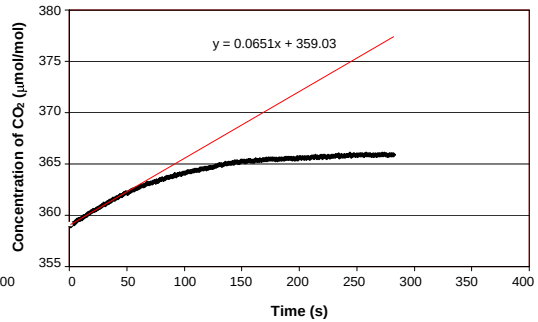

KM09220329

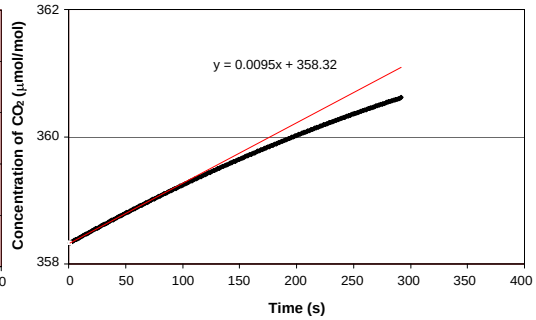

KM09220324

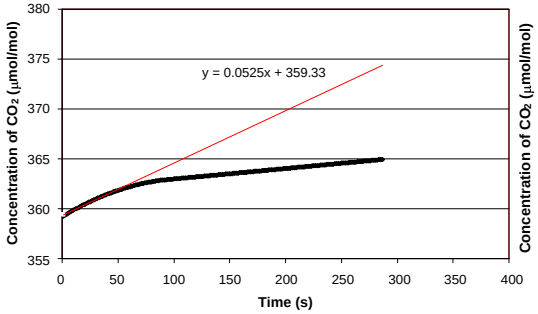

KM09220327

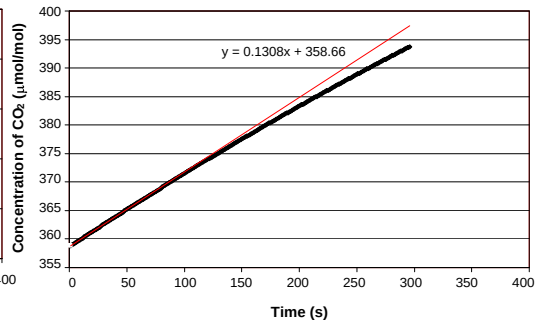

KM09220330

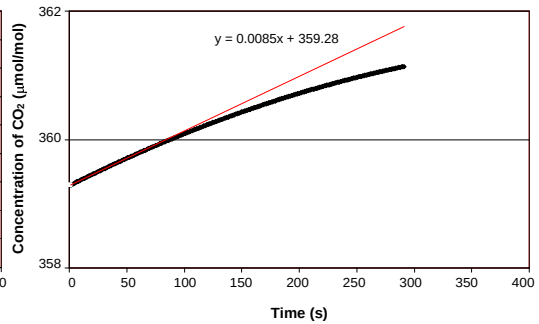

KM09220325

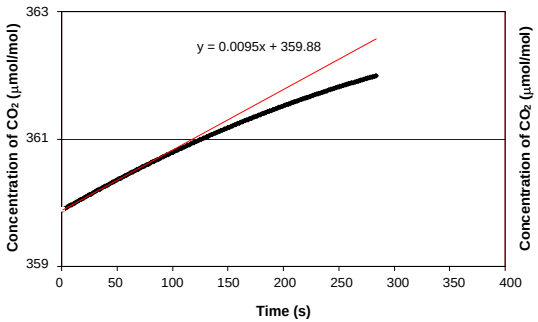

KM09220328

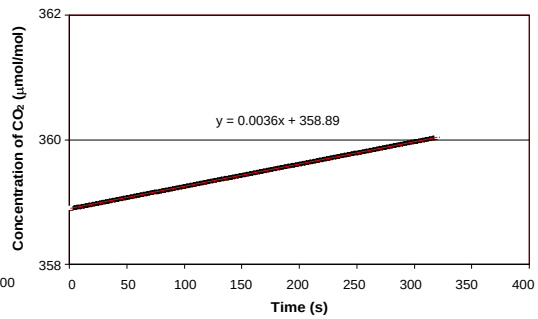

KM09220331

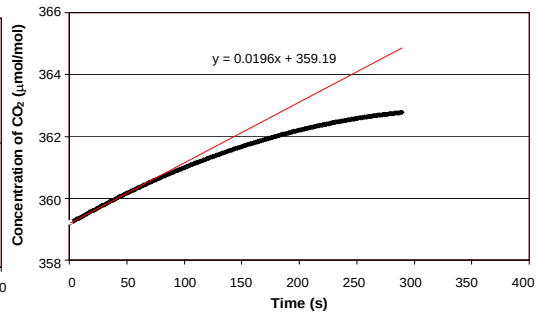

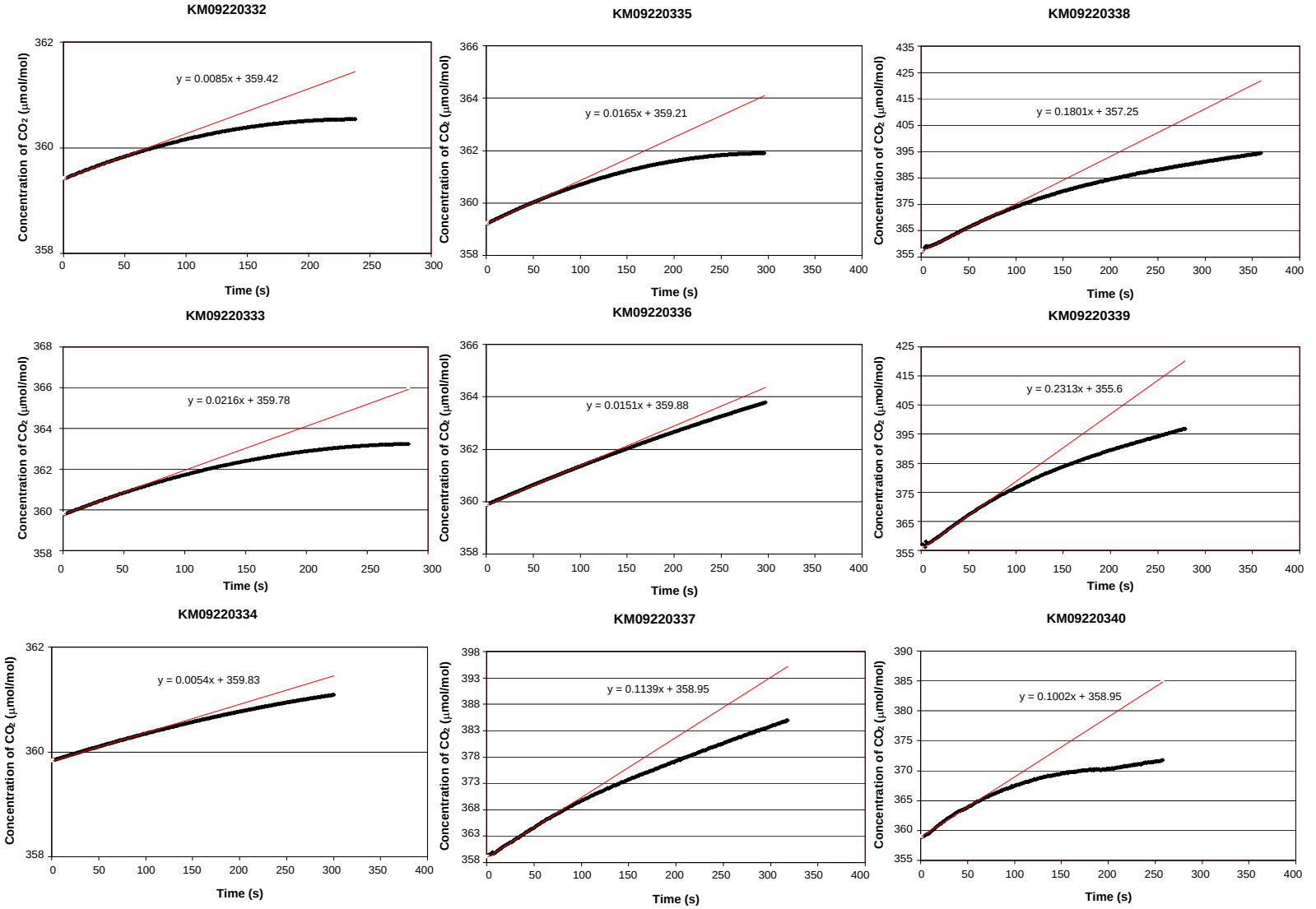
KM09220332
y = 0.0085x + 359.42
KM09220335
y = 0.0165x + 359.21
KM09220338
y = 0.1801x + 357.25
KM09220333
y = 0.0216x + 359.78
KM09220336
y = 0.0151x + 359.88
KM09220339
y = 0.2313x + 355.6
KM09220334
y = 0.0054x + 359.83
KM09220337
y = 0.1139x + 358.95
KM09220340
y = 0.1002x + 358.95
Concentration of CO2 (µmol/mol)
Time (s)

KM09220341

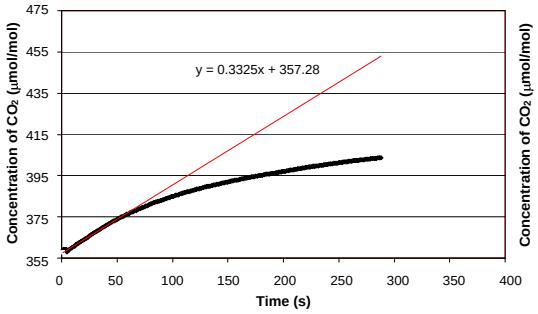

KM09220344

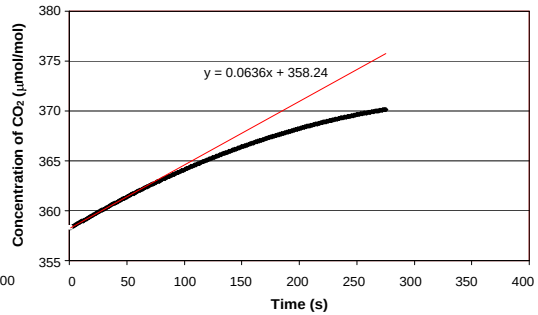

KM09220347

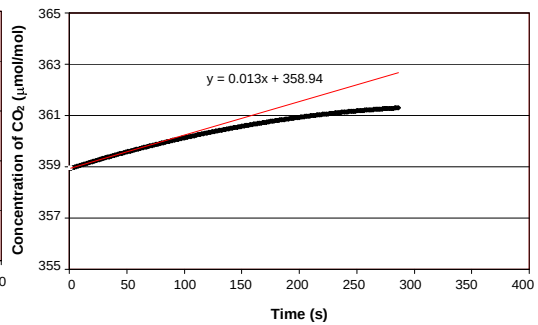

KM09220342

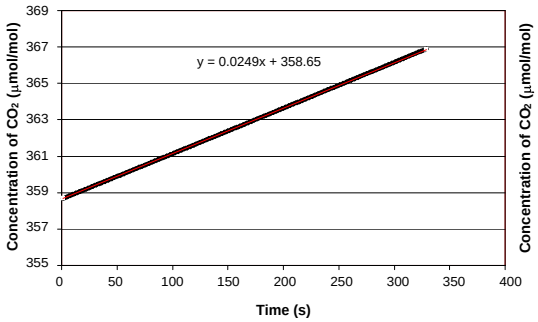

KM09220345

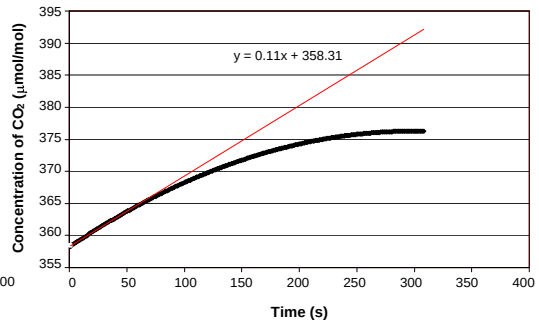

KM09220348

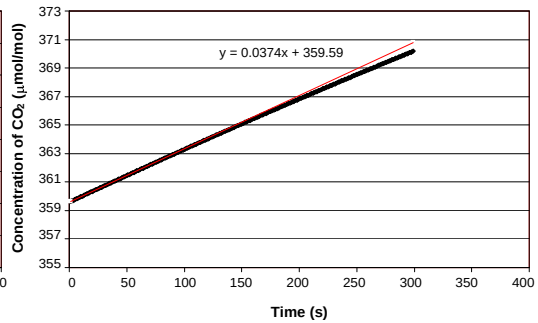

KM09220343

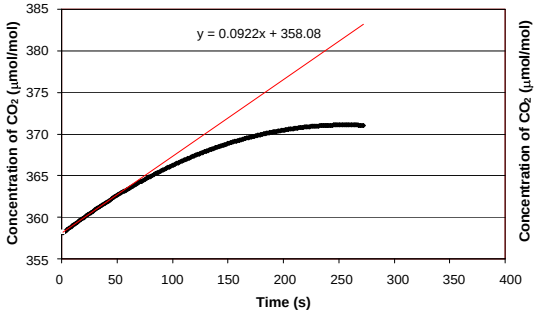

KM09220346

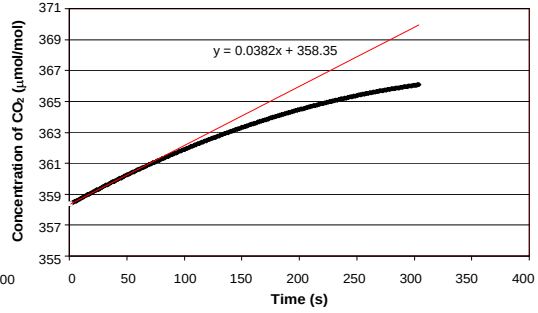

KM09220349

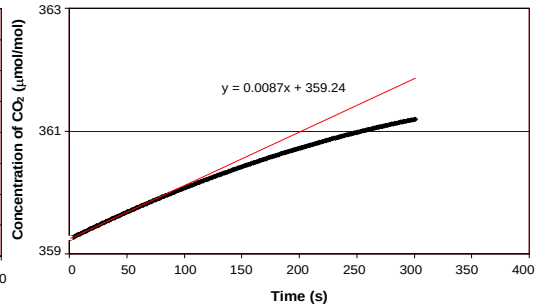

KM09220350

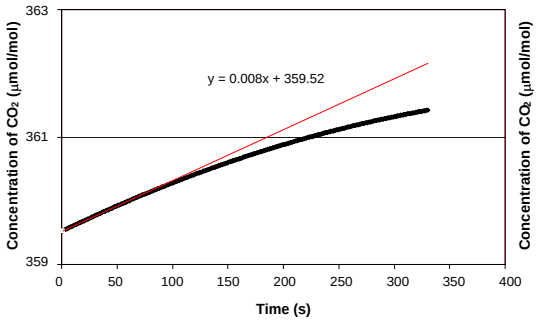

KM09220353

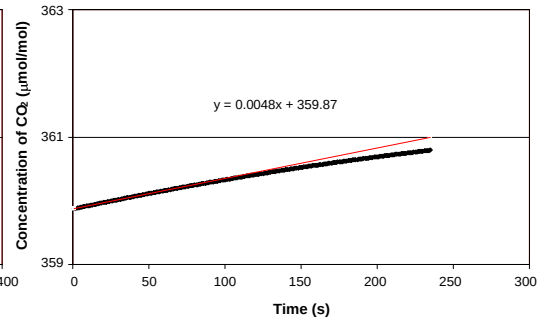

KM09220356

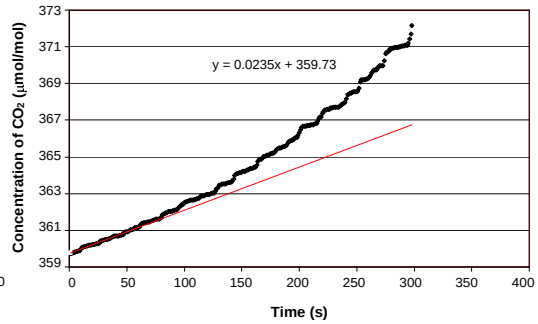

KM09220351

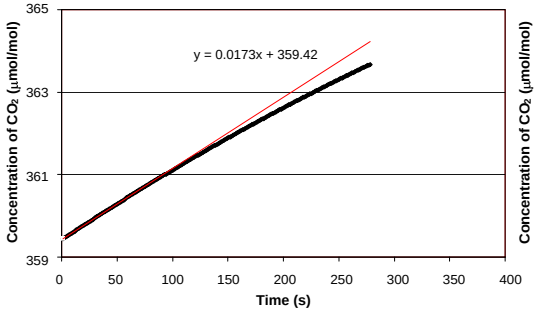

KM09220354

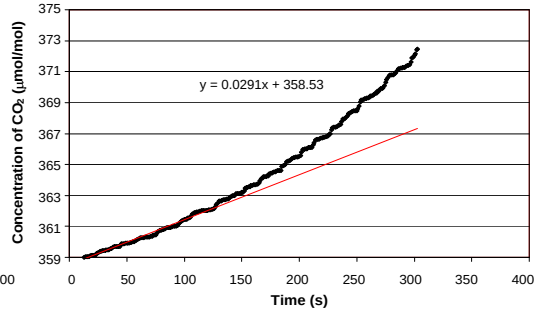

KM09220357

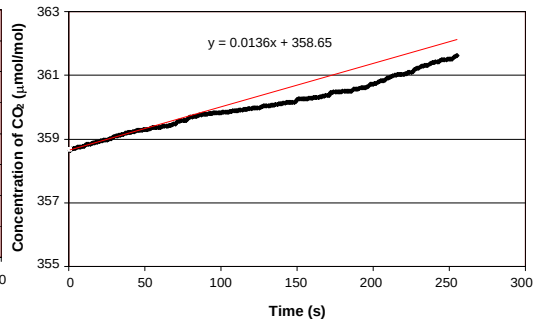

KM09220352

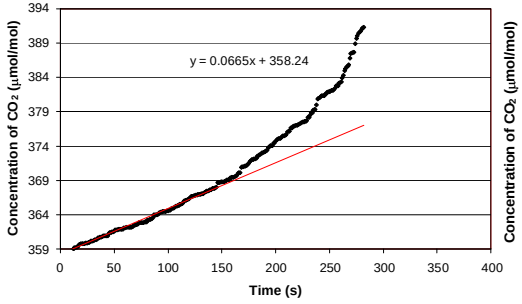

KM09220355

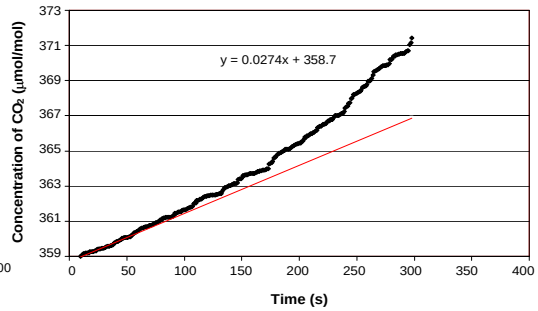

KM09220358

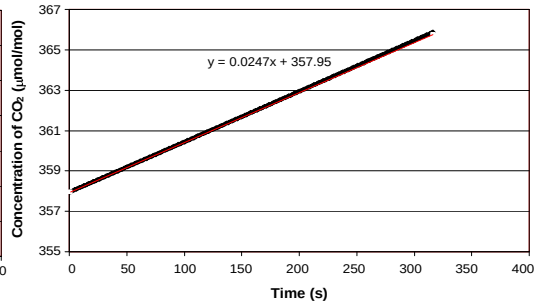

KM09220359

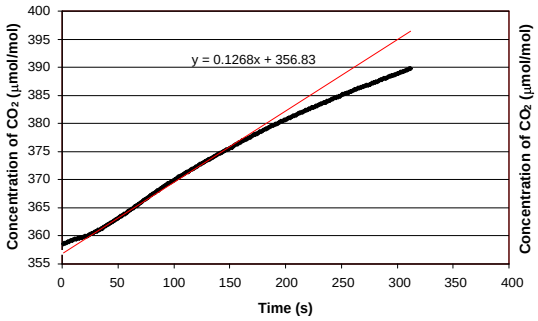

KM09220362

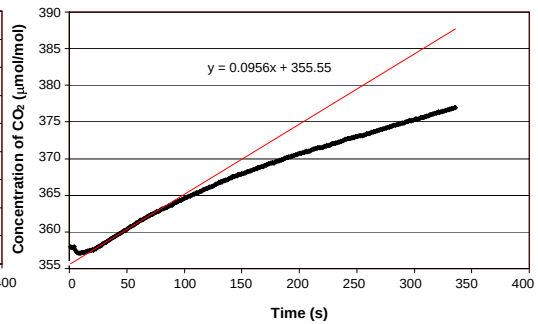

KM09220365

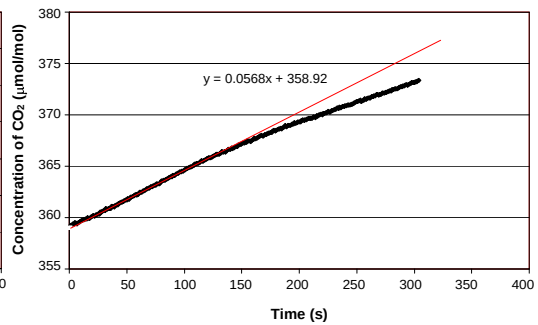

KM09220360

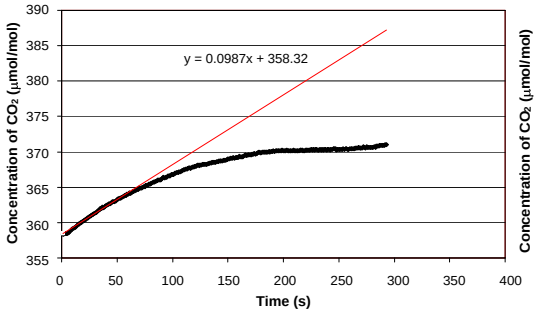

KM09220363

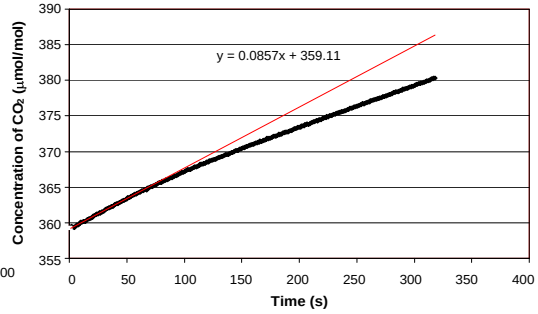

SG1

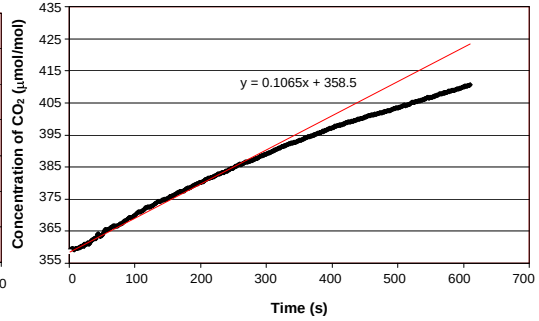

KM09220361

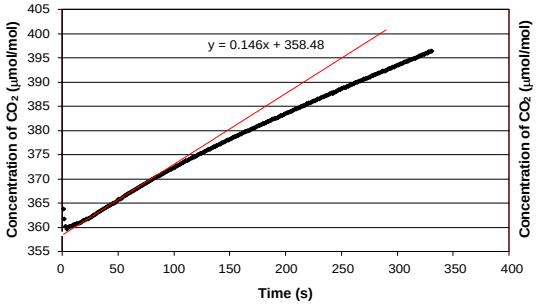

KM09220364

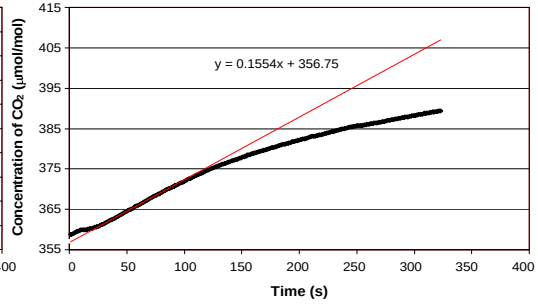

SG2

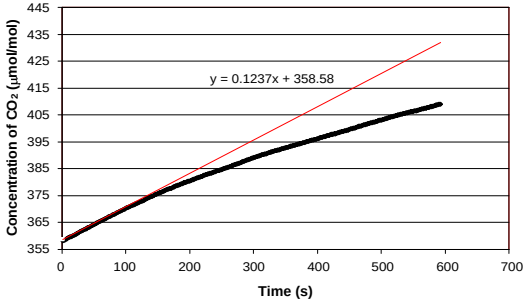

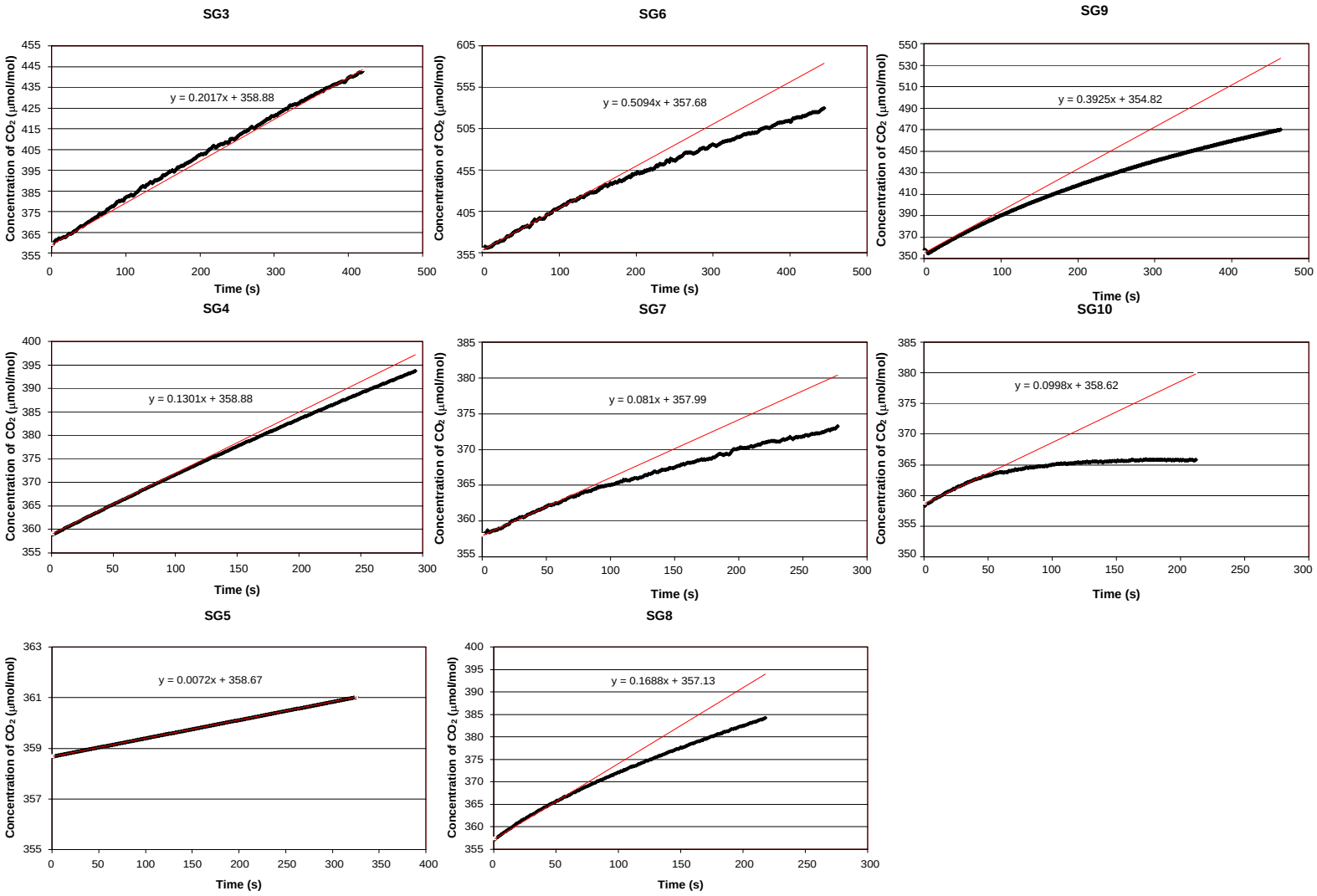
SG3
y = 0.2017x + 358.88
Concentration of CO2 (µmol/mol)
Time (s)
SG6
y = 0.5094x + 357.68
Concentration of CO2 (µmol/mol)
Time (s)
SG9
y = 0.3925x + 354.82
Concentration of CO2 (µmol/mol)
Time (s)
SG4
y = 0.1301x + 358.88
Concentration of CO2 (µmol/mol)
Time (s)
SG7
y = 0.081x + 357.99
Concentration of CO2 (µmol/mol)
Time (s)
SG10
y = 0.0998x + 358.62
Concentration of CO2 (µmol/mol)
Time (s)
SG5
y = 0.0072x + 358.67
Concentration of CO2 (µmol/mol)
Time (s)
SG8
y = 0.1688x + 357.13
Concentration of CO2 (µmol/mol)
Time (s)

APPENDIX B

Soil CO_2 flux measurement locations (UTM), dX/dt values ($\mu mol\ mol^{-1}\ s^{-1}$), atmospheric and soil temperatures (K), atmospheric pressures (kPa), air speed ($m\ s^{-1}$), and calculated flux values ($g\ m^{-2}\ day^{-1}$) for the LDKGRA are shown here. The accumulation chamber had a volume of 9.39 L and an area of 0.07 m^2 of soil was enclosed within the chamber. An example flux calculation for measurement DC1 follows:

$$Flux = (PV/RT*dX/dt)/A$$

$$Flux = ((0.1508\ \mu mol/mol/s)*(0.86\ atm)*(9.39\ L))/((0.082\ L*atm/K*mol)*(308\ K)*(0.07 m^2))$$

$$Flux = 0.7\ \mu mol/m^2/s$$

$$Flux = (0.7\ \mu mol/m^2/s)*(1mol/10^6 \mu mol)*(86400s/day)*(44.01g/mol)$$

$$Flux = 3\ g\ m^{-2}\ day^{-1}$$

Appendix B: Measurement locations, slopes acquired from graphs in Appendix A, temperatures, air speeds, and calculated flux values for all measurements taken in this study.

* Mesurements of atmospheric temperature and pressure were not taken for the first 126 measurements. Average daily temperatures and pressures for Lordsburg, NM in July were used for flux calculations (308 K and 0.86 atm).

Measurement	UTM E	UTM N	Slope (μmol/mol/sec)	Atmospheric Temperature* (K)	Soil Temperature (K)	Atmospheric Pressure* (kPa)	Air Speed (m/s)	Flux ($g/m^2/day$)
dc1	704722	3559246	0.1508	NT	NT	NT	NT	3
dc2	704775	3559246	0.1283	NT	NT	NT	NT	2
dc3	704800	3559246	0.1312	NT	NT	NT	NT	2
dc4	704851	3559246	0.0759	NT	NT	NT	NT	1
dc5	704886	3559244	0.1141	NT	NT	NT	NT	2
dc6	704936	3559246	0.3944	NT	NT	NT	NT	7
dc7	704975	3559246	0.3667	NT	NT	NT	NT	7
dc8	705025	3559246	0.2127	NT	NT	NT	NT	4
dc9	705077	3559245	0.0726	NT	NT	NT	NT	1
dc10	705126	3559246	0.0629	NT	NT	NT	NT	1
dc11	705168	3559246	0.059	NT	NT	NT	NT	1
dc12	705218	3559246	0.117	NT	NT	NT	NT	2
dc13	705257	3559246	0.0659	NT	NT	NT	NT	1
dc14	705307	3559246	0.0759	NT	NT	NT	NT	1
dc15	705349	3559246	0.0916	NT	NT	NT	NT	2
dc15b	705349	3559246	0.1265	NT	NT	NT	NT	2
dc16	705398	3559246	0.1175	NT	NT	NT	NT	2
dc17	705444	3559244	0.0739	NT	NT	NT	NT	1
dc18	705495	3559246	0.1201	NT	NT	NT	NT	2
dc19	705565	3559239	0.0981	NT	NT	NT	NT	2
dcn16	704893	3559702	0.1535	NT	NT	NT	NT	3
dcn17	704892	3559657	0.2331	NT	NT	NT	NT	4
dcn18	704892	3559562	0.1576	NT	NT	NT	NT	3
dcn19	704893	3559512	0.2198	NT	NT	NT	NT	4
dcn20	704895	3559443	0.2298	NT	NT	NT	NT	4
dcn21	704890	3559397	0.1118	NT	NT	NT	NT	2
dcn22	704896	3559323	0.0913	NT	NT	NT	NT	2
dcn23	704889	3559252	0.0587	NT	NT	NT	NT	1
dcn24	704898	3559199	0.067	NT	NT	NT	NT	1

Measurement	UTM E	UTM N	Slope (μmol/mol/sec)	Atmospheric Temperature* (K)	Soil Temperature (K)	Atmospheric Pressure* (kPa)	Air Speed (m/s)	Flux (g/m^2/day)
dcn24b	704898	3559199	0.0917	NT	NT	NT	NT	2
dcn25	704897	3559127	0.0866	NT	NT	NT	NT	2
dcn26	704900	3559079	0.0728	NT	NT	NT	NT	1
dcn27	704899	3559030	0.2922	NT	NT	NT	NT	5
dcn28	704903	3558980	0.1504	NT	NT	NT	NT	3
dcn29	704903	3558925	0.1799	NT	NT	NT	NT	3
dcn30	704902	3558882	0.3201	NT	NT	NT	NT	6
dcn31	704906	3558829	0.2076	NT	NT	NT	NT	4
dcn32	704905	3558780	0.4977	NT	NT	NT	NT	9
dcn33	704907	3558728	0.4893	NT	NT	NT	NT	9
dcn34	704912	3558680	0.406	NT	NT	NT	NT	7
dcn35	704921	3558631	0.5881	NT	NT	NT	NT	10
dcn36	704923	3558577	0.3222	NT	NT	NT	NT	6
dcn37	704928	3558523	0.4745	NT	NT	NT	NT	8
dcn37b	704928	3558523	0.4734	NT	NT	NT	NT	8
dcn38	704915	3558473	0.2148	NT	NT	NT	NT	4
dcn39	704922	3558418	0.2864	NT	NT	NT	NT	5
dcn40	704918	3558375	0.1558	NT	NT	NT	NT	3
dcn41	704917	3558329	0.2584	NT	NT	NT	NT	5
dcn42	704920	3558250	0.322	NT	NT	NT	NT	6
g1	704882	3559626	0.2068	NT	NT	NT	NT	4
g2	704947	3559627	0.2237	NT	NT	NT	NT	4
g3	704999	3559631	0.1016	NT	NT	NT	NT	2
g4	705051	3559625	0.1701	NT	NT	NT	NT	3
g5	705096	3559623	0.1874	NT	NT	NT	NT	3
g6	705183	3559623	0.2773	NT	NT	NT	NT	5
g7	705248	3559630	0.3347	NT	NT	NT	NT	6
g8	705311	3559622	0.4418	NT	NT	NT	NT	8
g9	705388	3559628	0.5132	NT	NT	NT	NT	9
g10	705442	3559627	0.1129	NT	NT	NT	NT	2
g11	705443	3559440	0.083	NT	NT	NT	NT	1
g12	705381	3559439	0.137	NT	NT	NT	NT	2
g13	705320	3559440	0.0859	NT	NT	NT	NT	2
g14	705249	3559440	0.2479	NT	NT	NT	NT	4
g15	705186	3559438	0.1688	NT	NT	NT	NT	3

Measurement	UTM E	UTM N	Slope (μmol/mol/sec)	Atmospheric Temperature* (K)	Soil Temperature (K)	Atmospheric Pressure* (kPa)	Air Speed (m/s)	Flux (g/m^2/day)
g16	705122	3559438	0.125	NT	NT	NT	NT	2
g17	705076	3559443	0.4048	NT	NT	NT	NT	7
g18	705010	3559446	0.1804	NT	NT	NT	NT	3
g19	704957	3559439	0.101	NT	NT	NT	NT	2
g20	704900	3559439	0.282	NT	NT	NT	NT	5
g20b	704900	3559439	0.2387	NT	NT	NT	NT	4
g21	704957	3559079	0.0856	NT	NT	NT	NT	2
g22	705023	3559079	0.1352	NT	NT	NT	NT	2
g23	705084	3559080	0.2331	NT	NT	NT	NT	4
g24	705139	3559080	0.1056	NT	NT	NT	NT	2
g25	705225	3559078	0.1555	NT	NT	NT	NT	3
g26	705281	3559081	0.171	NT	NT	NT	NT	3
g27	705344	3559075	0.1237	NT	NT	NT	NT	2
g28	705406	3559078	0.1193	NT	NT	NT	NT	2
g29	705460	3559084	0.1044	NT	NT	NT	NT	2
g30	705517	3559078	0.0864	NT	NT	NT	NT	2
g30b	705517	3559078	0.0332	NT	NT	NT	NT	1
g31	705517	3558828	0.1529	NT	NT	NT	NT	3
g32	705444	3558829	0.1275	NT	NT	NT	NT	2
g33	705391	3558838	0.1053	NT	NT	NT	NT	2
g34	705317	3558833	0.1076	NT	NT	NT	NT	2
g35	705268	3558818	0.1236	NT	NT	NT	NT	2
g36	705210	3558826	0.0923	NT	NT	NT	NT	2
g37	705142	3558838	0.2659	NT	NT	NT	NT	5
g37b	705142	3558838	0.2327	NT	NT	NT	NT	4
g38	705082	3558823	0.1879	NT	NT	NT	NT	3
g39	705021	3558828	0.2039	NT	NT	NT	NT	4
g40	704967	3558831	0.311	NT	NT	NT	NT	6
g41	704984	3558631	0.2273	NT	NT	NT	NT	4
g42	704945	3558627	0.2432	NT	NT	NT	NT	4
g43	705107	3558631	0.1689	NT	NT	NT	NT	3
g44	705177	3558647	0.2945	NT	NT	NT	NT	5
g45	705215	3558630	0.1383	NT	NT	NT	NT	2
g46	705268	3558628	0.1893	NT	NT	NT	NT	3
g47	705340	3558634	0.1206	NT	NT	NT	NT	2

Measurement	UTM E	UTM N	Slope (μmol/mol/sec)	Atmospheric Temperature* (K)	Soil Temperature (K)	Atmospheric Pressure* (kPa)	Air Speed (m/s)	Flux (g/m^2/day)
g48	705391	3558632	0.1151	NT	NT	NT	NT	2
g49	705463	3558627	0.1096	NT	NT	NT	NT	2
g50	705533	3558636	0.1287	NT	NT	NT	NT	2
g50b	705533	3558636	0.1389	NT	NT	NT	NT	2
g51	705538	3558376	0.1699	NT	NT	NT	NT	3
g52	705488	3558380	0.1454	NT	NT	NT	NT	3
g53	705428	3558380	0.2313	NT	NT	NT	NT	4
g54	705363	3558373	0.181	NT	NT	NT	NT	3
g55	705293	3558385	0.1869	NT	NT	NT	NT	3
g56	705240	3558387	0.2922	NT	NT	NT	NT	5
g57	705184	3558372	0.2558	NT	NT	NT	NT	5
g58	705126	3558373	0.1871	NT	NT	NT	NT	3
g59	705065	3558379	0.3291	NT	NT	NT	NT	6
g60	704994	3558368	0.1799	NT	NT	NT	NT	3
g60b	704994	3558368	0.1286	NT	NT	NT	NT	2
dcc1	701986	3559132	0.1921	NT	NT	NT	NT	3
dcc2	701960	3559133	0.1732	NT	NT	NT	NT	3
dcc3	701936	3559130	0.1715	NT	NT	NT	NT	3
dcc4	701829	3559127	0.212	NT	NT	NT	NT	4
dcc5	701811	3559127	0.202	NT	NT	NT	NT	4
dcc6	701792	3559127	0.2718	NT	NT	NT	NT	5
dcc7	701668	3559128	0.2024	NT	NT	NT	NT	4
dcc8	701648	3559128	0.2128	NT	NT	NT	NT	4
dcc9	701617	3559131	0.2109	NT	NT	NT	NT	4
dcc10	701508	3559129	0.121	NT	NT	NT	NT	2
dcc11	701455	3559128	0.1843	NT	NT	NT	NT	3
dcc12	701448	3559127	0.2526	NT	NT	NT	NT	4
dcb	704722	3559246	0.1273	NT	NT	NT	NT	2
dcb2	704722	3559246	0.1186	NT	NT	NT	NT	2
dcb3	704722	3559246	0.1666	NT	NT	NT	NT	3
dcb4	704722	3559246	0.1547	NT	NT	NT	NT	3
dcb5	704722	3559246	0.0967	NT	NT	NT	NT	2
dcb6	704722	3559246	0.1669	NT	NT	NT	NT	3
km01040301	704718	3559239	0.1068	283	277	88.78	0.0	2
km01040302	705450	3564800	0.0883	286	275	88.66	1.5	2

Measurement	UTM E	UTM N	Slope (μmol/mol/sec)	Atmospheric Temperature* (K)	Soil Temperature (K)	Atmospheric Pressure* (kPa)	Air Speed (m/s)	Flux (g/m^2/day)
km01040303	705350	3564800	0.0906	292	277	88.66	0.2	2
km01040304	705250	3564800	0.0467	292	280	88.63	1.2	1
km01040305	705150	3564800	0.1094	293	279	88.60	1.4	2
km01040306	705050	3564800	0.1205	295	280	88.55	1.2	2
km01040307	704950	3564800	0.1522	295	286	88.55	1.3	3
km01040308	704850	3564800	0.1234	295	283	88.52	2.3	2
km01040309	704750	3564800	0.1431	297	284	88.52	1.8	3
km01040310	704650	3564800	0.1061	297	285	88.52	2.0	2
km01040311	705350	3564800	0.1344	296	286	88.52	1.2	2
km01040312	705350	3564700	0.0883	297	287	88.40	1.5	2
km01040313	705250	3564700	0.0467	296	288	88.34	1.1	1
km01040314	705150	3564700	0.1094	299	285	88.40	0.0	2
km01040315	705050	3564700	0.1205	295	288	88.40	1.3	2
km01040316	704950	3564700	0.1564	294	288	88.40	0.7	3
km01040317	704850	3564700	0.1366	295	284	88.43	1.1	3
km01040318	704750	3564700	0.1944	294	278	88.43	1.3	4
km01040319	704650	3564700	0.1558	293	278	88.43	1.0	3
km01040320	704550	3564700	0.1065	293	286	88.46	0.6	2
km01050301	704718	3559239	0.0807	291	286	88.43	1.0	2
km01050302	703720	3564000	0.0467	294	283	88.34	1.3	1
km01050303	703770	3564000	0.0502	295	280	88.28	2.6	1
km01050304	703820	3564000	0.083	294	288	88.31	2.1	2
km01050305	703870	3564000	0.0876	294	285	88.28	2.2	2
km01050306	703920	3564000	0.0849	295	276	88.28	2.1	2
km01050307	703970	3564000	0.1027	294	286	88.25	1.0	2
km01050308	704020	3564000	0.163	295	283	88.25	2.1	3
km01050309	704070	3564000	0.2108	295	284	88.22	1.7	4
km01050310	704120	3564000	0.1459	296	280	88.19	1.6	3
km01050311	704170	3564000	0.0571	296	282	88.16	1.8	1
km01050312	704220	3564000	0.0853	294	284	89.02	1.5	2
km01070301	704718	3559239	0.0579	287	284	88.93	5.8	1
km01070302	705550	3560130	0.0809	287	287	88.90	7.2	2
km01070303	705500	3560130	0.1056	289	289	88.93	6.5	2
km01070304	705450	3560130	0.0421	286	285	88.87	3.3	1
km01070305	705400	3560130	0.0865	287	284	88.87	6.0	2

Measurement	UTM E	UTM N	Slope (μmol/mol/sec)	Atmospheric Temperature* (K)	Soil Temperature (K)	Atmospheric Pressure* (kPa)	Air Speed (m/s)	Flux (g/m^2/day)
km01070306	705300	3560100	0.0578	286	283	88.87	5.1	1
km01070307	705200	3560100	0.0962	287	283	88.87	6.3	2
km01070308	705100	3560100	0.0692	287	285	88.87	5.3	1
km01070309	705000	3560100	0.1281	288	285	88.84	5.0	2
km01070310	704900	3560100	0.0765	289	287	88.90	5.0	1
km01070311	704800	3560100	0.0925	288	288	88.90	4.5	2
km01070312	704700	3560100	0.1112	288	285	88.90	5.0	2
km01070313	704700	3559972	0.0568	288	286	88.93	4.5	1
km01100301	704718	3559239	0.0876	293	286	88.63	1.2	2
km01100302	703788	3558372	0.0287	293	281	88.63	1.2	1
km01100303	703900	3558373	0.1513	293	288	88.60	1.6	3
km01100304	704000	3558376	0.1511	293	281	88.52	1.7	3
km01100305	704161	3558410	0.2053	293	286	88.49	1.0	4
km01100306	704295	3558417	0.1289	293	289	88.46	1.5	2
km01100307	704297	3558300	0.1172	298	289	88.37	1.6	2
km01100308	704294	3558199	0.1036	293	291	88.37	1.4	2
km01100309	703750	3557900	0.3115	296	285	88.40	1.0	6
km01100310	703850	3557900	0.1827	299	285	88.40	0.6	3
km01100311	703950	3557900	0.1842	297	283	88.34	0.3	3
km01100312	704050	3557900	0.196	293	287	88.34	0.6	4
km01100313	704750	3557200	0.0307	299	298	88.19	1.0	1
km01100314	704650	3557200	0.0281	298	284	88.19	0.7	1
km01100315	704550	3557200	0.0333	295	281	88.19	0.0	1
km01100316	704450	3557200	0.0983	296	289	88.19	0.0	2
km01100317	704350	3557200	0.0919	293	291	88.22	0.0	2
km01100318	704250	3557200	0.1081	295	286	88.25	1.8	2
km01100319	704150	3557200	0.1218	293	287	88.28	3.3	2
km01100320	704050	3557200	0.4279	290	286	88.28	1.5	8
km01110301	704718	3559239	0.0204	280	279	88.46	0.0	0
km01110302	704797	3558164	0.1689	284	277	88.43	1.2	3
km01110303	704747	3558164	0.1029	288	282	88.43	0.0	2
km01110304	704697	3558164	0.0963	287	286	88.43	1.0	2
km01110305	704647	3558164	0.1129	284	285	88.43	0.0	2
km01110306	704597	3558164	0.0961	285	281	88.46	0.0	2
km01110307	704547	3558164	0.175	286	287	88.46	0.0	3

Measurement	UTM E	UTM N	Slope (μmol/mol/sec)	Atmospheric Temperature* (K)	Soil Temperature (K)	Atmospheric Pressure* (kPa)	Air Speed (m/s)	Flux (g/m^2/day)
km01110308	704497	3558164	0.1873	291	283	88.46	0.6	4
km01110309	704447	3558164	0.17	291	283	88.46	0.3	3
km01110310	704397	3558164	0.1711	289	286	88.40	0.5	3
km01110311	704347	3558164	0.1849	288	287	88.40	0.4	4
km01110312	704422	3558172	0.1984	290	285	88.34	1.0	4
km01110313	704422	3558222	0.2366	291	287	88.34	1.0	4
km01110314	704422	3558272	0.0836	292	288	88.31	0.0	2
km01110315	704487	3558167	0.2303	292	288	88.28	1.0	4
km01110316	704486	3558227	0.0529	292	285	88.28	0.8	1
km01110317	704487	3558267	0.107	291	286	88.28	2.5	2
km01110318	704571	3558165	0.2095	291	285	88.28	1.8	4
km01110319	704571	3558215	0.1178	290	288	88.25	2.5	2
km01110320	704571	3558265	0.1448	291	287	88.22	1.5	3
km01110321	704566	3558309	0.1435	294	289	88.22	2.5	3
km01110322	704561	3558357	0.5073	292	281	88.22	1.0	9
km01110323	704557	3558360	0.0329	292	285	88.22	1.5	1
km01110324	704561	3558402	0.1793	294	286	88.22	2.1	3
km01120301	704718	3559239	0.0769	289	281	88.96	1.0	1
km01120302	704690	3558168	0.1117	292	285	88.96	0.3	2
km01120303	704683	3558227	0.2629	292	286	88.99	1.3	5
km01120304	704677	3558288	0.3943	292	285	88.96	0.6	7
km01120305	704676	3558328	0.3828	292	282	88.96	1.0	7
km01120306	704683	3558377	0.563	292	291	88.96	0.5	11
km01120307	704687	3558432	0.3306	293	288	88.93	0.7	6
km01120308	704675	3558484	0.1334	293	285	88.93	2.5	3
km01120309	704670	3558528	0.1161	292	286	88.87	2.0	2
km01120310	704674	3558304	0.2847	292	287	88.84	0.5	5
km01120311	704637	3558300	0.1145	293	286	88.81	0.3	2
km01120312	704581	3558306	0.1341	296	284	88.81	1.0	2
km01120313	704531	3558306	0.1473	295	285	88.81	0.5	3
km01120314	704548	3558310	0.2141	292	281	88.81	1.0	4
km01120315	704474	3558306	0.1455	292	280	88.81	1.0	3
km01120316	704425	3558306	0.0739	290	285	88.81	0.8	1
km01120317	704372	3558305	0.1258	291	286	88.81	0.5	2
km01120318	704342	3558303	0.1764	290	289	88.81	0.5	3

Measurement	UTM E	UTM N	Slope (μmol/mol/sec)	Atmospheric Temperature* (K)	Soil Temperature (K)	Atmospheric Pressure* (kPa)	Air Speed (m/s)	Flux (g/m^2/day)
km01120319	704297	3558250	0.1239	292	281	88.81	1.0	2
km01130301	704718	3559239	0.0827	291	283	89.02	1.4	2
km01130302	704647	3558453	0.1665	292	287	88.99	1.5	3
km01130303	704599	3558453	0.1941	292	287	88.99	1.2	4
km01130304	704549	3558453	0.0778	292	287	88.96	1.7	1
km01130305	704499	3558453	0.1608	292	288	88.93	2.1	3
km01130306	704449	3558453	0.1037	291	286	88.90	3.1	2
km01130307	704689	3558442	0.067	291	286	88.87	0.5	1
km01130308	704740	3558433	0.1655	291	285	88.81	1.0	3
km01130309	704754	3558433	0.116	291	284	88.81	1.0	2
km01130310	704789	3558441	0.129	288	287	88.81	0.5	2
km01130311	704785	3558488	0.1851	290	288	88.81	2.0	4
km01130312	704793	3558548	0.3877	290	287	88.81	0.5	7
km01130313	704806	3558584	0.0457	290	285	88.81	0.0	1
km01130314	704753	3558578	0.0669	290	286	88.78	0.5	1
km01130315	704705	3558578	0.1498	290	288	88.78	0.0	3
km01130316	704637	3558567	0.1034	290	285	88.78	0.9	2
km01130317	704593	3558559	0.1868	292	286	88.81	0.5	4
km01130318	704536	3558584	0.118	292	284	88.81	0.5	2
km01140301	704718	3559239	0.081	290	288	88.96	0.0	2
km01140302	704124	3558800	0.1421	291	286	88.90	2.0	3
km01140303	704200	3558800	0.1127	293	282	88.90	1.2	2
km01140304	704268	3558800	0.1431	293	288	88.84	0.5	3
km01140305	704344	3558805	0.0856	293	284	88.84	1.5	2
km01140306	704400	3558800	0.1391	293	282	88.84	1.5	3
km01140307	704450	3558800	0.1595	293	285	88.84	1.0	3
km01140308	704600	3558824	0.0979	292	287	88.75	1.0	2
km01140309	704719	3558820	0.0797	293	287	88.66	1.0	1
km01140310	704800	3558805	0.064	293	287	88.60	0.5	1
km01140311	704697	3559229	0.0717	293	286	88.63	2.2	1
km09170301	704718	3559239	0.3054	305	302	88.54	0.1	5
km09170302	704234	3558766	0.0262	306	304	88.54	0.1	0
km09170303	704173	3558722	0.0523	306	306	88.55	3.1	1
km09170304	704120	3558766	0.0318	305	304	88.54	2.1	1
km09170305	704072	3558767	0.0343	306	306	88.55	2.3	1

Measurement	UTM E	UTM N	Slope (μmol/mol/sec)	Atmospheric Temperature* (K)	Soil Temperature (K)	Atmospheric Pressure* (kPa)	Air Speed (m/s)	Flux (g/m^2/day)
km09170306	704034	3558763	0.0414	306	304	88.56	1.1	1
km09170307	703983	3558762	0.0433	305	311	88.55	2.3	1
km09170308	703932	3558763	0.0338	310	311	88.56	0.8	1
km09170309	703881	3558759	0.0338	310	309	88.57	0.6	1
km09170310	703833	3558761	0.0438	315	310	88.55	0.5	1
km09170311	703784	3558760	0.0372	313	315	88.55	1.0	1
km09170312	703725	3558761	0.0337	310	312	88.62	0.1	1
km09170313	704034	3558445	0.201	314	309	88.62	1.8	4
km09170314	703979	3558440	0.0323	316	309	88.61	2.7	1
km09170315	703935	3558436	0.0256	310	308	88.61	2.0	0
km09170316	703888	3558431	0.0407	316	307	88.62	1.6	1
km09170317	703843	3558431	0.045	318	310	88.63	1.8	1
km09170318	703803	3558426	0.0438	316	311	88.63	1.8	1
km09170319	703748	3558436	0.0338	317	315	88.63	1.0	1
km09170320	703705	3558425	0.0284	316	311	88.62	0.4	0
km09180301	704011	3558709	0.0771	298	299	88.64	4.0	1
km09180302	703969	3558704	0.2045	298	299	88.63	4.4	4
km09180303	703924	3558699	0.1942	299	299	88.65	5.0	4
km09180304	703877	3558696	0.2578	300	300	88.64	5.6	5
km09180305	703831	3558697	0.153	300	300	88.64	4.1	3
km09180306	703788	3558693	0.1325	301	300	88.64	5.0	2
km09180307	703734	3558691	0.115	301	301	88.64	3.0	2
km09180308	703690	3558690	0.054	302	302	88.64	2.7	1
km09180309	703695	3558641	0.0843	304	303	88.64	3.9	2
km09180310	703739	3558645	0.1778	304	303	88.64	3.6	3
km09180311	703781	3558652	0.0454	303	303	88.62	6.1	1
km09180312	703836	3558654	0.1161	302	303	88.62	5.0	2
km09180313	703881	3558656	0.0727	302	304	88.62	5.1	1
km09180314	703924	3558661	0.0684	303	304	88.62	2.5	1
km09180315	703970	3558658	0.1014	303	303	88.62	4.2	2
km09180316	704010	3558659	0.1106	304	305	88.62	3.8	2
km09180317	704017	3558619	0.123	305	304	88.62	2.7	2
km09180318	703968	3558616	0.0215	302	305	88.62	2.5	0
km09180319	703929	3558611	0.1147	306	302	88.60	5.3	2
km09180320	703833	3558607	0.0761	304	306	88.60	4.4	1

Measurement	UTM E	UTM N	Slope (μmol/mol/sec)	Atmospheric Temperature* (K)	Soil Temperature (K)	Atmospheric Pressure* (kPa)	Air Speed (m/s)	Flux (g/m^2/day)
km09180321	703789	3558604	0.1092	304	304	88.60	2.1	2
km09180322	703737	3558602	0.0529	306	304	88.60	5.0	1
km09180323	703699	3558596	0.0196	306	303	88.60	2.5	0
km09180324	703696	3558553	0.0074	306	304	88.61	3.7	0
km09180325	703699	3558507	0.0366	306	305	88.62	5.1	1
km09180326	703707	3558459	0.0585	305	304	88.62	1.2	1
km09180327	703750	3558466	0.1138	305	307	88.62	2.5	2
km09180328	703800	3558465	0.1043	308	307	88.63	0.5	2
km09180329	703844	3558470	0.1392	307	308	88.62	4.0	2
km09180330	703889	3558474	0.0771	307	306	88.64	5.0	1
km09180331	703954	3558481	0.21	307	304	88.64	3.0	4
km09180332	703978	3558480	0.012	308	305	88.64	5.8	0
km09180333	704025	3558482	0.1273	309	311	88.64	2.6	2
km09180334	704021	3558530	0.0545	311	309	88.64	0.2	1
km09180335	703977	3558520	0.0559	307	312	88.64	0.5	1
km09180336	703935	3558524	0.1273	306	306	88.64	0.4	2
km09180337	703886	3558521	0.0291	308	305	88.63	2.2	1
km09180338	703842	3558518	0.1096	309	311	88.62	4.0	2
km09180339	703804	3558515	0.1525	310	308	88.62	2.0	3
km09180340	703747	3558506	0.0755	307	311	88.62	1.0	1
km09190301	704021	3558528	0.0486	306	306	88.58	1.8	1
km09190302	703880	3558611	0.106	306	304	88.58	2.0	2
km09190303	703743	3558555	0.2427	306	304	88.58	1.1	4
km09190304	703792	3558556	0.1143	306	303	88.58	1.5	2
km09190305	703832	3558558	0.0067	306	307	88.58	3.2	0
km09190306	703884	3558563	0.0355	307	306	88.57	1.5	1
km09190307	703928	3558564	0.026	307	310	88.57	1.6	0
km09190308	703975	3558570	0.029	307	303	88.56	1.9	1
km09190309	704021	3558575	0.0088	308	307	88.56	3.1	0
km09190310	704211	3559176	0.0185	311	313	88.56	1.7	0
km09190311	704167	3559175	0.0736	312	316	88.56	1.6	1
km09190312	704118	3559173	0.0247	312	305	88.56	0.6	0
km09190313	704067	3559173	0.191	313	311	88.56	2.5	3
km09190314	704024	3559171	0.1525	312	305	88.56	2.0	3
km09190315	703978	3559168	0.0861	314	306	88.56	1.7	2

Measurement	UTM E	UTM N	Slope (μmol/mol/sec)	Atmospheric Temperature* (K)	Soil Temperature (K)	Atmospheric Pressure* (kPa)	Air Speed (m/s)	Flux (g/m^2/day)
km09190316	703938	3559169	0.1127	313	317	88.55	1.4	2
km09190317	703890	3559162	0.1091	313	317	88.55	2.0	2
km09190318	703844	3559165	0.0253	313	317	88.55	1.5	0
km09190319	703805	3559169	0.0272	313	319	88.55	1.3	0
km09190320	703843	3558976	0.0098	313	317	88.55	1.0	0
km09190321	703884	3558976	0.1942	312	317	88.57	1.0	3
km09190322	703938	3558977	0.0132	311	319	88.57	1.1	0
km09190323	703978	3558980	0.019	310	316	88.57	1.0	0
km09190324	704025	3558985	0.0223	311	300	88.57	0.0	0
km09190325	704069	3558982	0.0459	310	315	88.57	1.0	1
km09190326	704120	3558986	0.0105	309	314	88.57	0.7	0
km09190327	704163	3558989	0.0559	310	313	88.57	0.1	1
km09190328	704208	3558995	0.0559	311	317	88.57	0.0	1
km09190329	704253	3558996	0.0808	310	314	88.56	0.2	1
km09190330	704299	3558996	0.4882	309	310	88.56	1.0	9
km09190331	704347	3559001	0.1125	309	313	88.56	0.7	2
km09200301	704021	3558528	0.125	310	313	88.60	2.0	2
km09200302	704916	3557952	0.0227	310	313	88.60	2.0	0
km09200303	704877	3557951	0.0283	310	313	88.60	1.0	1
km09200304	704832	3557947	0.3194	310	313	88.60	0.6	6
km09200305	704786	3557949	0.0463	311	313	88.60	2.0	1
km09200306	704742	3557948	0.0279	311	316	88.60	3.2	0
km09200307	704694	3557943	0.0198	311	312	88.60	1.0	0
km09200308	704650	3557943	0.0195	312	312	88.61	1.3	0
km09200309	704601	3557943	0.0292	312	309	88.62	2.6	1
km09200310	704563	3557939	0.0184	313	312	88.62	0.6	0
km09200311	704512	3557941	0.0549	313	313	88.61	1.6	1
km09200312	704467	3557941	0.023	313	312	88.60	1.8	0
km09200313	704420	3557941	0.0336	313	311	88.60	1.0	1
km09200314	704371	3557938	0.0214	313	316	88.60	0.7	0
km09200315	704338	3557929	0.052	314	313	88.60	1.3	1
km09200316	704281	3557935	0.0285	313	317	88.60	2.0	0
km09200317	704238	3557925	0.0133	313	316	88.62	0.6	0
km09200318	704195	3557926	0.0036	312	313	88.62	1.3	0
km09200319	704156	3557926	0.0489	312	317	88.62	0.2	1

Measurement	UTM E	UTM N	Slope (μmol/mol/sec)	Atmospheric Temperature* (K)	Soil Temperature (K)	Atmospheric Pressure* (kPa)	Air Speed (m/s)	Flux (g/m^2/day)
km09210301	704718	3559239	0.0937	302	301	88.57	1.0	2
km09210302	704168	3557582	0.2628	302	301	88.57	2.5	5
km09210303	704186	3557597	0.1817	303	303	88.57	2.5	3
km09210304	704229	3557599	0.2701	303	304	88.57	2.6	5
km09210305	704278	3557602	0.1046	303	304	88.58	3.0	2
km09210306	704145	3557600	0.1692	303	305	88.59	3.0	3
km09210307	704185	3557540	0.3001	304	305	88.58	3.7	5
km09210308	704176	3557510	0.2522	304	305	88.58	2.0	5
km09210309	704178	3557475	0.1449	305	305	88.58	3.2	3
km09210310	705680	3560158	0.0009	305	309	88.57	3.5	0
km09210311	705651	3560114	0.0091	304	310	88.57	1.6	0
km09210312	705638	3560054	0.0608	304	307	88.57	1.8	1
km09210313	705824	3560183	0.0275	303	309	88.57	2.0	0
km09220301	704718	3559239	0.1235	297	300	88.62	2.0	2
km09220302	704136	3558647	0.1675	297	300	88.62	2.3	3
km09220303	704183	3558648	0.1078	297	301	88.62	3.0	2
km09220304	704225	3558655	0.0976	297	299	88.62	3.2	2
km09220305	704269	3558659	0.0952	298	300	88.62	2.0	2
km09220306	704318	3558659	0.0506	297	299	88.63	3.3	1
km09220307	704361	3558665	0.0606	298	300	88.64	2.0	1
km09220308	704409	3558664	0.0948	298	302	88.65	1.2	2
km09220309	704451	3558668	0.1098	298	302	88.65	2.6	2
km09220310	704501	3558675	0.1375	299	303	88.66	3.0	3
km09220311	704636	3558679	0.165	300	303	88.65	2.3	3
km09220312	704682	3558679	0.1018	300	301	88.66	2.0	2
km09220313	704727	3558682	0.2018	300	302	88.66	1.6	4
km09220314	704764	3558680	0.113	301	304	88.66	2.0	2
km09220315	704450	3559003	0.1237	301	303	88.66	1.7	2
km09220316	704488	3558985	0.1007	301	304	88.66	0.8	2
km09220317	704525	3558987	0.084	301	300	88.67	1.2	2
km09220318	704573	3558991	0.0248	302	302	88.66	1.0	0
km09220319	704622	3558996	0.0117	301	303	88.66	2.7	0
km09220320	704664	3558994	0.0659	300	304	88.67	1.8	1
km09220321	704707	3558995	0.0204	300	304	88.67	0.7	0
km09220322	704758	3558990	0.0986	300	303	88.67	1.6	2

Measurement	UTM E	UTM N	Slope (μmol/mol/sec)	Atmospheric Temperature* (K)	Soil Temperature (K)	Atmospheric Pressure* (kPa)	Air Speed (m/s)	Flux (g/m^2/day)
km09220323	704801	3558995	0.0284	300	303	88.67	1.7	1
km09220324	704852	3558997	0.0525	300	301	88.67	1.2	1
km09220325	704893	3558996	0.0095	300	303	88.67	1.7	0
km09220326	704664	3559196	0.0651	300	300	88.67	2.0	1
km09220327	704631	3559194	0.1308	300	302	88.67	2.3	2
km09220328	704571	3559233	0.0036	300	303	88.67	0.8	0
km09220329	704530	3559227	0.0095	300	300	88.67	1.2	0
km09220330	704485	3559220	0.0085	300	301	88.69	0.8	0
km09220331	704472	3559211	0.0196	299	302	88.68	1.4	0
km09220332	704294	3559208	0.0085	300	302	88.68	1.8	0
km09220333	704353	3559204	0.0216	300	302	88.69	2.3	0
km09220334	704305	3559201	0.0054	301	304	88.69	0.8	0
km09220335	704258	3559197	0.0165	300	303	88.69	1.2	0
km09220336	704212	3559192	0.0151	301	301	88.69	0.2	0
km09220337	703747	3558121	0.1139	301	301	88.69	0.7	2
km09220338	703795	3558128	0.1801	301	301	88.69	0.0	3
km09220339	703835	3558120	0.2313	301	302	88.69	0.0	4
km09220340	703886	3558125	0.1002	302	299	88.69	1.0	2
km09220341	703930	3558127	0.3325	302	299	88.67	1.0	6
km09220342	703976	3558130	0.0249	302	302	88.66	1.0	0
km09220343	704023	3558135	0.0922	302	300	88.67	1.2	2
km09220344	704062	3558136	0.0636	303	301	88.64	0.5	1
km09220345	704058	3557894	0.11	303	303	88.64	0.3	2
km09220346	704041	3557899	0.0382	305	307	88.64	0.0	1
km09220347	703960	3557899	0.013	304	305	88.64	0.0	0
km09220348	703917	3557892	0.0374	304	303	88.64	0.5	1
km09220349	703875	3557888	0.0087	304	302	88.63	0.7	0
km09220350	703829	3557887	0.008	303	304	88.64	1.2	0
km09220351	703760	3557578	0.0173	304	305	88.63	0.3	0
km09220352	703806	3557576	0.0665	304	302	88.63	0.8	1
km09220353	703852	3557581	0.0048	303	303	88.63	1.5	0
km09220354	703900	3557582	0.0291	303	304	88.64	2.2	1
km09220355	703947	3557587	0.0274	302	301	88.64	0.3	0
km09220356	703988	3557587	0.0235	302	302	88.64	0.2	0
km09220357	704035	3557590	0.0136	302	299	88.62	0.0	0

Measurement	UTM E	UTM N	Slope (μmol/mol/sec)	Atmospheric Temperature* (K)	Soil Temperature (K)	Atmospheric Pressure* (kPa)	Air Speed (m/s)	Flux (g/m^2/day)
km09220358	704088	3557589	0.0247	302	301	88.62	0.0	0
km09220359	704332	3557601	0.1268	301	299	88.63	0.0	2
km09220360	704376	3557600	0.0987	302	300	88.63	1.0	2
km09220361	704425	3557603	0.146	301	303	88.62	1.0	3
km09220362	704488	3557599	0.0956	300	305	88.62	1.5	2
km09220363	704536	3557599	0.0857	301	302	88.62	0.2	2
km09220364	704584	3557604	0.1554	301	303	88.62	0.4	3
km09220365	704625	3557601	0.0568	302	303	88.62	1.0	1
Sg1	704722	3559246	0.1065	286	282	88.55	0.5	2
Sg2	704677	3559267	0.1237	288	288	88.54	1.2	2
Sg3	704038	3559283	0.2071	288	283	88.54	2.4	4
Sg4	704682	3558372	0.1301	287	286	88.54	1.7	2
Sg5	704395	3558190	0.0072	288	289	88.55	1.0	0
Sg6	704432	3557929	0.5094	289	290	88.53	1.4	10
Sg7	704049	3557205	0.081	290	284	88.54	0.3	2
Sg8	703734	3558132	0.1688	289	282	88.53	1.1	3
Sg9	703729	3557919	0.3925	286	288	88.52	0.7	7
Sg10	704912	3558643	0.0998	285	285	88.52	0.9	2

APPENDIX C

These spreadsheets show the raw data for the soil gas compositional analyses. They are in the order in which they were analyzed. The gases correspond to a number in the "Data" column. He is 0, CH_4 is 1, N_2 is 2, C_2H_6 is 3, O_2 is 4, Ar is 5, CO_2 is 6, and SO_2 is 7. All ten cycles are shown for each analysis, as well as maximum and minimum values.

ASCII SAMPLE CYCLES : Background 1
DATE : 4/10/2004
CONVERTED CYCLES : 10

Number of stored cycles 10
Printed start cycle 1
Printed end cycle 10
Number of stored datablocks 1

Data	block	Ion Current			
0	4	min:	9.27E-13	max:	1.14E-12
1	15	min:	4.17E-12	max:	5.56E-12
2	28	min:	2.91E-10	max:	2.96E-10
3	30	min:	4.84E-12	max:	6.43E-12
4	32	min:	2.94E-10	max:	2.99E-10
5	40	min:	3.76E-12	max:	4.83E-12
6	44	min:	6.22E-11	max:	6.56E-11
7	48	min:	8.70E-13	max:	9.58E-13

Cycle	Date	Time	RelTime[s]	0	1	2	3	4	5	6	7
1	4/10/2004	12:07:06 PM:00	0	9.65E-13	5.14E-12	2.93E-10	5.23E-12	2.95E-10	4.51E-12	6.47E-11	8.70E-13
2	4/10/2004	12:07:23 PM:35	17.35	1.14E-12	4.17E-12	2.91E-10	5.89E-12	2.95E-10	4.36E-12	6.22E-11	8.86E-13
3	4/10/2004	12:07:40 PM:49	34.49	1.13E-12	4.58E-12	2.93E-10	6.43E-12	2.99E-10	3.76E-12	6.46E-11	9.13E-13
4	4/10/2004	12:07:57 PM:90	51.9	9.27E-13	4.36E-12	2.92E-10	5.86E-12	2.99E-10	4.68E-12	6.53E-11	9.35E-13
5	4/10/2004	12:08:15 PM:20	69.2	1.10E-12	4.83E-12	2.92E-10	5.46E-12	2.95E-10	4.19E-12	6.33E-11	8.83E-13
6	4/10/2004	12:08:32 PM:61	86.61	9.95E-13	5.18E-12	2.96E-10	5.79E-12	2.94E-10	4.51E-12	6.56E-11	9.58E-13
7	4/10/2004	12:08:49 PM:75	103.75	1.12E-12	4.79E-12	2.94E-10	5.55E-12	2.95E-10	4.62E-12	6.34E-11	8.99E-13
8	4/10/2004	12:09:07 PM:00	121	1.13E-12	4.86E-12	2.93E-10	5.01E-12	2.99E-10	3.82E-12	6.36E-11	8.81E-13
9	4/10/2004	12:09:24 PM:63	138.63	1.06E-12	5.25E-12	2.92E-10	5.42E-12	2.96E-10	4.83E-12	6.39E-11	8.86E-13
10	4/10/2004	12:09:42 PM:04	156.04	1.04E-12	5.56E-12	2.94E-10	4.84E-12	2.94E-10	3.91E-12	6.32E-11	8.94E-13

ASCII SAMPLE CYCLES : Air 1
DATE : 4/10/2004
CONVERTED CYCLES : 10

Number of stored cycles 10
Printed start cycle 1
Printed end cycle 10
Number of stored datablocks 1

Data	block 0	Ion Current			
0	4	min:	3.03E-12	max:	3.67E-12
1	15	min:	1.28E-10	max:	1.67E-10
2	28	min:	7.32E-08	max:	8.69E-08
3	30	min:	3.82E-10	max:	1.22E-09
4	32	min:	1.48E-08	max:	1.75E-08
5	40	min:	6.15E-10	max:	7.38E-10
6	44	min:	2.57E-10	max:	3.46E-10
7	48	min:	1.74E-12	max:	2.13E-12

Cycle	Date	Time	Rel Time	0	1	2	3	4	5	6	7
1	4/10/2004	12:14:02 PM:00	0	3.67E-12	1.67E-10	8.67E-08	1.22E-09	1.75E-08	7.38E-10	3.46E-10	2.13E-12
2	4/10/2004	12:14:18 PM:86	16.86	3.25E-12	1.65E-10	8.69E-08	9.74E-10	1.75E-08	7.36E-10	3.31E-10	1.91E-12
3	4/10/2004	12:14:35 PM:83	33.83	3.45E-12	1.57E-10	8.47E-08	8.18E-10	1.70E-08	7.15E-10	3.17E-10	2.00E-12
4	4/10/2004	12:14:52 PM:86	50.86	3.38E-12	1.48E-10	7.97E-08	6.94E-10	1.60E-08	6.65E-10	2.97E-10	1.99E-12
5	4/10/2004	12:15:09 PM:77	67.77	3.56E-12	1.41E-10	7.72E-08	6.02E-10	1.57E-08	6.59E-10	2.89E-10	2.03E-12
6	4/10/2004	12:15:26 PM:64	84.64	3.32E-12	1.38E-10	7.59E-08	5.41E-10	1.54E-08	6.38E-10	2.76E-10	2.02E-12
7	4/10/2004	12:15:43 PM:50	101.5	3.28E-12	1.35E-10	7.68E-08	4.91E-10	1.57E-08	6.59E-10	2.78E-10	1.95E-12
8	4/10/2004	12:16:00 PM:31	118.31	3.54E-12	1.35E-10	7.52E-08	4.48E-10	1.53E-08	6.39E-10	2.67E-10	1.74E-12
9	4/10/2004	12:16:17 PM:17	135.17	3.03E-12	1.30E-10	7.42E-08	4.11E-10	1.51E-08	6.28E-10	2.65E-10	1.87E-12
10	4/10/2004	12:16:34 PM:08	152.08	3.57E-12	1.28E-10	7.32E-08	3.82E-10	1.48E-08	6.15E-10	2.57E-10	1.76E-12

ASCII SAMPLE CYCLES : Air 2
DATE : 4/10/2004
CONVERTED CYCLES : 10

Number of stored cycles 10
Printed start cycle 1
Printed end cycle 10
Number of stored datablocks 1

Data	block	Ion Current			
0	4	min:	3.30E-12	max:	4.32E-12
1	15	min:	1.43E-10	max:	1.49E-10
2	28	min:	9.37E-08	max:	9.75E-08
3	30	min:	1.43E-10	max:	1.68E-10
4	32	min:	1.93E-08	max:	1.97E-08
5	40	min:	7.95E-10	max:	8.25E-10
6	44	min:	2.74E-10	max:	2.81E-10
7	48	min:	1.84E-12	max:	2.26E-12

Cycle	Date	Time	RelTime[s]	0	1	2	3	4	5	6	7
1	4/10/2004	12:23:29 PM:00	0	3.79E-12	1.44E-10	9.75E-08	1.68E-10	1.97E-08	8.25E-10	2.74E-10	2.00E-12
2	4/10/2004	12:23:45 PM:80	16.8	3.46E-12	1.45E-10	9.69E-08	1.61E-10	1.96E-08	8.23E-10	2.76E-10	1.96E-12
3	4/10/2004	12:24:02 PM:83	33.83	4.17E-12	1.49E-10	9.65E-08	1.59E-10	1.96E-08	8.14E-10	2.77E-10	2.04E-12
4	4/10/2004	12:24:19 PM:80	50.8	4.32E-12	1.46E-10	9.59E-08	1.59E-10	1.95E-08	8.16E-10	2.76E-10	1.93E-12
5	4/10/2004	12:24:36 PM:83	67.83	3.45E-12	1.43E-10	9.56E-08	1.56E-10	1.95E-08	8.12E-10	2.78E-10	2.26E-12
6	4/10/2004	12:24:53 PM:75	84.75	3.80E-12	1.44E-10	9.51E-08	1.55E-10	1.94E-08	8.06E-10	2.75E-10	1.87E-12
7	4/10/2004	12:25:10 PM:72	101.72	3.82E-12	1.46E-10	9.47E-08	1.50E-10	1.94E-08	8.04E-10	2.78E-10	1.90E-12
8	4/10/2004	12:25:27 PM:64	118.64	3.30E-12	1.43E-10	9.44E-08	1.47E-10	1.93E-08	7.98E-10	2.77E-10	1.86E-12
9	4/10/2004	12:25:44 PM:61	135.61	3.90E-12	1.43E-10	9.41E-08	1.45E-10	1.93E-08	8.00E-10	2.81E-10	2.18E-12
10	4/10/2004	12:26:01 PM:47	152.47	3.49E-12	1.44E-10	9.37E-08	1.43E-10	1.93E-08	7.95E-10	2.75E-10	1.84E-12

ASCII SAMPLE CYCLES : Soil Gas 1
DATE : 4/10/2004
CONVERTED CYCLES : 10

Number of stored cycles 10
Printed start cycle 1
Printed end cycle 10
Number of stored datablocks 1

Data	block	Ion Current			
0	4	min:	8.67E-12	max:	1.20E-11
1	15	min:	3.19E-10	max:	3.27E-10
2	28	min:	2.68E-07	max:	2.83E-07
3	30	min:	1.61E-10	max:	1.72E-10
4	32	min:	5.44E-08	max:	5.68E-08
5	40	min:	2.24E-09	max:	2.35E-09
6	44	min:	4.31E-10	max:	4.41E-10
7	48	min:	2.90E-12	max:	3.42E-12

Cycle	Date	Time	RelTime[s]	0	1	2	3	4	5	6	7
1	4/10/2004	12:34:10 PM:00	0	8.67E-12	3.25E-10	2.83E-07	1.69E-10	5.68E-08	2.35E-09	4.41E-10	2.96E-12
2	4/10/2004	12:34:26 PM:97	16.97	1.15E-11	3.22E-10	2.81E-07	1.72E-10	5.66E-08	2.35E-09	4.40E-10	3.07E-12
3	4/10/2004	12:34:43 PM:89	33.89	1.06E-11	3.27E-10	2.79E-07	1.71E-10	5.62E-08	2.33E-09	4.35E-10	2.93E-12
4	4/10/2004	12:35:00 PM:86	50.86	9.10E-12	3.21E-10	2.78E-07	1.67E-10	5.60E-08	2.33E-09	4.36E-10	2.96E-12
5	4/10/2004	12:35:17 PM:84	67.84	9.22E-12	3.25E-10	2.76E-07	1.68E-10	5.57E-08	2.32E-09	4.38E-10	3.42E-12
6	4/10/2004	12:35:34 PM:75	84.75	9.43E-12	3.19E-10	2.74E-07	1.65E-10	5.54E-08	2.30E-09	4.35E-10	3.30E-12
7	4/10/2004	12:35:51 PM:89	101.89	1.20E-11	3.20E-10	2.73E-07	1.65E-10	5.52E-08	2.28E-09	4.39E-10	2.90E-12
8	4/10/2004	12:36:08 PM:92	118.92	9.71E-12	3.23E-10	2.71E-07	1.65E-10	5.49E-08	2.27E-09	4.33E-10	2.92E-12
9	4/10/2004	12:36:25 PM:89	135.89	8.88E-12	3.19E-10	2.70E-07	1.64E-10	5.46E-08	2.25E-09	4.31E-10	3.17E-12
10	4/10/2004	12:36:42 PM:81	152.81	1.08E-11	3.19E-10	2.68E-07	1.61E-10	5.44E-08	2.24E-09	4.34E-10	2.93E-12

ASCII SAMPLE CYCLES : Soil Gas 2
DATE : 4/10/2004
CONVERTED CYCLES : 10

Number of stored cycles 10
Printed start cycle 1
Printed end cycle 10
Number of stored datablocks 1

Data	block	Ion Current			
0	4	min:	1.20E-11	max:	1.69E-11
1	15	min:	4.47E-10	max:	4.59E-10
2	28	min:	4.36E-07	max:	4.68E-07
3	30	min:	1.82E-10	max:	1.87E-10
4	32	min:	8.81E-08	max:	9.37E-08
5	40	min:	3.65E-09	max:	3.90E-09
6	44	min:	6.13E-10	max:	6.27E-10
7	48	min:	3.37E-12	max:	4.25E-12

Cycle	Date	Time	RelTime[s]	0	1	2	3	4	5	6	7
1	4/10/2004	12:44:02 PM:00	0	1.63E-11	4.59E-10	4.68E-07	1.83E-10	9.37E-08	3.90E-09	6.27E-10	3.55E-12
2	4/10/2004	12:44:18 PM:98	16.98	1.53E-11	4.59E-10	4.63E-07	1.87E-10	9.28E-08	3.85E-09	6.25E-10	4.03E-12
3	4/10/2004	12:44:35 PM:78	33.78	1.58E-11	4.57E-10	4.59E-07	1.87E-10	9.20E-08	3.83E-09	6.23E-10	3.72E-12
4	4/10/2004	12:44:52 PM:76	50.76	1.53E-11	4.58E-10	4.55E-07	1.83E-10	9.14E-08	3.80E-09	6.19E-10	4.25E-12
5	4/10/2004	12:45:09 PM:73	67.73	1.52E-11	4.50E-10	4.51E-07	1.84E-10	9.08E-08	3.77E-09	6.16E-10	3.81E-12
6	4/10/2004	12:45:26 PM:64	84.64	1.24E-11	4.53E-10	4.48E-07	1.84E-10	9.03E-08	3.74E-09	6.21E-10	3.89E-12
7	4/10/2004	12:45:43 PM:56	101.56	1.36E-11	4.53E-10	4.45E-07	1.82E-10	8.97E-08	3.73E-09	6.14E-10	3.87E-12
8	4/10/2004	12:46:00 PM:42	118.42	1.20E-11	4.52E-10	4.41E-07	1.85E-10	8.92E-08	3.69E-09	6.13E-10	3.91E-12
9	4/10/2004	12:46:17 PM:29	135.29	1.69E-11	4.52E-10	4.38E-07	1.84E-10	8.87E-08	3.67E-09	6.14E-10	3.46E-12
10	4/10/2004	12:46:34 PM:37	152.37	1.64E-11	4.47E-10	4.36E-07	1.84E-10	8.81E-08	3.65E-09	6.15E-10	3.37E-12

ASCII SAMPLE CYCLES : Air 3
DATE : 4/10/2004
CONVERTED CYCLES : 10

Number of stored cycles 10
Printed start cycle 1
Printed end cycle 10
Number of stored datablocks 1

Data	block	Ion Current			
0	4	min:	9.35E-12	max:	1.42E-11
1	15	min:	3.57E-10	max:	3.63E-10
2	28	min:	3.02E-07	max:	3.16E-07
3	30	min:	1.28E-10	max:	1.31E-10
4	32	min:	6.20E-08	max:	6.45E-08
5	40	min:	2.54E-09	max:	2.64E-09
6	44	min:	4.70E-10	max:	4.79E-10
7	48	min:	2.81E-12	max:	3.25E-12

Cycle	Date	Time	RelTime[s]	0	1	2	3	4	5	6	7
1	4/10/2004	12:53:59 PM:00	0	1.35E-11	3.63E-10	3.16E-07	1.30E-10	6.45E-08	2.64E-09	4.79E-10	2.92E-12
2	4/10/2004	12:54:15 PM:98	16.98	1.20E-11	3.60E-10	3.15E-07	1.30E-10	6.42E-08	2.63E-09	4.74E-10	3.25E-12
3	4/10/2004	12:54:32 PM:78	33.78	1.25E-11	3.61E-10	3.13E-07	1.30E-10	6.39E-08	2.61E-09	4.76E-10	3.03E-12
4	4/10/2004	12:54:49 PM:81	50.81	1.26E-11	3.59E-10	3.11E-07	1.30E-10	6.35E-08	2.60E-09	4.76E-10	3.05E-12
5	4/10/2004	12:55:06 PM:78	67.78	1.07E-11	3.57E-10	3.10E-07	1.31E-10	6.33E-08	2.58E-09	4.75E-10	3.08E-12
6	4/10/2004	12:55:23 PM:70	84.7	1.19E-11	3.60E-10	3.08E-07	1.30E-10	6.30E-08	2.57E-09	4.74E-10	3.15E-12
7	4/10/2004	12:55:40 PM:67	101.67	1.29E-11	3.58E-10	3.06E-07	1.28E-10	6.26E-08	2.56E-09	4.70E-10	2.98E-12
8	4/10/2004	12:55:57 PM:48	118.48	1.42E-11	3.61E-10	3.05E-07	1.29E-10	6.24E-08	2.56E-09	4.78E-10	3.01E-12
9	4/10/2004	12:56:14 PM:56	135.56	1.17E-11	3.59E-10	3.04E-07	1.31E-10	6.23E-08	2.55E-09	4.75E-10	2.96E-12
10	4/10/2004	12:56:31 PM:59	152.59	9.35E-12	3.59E-10	3.02E-07	1.29E-10	6.20E-08	2.54E-09	4.71E-10	2.81E-12

ASCII SAMPLE CYCLES : Soil Gas 3
DATE : 4/10/2004
CONVERTED CYCLES : 10

Number of stored cycles 10
Printed start cycle 1
Printed end cycle 10
Number of stored datablocks 1

Data	block	Ion Current			
0	4	min:	3.62E-12	max:	5.32E-12
1	15	min:	1.55E-10	max:	1.61E-10
2	28	min:	9.88E-08	max:	1.00E-07
3	30	min:	1.76E-10	max:	3.46E-10
4	32	min:	2.05E-08	max:	2.07E-08
5	40	min:	8.25E-10	max:	8.42E-10
6	44	min:	2.24E-10	max:	2.31E-10
7	48	min:	1.64E-12	max:	2.24E-12

Cycle	Date	Time	RelTime[s]	0	1	2	3	4	5	6	7
1	4/10/2004	1:06:13 PM:00	0	5.32E-12	1.61E-10	9.92E-08	3.46E-10	2.05E-08	8.35E-10	2.28E-10	1.90E-12
2	4/10/2004	1:06:30 PM:03	17.03	3.98E-12	1.60E-10	9.94E-08	3.05E-10	2.05E-08	8.27E-10	2.29E-10	1.76E-12
3	4/10/2004	1:06:46 PM:95	33.95	3.74E-12	1.60E-10	9.91E-08	2.76E-10	2.05E-08	8.25E-10	2.27E-10	1.88E-12
4	4/10/2004	1:07:03 PM:92	50.92	4.34E-12	1.55E-10	9.88E-08	2.54E-10	2.05E-08	8.29E-10	2.24E-10	1.86E-12
5	4/10/2004	1:07:20 PM:78	67.78	3.91E-12	1.56E-10	1.00E-07	2.35E-10	2.07E-08	8.42E-10	2.27E-10	1.89E-12
6	4/10/2004	1:07:37 PM:75	84.75	4.40E-12	1.59E-10	9.98E-08	2.20E-10	2.07E-08	8.36E-10	2.29E-10	2.24E-12
7	4/10/2004	1:07:54 PM:73	101.73	3.79E-12	1.57E-10	9.97E-08	2.05E-10	2.07E-08	8.38E-10	2.31E-10	2.13E-12
8	4/10/2004	1:08:11 PM:75	118.75	4.92E-12	1.59E-10	9.95E-08	1.95E-10	2.07E-08	8.37E-10	2.25E-10	2.09E-12
9	4/10/2004	1:08:28 PM:89	135.89	4.16E-12	1.60E-10	9.92E-08	1.84E-10	2.07E-08	8.37E-10	2.28E-10	1.64E-12
10	4/10/2004	1:08:45 PM:92	152.92	3.62E-12	1.59E-10	9.90E-08	1.76E-10	2.06E-08	8.38E-10	2.28E-10	2.02E-12

ASCII SAMPLE CYCLES : Soil Gas 4
DATE : 4/10/2004
CONVERTED CYCLES : 10

Number of stored cycles 10
Printed start cycle 1
Printed end cycle 10
Number of stored datablocks 1

Data	block	Ion Current			
0	4	min:	1.17E-12	max:	1.44E-12
1	15	min:	1.85E-11	max:	2.33E-11
2	28	min:	5.63E-09	max:	5.66E-09
3	30	min:	2.45E-11	max:	2.68E-11
4	32	min:	1.29E-09	max:	1.31E-09
5	40	min:	5.00E-11	max:	5.23E-11
6	44	min:	6.78E-11	max:	7.06E-11
7	48	min:	9.75E-13	max:	1.19E-12

Cycle	Date	Time	RelTime[s]	0	1	2	3	4	5	6	7
1	4/10/2004	2:47:15 PM:00	0	1.30E-12	2.02E-11	5.63E-09	2.64E-11	1.29E-09	5.06E-11	6.89E-11	1.07E-12
2	4/10/2004	2:47:32 PM:03	17.03	1.36E-12	2.04E-11	5.66E-09	2.60E-11	1.29E-09	5.07E-11	6.93E-11	1.00E-12
3	4/10/2004	2:47:49 PM:16	34.16	1.33E-12	1.95E-11	5.65E-09	2.68E-11	1.29E-09	5.07E-11	7.06E-11	1.16E-12
4	4/10/2004	2:48:06 PM:19	51.19	1.17E-12	1.93E-11	5.65E-09	2.48E-11	1.30E-09	5.18E-11	6.86E-11	1.08E-12
5	4/10/2004	2:48:23 PM:27	68.27	1.21E-12	2.13E-11	5.64E-09	2.64E-11	1.30E-09	5.13E-11	7.03E-11	1.19E-12
6	4/10/2004	2:48:40 PM:52	85.52	1.25E-12	1.85E-11	5.64E-09	2.45E-11	1.30E-09	5.06E-11	6.91E-11	1.18E-12
7	4/10/2004	2:48:57 PM:55	102.55	1.44E-12	2.12E-11	5.65E-09	2.52E-11	1.29E-09	5.23E-11	6.78E-11	1.07E-12
8	4/10/2004	2:49:14 PM:57	119.57	1.32E-12	2.16E-11	5.64E-09	2.56E-11	1.30E-09	5.00E-11	6.90E-11	1.06E-12
9	4/10/2004	2:49:31 PM:71	136.71	1.25E-12	2.33E-11	5.66E-09	2.60E-11	1.31E-09	5.12E-11	7.02E-11	1.10E-12
10	4/10/2004	2:49:48 PM:79	153.79	1.18E-12	2.14E-11	5.65E-09	2.56E-11	1.31E-09	5.12E-11	6.94E-11	9.75E-13

ASCII SAMPLE CYCLES : Air 4
DATE : 4/10/2004
CONVERTED CYCLES : 10

Number of stored cycles 10
Printed start cycle 1
Printed end cycle 10
Number of stored datablocks 1

Data	block	Ion Current			
0	4	min:	1.28E-12	max:	1.49E-12
1	15	min:	2.50E-11	max:	2.72E-11
2	28	min:	9.97E-09	max:	1.00E-08
3	30	min:	2.29E-11	max:	2.67E-11
4	32	min:	1.95E-09	max:	1.99E-09
5	40	min:	8.40E-11	max:	8.79E-11
6	44	min:	7.76E-11	max:	8.05E-11
7	48	min:	9.84E-13	max:	1.14E-12

Cycle	Date	Time	RelTime[s]	0	1	2	3	4	5	6	7
1	4/10/2004	2:57:04 PM:00	0	1.32E-12	2.61E-11	1.00E-08	2.56E-11	1.95E-09	8.73E-11	7.82E-11	1.03E-12
2	4/10/2004	2:57:21 PM:03	17.03	1.28E-12	2.72E-11	1.00E-08	2.67E-11	1.97E-09	8.57E-11	7.98E-11	1.13E-12
3	4/10/2004	2:57:38 PM:05	34.05	1.39E-12	2.50E-11	1.00E-08	2.38E-11	1.97E-09	8.45E-11	7.90E-11	1.07E-12
4	4/10/2004	2:57:55 PM:19	51.19	1.43E-12	2.57E-11	1.00E-08	2.54E-11	1.97E-09	8.45E-11	7.76E-11	1.13E-12
5	4/10/2004	2:58:12 PM:33	68.33	1.47E-12	2.62E-11	1.00E-08	2.52E-11	1.97E-09	8.76E-11	7.87E-11	1.14E-12
6	4/10/2004	2:58:29 PM:36	85.36	1.49E-12	2.61E-11	1.00E-08	2.54E-11	1.98E-09	8.57E-11	7.89E-11	1.09E-12
7	4/10/2004	2:58:46 PM:44	102.44	1.48E-12	2.53E-11	1.00E-08	2.47E-11	1.99E-09	8.50E-11	7.96E-11	9.84E-13
8	4/10/2004	2:59:03 PM:46	119.46	1.38E-12	2.58E-11	9.97E-09	2.29E-11	1.98E-09	8.73E-11	7.93E-11	1.01E-12
9	4/10/2004	2:59:20 PM:60	136.6	1.30E-12	2.57E-11	9.98E-09	2.58E-11	1.99E-09	8.79E-11	8.05E-11	1.12E-12
10	4/10/2004	2:59:37 PM:68	153.68	1.48E-12	2.61E-11	9.99E-09	2.44E-11	1.99E-09	8.40E-11	8.01E-11	1.06E-12

ASCII SAMPLE CYCLES : Soil Gas 5
DATE : 4/10/2004
CONVERTED CYCLES : 10

Number of stored cycles 10
Printed start cycle 1
Printed end cycle 10
Number of stored datablocks 1

Data	block	Ion Current			
0	4	min:	1.16E-12	max:	1.39E-12
1	15	min:	1.94E-11	max:	2.20E-11
2	28	min:	6.13E-09	max:	6.16E-09
3	30	min:	2.05E-11	max:	2.42E-11
4	32	min:	1.34E-09	max:	1.36E-09
5	40	min:	5.35E-11	max:	5.59E-11
6	44	min:	6.80E-11	max:	7.10E-11
7	48	min:	9.58E-13	max:	1.13E-12

Cycle	Date	Time	RelTime[s]	0	1	2	3	4	5	6	7
1	4/10/2004	3:07:24 PM:00	0	1.18E-12	2.09E-11	6.16E-09	2.27E-11	1.34E-09	5.55E-11	6.95E-11	1.13E-12
2	4/10/2004	3:07:40 PM:97	16.97	1.24E-12	1.94E-11	6.16E-09	2.42E-11	1.34E-09	5.59E-11	7.04E-11	1.04E-12
3	4/10/2004	3:07:58 PM:06	34.06	1.16E-12	1.98E-11	6.16E-09	2.25E-11	1.36E-09	5.48E-11	7.10E-11	9.58E-13
4	4/10/2004	3:08:15 PM:14	51.14	1.39E-12	1.97E-11	6.15E-09	2.12E-11	1.35E-09	5.52E-11	7.03E-11	1.04E-12
5	4/10/2004	3:08:32 PM:33	68.33	1.33E-12	2.18E-11	6.16E-09	2.33E-11	1.34E-09	5.48E-11	6.91E-11	1.11E-12
6	4/10/2004	3:08:49 PM:41	85.41	1.28E-12	2.05E-11	6.14E-09	2.22E-11	1.35E-09	5.35E-11	6.93E-11	1.06E-12
7	4/10/2004	3:09:06 PM:44	102.44	1.36E-12	2.10E-11	6.13E-09	2.21E-11	1.35E-09	5.43E-11	6.93E-11	1.05E-12
8	4/10/2004	3:09:23 PM:52	119.52	1.27E-12	2.07E-11	6.14E-09	2.06E-11	1.35E-09	5.48E-11	6.90E-11	1.03E-12
9	4/10/2004	3:09:40 PM:66	136.66	1.30E-12	2.20E-11	6.15E-09	2.05E-11	1.36E-09	5.48E-11	6.80E-11	1.12E-12
10	4/10/2004	3:09:57 PM:74	153.74	1.27E-12	2.15E-11	6.15E-09	2.12E-11	1.36E-09	5.35E-11	6.95E-11	1.01E-12

ASCII SAMPLE CYCLES : Soil Gas 6
DATE : 4/10/2004
CONVERTED CYCLES : 10

Number of stored cycles 10
Printed start cycle 1
Printed end cycle 10
Number of stored datablocks 1

Data	block	Ion Current			
0	4	min:	1.15E-12	max:	1.33E-12
1	15	min:	1.69E-11	max:	2.17E-11
2	28	min:	6.15E-09	max:	6.22E-09
3	30	min:	1.84E-11	max:	2.18E-11
4	32	min:	1.36E-09	max:	1.38E-09
5	40	min:	5.30E-11	max:	5.67E-11
6	44	min:	6.77E-11	max:	7.32E-11
7	48	min:	9.92E-13	max:	1.13E-12

Cycle	Date	Time	RelTime[s]	0	1	2	3	4	5	6	7
1	4/10/2004	3:17:24 PM:00	0	1.25E-12	2.02E-11	6.22E-09	2.18E-11	1.36E-09	5.63E-11	7.32E-11	1.08E-12
2	4/10/2004	3:17:41 PM:03	17.03	1.26E-12	1.92E-11	6.21E-09	2.15E-11	1.37E-09	5.63E-11	6.89E-11	1.03E-12
3	4/10/2004	3:17:58 PM:06	34.06	1.29E-12	1.69E-11	6.18E-09	2.06E-11	1.38E-09	5.55E-11	6.77E-11	1.00E-12
4	4/10/2004	3:18:15 PM:14	51.14	1.24E-12	2.00E-11	6.17E-09	2.14E-11	1.38E-09	5.67E-11	6.98E-11	1.13E-12
5	4/10/2004	3:18:32 PM:22	68.22	1.30E-12	2.17E-11	6.18E-09	2.08E-11	1.37E-09	5.53E-11	7.06E-11	1.06E-12
6	4/10/2004	3:18:49 PM:41	85.41	1.33E-12	2.04E-11	6.18E-09	1.84E-11	1.37E-09	5.40E-11	7.01E-11	1.00E-12
7	4/10/2004	3:19:06 PM:49	102.49	1.15E-12	2.09E-11	6.17E-09	2.02E-11	1.38E-09	5.48E-11	7.03E-11	1.01E-12
8	4/10/2004	3:19:23 PM:58	119.58	1.30E-12	1.94E-11	6.15E-09	2.08E-11	1.38E-09	5.53E-11	6.91E-11	1.04E-12
9	4/10/2004	3:19:40 PM:66	136.66	1.23E-12	2.00E-11	6.16E-09	2.09E-11	1.38E-09	5.64E-11	6.97E-11	9.96E-13
10	4/10/2004	3:19:57 PM:79	153.79	1.28E-12	2.01E-11	6.15E-09	1.98E-11	1.38E-09	5.30E-11	6.87E-11	9.92E-13

ASCII SAMPLE CYCLES : Air 5
DATE : 4/10/2004
CONVERTED CYCLES : 10

Number of stored cycles 10
Printed start cycle 1
Printed end cycle 10
Number of stored datablocks 1

Data	block	Ion Current			
0	4	min:	1.51E-12	max:	1.83E-12
1	15	min:	3.07E-11	max:	3.28E-11
2	28	min:	1.47E-08	max:	1.49E-08
3	30	min:	1.73E-11	max:	2.00E-11
4	32	min:	2.92E-09	max:	2.94E-09
5	40	min:	1.21E-10	max:	1.23E-10
6	44	min:	7.27E-11	max:	7.58E-11
7	48	min:	1.01E-12	max:	1.16E-12

Cycle	Date	Time	RelTime[s]	0	1	2	3	4	5	6	7
1	4/10/2004	3:55:39 PM:00	0	1.68E-12	3.15E-11	1.49E-08	1.73E-11	2.93E-09	1.22E-10	7.27E-11	1.07E-12
2	4/10/2004	3:55:56 PM:03	17.03	1.83E-12	3.27E-11	1.49E-08	1.92E-11	2.92E-09	1.23E-10	7.58E-11	1.07E-12
3	4/10/2004	3:56:13 PM:16	34.16	1.61E-12	3.27E-11	1.48E-08	1.95E-11	2.92E-09	1.22E-10	7.30E-11	1.04E-12
4	4/10/2004	3:56:30 PM:08	51.08	1.60E-12	3.10E-11	1.49E-08	1.82E-11	2.93E-09	1.23E-10	7.40E-11	1.11E-12
5	4/10/2004	3:56:47 PM:22	68.22	1.61E-12	3.20E-11	1.48E-08	1.94E-11	2.93E-09	1.23E-10	7.31E-11	1.11E-12
6	4/10/2004	3:57:04 PM:24	85.24	1.83E-12	3.17E-11	1.48E-08	2.00E-11	2.93E-09	1.21E-10	7.37E-11	1.15E-12
7	4/10/2004	3:57:21 PM:27	102.27	1.51E-12	3.19E-11	1.48E-08	2.00E-11	2.92E-09	1.23E-10	7.27E-11	1.13E-12
8	4/10/2004	3:57:38 PM:30	119.3	1.60E-12	3.20E-11	1.48E-08	1.97E-11	2.94E-09	1.22E-10	7.46E-11	1.01E-12
9	4/10/2004	3:57:55 PM:27	136.27	1.81E-12	3.28E-11	1.47E-08	1.91E-11	2.93E-09	1.22E-10	7.49E-11	1.16E-12
10	4/10/2004	3:58:12 PM:24	153.24	1.58E-12	3.07E-11	1.47E-08	1.93E-11	2.94E-09	1.21E-10	7.35E-11	1.10E-12

ASCII SAMPLE CYCLES : Soil Gas 7
DATE : 4/10/2004
CONVERTED CYCLES : 10

Number of stored cycles 10
Printed start cycle 1
Printed end cycle 10
Number of stored datablocks 1

Data	block	Ion Current			
0	4	min:	1.00E-12	max:	1.28E-12
1	15	min:	1.18E-11	max:	1.43E-11
2	28	min:	4.05E-09	max:	4.07E-09
3	30	min:	9.21E-12	max:	1.19E-11
4	32	min:	9.30E-10	max:	9.39E-10
5	40	min:	3.63E-11	max:	3.81E-11
6	44	min:	4.78E-11	max:	4.94E-11
7	48	min:	9.33E-13	max:	1.08E-12

Cycle	Date	Time	RelTime[s]	0	1	2	3	4	5	6	7
1	4/10/2004	4:56:11 PM:00	0	1.04E-12	1.20E-11	4.05E-09	1.07E-11	9.30E-10	3.72E-11	4.87E-11	9.74E-13
2	4/10/2004	4:56:28 PM:08	17.08	1.02E-12	1.32E-11	4.06E-09	9.21E-12	9.32E-10	3.63E-11	4.80E-11	9.94E-13
3	4/10/2004	4:56:45 PM:27	34.27	1.28E-12	1.37E-11	4.06E-09	1.19E-11	9.30E-10	3.69E-11	4.85E-11	9.61E-13
4	4/10/2004	4:57:02 PM:52	51.52	1.14E-12	1.26E-11	4.05E-09	9.53E-12	9.35E-10	3.72E-11	4.84E-11	1.08E-12
5	4/10/2004	4:57:19 PM:71	68.71	1.19E-12	1.42E-11	4.05E-09	9.75E-12	9.35E-10	3.81E-11	4.86E-11	9.39E-13
6	4/10/2004	4:57:36 PM:96	85.96	1.19E-12	1.18E-11	4.05E-09	9.48E-12	9.34E-10	3.73E-11	4.88E-11	9.74E-13
7	4/10/2004	4:57:54 PM:15	103.15	1.00E-12	1.43E-11	4.06E-09	1.15E-11	9.35E-10	3.76E-11	4.78E-11	9.33E-13
8	4/10/2004	4:58:11 PM:29	120.29	1.15E-12	1.30E-11	4.06E-09	1.02E-11	9.39E-10	3.68E-11	4.94E-11	9.67E-13
9	4/10/2004	4:58:28 PM:43	137.43	1.17E-12	1.37E-11	4.07E-09	9.35E-12	9.35E-10	3.68E-11	4.88E-11	9.69E-13
10	4/10/2004	4:58:45 PM:62	154.62	1.10E-12	1.26E-11	4.05E-09	1.17E-11	9.31E-10	3.69E-11	4.94E-11	1.02E-12

ASCII SAMPLE CYCLES : Soil Gas 8
DATE : 4/10/2004
CONVERTED CYCLES : 10

Number of stored cycles 10
Printed start cycle 1
Printed end cycle 10
Number of stored datablocks 1

Data	block	Ion Current			
0	4	min:	1.01E-12	max:	1.26E-12
1	15	min:	1.11E-11	max:	1.50E-11
2	28	min:	4.28E-09	max:	4.31E-09
3	30	min:	9.09E-12	max:	1.21E-11
4	32	min:	9.20E-10	max:	9.34E-10
5	40	min:	3.70E-11	max:	3.86E-11
6	44	min:	4.71E-11	max:	4.91E-11
7	48	min:	9.12E-13	max:	1.02E-12

Cycle	Date	Time	RelTime[s]	0	1	2	3	4	5	6	7
1	4/10/2004	5:05:20 PM:00	0	1.18E-12	1.50E-11	4.31E-09	1.21E-11	9.26E-10	3.86E-11	4.76E-11	9.85E-13
2	4/10/2004	5:05:37 PM:19	17.19	1.14E-12	1.30E-11	4.31E-09	1.11E-11	9.21E-10	3.78E-11	4.91E-11	9.50E-13
3	4/10/2004	5:05:54 PM:33	34.33	1.12E-12	1.41E-11	4.30E-09	9.09E-12	9.20E-10	3.70E-11	4.84E-11	1.02E-12
4	4/10/2004	5:06:11 PM:74	51.74	1.01E-12	1.40E-11	4.28E-09	9.29E-12	9.21E-10	3.79E-11	4.71E-11	9.56E-13
5	4/10/2004	5:06:28 PM:87	68.87	1.26E-12	1.40E-11	4.30E-09	9.32E-12	9.33E-10	3.80E-11	4.79E-11	9.89E-13
6	4/10/2004	5:06:46 PM:01	86.01	1.02E-12	1.39E-11	4.29E-09	1.14E-11	9.27E-10	3.80E-11	4.84E-11	9.87E-13
7	4/10/2004	5:07:03 PM:26	103.26	1.19E-12	1.33E-11	4.28E-09	1.09E-11	9.28E-10	3.81E-11	4.73E-11	9.12E-13
8	4/10/2004	5:07:20 PM:56	120.56	1.05E-12	1.37E-11	4.29E-09	9.81E-12	9.34E-10	3.81E-11	4.79E-11	9.30E-13
9	4/10/2004	5:07:37 PM:97	137.97	1.10E-12	1.11E-11	4.28E-09	9.21E-12	9.29E-10	3.81E-11	4.80E-11	9.75E-13
10	4/10/2004	5:07:55 PM:27	155.27	1.10E-12	1.41E-11	4.29E-09	9.93E-12	9.33E-10	3.78E-11	4.85E-11	9.81E-13

ASCII SAMPLE CYCLES : Air 6
DATE : 4/10/2004
CONVERTED CYCLES : 10

Number of stored cycles 10
Printed start cycle 1
Printed end cycle 10
Number of stored datablocks 1

Data	block	Ion Current			
0	4	min:	1.00E-12	max:	1.25E-12
1	15	min:	1.16E-11	max:	1.49E-11
2	28	min:	4.34E-09	max:	4.39E-09
3	30	min:	8.27E-12	max:	1.04E-11
4	32	min:	9.75E-10	max:	9.89E-10
5	40	min:	3.95E-11	max:	4.14E-11
6	44	min:	4.80E-11	max:	5.00E-11
7	48	min:	8.92E-13	max:	1.02E-12

Cycle	Date	Time	RelTime[s]	0	1	2	3	4	5	6	7
1	4/10/2004	5:18:20 PM:00	0	1.20E-12	1.18E-11	4.39E-09	9.67E-12	9.75E-10	3.95E-11	4.82E-11	9.73E-13
2	4/10/2004	5:18:37 PM:09	17.09	1.08E-12	1.48E-11	4.38E-09	9.76E-12	9.81E-10	4.01E-11	4.93E-11	9.88E-13
3	4/10/2004	5:18:54 PM:33	34.33	1.20E-12	1.31E-11	4.39E-09	1.04E-11	9.78E-10	4.04E-11	4.93E-11	1.02E-12
4	4/10/2004	5:19:11 PM:47	51.47	1.13E-12	1.40E-11	4.37E-09	1.01E-11	9.81E-10	4.14E-11	4.92E-11	1.02E-12
5	4/10/2004	5:19:28 PM:66	68.66	1.12E-12	1.49E-11	4.37E-09	1.03E-11	9.87E-10	4.02E-11	4.99E-11	9.81E-13
6	4/10/2004	5:19:45 PM:96	85.96	1.09E-12	1.43E-11	4.36E-09	9.50E-12	9.79E-10	3.96E-11	4.92E-11	9.81E-13
7	4/10/2004	5:20:03 PM:15	103.15	1.25E-12	1.36E-11	4.37E-09	8.27E-12	9.85E-10	3.99E-11	4.90E-11	9.52E-13
8	4/10/2004	5:20:20 PM:29	120.29	1.04E-12	1.24E-11	4.36E-09	1.02E-11	9.86E-10	3.99E-11	4.87E-11	8.92E-13
9	4/10/2004	5:20:37 PM:54	137.54	1.00E-12	1.34E-11	4.35E-09	8.77E-12	9.89E-10	4.01E-11	5.00E-11	9.66E-13
10	4/10/2004	5:20:54 PM:73	154.73	1.06E-12	1.16E-11	4.34E-09	1.02E-11	9.87E-10	4.04E-11	4.80E-11	9.17E-13

ASCII SAMPLE CYCLES : Soil Gas 9
DATE : 4/10/2004
CONVERTED CYCLES : 10

Number of stored cycles 10
Printed start cycle 1
Printed end cycle 10
Number of stored datablocks 1

Data	block	Ion Current			
0	4	min:	1.06E-12	max:	1.18E-12
1	15	min:	1.18E-11	max:	1.49E-11
2	28	min:	4.33E-09	max:	4.37E-09
3	30	min:	8.41E-12	max:	1.05E-11
4	32	min:	9.68E-10	max:	9.85E-10
5	40	min:	3.91E-11	max:	4.04E-11
6	44	min:	4.78E-11	max:	4.93E-11
7	48	min:	9.19E-13	max:	1.02E-12

Cycle	Date	Time	RelTime[s]	0	1	2	3	4	5	6	7
1	4/10/2004	5:30:05 PM:00	0	1.12E-12	1.26E-11	4.37E-09	8.41E-12	9.72E-10	3.97E-11	4.93E-11	9.62E-13
2	4/10/2004	5:30:22 PM:47	17.47	1.15E-12	1.35E-11	4.36E-09	8.71E-12	9.73E-10	3.91E-11	4.84E-11	9.39E-13
3	4/10/2004	5:30:39 PM:77	34.77	1.10E-12	1.39E-11	4.35E-09	9.07E-12	9.72E-10	4.02E-11	4.87E-11	9.51E-13
4	4/10/2004	5:30:56 PM:91	51.91	1.11E-12	1.49E-11	4.34E-09	1.01E-11	9.68E-10	3.92E-11	4.79E-11	1.01E-12
5	4/10/2004	5:31:13 PM:88	68.88	1.07E-12	1.27E-11	4.33E-09	1.05E-11	9.79E-10	4.00E-11	4.84E-11	9.19E-13
6	4/10/2004	5:31:31 PM:13	86.13	1.17E-12	1.43E-11	4.35E-09	8.58E-12	9.79E-10	4.01E-11	4.91E-11	9.74E-13
7	4/10/2004	5:31:48 PM:21	103.21	1.08E-12	1.37E-11	4.33E-09	9.59E-12	9.80E-10	3.96E-11	4.78E-11	9.62E-13
8	4/10/2004	5:32:05 PM:40	120.4	1.12E-12	1.18E-11	4.34E-09	8.93E-12	9.84E-10	4.02E-11	4.85E-11	9.40E-13
9	4/10/2004	5:32:22 PM:65	137.65	1.06E-12	1.38E-11	4.33E-09	8.69E-12	9.82E-10	4.04E-11	4.88E-11	1.02E-12
10	4/10/2004	5:32:39 PM:73	154.73	1.18E-12	1.26E-11	4.34E-09	8.76E-12	9.85E-10	4.03E-11	4.85E-11	9.36E-13

ASCII SAMPLE CYCLES : Background 2
DATE : 4/10/2004
CONVERTED CYCLES : 10

Number of stored cycles 10
Printed start cycle 1
Printed end cycle 10
Number of stored datablocks 1

Data	block	Ion Current			
0	4	min:	8.83E-13	max:	9.44E-13
1	15	min:	3.27E-12	max:	4.04E-12
2	28	min:	1.58E-10	max:	1.62E-10
3	30	min:	6.21E-12	max:	8.34E-12
4	32	min:	1.95E-10	max:	2.00E-10
5	40	min:	2.66E-12	max:	2.98E-12
6	44	min:	3.92E-11	max:	4.18E-11
7	48	min:	8.79E-13	max:	9.68E-13

Cycle	Date	Time	RelTime[s]	0	1	2	3	4	5	6	7
1	4/10/2004	5:41:05 PM:00	0	8.84E-13	3.27E-12	1.60E-10	7.65E-12	2.00E-10	2.92E-12	4.13E-11	9.15E-13
2	4/10/2004	5:41:22 PM:25	17.25	8.88E-13	3.33E-12	1.60E-10	6.94E-12	1.99E-10	2.98E-12	4.01E-11	9.33E-13
3	4/10/2004	5:41:39 PM:61	34.61	9.06E-13	4.04E-12	1.59E-10	6.66E-12	1.95E-10	2.96E-12	4.07E-11	9.31E-13
4	4/10/2004	5:41:57 PM:02	52.02	9.05E-13	3.58E-12	1.60E-10	7.82E-12	1.98E-10	2.83E-12	4.07E-11	9.09E-13
5	4/10/2004	5:42:14 PM:32	69.32	8.84E-13	3.64E-12	1.61E-10	7.61E-12	1.96E-10	2.89E-12	4.15E-11	8.97E-13
6	4/10/2004	5:42:31 PM:57	86.57	8.98E-13	3.66E-12	1.58E-10	7.91E-12	1.97E-10	2.92E-12	4.18E-11	8.79E-13
7	4/10/2004	5:42:48 PM:81	103.81	9.44E-13	3.63E-12	1.61E-10	8.34E-12	1.97E-10	2.93E-12	4.12E-11	9.42E-13
8	4/10/2004	5:43:06 PM:22	121.22	9.35E-13	3.98E-12	1.60E-10	6.55E-12	1.97E-10	2.66E-12	3.92E-11	9.32E-13
9	4/10/2004	5:43:23 PM:69	138.69	8.86E-13	3.50E-12	1.62E-10	6.21E-12	1.98E-10	2.70E-12	4.16E-11	9.45E-13
10	4/10/2004	5:43:40 PM:88	155.88	8.83E-13	3.34E-12	1.58E-10	6.66E-12	1.96E-10	2.75E-12	4.08E-11	9.68E-13

ASCII SAMPLE CYCLES : Soil Gas 10
DATE : 4/10/2004
CONVERTED CYCLES : 10

Number of stored cycles 10
Printed start cycle 1
Printed end cycle 10
Number of stored datablocks 1

Data	block	Ion Current			
0	4	min:	1.18E-12	max:	1.29E-12
1	15	min:	1.66E-11	max:	1.86E-11
2	28	min:	6.30E-09	max:	6.38E-09
3	30	min:	7.79E-12	max:	1.11E-11
4	32	min:	1.32E-09	max:	1.34E-09
5	40	min:	5.51E-11	max:	5.79E-11
6	44	min:	5.11E-11	max:	5.31E-11
7	48	min:	8.90E-13	max:	9.97E-13

Cycle	Date	Time	RelTime[s]	0	1	2	3	4	5	6	7
1	4/10/2004	5:46:14 PM:00	0	1.25E-12	1.69E-11	6.38E-09	8.98E-12	1.32E-09	5.79E-11	5.20E-11	9.36E-13
2	4/10/2004	5:46:31 PM:08	17.08	1.28E-12	1.68E-11	6.37E-09	9.97E-12	1.32E-09	5.65E-11	5.25E-11	9.54E-13
3	4/10/2004	5:46:48 PM:33	34.33	1.20E-12	1.74E-11	6.36E-09	1.02E-11	1.32E-09	5.67E-11	5.11E-11	9.35E-13
4	4/10/2004	5:47:05 PM:46	51.46	1.21E-12	1.71E-11	6.35E-09	9.53E-12	1.33E-09	5.75E-11	5.21E-11	9.84E-13
5	4/10/2004	5:47:22 PM:71	68.71	1.29E-12	1.86E-11	6.33E-09	9.25E-12	1.33E-09	5.70E-11	5.25E-11	9.31E-13
6	4/10/2004	5:47:39 PM:85	85.85	1.18E-12	1.66E-11	6.35E-09	7.79E-12	1.33E-09	5.64E-11	5.19E-11	8.90E-13
7	4/10/2004	5:47:56 PM:98	102.98	1.19E-12	1.71E-11	6.32E-09	8.69E-12	1.33E-09	5.75E-11	5.27E-11	9.86E-13
8	4/10/2004	5:48:14 PM:17	120.17	1.24E-12	1.85E-11	6.31E-09	1.11E-11	1.33E-09	5.51E-11	5.23E-11	9.97E-13
9	4/10/2004	5:48:31 PM:48	137.48	1.28E-12	1.71E-11	6.31E-09	1.06E-11	1.33E-09	5.63E-11	5.25E-11	9.47E-13
10	4/10/2004	5:48:48 PM:72	154.72	1.20E-12	1.72E-11	6.30E-09	1.11E-11	1.34E-09	5.69E-11	5.31E-11	9.54E-13

ASCII SAMPLE CYCLES : Air 7
DATE : 4/10/2004
CONVERTED CYCLES : 10

Number of stored cycles 10
Printed start cycle 1
Printed end cycle 10
Number of stored datablocks 1

Data	block	Ion Current			
0	4	min:	1.04E-12	max:	1.29E-12
1	15	min:	1.34E-11	max:	1.63E-11
2	28	min:	5.11E-09	max:	5.19E-09
3	30	min:	6.74E-12	max:	1.04E-11
4	32	min:	1.12E-09	max:	1.14E-09
5	40	min:	4.64E-11	max:	4.80E-11
6	44	min:	4.94E-11	max:	5.08E-11
7	48	min:	8.73E-13	max:	1.00E-12

Cycle	Date	Time	RelTime[s]	0	1	2	3	4	5	6	7
1	4/10/2004	5:59:41 PM:00	0	1.04E-12	1.59E-11	5.19E-09	8.05E-12	1.12E-09	4.65E-11	5.03E-11	9.55E-13
2	4/10/2004	5:59:58 PM:03	17.03	1.19E-12	1.50E-11	5.18E-09	8.33E-12	1.12E-09	4.67E-11	5.04E-11	9.78E-13
3	4/10/2004	6:00:15 PM:22	34.22	1.19E-12	1.63E-11	5.15E-09	8.92E-12	1.13E-09	4.73E-11	4.97E-11	9.94E-13
4	4/10/2004	6:00:32 PM:46	51.46	1.11E-12	1.47E-11	5.14E-09	9.12E-12	1.14E-09	4.80E-11	5.05E-11	8.73E-13
5	4/10/2004	6:00:49 PM:77	68.77	1.24E-12	1.34E-11	5.15E-09	7.64E-12	1.13E-09	4.73E-11	4.94E-11	9.55E-13
6	4/10/2004	6:01:06 PM:85	85.85	1.13E-12	1.49E-11	5.14E-09	8.23E-12	1.14E-09	4.72E-11	4.96E-11	1.00E-12
7	4/10/2004	6:01:24 PM:15	103.15	1.27E-12	1.36E-11	5.12E-09	7.18E-12	1.13E-09	4.64E-11	4.97E-11	9.33E-13
8	4/10/2004	6:01:41 PM:12	120.12	1.23E-12	1.38E-11	5.12E-09	8.71E-12	1.13E-09	4.76E-11	4.96E-11	9.35E-13
9	4/10/2004	6:01:58 PM:31	137.31	1.20E-12	1.61E-11	5.12E-09	1.04E-11	1.13E-09	4.65E-11	4.95E-11	9.93E-13
10	4/10/2004	6:02:15 PM:50	154.5	1.29E-12	1.43E-11	5.11E-09	6.74E-12	1.13E-09	4.79E-11	5.08E-11	9.23E-13